



Università degli studi di Milano
Dipartimento di Chimica

Ph.D. course in Chemistry
XXXIV cycle

**The non-invasive analysis of organic materials in
cultural heritage: development of strategies based
on molecular spectroscopies**

CHIM/01 – CHIM/12

Ph.D. student:
Margherita Longoni

Tutor:
Prof. Silvia Bruni

Ph.D. coordinator:
Prof. Daniele Passarella

Academic Year 2020/2021

Table of contents

Aim of the thesis	8
Chapter 1 - Organic materials in art and their chemical characterisation: state of the art	
Abstract	10
1. Organic materials in art	10
1.1 Lipids	10
1.2 Proteins	12
1.2.1 Egg	13
1.2.2 Milk derivatives	13
1.2.3 Animal glue	14
1.3 Polysaccharides	15
1.4 Natural resins	16
1.5 Organic colourants	16
1.6 Synthetic resins	16
2. The chemical characterisation of organic materials: state of the art	17
2.1 Painting materials	18
2.2 Natural dyes	19
2.3 Synthetic pigments	20
References	20
Chapter 2 - Visible and UV-excited spectrofluorimetry for the non- invasive identification of synthetic organic pigments of contemporary art	
Abstract	24
1. Introduction	24
2. Object of study	27
2.1 Synthetic organic pigments	27
2.1.1 Azo pigments	27
2.1.1.1 Arylide yellows	27
2.1.1.2 Diarylide yellows and oranges	28
2.1.1.3 β -Naphthol pigments	28
2.1.1.4 β -Naphthol reds	28

2.1.1.5 Benzimidazolones	29
2.1.2 Non-azo pigments	29
2.1.2.1 Phthalocyanines	29
2.1.2.2 Quinacridones	30
2.1.2.3 Perylene and Perinone pigments	30
2.1.2.4 Isoindolinone and isoindoline pigments	30
2.1.2.5 Other pigments	31
3. Analytical and imaging fluorescence methods	31
3.1 Spectrofluorimetry	31
3.2 UV-imaging	32
4. Materials and methods	33
4.1 Reference materials	33
4.2 Instrumentation	39
4.3 Multivariate analysis of data	40
4.4 Kubelka-Munk correction for self-absorption of fluorescence emission	40
4.5 Case studies	41
5. Results and discussion	41
5.1 Visible reflectance spectroscopy	41
5.1.1 Red and orange pigments	41
5.1.2 Yellow pigments	42
5.1.3 Violet and blue pigments	43
5.2 Visible-excited spectrofluorimetry	44
5.2.1 Red and orange pigments	45
5.2.2 Yellow pigments	45
5.2.3 Violet and blue pigments	47
5.2.4 Inorganic cadmium-based pigments	51
5.2.5 Self-absorption correction applied to mixtures of pigments	51
5.3 Case studies	54
5.3.1 <i>Addetta near Zoate</i> by G. Faraone	54
5.3.2 Paintings by S. Pasotti	56
5.4 UV-excited spectrofluorimetry	59
5.4.1 Red and orange pigments	59
5.4.2 Yellow pigments and binders	60

5.4.3 Blue, green, violet and cadmium-based inorganic pigments	61
5.5 UV-imaging	61
5.5.1 Red, orange and yellow pigments	63
5.5.2 Violet pigments	65
5.5.3 Blue and green pigments	67
5.5.4 Cadmium-based pigments	67
5.6 Case study	67
6. Conclusions	69
References	70
Appendix A	
1. Reflectance and emission spectra	73
2. Score plots from PCA of emission spectra of reference samples	86
Appendix B - Identification of quinacridone pigments in artists' paints by micro-invasive IR and Raman methods	
Abstract	88
1. Introduction	89
2. Materials and methods	89
2.1 Materials	90
2.2 Sample treatment	90
2.3 Instrumentation	90
3. Results and discussion	91
4. Conclusion	94
References	95
Chapter 3 - FT-NIR Spectroscopy for the non-invasive study of binders and multi-layered structures in paintings	
Abstract	96
1. Introduction	96
2. Object of study	98
2.1 Artistic binders	98
2.2 Preparatory layers	98
3. Near-infrared (NIR) spectroscopy	101
4. Materials and methods	103
4.1 Materials	103

4.2 Instrumentation	103
4.3 Sample preparation	103
4.3.1 Pure reference materials	103
4.3.2 Mock-up painting samples	104
4.4 Preparation of cross sections	104
4.5 Multivariate analysis of data	105
4.6 Ratio calculation	105
4.7 Synthesis of lead palmitate	105
4.8 Ancient paintings	106
5. Results and discussion	107
5.1 Pure reference materials	107
5.2 Model samples with CaCO ₃ preparatory layer	115
5.3 Model samples with CaSO ₄ · 2H ₂ O preparatory layer	125
5.4 Case studies	134
5.4.1 Paintings of the Lombard Renaissance (late 15 th - early 16 th century)	134
5.4.1.1 Paintings by Leonardo's pupils	135
5.4.1.2 <i>SS. Augustine and Jerome</i> by Bergognone	139
5.4.1.3 <i>St. John the Baptist</i> by B. Zenale	140
5.4.2 <i>Ecce Homo</i> by A. Solario	141
5.4.3 A late baroque Italian painting: <i>Porter boy sitting on a basket</i> by Pitocchetto	143
5.4.4 A neoclassical Italian painting: <i>Napoleon</i> by A. Appiani	145
6. Conclusions	147
References	148
Appendix A	
1. Reference FT-IR spectra and band assignment	151
2. Score plots from PCA of NIR spectra of model samples	163
Appendix B- Analyses on micro-samples from the painting Porter boy sitting on a basket by Pitocchetto	
1. Introduction	166
2. Materials and methods	166
3. Results and discussion	166
4. Conclusions	169
References	170

Chapter 4 - *Dry-state* SERS for the non-invasive investigation of natural dyes in textiles

Abstract	171
1. Introduction	171
2. Object of study	174
2.1 Natural dyes	174
2.1.1 Madder	176
2.1.2 Lac dye	176
2.1.3 Indigoids	177
3. SERS spectroscopy	176
3.1. Optical properties of metals	178
3.2 The SERS effect	180
3.2.1 Electromagnetic mechanism	181
3.2.2 Chemical mechanism	182
3.2.3 Hot spots and SERS enhancement	183
3.2.4 Quenching of the fluorescence emission	183
3.3 SERS in cultural heritage diagnostics	184
4. Materials and methods	186
4.1 Materials	186
4.2 Syntheses of silver colloids	186
4.2.1 Lee-Meisel nanospheres	186
4.2.2 Leopold-Lendl nanospheres	187
4.2.3 Garcia-Leis nanostars	188
4.2.4 Nanorods	189
4.3 Syntheses of gold colloids	191
4.3.1 Frens nanospheres	191
4.3.2 Gold nanostars	191
4.4 Preparation of the substrates	192
4.4.1 Functionalization of glass slides	192
4.4.2 Drop deposition	194
4.4.3 Multi-layered deposition	195
4.4.4 Films based on modified coffee-ring effect	196
4.5 Silver nanoparticles embedded into polymeric matrixes	196

4.5.1 Exodisp C 4502 substrates	196
4.5.2 Hydroxyethylcellulose substrates	196
4.5.3 Silver nanoparticle-doped polyvinyl alcohol substrates	197
4.6 Commercial SERS substrates	197
4.7 Electrochemical deposition of silver nanoparticles	197
4.8 Cleaning of the substrates by TiO ₂	198
4.9 Preparation of reference mock-up samples	198
4.10 Instrumentation	199
4.10.1 Raman spectroscopy	199
4.10.2 UV-visible spectroscopy	199
4.10.3 Scanning Electron Microscopy (SEM-EDX)	199
4.10.4 Profilometry	199
4.9.5 Potentiometry	200
5. Results and discussion	201
5.1 Silver substrates	201
5.1.1 Lee-Meisel nanosphere substrates	201
5.1.2 Leopold-Lendl nanosphere substrates	209
5.1.3 Garcia-Leis nanostar substrates	216
5.1.4 Nanorod substrates	225
5.1.5 Multi-layered substrates: nanostars on nanospheres	226
5.2 Silver nanoparticles embedded into polymeric matrixes	228
5.3 Gold substrates	234
5.3.1 Frens nanosphere substrates	234
5.3.2 Nanostar substrates	243
5.4 Commercial SERS substrates	247
5.5 Electrochemically-deposited substrates	249
5.6 Exploiting the self-cleaning properties of titanium dioxide	251
6. Conclusion and future perspectives	252
References	253
Final conclusions	259
Lists of publications and attended congresses	261

Aim of the thesis

The importance of scientific analyses on artworks has become more and more crucial in the articulate processes of conservation and restoration. Moreover, the complexity of artistic materials, composed by organic and inorganic substances mixed together and often aged, requires extremely sensitive but user-friendly analytical tools. For this reason, the request of effective non-invasive diagnostic techniques is steadily increasing. In particular, a challenging task is represented by organic compounds, which can be found in the artistic field with a wide range of applications: they are binders used to spread pigments in paintings, varnishes, coatings and adhesives applied by the artist himself or during the restoration works, and colouring substances. Among the latter two different typologies can be individuated, namely natural dyes, used from the antiquity to dye textiles and in paintings in form of lakes, and a quite recent family of pigments, the synthetic organic ones. The detection of such materials can be hardly achieved by the non-invasive and in-situ applicable analytical techniques commonly employed in the field of conservation science. Briefly, X-ray fluorescence cannot provide useful information as it detects only elements with medium to high atomic number, while infrared and Raman spectroscopies are affected by the problem of fluorescence emission and of the matrix interference respectively.

This thesis work was intended to develop innovative strategies based on molecular spectroscopies, pursuing the objective of non-invasively identifying the most common organic materials which can be found in museum objects, mainly focusing the attention on paintings and ancient textiles.

In particular, chapter 1 provides an overview of these substances and of the analytical methods commonly employed for their detection, underlining the lack, and the consequent need, of non-invasive and in-situ applicable strategies.

The following chapters deal with the issue of analysing different kinds of organic substances by specific and innovative spectroscopic methods aimed at recognising them.

Chapter 2 deals with the identification of synthetic organic pigments, a quite recent category of colourants since they were introduced by Perkin in the second half of the 19th century.

The fluorescence emission upon visible excitation exhibited by several organic pigments used in contemporary artworks is demonstrated and an analytical approach combining visible-induced spectrofluorimetry and visible-reflectance spectroscopy with a multivariate processing

of data is established. The effectiveness of the method is finally confirmed by its application to three contemporary paintings. In addition, the possibility of exploiting fluorescence emission induced by UV radiation is considered, as well as the prospect of investigating such materials by ultraviolet fluorescence (UVF), visible and infrared luminescence (VIVF and VIL) images.

Chapter 3 is dedicated to the use of near-infrared (NIR) spectroscopy for the detection of organic binders and to understand the complex stratigraphy in paintings. This spectral region, in particular in the range 6500-4000 cm^{-1} , is dominated by combination and overtone bands due to functional groups typical of the lipidic and proteinaceous materials used as binding media, therefore it can be exploited for identification purposes. Moreover, the greater penetration depth of the NIR radiation in comparison with the mid-infrared (MIR) one allows the investigation of the preparatory layers possibly applied by the artist on the painting support. In this respect, an exhaustive study is carried out at first on a consistent number of reference mock-up samples, prepared on the basis of ancient recipes, and then on eight paintings, dating from the end of the 15th century to the end of the 18th century and exemplifying different artistic techniques on different supports.

Finally, chapter 4 is dedicated to surface-enhanced Raman spectroscopy (SERS) for the identification of natural dyes in textiles. This technique, which exploits the strong intensification by several orders of magnitude of the Raman scattering of organic molecules in the proximity of metal nanoparticles and nanostructured surfaces, is a well-established method for the detection of dyes, but generally requires the extraction of the target analyte from a sample. In this work many experiments were performed to develop SERS-sensors suitable for performing measurements directly from dyed fibres in dry-state condition, i.e without requiring extraction protocols or the placement of a wet substrate in contact with the artefact. In this respect, a general, easy-to-apply protocol involving the deposition of colloidal nanoparticles on glass supports was developed. The importance of hot spots, areas of strong SERS intensification of the Raman signal formed between close nanoparticles or on anisotropic structures rich in tips, leads to experiment different aggregation procedures and nanoparticle shapes, ranging from nanospheres to nanostars and nanorods. The final aim is to create reproducible and homogeneous sensors, able to provide a high SERS enhancement when just put in contact in dry-state conditions with the artistic object under investigation. Finally, also some related issues are faced, such as the release of metal on the sample and the cleaning of the substrate surface.

Chapter 1:

Organic materials in art and their chemical characterisation: state of the art

Abstract

This introductory chapter is intended to provide a short overview of the organic materials which can be found in the artistic field and of their use. Their chemical classes will be briefly described, as well as the analytical methods commonly employed for their detection. The availability of mainly destructive methods will be underlined, as opposed to the highly desirable request of a non-invasive approach in the field of diagnostics.

1. Organic materials in art

Organic materials represent a major component in art and archaeology. Such substances have been extensively used since antiquity to create different kinds of artefacts, including textiles, paintings and archaeological objects. Organic compounds were, in fact, employed for a wide range of applications: proteinaceous, lipidic and polysaccharide materials were used as paint binders, natural dyes as colouring substances both for fabrics and paintings, natural waxes and resins as varnishes and coatings in sculptures and paintings. Moreover, in recent times, synthetic organic materials joined the traditional ones. Artificial polymers, such as acrylic and alkyd resins, were increasingly used as binders in contemporary art, thanks to their shorter drying time. At the same time, synthetic organic pigments became rapidly appreciated by artists for their brightness. In the following sections, the main classes of organic compounds of artistic interest will be briefly discussed, focusing on their chemical composition and on their use in the artistic field.

1.1 Lipids

Lipids are a wide category of natural compounds, both of vegetable and animal origin. The former are referred as oils and have a liquid nature, the latter, known as animal fats, are solid or semi-solid compounds. Oils and fats are mixtures of triglycerides, basically esters of glycerol with fatty acids, and smaller amounts of other compounds, i.e. sterols and vitamins [1, 2].

In particular, referring to paintings, a key-role is played by siccative oils. They are unsaturated triglycerides, derived from the reaction between a molecule of glycerol and three long chain

molecules of fatty acids (Fig. 1). The principal ones are oleic ($C_{18}H_{34}O_2$), linoleic ($C_{18}H_{32}O_2$) and linolenic ($C_{18}H_{30}O_2$) acids which can be associated with minor amounts of saturated fatty acids, especially the palmitic ($C_{16}H_{32}O_2$) and the stearic ($C_{18}H_{36}O_2$) ones [3].

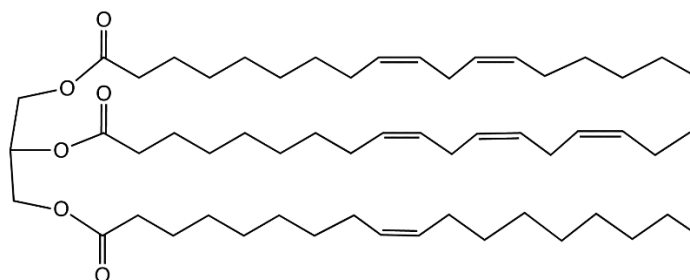


Figure 1. Representative triglyceride found in a drying oil. The triester is derived from three different unsaturated fatty acids, linoleic, alpha-linolenic and oleic acids.

The reactivity of the double bonds in the unsaturated chains of fatty acids determines the chemical behaviour of oils and the radical transformations which can alter their composition because of degradation phenomena [4-7]. The hydrolysis of triacylglycerols leads to the formation of free fatty acids, while oxidation via radical reactions causes the inclusion of oxygen in the acyl chain, carbon-carbon bond cleavage and the formation of lower molecular weight species [2, 7, 8]. Oxidation is a key-phenomenon in painting as induces polymerisation and cross-linking processes during the curing of drying oils, leading to the formation of a polymeric network which generates the solid paint film. This process is quite slow: the drying of the whole thickness of a siccativ oil film can take a long time, which depends on different factors, i.e. temperature and presence of substances having a catalytic effect. For these reasons, since ancient times heating procedures were adopted to speed up the polymerisation process, as well as the addition of substances promoting drying. In particular, it is the case of some metal ions derived from pigments, such as Pb^{2+} , Co^{2+} and Mn^{2+} , which fasten oxidation [3].

The most common used oil in painting is linseed oil: it was employed in northern Europe from the 13th century and spread in Italy from the 15th one, replacing walnut oil. Its extensive use is due to the excellent properties of the film it forms once cured and dried: the network structure containing residual molecules of free fatty acids in the structural voids confers flexibility, cohesion and elasticity [3]. Anyway, it suffers from yellowing issues and tends to lose its optical property of transparency over time. This phenomenon is less accentuated for poppy and walnut oils, although they give rise to films having worse properties and, for these reasons, were adopted by artists only in limited cases, for example to spread white pigments, often in mixture with linseed oil. Poppy oil films, in fact, have low resistance and are prone to cracking, while walnut oil is more subject to degradation phenomena for its intrinsic nature. [3]

1.2 Proteins

Proteins are macromolecules constituted of one or more linear chains of amino acids (Fig. 2) joined together by peptide bonds between the carboxyl ($-\text{COOH}$) and amino ($-\text{NH}_2$) groups of adjacent amino acid residues. The resulting structure is known as polypeptide. [1, 2]

Twenty amino acids are commonly found in animal and vegetable proteins: glycine (Gly), alanine (Ala), valine (Val), leucine (Leu), isoleucine (Ile), methionine (Met), proline (Pro), hydroxyproline, (Hyp), threonine (Thr), asparagine (Asn), glutamine (Gln), tyrosine (Tyr), cysteine (Cys), lysine (Lys), arginine (Arg), aspartic acid (Asp), phenylalanine (Phe), tryptophan (Trp), serine (Ser), glutamic acid (Glu), and histidine (His) [9]. Their number and type and their sequence determine the molecular configuration of the protein and its unique chemical and physical properties. The three-dimensional structure influences instead the function of a polypeptide. The presence of chemical groups able to form hydrogen bonds confers to protein a hydrophilic nature: in most cases, they dissolve forming aqueous solutions which have a colloidal nature, i. e. are composed of *micelle* (large aggregates of molecules) stably dispersed in the aqueous phase. [3]

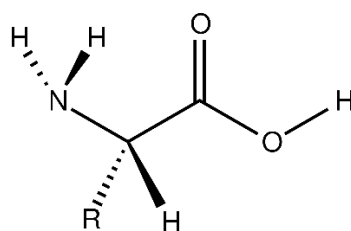


Figure 2. Structure of a generic amino acid with its amino ($-\text{NH}_2$) and carboxylate ($-\text{COOH}$) functional groups and a side chain (R group), specific to each amino acid.

Proteinaceous substances are rather stable to oxidation and undergo little chemical changes under normal conditions of temperature and humidity thanks to the low reactivity of the amino and peptide bonds. Anyway, their main enemy is moisture, not only as it causes slow hydrolysis of the peptide linkage and, as a consequence, reduces the average molecular weight, but also because it permits fungi and bacteria to flourish. The enzymatic and biological route is, in fact, the main cause of protein degradation. Moreover, the complex chemical structure of these macromolecules can be irremediably altered by chemical and physical agents or simply because of aging. This process is called denaturation and can be induced by different factors, such as time, heat, UV radiation, pH and salts. Denaturation makes the identification of proteins a matter of some difficulty in the case of museum materials [2, 3]. They have rather to be analysed in terms of their constituent amino acids, released by acid hydrolysis, and, since there are no

unique amino acids allowing the identification of a given protein, an evaluation can be made only on the basis of a quantitative assay of the amino acids themselves [2, 10].

In paintings, animal proteins such as egg and casein were frequently used as binders for pigments in the tempera technique, while animal glues were one of the main ingredients of preparatory layers for panels and canvases [3]. In the following, a brief description of these material will be presented.

1.2.1 Egg

Egg has been extensively used in the artistic field, as it is the main component of tempera technique. It is composed of two parts, yolk and white, whose chemical composition and properties are slightly different.

Yolk is an emulsion of a colloidal solution of some phosphorated proteins and a mixture of lipidic components. White is basically an aqueous colloidal suspension of proteins (the main is albumin), coupled with a small amount of lipids and mineral salts. Egg, because of water loss or heat effect, becomes an irreversible gel. This means that, once dried, it loses its solubility. This property is exploited in painting: when used as binder, it rapidly forms a film characterised by a strong cohesion. White gives a more fragile and water-sensitive film in comparison with yolk because of the absence of the lipidic component, which confers better mechanical and water-proof properties, adhesion, cohesion and flexibility. Moreover, while white can easily deteriorate because of ageing, yolk is more stable and maintains its optical properties. For all these reasons, yolk has been extensively mixed with pigments in painting since antiquity, whereas the use of white was limited to illuminations in manuscripts. [2, 3]

1.2.2 Milk derivatives

Milk is an aqueous emulsion of proteins and lipids: dry milk contains about 26% proteins, 26% lipids and the remaining is composed of sugars, vitamins and mineral salts [11]. Casein is a phosphoprotein which can be found in milk as calcium salt, forming a colloidal dispersion. It is formed by acidic, enzymatic or thermal treatment and its main constituents are α , β , γ and δ -casein. This protein is insoluble in water, unless its acid carboxylic groups react with alkaline substances forming caseinates. The most common ones are ammonium or calcium caseinates, derived respectively from the reaction with ammonia or ammonium carbonate and calcium hydroxide. [2, 3] The former, although less frequently than egg, was used as binder in wall paintings and for water colours; on the other hand, the adoption of the latter as binding medium is only occasionally documented in emulsion with oil. Since the 19th century, the application of casein in art was limited to the preparatory ground of panels and canvases. This restricted use

is due to the fastness of the degradation processes undergone by the film because of ageing and leading to a loss of mechanical and physical properties. [3]

Despite only little documentation is available in the literature about the use of pure milk as binder, it is likely that this proteinaceous material has been historically employed both to make and restore paintings. In fact, being an emulsion of casein with lipids, when used to disperse pigments, it gives a paint similar to egg tempera. [3] It is worth noticing that their composition is, in fact, quite similar. [2]

1.2.3 Animal glue

The definition “animal glue” refers to a specific chemical class of materials derived from rabbit skins, cartilages and bones and mainly composed of proteins (collagen is the most important) and, in smaller amount, other non-proteinaceous substances [1]. Glycine and hydroxyproline are the main amino acids [2]. Glues can show different behaviours according to their chemical composition and their physical properties can vary as a function of their origin and of the purification treatments. Purer glues, called gelatines, are mainly composed of collagen; raw glues are known as strong glue because of their higher adhesive power. In comparison with egg, glues give rise to aqueous colloidal solutions which are reversible: this means that, once dried by solvent evaporation, they recover the original properties and can be re-used [3]. In art, animal glues were mainly adopted for their adhesive properties, but also as painting medium for preparatory layers. It is, in fact, well assessed that the most common ground layers in historical Italian painting were made of gypsum in mixture with aqueous glue solutions. For this application, gelatines were preferred because of their higher solubility in water. Moreover, since the 16th century, glues have been mixed with oils or natural resins to obtain a more flexible preparatory layer, the so-called *mestica*, especially suitable for canvas. Finally, they found application also for illuminations, used pure or more typically in mixture with egg [3]. Many degradation phenomena, leading to a loss of cohesion and adhesion and, as a consequence, to the detachment of the paint layers, can be attributed to glue. The nature of such processes, both chemical and physical, is still undefined, but they are probably due to the interaction with water, even in form of environmental humidity [2]. Its variations, in fact, leads to cycles of swelling and shrinking phenomena, which cause mechanical damages. Moreover, water can hydrolyse the proteinaceous component, inducing a loss of the binding properties, and promotes the microbiological attack [2, 12].

1.3 Polysaccharides

Polysaccharides are polymers derived from condensation of many monosaccharides, joined together by glycoside bonds (Fig. 3). Such compounds, being rich in hydroxyl groups, have a strong affinity with water and show a hydrophilic behaviour. On the other hand, they are insoluble in organic solvents.

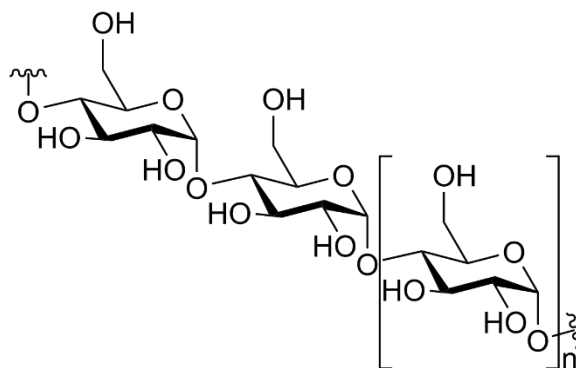


Figure 3. Structure of a polysaccharide molecule.

In art, the most typical polysaccharides are vegetable gums, amorphous materials exudated or contained in some plants [3]. These substances have a very complex chemical structure made of sequences of monomers of simple sugars, sometimes salified with Ca^{2+} , Mg^{2+} and K^{+} ions. The gums traditionally employed were gum Arabic (exuded by *Acacia* trees), tragacanth gum (produced by *Astragalus*) and fruit tree gum (mainly obtained from cherry, apricot, peach and plum trees). [1]

Their application ranges from adhesives to binders, especially in manuscripts and illuminations, thanks to the brightness and the chromatic properties they confer to pigments. In the traditional painting techniques, their use is instead extremely rare and only in mixture with oil, casein or egg, forming an emulsion.

Another common polysaccharide is starch. It is made of glucose, amylose (a linear chain polymer) and amylopectin (a partially branched polymer) and derives from seeds or other vegetable parts [1, 2]. The use of starch is documented only in some paint preparations or in the production of paper. Its complex chemical structure, in fact, prevents its solubility in water and, as a consequence, makes this substance unsuitable to be used as medium to disperse pigments [3]. On the other hand, acid treatment of starch produces dextrans, which are exploited as adhesives and additives in water colour paintings, generally mixed with natural gums. [1, 12]

1.4 Natural resins

Natural resins can have vegetable or animal origin. Resins derived from plants are lipid-soluble mixtures of volatile and non-volatile terpenoid and/or phenolic secondary compounds. From a chemical point of view, vegetable resins are a complex mixture of mono-, sesqui-, di- and triterpenes, which have, respectively, 10, 15, 20 and 30 carbon atoms per molecule [1, 2]. Resins are formed in the so-called 'resiniferous canals' of several trees: many varieties of plants spontaneously produce and exude them as a product of their metabolism, to protect themselves against loss of water and microbiological attacks. [1, 12]

Natural terpenoid resins and resinous materials played a prominent role in ancient times: they were used as adhesives, hydro-repellents, and coating and sealing agents [13]. Their high viscosity and insolubility in water prevent their application as binding media [1, 3].

Referring to animal resins, the most common is shellac, produced by an Indian scale insect (*Laccifer lacca* Kerr, also known as *Kerria lacca*) [14]. Shellac is a complex mixture made of mono- and polyesters of hydroxy-aliphatic and sesquiterpene acids. It began to be used in Europe towards the end of the 16th century [15], mainly as varnish for paintings and wooden objects.

1.5 Organic colourants

Organic colourants include natural dyes and a quite recent category of substances, synthetic organic dyes and pigments. Natural dyes have been used since antiquity both to dye textile fibres and in form of lakes (i.e. adsorbed onto an inorganic substrate such as alum) in paintings. They were extracted from vegetable or animal sources and, according to their chemical nature, can be divided into different classes. Their colouring molecules are mainly flavonoids, anthraquinoids, indigoids and gallotannins or other molecular types such as carotenoids, benzoquinones and anthocyanidins. [16-19] More details about natural dyes will be provided in chapter 4.

In 1856 William Perkin discovered the first dye obtained by synthetic route, mauve: from this moment on, a wide range of new substances were produced and, thanks to their brightness and the variety of hues, adopted by modern and contemporary artists. They were both water soluble (synthetic dyes) and insoluble (organic pigments) materials, but their basic chemical structure is in most cases the same: the necessary insolubility for pigments, in fact, is achieved by replacing in the molecule the functional groups that favour solubility or by forming insoluble organic complexes. [20, 21] More detail about synthetic organic pigment will be given in chapter 2.

1.6 Synthetic resins

Since the mid-19th century, artists and restorers have explored the use of synthetic materials and nearly all the polymers that industry made available have been adopted in art or conservation

[22]. Synthetic resins found application as solidifiers, varnishes, coatings, paint binders, moulding and casting substances. Industrial varnishes, which are transparent and give colourless protective films, progressively replaced traditional natural paint coatings (i.e. dammar and mastic resin, copal or colophony). These modern polymers include ketonic, acrylic and methacrylic resins, really appreciated thanks to their good refraction index, resistance to yellowing and high transition temperatures (low glass transition temperatures lead, with time, to the incorporation of particulate in the coating layer, with a loss of transparency and gloss). In paintings, beside the traditional binding media such as drying oils and proteinaceous temperas, a wide range of industrial binders were experimented: it is the case of alkyd and acrylic resins, extensively employed in the 20th century artworks [1]. As yet we are not fully aware of the chemical and physical behaviour of modern synthetic materials, their conservation is challenging. This is particularly true regarding the interactions with the other components in art objects (i.e. additives, fillers, plasticizers and colourants) and the changes in their properties during ageing.

2. The chemical characterisation of organic materials: state of the art

The analysis of the materials which constitute artistic and archaeological objects represents a fundamental task in the field of cultural heritage diagnostics. Such a knowledge, in fact, is indispensable for their conservation and valorisation, besides providing interesting information about their history. From an historical point of view, it permits to discover what resources were available in a certain age and in a certain geographical area, giving interesting anthropological indications. From an artistic perspective, recognising the materials can be useful to understand the artist's painting technique and its evolution, as well as to date artefacts, leading sometimes to find out forgeries and counterfeiting. Finally, scientific analyses give an insight into degradation phenomena, directing in this way conservative and restoration works.

In this scenario, the pursuit of chemical techniques which are non-destructive or require a minimal amount of sample can be considered the main challenge of the current research in the conservation field. Nowadays, different analytical methods allowing non-invasive and in-situ analyses have been developed, thanks to portable and easy-to-use analytical devices suitable to provide quick, but reliable chemical information. Among these methods, it is worth mentioning X-ray fluorescence (XRF), Raman spectroscopy and Fourier-transform infrared spectroscopy (FT-IR) in reflection mode. Their use, in fact, is well assessed for the detection of materials directly on artistic artefacts, but these techniques suffer from many limitations when applied for the analysis of organic compounds. XRF is an elemental technique, aimed at detecting high

atomic number elements (typically $Z > 16$); Raman spectroscopy is affected by the problem of fluorescence emission; FT-IR is, in principle, an ideal tool, but the identification of the target analyte can be made difficult because of the matrix interference. In fact, the majority of artworks are complex objects, made of different materials, often assembled in multiple layers and/or mixed together. Organic substances, for example, can be found as binders used to disperse and apply pigments on supports, as dyes in the ancient art of dyeing textiles and as consolidants, adhesives, paints and varnishes applied during restoration works. Finally, in recent years, the spreading of new synthetic colourants amplified the range of organic substances available in the artistic field. For all these reasons, the traditional approach to the detection of such compounds mainly involves the use of destructive, sample-requiring techniques. A key-role, in particular, is played by separative methods as they allow the separation of the organic analyte from its matrix, enabling its univocal identification. In this respect, the use of chromatographic techniques, possibly coupled with mass spectrometry, is the most established protocol.

2.1 Painting materials

Dealing with paintings, proteins, glycerolipids and polysaccharides used as binders are the main objects of study, together with waxes, lacquers and natural or synthetic resins used as additives, varnishes and consolidants. Since it was introduced in conservation science in the 1970s, gas chromatography coupled with mass spectrometry (GC/MS) have been one of the most commonly exploited analytical method for the detection of such substances [23-29]. Being macromolecular, polar and low volatility compounds, for GC/MS analyses they must be subjected to chemical or thermal treatments aimed at obtaining from the original macromolecules low-polarity, low-molecular weight components. In this way, their volatilisation and the subsequent separation through a gas chromatographic column are facilitated. This can be achieved by coupling analytical pyrolysis with GC/MS (Py-GC/MS) [29-31] or by a wet chemical treatment of the samples involving hydrolysis and derivatisation [29]. Hydrolysis conditions vary from material to material: for example, glycerolipids and waxes are hydrolysed by an alkaline solution, while proteins and polysaccharides require acidic solutions. Moreover, recent studies have demonstrated that GC/MS is a valuable technique also for the identification of synthetic binders of contemporary art such as alkyd and acryl resins [32, 33]. Obviously, in all cases we deal with a destructive approach.

In addition, spectroscopic techniques allowing micro-analysis (such as FT-IR and scanning electron microscopy with energy dispersive X-ray analyses SEM-EDX) can be used to individuate both organic and inorganic materials in cross sections [34, 35]. Again, a sample is required, preventing non-destructivity, but thanks to these techniques it is possible to achieve

information layer by layer, disclosing the stratigraphy of the painting. This is clearly impossible when the whole sample is subjected to extraction procedures.

2.2 Natural dyes

Natural dyes are inserted in complex matrixes such as textile fibres or paint layers, where they are mixed with other substances, including binding media and mordants. Moreover, because of their high tinting strength, they were used in very small amounts, leading to the necessity of a very sensitive detection method. Since the beginning of 1980s, when it was introduced by Wouters and collaborators [36], high-performance liquid chromatography (HPLC) equipped with a diode array detector (DAD) and/or coupled with mass spectrometry (HPLC/MS) has been successfully exploited for the characterisation of natural colourants. As a result, dye molecules can be characterised in terms of retention time from the HPLC column and on the basis of their electronic or mass spectra respectively from UV-visible spectroscopy and MS analysis. The former of these techniques, basing the identification of the analyte on its electronic spectrum, is scarcely specific and fails when dealing with mixture of colours having similar hue [37]; the latter provides a unique fingerprint of the compounds under investigation as the molecular masses are generally typical of a given dye. The usual procedure involves the extraction of the dye from a micro-sample (0.1-1 mg) with a suitable solvent (typically a mixture of hydrochloric acid and methanol [38], followed by its chromatographic analysis. The application of HPLC/MS has been largely documented for the detection of a consistent number of dyes belonging to the main chemical classes both in reference materials [39-41] and in extracts from ancient artefacts [42-47]. Finally, although nuclear magnetic resonance (NMR) is the most widely used spectrometric technique for characterising organic compounds, it has never been applied to textile dye analysis as it is not sensitive enough to the minute amounts of material generally available for the analysis. [48]

Among the non-invasive spectroscopic methods, the use of IR, UV-visible and Raman spectroscopies is well documented for the identification of natural dyes [36, 50-53]. However, FT-IR is not the ideal method to characterise dyes as it is strongly affected by the matrix interference effect which occurs in the presence of the mordanted textile fibres, whose signals dominate the spectrum [54]. UV-visible spectroscopy suffers, on the other hand, from a lack of specificity: being based on electronic absorptions, it gives rise to broad bands that can be similar for dyes having similar hue and can also be affected by the problem of dye fading. [55] Finally, normal Raman spectroscopy encounters the problem of fluorescence emission especially when natural organic dyes are involved, and, even in cases when such emission can be limited by proper choice of the experimental conditions, for example by using red or near-IR emitting

lasers, the response of the textile fibre prevails. [56] A valid solution to most of these issues is offered by surface-enhanced Raman spectroscopy (SERS), as will be described in the detail in chapter 4.

2.3 Synthetic pigments

Even the identification of the more recent synthetic organic pigments represents a challenging task. X-ray diffraction (XRD) is a valuable technique and its application was reported for the characterisation of the chemical and crystalline structure both of pure powder pigments [57] and commercial alkyd and acrylic paints [58]. Also chromatographic methods were successfully used: thin layer chromatography (TLC) [59, 60], high-performance liquid chromatography (HPLC) [61] and pyrolysis gas chromatography (pyGC) [62] allowed the identification of a consistent number of pigments, both pure and in commercial paints, and the same goal was achieved by mass spectrometry (MS) techniques [63, 64, 65].

Referring to spectroscopic methods, Raman spectroscopy was exploited to create a spectral database of synthetic organic pigments [65, 66] but, when analyses are performed directly on works of art, the colourants themselves and/or the binding media, especially if aged, can cause a huge fluorescence that hides the weak Raman signals due to the target analytes. Even if this limitation can be overcome by using new generation handheld Raman spectrometers based on the patented SSETM (Sequentially Shifted Excitation) technology [67], this instrumentation is at present not commonly available in diagnostic laboratories. FT-IR spectroscopy can provide a univocal spectrum, but the presence of binders and fillers often hides with their stronger absorptions the bands of the pigments. This makes impossible their identification without preliminary treatments aimed at extracting the colourants or/and at eliminating, at least partially, the fillers [68, 69]. However, the detection of these synthetic pigments remains of great interest as only little is known about their stability over time and degradation processes because of their quite recent introduction.

References

- [1] Organic Materials in Art and Archaeology Maria Perla Colombini and Francesca Modugno
- [2] J. S. Mills, R. White, The Organic Chemistry of Museum Objects, Butterworths, London, 1999.
- [3] M. Matteini, A. Moles, La Chimica nel Restauro. I Materiali dell'arte Pittorica, Nardini Editore, Florence, 1989.
- [4] M. P. Colombini, F. Modugno, E. Ribechini, *J. Mass Spectrom* 2005, 40, 890–898.
- [5] R.P. Evershed, S.N. Dudd, M.S. Copley, R. Berstan, A.W. Stott, H. Mottram, S.A. Buckley,

- Z. Crossman, *Acc. Chem. Res.* 2002, 35, 660–668 (2002).
- [6] M. Regert, H.A. Bland, S.N. Dudd, P.F. van Bergen, R.P. Evershed, Free and bound fatty acid oxidation products in archaeological ceramic vessels, *Proceedings of the Royal Society London B*, 265, 2027–2032, 1998.
- [7] R.J. Hamilton, C. Kalu, E. Prisk, F.B. Padley, H. Pierce, *Food Chem.* 1997, 60, 193–199.
- [8] N.A. Porter, *Methods Enzymol.* 1984, 105, 273–282.
- [9] T.E. Creighton, *Proteins: Structures and Molecular Properties*, W.H. Freeman, New York, 1993.
- [10] M. G. Giuffrida, R. Mazzoli, Enrica Pessione, *Appl. Microbiol. Biotechnol.* 2018, 102, 5445–5455.
- [11] P. Cok, B. De Bernard, M.P. Radillo, F. Francescato, *Synoptic Food Composition Tables*, Edizioni Piccini, Padova, 1986.
- [12] O. Ciferri, *Appl. Environ. Microbiol.* 2020, 65, 3.
- [13] A.M. Pollard, C. Heron, *Archaeological Chemistry*, Royal Society of Chemistry, Cambridge, 1996, 239–270.
- [14] K.S. Brown, *Chem. Soc. Rev.* 1975, 4, 263–288.
- [15] L. Masschelein-Kleiner, *Ancient Binding Media, Varnishes and Adhesives*, ICCROM Ed., Rome, 1995.
- [16] J. H. Hofenk de Graaff, *The Colorful Past. Origin, Chemistry and Identification of Natural Dyestuffs*, Abegg-Stiftung, Riggisberg, 2004.
- [17] J. Cannon, M. Cannon, *Dye Plants and Dyeing*, The Herbert Press, London, 1994.
- [18] D. Cardon, *Natural Dyes: Sources, Tradition, Technology and Science*, Archetype Publications, London, 2007.
- [19] H. Zollinger, *Color Chemistry. Syntheses, Properties and Applications of Organic Dyes and Pigments*, Wiley-VCH, Weinheim, 2003.
- [20] H. Zollinger, *Color Chemistry. Syntheses, Properties and Applications of Organic Dyes and Pigments*, Wiley-VCH, Weinheim, 2003.
- [21] S. Q. Lomax, T. Learner, *JAIIC* 2006, 45, 107-125.
- [22] C. V Horie, *Materials for Conservation, Organic Consolidants, Adhesives and Coatings*, Butterworth Heinemann, Oxford, 1987.
- [23] P. H. Ostrom, M. Schall, G. Hasand, T. Shen, P. V. Hauschra, J. R. Strahler, D. A. Gage, *Geochim. Cosmochim. Acta* 2000, 64, 1043-1050.
- [24] S. L. Vallance, *Analyst* 1997, 122, 75R-81R
- [25] R. M. Castro, M.T. D. Carbó, V. P. Martínez, J. V. G. Adelantado, F. B. Reig, *J. Chromatogr. A* 1997, 778, 373-381.

- [26] M. P. Colombini, F. Modugno, E. Menicagli, R. Fuoco, A. Giacomelli, *Microchem. J.* 2000, 67, 291-300.
- [27] M. P. Colombini, F. Modugno, M. Giacomelli, S. Francesconi, *J. Chromatogr. A* 1999, 846, 113-124.
- [28] M. P. Colombini, A. Andreotti, I. Bonaduce, F. Modugno, E. Ribechini, *Acc. Chem. Res.* 2010, 43, 715-727.
- [29] M. P. Colombini, F. Modugno, *J. Sep. Sci.* 2004, 27, 147-160 and papers therein.
- [30] I. Bonaduce, A. Andreotti. Py-GC/MS of organic paint binders in Organic mass spectrometry in art and archaeology, Wiley, Chichester, 2009, 304-326.
- [31] G. Chiavari, N. Gandini, P. Russo, D. Fabbri, *Chromatographia* 1998, 47, 420-426.
- [32] J. Peris-Vicente, U. Baumer, H. Stege, K. Lutzenberger, J. V. Gimeno Adelantado, *Anal. Chem.* 2009, 81, 8, 3180–3187.
- [33] J. La Nasa, S. Orsini, I. Degano, A. Rava, F. Modugno, M. P. Colombini, *Microchem. J.* 2016, 124, 940–948.
- [34] D. Pinna, M. Galeotti, R. Mazzeo, Scientific examination for the investigation of paintings. A handbook for restorers, Centro Di, Firenze, 2011.
- [35] S. Prati, D. Fuentes, G. Sciutto, R. Mazzeo, *J. Anal. Appl. Pyrolysis* 2014, 105, 327–334.
- [36] J. Wouters, *Stud. Conserv.* 1985, 30, 119-128.
- [37] D. Mantzouris, I. Karapanagiotis, L. Valianou, C. Panayiotou, *Anal. Bioanal. Chem.* 2011, 399, 3065–3079.
- [38] M. Trojanowicz, J. Orska-Gawrys, L. Surowiec, B. Szostek, K. Urbaniak-Walczak, J. Kehl, M. Wróbel, *Stud. Conserv.* 49 (2004) 115-130.
- [39] M. R. Van Bommel, I. Vanden Berghe, A. M. Wallert, R. Boitelle, J. Wouters, *J. Chromatogr. A* 2007, 1157, 260-272.
- [40] J. Orska-Gawrys, I. Surowiec, J. Kehl, H. Rejniak, K. Urbaniak-Walczak, M. Trojanowicz, *J. Chromatogr. A* 2003, 989 (2), 239-248.
- [41] P. Novotná, V. Pacáková, Z. Bosáková, K. Štulík, *J. Chromatogr. A* 1999, 863 (2), 235-241.
- [42] E. Rosenberg, *Anal. Bioanal. Chem.* 2008, 391, 33–57.
- [43] I. Petroviciu, F. Albu, A. Medvedovici, *Microchem. J.* 2010, 95, 247-254.
- [44] G. G. Balakina, V. G. Vasiliev, E. V. Karpova, V. I. Mamatyuk, *Dyes Pigm.* 2006, 71, 54-60.
- [45] I. Joosten, M. R. Van Bommel, R. Hofmann de Keijzer, H. Reschreiter, *Microchim. Acta*, 2006, 155, 169-174.
- [46] X. Zhang, I. Good, R. Laursen, *J. Archaeol. Sci.* 2008, 35, 1095-1103.
- [47] X. Zhang, K. Corrigan, B. Mac Laren, M. Leveque, R. Laursen, *Stud. Cons.* 2007, 52, 211-220.

- [48] X. Zhang, R. Laursen, *Int. J. Mass* 2009, 284, 108-114.
- [50] G.W. Taylor, *Stud. Conserv.* 1983, 28, 153-160.
- [51] M. Bacci, F. Baldini, R. Carla, R. Linari, *Appl. Spectrosc.* 1991, 45, 26-31.
- [52] M. Bacci, A. Casini, F. Lotti, M. Picollo, Proceedings of the 18th International Symposium on the Conservation and Restoration of Cultural Property – Spectrometric Examination in Conservation, Tokyo National Research Institute of Cultural Properties, p. 97, 1994.
- [53] J. Wouters, A. Verhecken, *Stud. Conserv.* 1989, 34, 189-200.
- [54] E. De Luca, S. Bruni, D. Sali, V. Guglielmi, P. Belloni, *Appl. Spectrosc.* 2015, 69, 222-229.
- [55] M. Gulmini, A. Idone, E. Diana, D. Gastaldi, D. Vaudan, M. Aceto, , *Dyes Pigm.* 2013, 98, 136-145
- [56] Isabella Cavaliere, Bachelor thesis, Università degli Studi di Milano, 2017.
- [57] S. Q. Lomax, *J. Coat. Technol. Res.* 2010, 7, 331-346.
- [58] S.Q. Lomax, *J. Coat. Technol. Res.* 2010, 7, 325-330.
- [59] G. A. Milovanovic, M. Ristic-Solajic, T. J. Janjic, *J. Chromatogr.* 1982, 249, 149-154.
- [60] G. Massonnet, W. Stoecklein, *Sci. Justice* 1999, 39, 128-134.
- [61] J. W Wegener, J. C. Klammer, H.Govers H., U. A. Brinkman, *Chromatographia* 1987, 24, 865-875.
- [62] J. Russell, B. W. Singer, J. J. Perry, A. Bacon, *Anal. Bioanal. Chem.* 2011, 400, 1473-1491.
- [63] D. P. Kirby D.P., N. Khandekar, K. Sutherland, B. A. Price, *Int. J. Mass Spectrom.* 2009, 284, 115-122.
- [64] C. A. Menke, R. Rivenc, T. Learner, *Int. J. Mass Spectrom.* 2009, 284, 2-11.
- [65] N. C. Scherrer, S. Zumbuehl., F. Delavy, A. Fritsch, R. Kuehnen, *Spectrochim. Acta A* 2009, 73, 505-524.
- [66] W. Fremout, S. Saverwyns, *J. Raman Spectrosc.* 2012, 43, 1536-1544.
- [67] S. Bruni, V. Guglielmi, Raman Spectroscopy for the Identification of Materials in Contemporary Painting, in Vandenabeele P., Edwards H. (eds.), Raman Spectroscopy in Archaeology and Art History (Vol.2), The Royal Society of Chemistry, 168, 2019.
- [68] J. Jonsson, T. Learner, Separation of acrylic paint components and their identification with FTIR spectroscopy. Proceedings of the 6th Infrared and Raman Users Group (IRUG 6). Ed. M. Picollo. Florence: Il Prato, 58-63. 2004.
- [69] M. Longoni, S. Bruni, *J. Chem. Educ.* 2021, 98, 966–972.

Chapter 2

Visible and UV-excited spectrofluorimetry for the non-invasive identification of synthetic organic pigments of contemporary art

Abstract

In this chapter, an innovative non-invasive analytical method which combines spectrofluorimetry and visible reflectance spectroscopy is proposed to investigate a wide number of synthetic organic pigments, belonging to the most representative chemical classes and currently employed in contemporary art paintings. In order to consider for identification purposes not only the wavelength of the emission maxima (scarcely specific for broad-band spectra) but the entire spectral pattern, data were processed through a multivariate approach, based on principal component analysis (PCA). The issue of identifying the components of binary mixtures of pigments of similar or complementary colours was also faced. This protocol was first validated on mock-up samples and then successfully applied to analyse organic pigments in three contemporary paintings.

In addition, the fluorescence emission exhibited by such pigments upon visible light was confirmed using a UV radiation as excitation source. Subsequently the possibility of individuating such materials by ultraviolet fluorescence imaging was explored on the mock-up painting samples and on a case of study. This discloses the possible applicability of this imaging technique, really appreciated by restorers, also for the identification of modern pigments.

1. Introduction

Since 1856, when William Perkin discovered the first synthetic dye, mauveine, the colouring materials adopted by artists have radically changed. The traditional inorganic pigments, derived from natural mineral sources, were in fact progressively joined, and in some cases replaced, by new artificial substances: the synthetic organic pigments. They are water-insoluble compounds containing carbocyclic ring systems, often aromatic and sometimes coupled with metal ions. According to their chemical nature, they can be distinguished in different classes: arylide, benzimidazolone, diketo-pyrrolo pyrrole, naphthol, quinacridone, perylene and phthalocyanine are only some of the most common ones [1]. Organic pigments span the entire colour range from red to orange, yellow, green, blue and violet depending on their chemical and crystalline

structure and their success is due to excellent physical and chemical properties, such as brightness, heat stability and high tinting strength. All these features made these new pigments really appreciated by contemporary artists, introducing on the other hand a new challenge in the field of diagnostics. In fact, the knowledge of the composition of paints is of great importance for the solution of problems related to the conservation and the restoration of paintings, as well as for their valorisation and dating. In addition, many of the early synthetic organic pigments were not particularly lightfast, so their identification can provide information about the degradation and the original appearance of an artwork.

As already described in section 2.3 of chapter 1, until now different analytical techniques have been applied to this purpose, but most of them are sample-requiring and destructive, such as chromatographic methods [2-5]. Moreover, the identification is often difficult because, thanks to their high tinting strength, synthetic organic pigments are generally present in commercial paints in relatively small amounts and mixed with other substances, such as binders, fillers and extenders. This leads to the need of a pre-treatment of the samples, aimed at eliminating at least partially these interferents [6, 7]. However, when dealing with artistic objects, the importance of non-invasive and in-situ applicable analytical methods must be taken into account, but organic pigments represent a challenge precisely in this respect. Being carbon-based compounds, they cannot be analysed by the elemental techniques commonly used in situ for the identification of traditional inorganic pigments, such as X-ray fluorescence (XRF). On the other hand, vibrational spectroscopies provide characteristic spectra but, when applied directly on paintings, are affected by some limitations connected to the presence of binders and additives which can hide the signals due to the target analytes, preventing their detection. In the specific case of Raman spectroscopy, even if pure synthetic organic pigments give often intense and characteristic spectra, they can be hardly obtained from real paintings.

In the first part of this chapter, the potentiality for the identification of synthetic organic pigments of two spectrophotometric techniques applicable to paintings in situ and in a totally non-invasive way - visible reflectance spectroscopy and visible-excited spectrofluorimetry- are demonstrated both for the study of reference materials and of three paintings of contemporary art. Visible reflectance spectroscopy has been already accepted as a common technique in the field of conservation due to its non-destructive nature and easiness of use. However, it is affected by the scarce specificity of the spectral response, characterised by large bands and by absorption maxima obviously similar for pigments of analogous hue [8, 9]. In addition, spectra often exhibit an s-shaped, and thus even less characteristic patterns, especially for highly concentrated pigments [10]. Spectrofluorimetry, already applied for the in-situ identification of

natural dyes [9], may instead represent an innovative technique for the analysis of modern colouring substances. In fact, the molecules of synthetic organic pigments are rich in multiple bonds and aromatic rings, condition which can promote fluorescence emission, associated with electronic transitions between π orbitals. It should be emphasised that for highly concentrated compounds the emission intensity, although in principle increases with increasing concentration of the emitter [11], can be completely self-absorbed by the substance itself. However, it is reasonable that, when the pigments are diluted in binders and fillers to be used as paints, their fluorescence becomes more appreciable.

In order to consider for identification purposes the entire pattern of the fluorescence and reflectance spectra and not only the wavelength of the emission or absorption maxima, the obtained data were then processed through a multivariate approach, based on principal component (PCA) analysis, revealing the possibility of recognising a consistent number of organic pigments by combining the information given by the two techniques. Moreover, the Kubelka-Munk correction for self-absorption of fluorescence emission, proposed in the literature for paint layers with different concentration of natural dyes [6, 12], was in this case tested to recognise the components of binary mixtures of pigments of similar or complementary colours. Finally, the protocol based on the combination of the two spectrophotometric techniques and multivariate analysis was applied to identify some of the organic pigments used by a contemporary Italian landscape painter, Giuseppe Faraone, and by the Pop artist Silvio Pasotti.

The second part of the work consisted in repeating spectrofluorimetric analyses on synthetic organic pigments upon a different excitation wavelength, in the UV range (365 nm). The final aim was to establish a comparison between the spectrofluorimetric method and the UV fluorescence imaging technique. Visible luminescence induced by UV emission is, in fact, a well-known and widespread imaging technique in the field of conservation and restoration since the 1930s [13-14]. Direct fluorescence light analysis, thanks to the intrinsic limited capacity in the penetration of lower painting layers due to the relatively short wavelength of the UV radiation, is mainly used in the examination of external layers and can non-invasively provide a mapping of the distribution of varnishes, retouches and in some case of specific pigments on the pictorial surfaces [15-19]. Once confirmed by spectrofluorimetry the possibility of recognising synthetic organic pigments exciting their fluorescence emission also in the UV range, we successfully assessed the potentiality of the imaging method for the identification of these materials on the basis of the colour they exhibit under UV-light.

2. Objects of study

2.1 Synthetic organic pigments

Since the accidental discovery of mauveine by William Perkin in 1856, a rush to synthesise new dyes and pigments followed and soon new colourants were available. The term *synthetic organic pigments* refers to manufactured coloured compounds, whose chemical structure is characterised by a carbocyclic ring skeleton. Many of these rings are aromatic in structure and, because of their mobile clouds of electrons, they are the main chromophores (i.e. characteristic groups of atoms responsible for the colour). Moreover, other functional groups, such as keto, thio, nitro and nitroso, can confer different hues. [1] All these materials are referred as pigments and not dyes as, even if organic in nature, they are insoluble in water and in binding media. They span the entire chromatic range from blue and violet to green, yellow, orange and red and, because of their excellent physical and chemical properties (i.e. heat stability, lightfastness, resistance to most solvents), now dominate the market of colourants and are used in a variety of industrial applications.

Synthetic organic pigments are classified on the basis of their chemical class and, for simplicity, they are commonly named according to the colour Index (CI) nomenclature system. It involves that each colourant is designed by a CI name (i.e. Pigment Red 1, or PR1) and a CI number, which is linked to the chemical class and can convey information about the composition of the pigment itself.

In the following sections, the most common chemical groups and classes of pigments will be briefly presented. Only few examples of structural formulas will be provided in this section (for more of them refer to Tab. 1 in section 4.1).

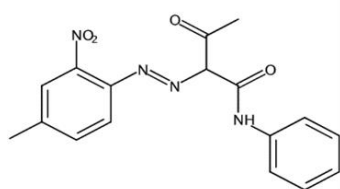
2.1.1 Azo pigments

Azo pigments were the first group to be introduced in the late 19th and early 20th century. They are characterised by one or more azo group ($-N=N-$) and synthesised by the diazotization reaction between a diazonium salt and a coupling component. The different classes of pigments (briefly presented below) are obtained by altering the coupling agent, while the variation of substituents within the same class leads to different hues. Azo pigments span the colour range of yellow, orange and red. [1]

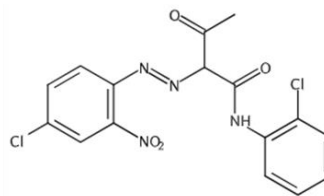
2.1.1.1 Arylide yellows

The arylide yellows are mono-azo pigments having acetoacetarylamide coupling components. This class includes almost 30 pigments, commonly referred as Hansa, arylide or monoarylide yellows, in the colour range from greenish to reddish yellow. These pigments were historically -

and still are nowadays- used in paints, printing inks and coloured pencil and crayons. [1] PY1 (Hansa Yellow G) and PY3 (Hansa yellow 10G) are the two most important member of this class in artists paints.



PY1



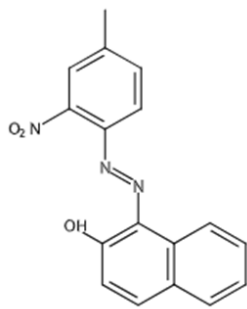
PY3

2.1.1.2 Diarylide yellow and orange

Diarylide yellows and oranges are diazo pigments obtained by combining 3,3' - dichlorobenzidine with two equivalents of acetoacetylide. Because of their limited lightfastness in comparison with monoazo yellows, their use in paint is less established and currently their main application is in the printing ink industry. PY12 (Benzidine yellow) and PY14 (Diarylide yellow AAOT) are the most employed pigments in this class, while PO16 is almost the only orange commercially available. [1]

2.1.1.3 β -Naphthol pigments

Among the oldest and most widespread, β -naphthol pigments are obtained by coupling a substituted aniline with β -naphthol. They can assume different hues, from yellowish orange to



PR3

bluish red, although their tinting power is not so strong as their lightfastness. A further distinction in this class can be made between neutral species and salts from carboxylate or sulfonate groups. The former include PR3 (Toluidine red), an extensively used red colourant introduced in 1905, while PR57 (Lithol rubine), a calcium salt having a blue shade and a high lightfastness patented in 1903, belongs to the latter. [1]

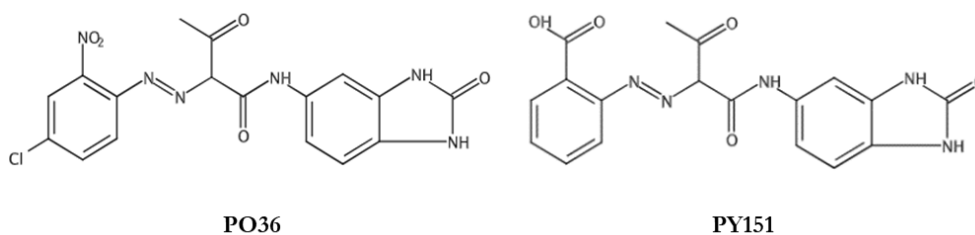
2.1.1.4 β -Naphthol reds

This class of pigments was discovered in 1911 in Germany, when the procedure for their synthesis was developed, and includes a large variety of materials. They are commonly referred also as Naphthol AS pigments, from *Amide einer Säure* (amide of an acid), as they derive from 2-hydroxy-3 naphthoic acid. Their high tinting strength, low-cost and relatively high lightfastness make these colourants suitable for a wide range of applications, including paint industry. [1]

Among the most common ones, there is PR177, which shows an improved lightfastness thanks to an additional amide functionality in its structure.

2.1.1.5 Benzimidazolones

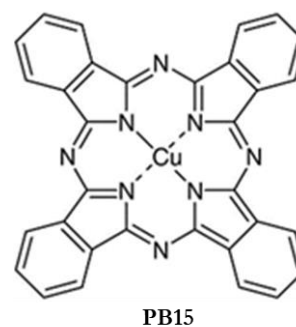
First patented in 1960s, this class includes a large number of yellow, orange and red pigments. Their main chemical feature is the presence of the 5-aminocarbonyl benzimidazolone group, which confers lightfastness. Benzimidazolones can be further divided into two groups on the basis of their structure: the Hansa and the Naphtol AS type, derived respectively from acetoacetyl amides and 2-hydroxy-3-naphthoic acid anilide. The former have yellow and red hues, the latter blue and violet. This wide range of colours and the excellent lightfastness of these substances promote their extensive use in many application fields, from paint to ink printing industry. [1] To provide some examples, PY175, PO36, PO60 and PY151 are benzimidazolones.



2.1.2 Non-azo pigments

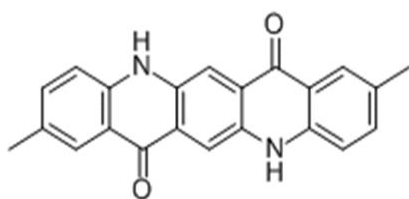
2.1.2.1 Phthalocyanines

Copper phthalocyanines, available from the 1930s, are organometallic compounds with a porphyrin ring structure. The most part of blue and green pigments belong to this chemical class. In particular, blue phthalocyanines are unhalogenated compounds, while the green ones are halogenated. The most common blue phthalocyanines are the metallised complex PB15 in its five crystalline polymorphs and the unmetallised PB16, the only



pigments without a copper ion in its porphyrin ring. Referring to green pigments, PG7 and PG36, respectively a chlorinated and a chlorinated and brominated phthalocyanine, are the most common. As the shade is a function of the degree of halogenation, PG7 is green blue, whereas PG36 is yellowish. [1] For their lightfastness, solvent resistance and stability, phthalocyanines are well established as artistic materials in contemporary paintings.

2.1.2.2 Quinacridones



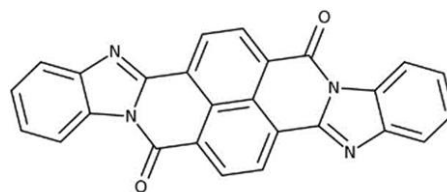
PR122

Quinacridones are a class of synthetic organic pigments whose colour varies from yellow to red and violet. They have a polycyclic structure and, despite of being synthesised in two linear form, only the trans one gained great importance in paint industry [1]. The most common

quinacridone red is the dimethylated PR122, while the unsubstituted form corresponds to the violet PV19, whose chromatic shade differs slightly as a function of the crystalline phase, if γ (reddish) or β (violet). In addition, quinacridones exist also as solid solutions with other quinacridones or quinacridone quinones: it is the case of PR206. [1] For their excellent properties (lightfastness, heat and solvent stability), these colourants are referred as high-performance pigments and find wide application in both industrial and artistic field.

2.1.2.3 Perylene and perinone pigments

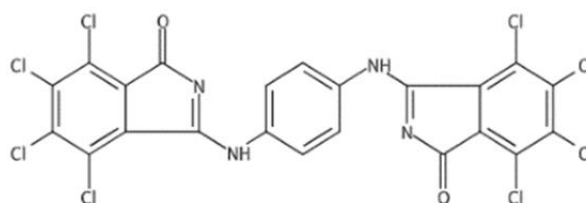
Perylenes are, from a chemical viewpoint, diimides of perylene tetracarboxylic acid and have been used as red, bordeaux, violet and brown pigments since the second half of the 20th century. Perinones were introduced in the same period and were synthesised from naphthalene-1,4,5,8-tetracarboxylic acid or its monohydride. Both perylenes and perinones have excellent solvent and lightfastness, which justify their application in many industrial sectors, including paint production. [1] PR149 and PO43 are an example of a perylene and a perinone pigment respectively.



PO43

2.1.2.4 Isoindolinone and isoindoline pigments

Isoindolinone and isoindoline reds, oranges and yellows spread in the second half of the 20th century. Their chemical structure has in common the isoindoline ring and, in general, they are lightfast and resistant to heat and solvents. [1] Isoindolinones, or azomethine type, includes PY109 and PY110, while PY139 is an example of isoindoline, or methine type.



PY110

2.1.2.5 Other pigments

Diketopyrrolo-Pyrrole pigments- Introduced in the 1980s, DPP pigments are a class of red colourants having considerable fastness properties. [1] PR254 is the most important pigment in this minor class.

Dioxazine violet- A dioxazine type structure is the main feature of this class, of which PV23 (carbazole violet) is the main representant. It has a very high tinting strength, a dark bluish violet colour and excellent chemical and physical properties. [1]

Indanthrone blue- PB60 is the only pigment belonging to this class. Even if, because of its expensiveness, it was outclassed by phthalocyanine blues [1], PB60 its frequently employed in artists' paints.

3. Analytical and imaging fluorescence methods

3.1 Spectrofluorimetry

Spectrofluorimetry is an analytical technique based on the detection of the fluorescence emission from the analyte.

Fluorescence is a process involving the emission of light by a substance which has absorbed electromagnetic radiation of a suitable wavelength, generally in the visible or UV range. The phenomenon evolves through a series of steps, schematically represented in Fig. 1. The initial one involves that an incoming photon is absorbed by the molecule and excites an electron, thus promoting the molecule from its ground singlet state S_0 to a higher energy state in the vibrational substructure of the first singlet state S_1 . The photon must obviously have enough energy to be absorbed and start the fluorescence event. Once the molecule is in the excited state, it undergoes a series of rapid relaxation processes, reaching the vibrational ground state of S_1 . These are mainly non-radiative events and energy is dissipated in different forms, for example as heat. Finally, the molecule radiatively relaxes to the vibrational levels of the ground state S_0 , thus emitting a photon whose energy will be necessarily lower than that of the incoming one. During radiative transition, the molecule may descend into any of the several vibrational levels in the ground state and, as a result, the emitted photons will have different energies, and thus different frequencies. For this reason, fluorescence spectra are characterised by broad and scarcely resolved bands. [20, 21]

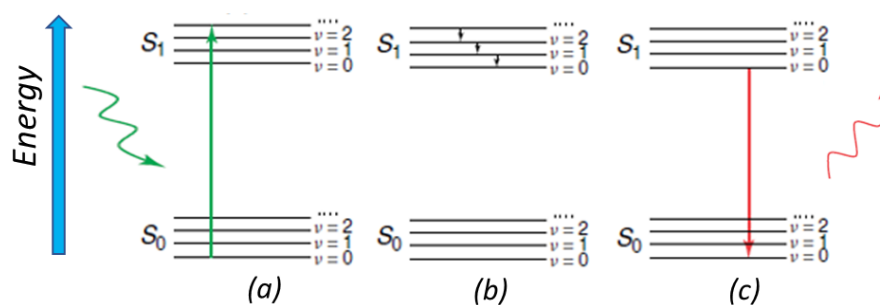


Figure 1. Schematic representation of the fluorescence process. a) a photon is absorbed; b) the molecule undergoes vibrational relaxations in the first electronically excited state S_1 ; c) the molecule relaxes to the vibrational levels of S_0 , thus emitting a photon.

3.2 UV-imaging

The definition “imaging” refers to a series of techniques whose final output is an image [22]. Multispectral imaging methods (i.e X-ray radiography, near-infrared reflectography and ultraviolet fluorescence) have been largely employed in the field of diagnostics, aiming to deeply understand the structure of a painting, the artists’ technique and previous restoration works [19, 22-26]. In particular, UV fluorescence imaging, better known as Wood or UV photography, is a well appreciated method not only by conservation scientists, but also by restorers because of its relative easiness of use and interpretation. It involves that the object under investigation, typically a painting, is illuminated by an UV source and a colour picture of its emission is recorded by a suitable digital camera [26]. The examination of the fluorescence emission allows restorers to identify the presence of not-fluorescent restoration treatments, as well as superficial varnishes, aged binders and some fluorescent inorganic pigments without inducing any damage to the work of art (Fig. 2). On the other hand, from a scientific viewpoint, fluorescence can provide an indication on the chemical nature of a specific material, since fluorescent compounds of different kind typically show different emission spectra.

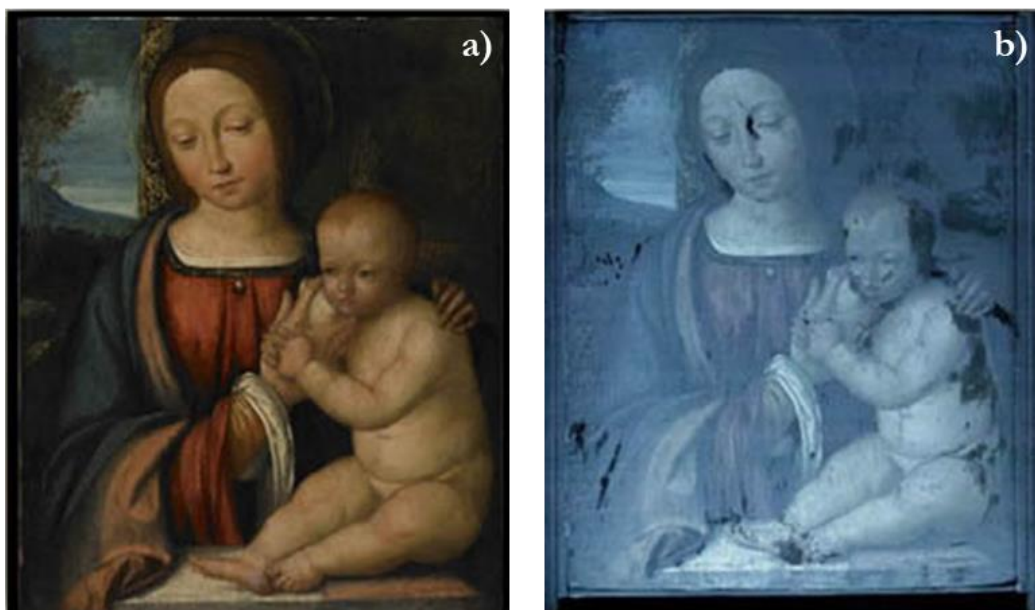


Figure 2. *Madonna Suckling the Child* by an artist of the Ferrarese School from the early 16th century under a) visible and b) UV light: the milky blue fluorescence is due to the aged varnish, while the darker areas are solid evidence of retouching. From [27]

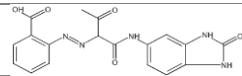
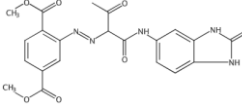
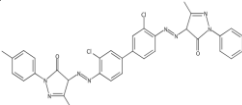
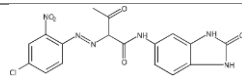
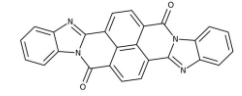
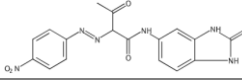
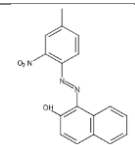
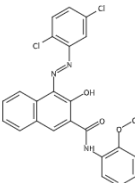
4. Materials and methods

4.1 Reference materials

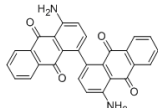
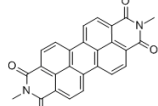
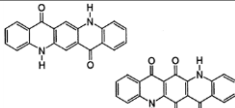
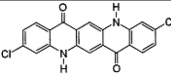
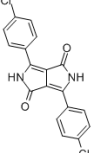
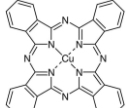
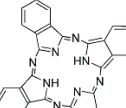
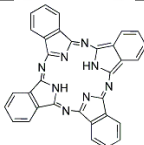
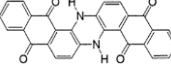
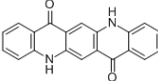
Synthetic organic pigments were acquired from some of the main pigment manufacturers. They were both pure powders applied on canvas by means of different binders (oil or acrylic) or commercial formulations (oil, acrylic or alkyd-based), that were spread on canvas as well. The choice was made in order to consider pigments employed by artists and belonging to the main chemical classes. Moreover, when available, the same pigment was purchased from different manufacturers to make a comparison between the corresponding reflectance and fluorescence spectra. Tab. 1 reports the analysed pigments with their CI name, the chemical class, the chemical group, the typology (formulation or powder plus binder) and the manufacturer. Moreover, the following inorganic pigments were analysed for comparison as they are used as well in contemporary painting: cadmium red (PR108), cadmium orange (PO20), cadmium yellow (PY35), Prussian blue (PB27), cobalt blue (PB28) and ultramarine blue (PB29). The cadmium pigments were purchased as powders from Zecchi (Firenze) and as oil paint from Royal Talens; the inorganic blues were pure powders commercialised by Zecchi (Firenze).

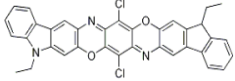
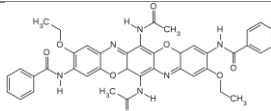
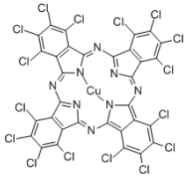
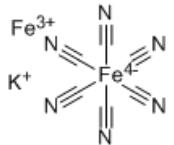
Table 1. Summary of the organic pigments analysed in this work and their main features (colour index and common name, chemical class and family, structural formula, typology and manufacturer).

CI name	Common name	Chemical class	Chemical group	Structural formula	Typology	Manufacturer
Yellow						
PY1	Hansa Yellow G	Monoazo	Acetoacetic arylide		Pure powder	Maimeri
PY3	Hansa Yellow 10G	Monoazo	Acetoacetic arylide		Commercial oil Powder Powder Commercial acrylic	Old Holland Classic Oil Kremer Pecchio Maimeri Acrylic
PY74	Arylide Yellow 5GX	Monoazo	Acetoacetic arylide		Powder	Kremer
PY83	Diarylide Yellow HR	Disazo	Diarylide		Powder Commercial acrylic	Maimeri Maimeri Acrylic
PY97	Diarylide Yellow FGL	Monoazo	Acetoacetic arylide		Commercial acrylic	Maimeri Brera
PY109	Isoindole Yellow	Isoindolinone	Azomethine-type		Powder	Kremer
PY110	Isoindolinone Yellow	Isoindolinone	Azomethine-type		Powder	Kremer
PY139	Isoindoline Yellow	Isoindoline	Azomethine-type		Powder Commercial alkyd	Maimeri Winsor Griffin

PY151	Benzimidazolone Yellow H4G	Monoazo	Benzimidazolone		Powder	Kremer
PY175	Benzimidazolone Yellow H6G	Monoazo	Benzimidazolone		Commercial oil	Maimeri Classic Oil
Orange						
PO34	Pyrazolone Orange	Disazo	Pyrazolone		Commercial acrylic	Maimeri
PO36	Benzimidazolone Orange HSL	Monoazo	Benzimidazolone		Powder Commercial acrylic	Maimeri Maimeri Polycolor
PO43	Perinone Orange	Polycyclic	Perinone		Powder Commercial oil Commercial acrylic	Maimeri Maimeri Classic Oil Maimeri Brera Acrylic
PO62	Benzimidazolone Orange H5G	Monoazo	Benzimidazolone		Commercial acrylic	Maimeri Polycolor
Red						
PR3	Toluidine Red	Monoazo	B-Naphthol		Powder Powder	Kremer Pecchio
PR9	Naphthol AS Red	Monoazo	Naphthol-AS		Powder	Kremer

PR12	Permanent Bordeaux TRR	Monoazo	Naphthol-AS		Commercial acrylic	Maimeri Polycolor
PR57:1	Lithol Rubine	Monoazo	BON lake		Powder	Maimeri
PR88	Thioindigoid Violet	Polycyclic	Thioindigo		Powder	Kremer
PR112	Naphthol Red AS-D	Monoazo	Naphthol-AS		Powder Commercial acrylic Commercial oil	Kremer Maimeri Old Holland
PR122	Quinacridone Magenta	Polycyclic	Quinacridone		Powder	Kremer
PR146	Naphthol Red AS	Monoazo	Naphthol-AS		Commercial a crylic	Maimeri
PR168	Anthraquinone Scarlet	Polycyclic	Anthraquinone		Commercial acrylic	Maimeri Brera
PR170	Naphthol Red AS	Monoazo	Naphthol-AS		Powder	Kremer

PR177	Anthraquinone Red	Polycyclic	Anthraquinone		Powder	Kremer
PR179	Perylene Maroon	Polycyclic	Perylene&Perino- ne		Powder	Kremer
PR206	Quinacridone Burnt Scarlet	Polycyclic	Quinacridone		Powder	Maimeri
PR209	Quinacridone Red	Polycyclic	Quinacridone		Commercial oil	Maimeri Classic Oil
PR254	Pyrrole Red	Polycyclic	Diketopyrrolo- pyrrole		Powder Commercial oil	Maimeri Winsor Griffin
Blue						
PB15:1	Phthalocyanine Blue	Polycyclic	Phthalocyanine		Acrylic	Maimeri
PB15:3		Polycyclic	Phthalocyanine		Acrylic	Maimeri
PB16	Phthalocyanine Turquoise	Polycyclic	Phthalocyanine		Powder	Maimeri
PB60	Indanthrone Blue	Polycyclic	Antraquinone		Powder	Maimeri
Violet						
PV19	Quinacridone Violet	Polycyclic	Quinacridone		Powder Commercial acrylic	Kremer Maimeri

PV23	Dioxazine Violet	Polycyclic	Dioxazine		Powder Commercial alkyd	Maimeri Winsor Griffin
PV37	Dioxazine Violet	Polycyclic	Dioxazine		Powder	Kremer
Green						
PG7	Phthalocyanine Green	Polycyclic	Phthalocyanine		Commercial oil	Maimeri
Inorganic Pigments						
PY35	Cadmium Yellow	Inorganic	Cadmium sulphide	CdS	Powder Commercial oil	Zecchi
PO20	Cadmium Orange	Inorganic	Cadmium-seleno sulphide	CdS/CdSe	Powder Commercial oil	Zecchi Royal Talens
PR108	Cadmium Red	Inorganic	Cadmium selenide	CdSe	Powder Commercial oil	Zecchi Royal Talens
PB27	Prussian Blue	Inorganic	Ferric ferricyanide		Powder	Zecchi
PB28	Cobalt Blue	Inorganic	Cobalt aluminate		Powder	Zecchi
PB29	Ultramarine Blue	Inorganic	Complex sulphur-containing sodium-silicate		Powder	Zecchi

In the graphs shown in the following discussion, each pigment will be referred as its CI name followed by two letters, indicating respectively the binder and the manufacturer. The legend is reported in Tab. 2.

Table 2. Legend of binders and manufacturers.

a	Acrylic
al	Alkyd
o	Oil
P	Acrylic (Primal®)
K	Kremer
M	Maimeri
OH	Old Holland
P	Pecchio
RT	Royal Talens
WG	Winsor&Griffin
Z	Zecchi

4.2 Instrumentation

Spectrofluorimetric analyses were performed using a portable microprobe, suitable for both visible reflectance and fluorescence measurements. The microprobe, equipped with an Olympus 20× objective, is connected by optical fibres to a halogen source (maximum power 150 W) and to a Lot Oriel MS125 spectrometer (grid 400 lines/mm) provided with an Andor CCD detector (1024 × 128 pixel) cooled by means of a Peltier device. The wavelength calibration was based on the emission spectrum of a neon lamp. The radiation from the source is sent along a direction perpendicular to the microscope objective.

For fluorescence analyses the microprobe is equipped with an interference filter to select the excitation wavelength and a dichroic filter to eliminate from the spectrum the component due to the exciting radiation. In particular, two different interference filters, centred respectively at 435 nm and 562 nm, were used, while two dichroic filters were available with transmission ranges 458-680 nm and 635-890 nm respectively. Most yellow, orange and red pigments were analysed with excitation at 435 nm, while the wavelength of 562 nm was mainly used to excite the emission of most blue and violet pigments. For UV excitation, a LED source emitting at 365 nm with a power of 5.5 mW was used. The radiation from the source is sent on the measurement area with an incidence angle of 45° and the emitted radiation is collected through the objective of the above-described microprobe. Both visible- and UV-induced fluorescence spectra were collected as sum of 30 scans with an exposure time of 2 seconds and the analyses were preceded by the acquisition of a background spectrum in the absence of the incident

radiation. For visible reflectance analyses the interference filter was removed and the dichroic one was replaced by a beamsplitter 30/70 for the spectral range 400-700 nm. Reflectance spectra were acquired as sum of 30 scans with an exposure time of 0.05 seconds and the analyses were preceded by the acquisition of background and reference spectra. A metal target coated with barium sulphate was used as reference.

Imaging analyses were carried out thanks to the collaboration with Dr. Marco Gargano of the Department of Physics of the Università degli Studi di Milano. Briefly, the images were acquired with a digital single-lens reflex (DSLR) Nikon D810, modified to extend the sensitivity from 350 nm to 1000 nm. Two lighting sources (emitting at 365 and 420 nm) were chosen according to the different purposes and different high-pass filters were mounted on the lens to correctly acquire the images in the desired range. The cut-on wavelengths were 420 nm for $\lambda_{exc} = 365$ nm, 480 for $\lambda_{exc} = 420$ nm and 850 to collect the response in the NIR region. All the acquired images were post-processed to make the chromatic response less dependent on the instrumentation and on the acquisition conditions. All the images that will be showed in Section 5.5 are kindly granted by Dr. M. Gargano.

4.3 Multivariate analysis of data

Reflectance and emission spectra were processed by principal component analysis (PCA), performed by the statistical package MINITAB 14. The spectra were first normalised between zero and one to avoid the possible variability due to the reflectance percentage or emission intensity. To perform PCA, the covariance matrix was selected to reduce the baseline contribution.

4.4 Kubelka-Munk correction for self-absorption of fluorescence emission

To take into account fluorescence self-absorption and reemission in the solid state, a model based on the Kubelka-Munk theory of diffuse reflectance was applied [28, 29]. According to it, it is possible to obtain true emission spectra dividing the experimental data by a function $\gamma(\lambda, \lambda_0)$, defined by equation 1:

$$\gamma(\lambda, \lambda_0) = \left(\frac{1}{1 + \sqrt{\frac{Rem[R(\lambda)]}{Rem[R(\lambda)]+2}}} \right) \times \left(\frac{1}{1 + \sqrt{\frac{Rem[R(\lambda)]\{Rem[R(\lambda)]+2\}}{Rem[R(\lambda_0)]\{Rem[R(\lambda_0)]+2\}}} \right) \quad (1)$$

where λ and λ_0 are the emission and excitation wavelength and $Rem[R(\lambda)]$ is the total remission function defined by the following equation 2:

$$Rem[R(\lambda)] = \frac{k(\lambda)}{s(\lambda)} = \frac{[1-R(\lambda)]^2}{2R(\lambda)} \quad (2)$$

where $s(\lambda)$ and $k(\lambda)$ are respectively the scattering and the absorption coefficient and $R(\lambda)$ is the diffuse reflectance at the corresponding wavelength λ .

The self-absorption correction was performed by means of GRAMS/AI software.

4.5 Case studies

The first case study was *Addetta near Zoate*, an oil painting by the contemporary post-impressionist landscape painter Giuseppe Faraone, dated 2001. The artwork, belonging to a private collection, was made available both for visible and UV-excited spectrofluorimetric measurements and for imaging analyses.

Two paintings of the Italian Pop artist Silvio Pasotti, namely *The monster* (1966) and the right panel of the triptych *The daily neo-mythology* (1966-1967) were studied by visible-excited spectrofluorimetry. Both artworks are realised on an aluminium support: in the 60s Silvio Pasotti, after encountering the American Pop art, was the author of works often combining metal and painting, in which images of everyday life objects were used to develop reflections on social themes. The former painting was examined during an exhibition dedicated to the artist, which took place in 2018 in Segrate (Milan, Italy). The latter is permanently on show in the Auditorium “Giuseppe Verdi” in Segrate.

5. Results and discussion

In the following sections, the obtained results will be discussed at first for visible reflectance spectroscopy and then for visible and UV-excited spectrofluorimetry. Finally, the preliminary comparative study with the UV-imaging method will be presented.

5.1 Visible-reflectance spectroscopy

5.1.1 Red and orange pigments

Visible reflectance spectroscopy is generally affected by scarce specificity for identification purposes and reflectance spectra of pigments having the same colour are very similar (Appendix A), so their identification is challenging. Consequently, PCA analysis allowed the discrimination of only few groups in the multivariate space (Fig. 3), as almost all red and orange pigments are close to one another. In particular, the identification was possible only for those colourants with a peculiar hue, for example brown (PR206), or a different shade of red (PR88, PR177, PR179).

It is instead difficult when their colour is very similar, as almost all the orange pigments occupy the same region of the score plot, and the same happens for the red ones.

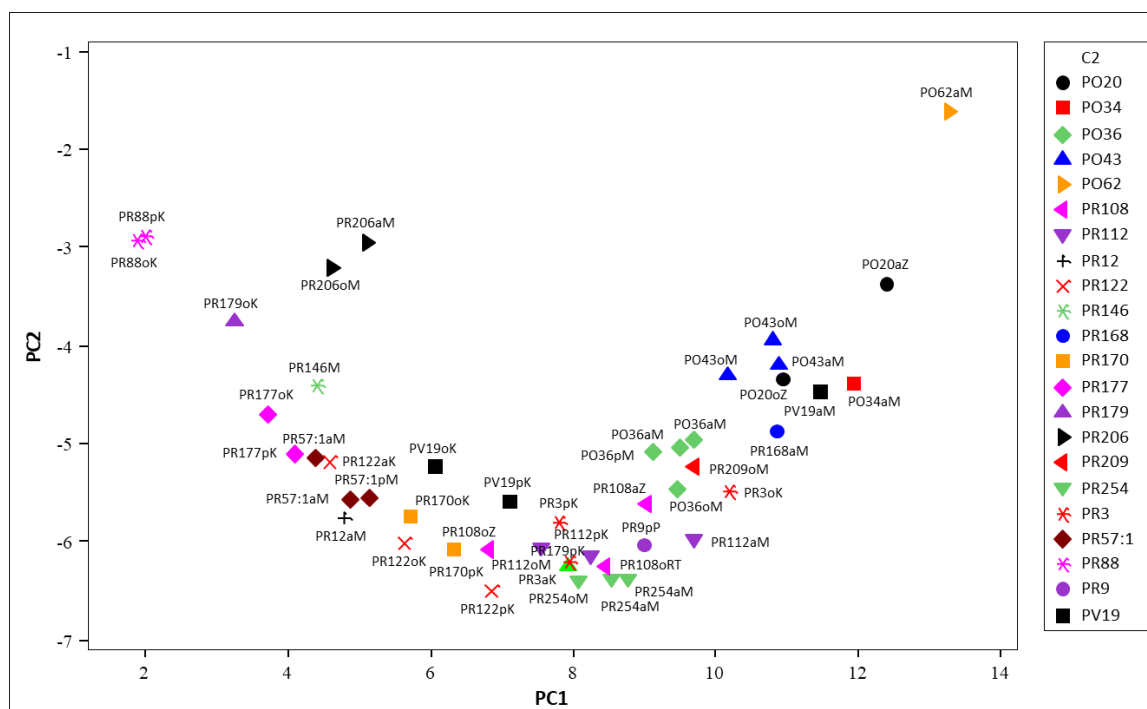


Figure 3. Score plot of the first two principal components of the visible reflectance spectra of red and orange pigments in painting mock-up samples on canvas.

5.1.2 Yellow pigments

As for the red ones, only few yellow pigments were identifiable by their visible reflectance spectra (Appendix A). In particular, PCA allowed us to recognise in the score plot (Fig. 4) only two of the colourants analysed, PY109 and PY110. Again, this spectroscopic technique suffers from low specificity for the identification of pigments having similar colour.

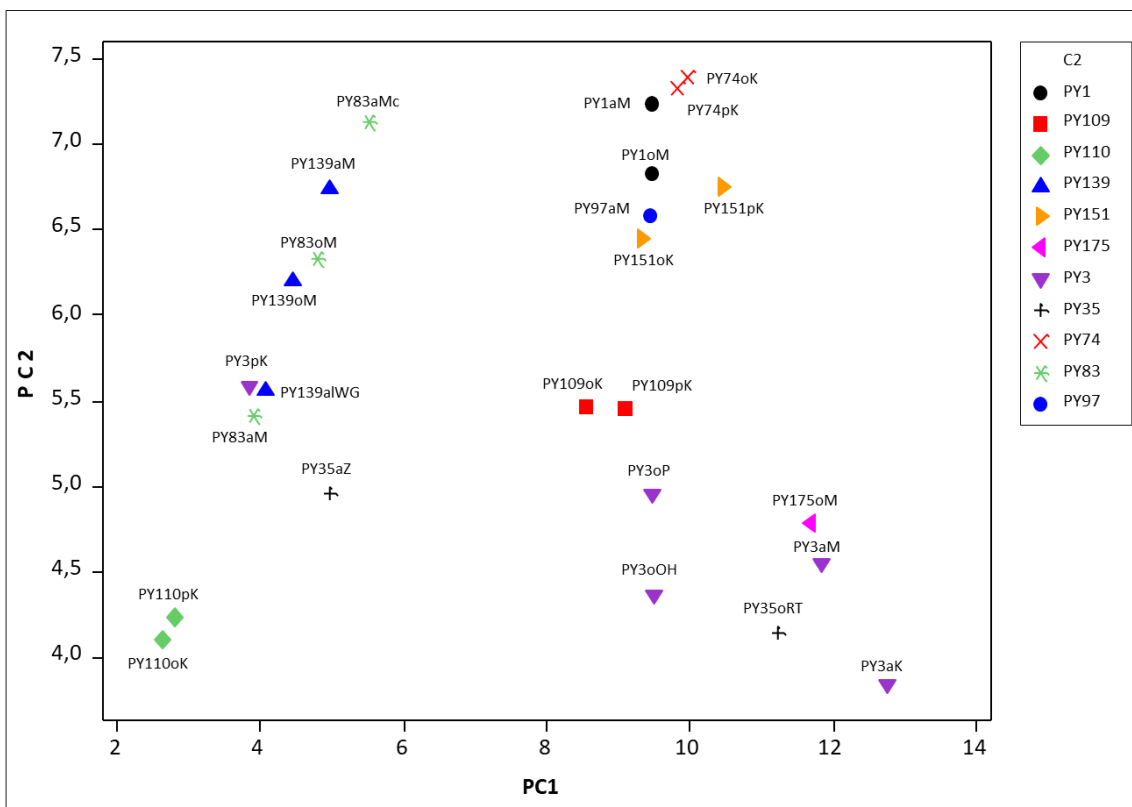


Figure 4. Score plot of the first two principal components of the visible reflectance spectra of yellow pigments in painting mock-up samples on canvas.

5.1.3 Violet and blue pigments

Among the analysed pigments, PV19 belongs to the quinacridone family and is characterised by a pink-reddish hue; PV23 and PV37 are member of the dioxazine group and their colour has a blue shade. For this reason, the former was considered together with red and orange pigments (section 5.1.1), while the latter were analysed together with the blue colourants. It is worth noticing that PV19 formed in the score plot (Fig. 3) two different groups, one corresponding to the pure pigment purchased from Kremer and mixed with acrylic and oil binders and the other corresponding to the commercial acrylic paint sold by Maimeri. This behaviour is due to the fact that the two pigments correspond to different crystalline phases of quinacridone [30, 31], respectively β for Maimeri and γ for Kremer, as confirmed by XRD, FT-IR and FT-Raman analyses (see Appendix B and [7]). The γ -phase is characterised by a bluish shade, the β one is instead reddish, explaining their different reflectance spectra.

The score plot of the PCA (Fig. 5) performed on violet and blue pigments revealed the impossibility of distinguishing the dioxazine violets PV23 and PV37, whose colour is very similar. The inorganic pigments cobalt blue (PB28) and ultramarine blue (PB29) are well recognisable, while Prussian blue (PB27) is located close to the indanthrone and phthalocyanine

blue PB60 and PB16, which cannot be distinguished from their reflectance spectra. Finally, the two crystalline phases of phthalocyanine blue PB15, PB15:1 and PB15:3, occupy two different areas in the centre of the score plot. This is attributable to the fact that the two forms of copper phthalocyanine, α and β respectively, have different chromatic shades, reddish-blue for the former and greenish for the latter. [32]

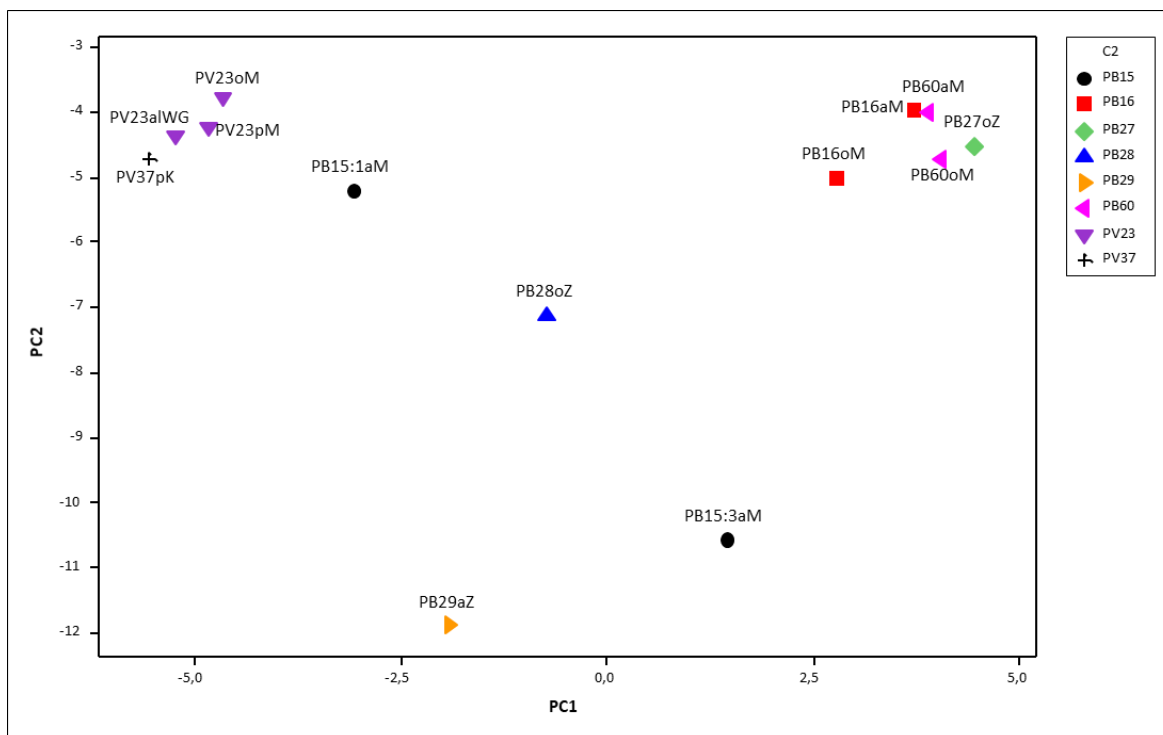


Figure 5. Score plot of the first two principal components of the visible reflectance spectra of blue and violet pigments in painting mock-up samples on canvas.

5.2 Visible-excited spectrofluorimetry

Most of the analysed pigments showed fluorescence emission, more or less intense according to their chemical structure. The corresponding spectra are reported in Appendix A, together with a table summarising their emission maxima. Only a limited number of pigments resulted to be not fluorescent, namely PR170, PR177, PR179, PR88 and PR206. On the other hand, it is worth noticing that three of them, PR206, PR179 and PR88, are among the few pigments recognisable from their reflectance spectrum.

In the following sections, multivariate analysis performed on red, orange and yellow fluorescent pigments will be presented. Given their small number, blue and violet pigments were instead compared and discussed just on the basis of their spectral pattern and emission maxima.

5.2.1 Red and orange pigments

PCA analysis allowed us to verify that almost all paint samples of the same pigment are located in the same region of the score plot (Fig. 6), forming an independent group regardless of the manufacturer and the binders employed. In particular, PR3, PR12, PR122, PR146, PR168, PR209, PR254, PO34, PO36, PO43 and PO62 were discernible, while some overlapping was observed for the paint samples of a few other pigments, as detailed below. PV19 formed again two different groups in the score plot, each corresponding to a different crystalline form. The γ -phase of PV19 (Kremer) has a fluorescence emission similar to PR57:1, but, being of two different colours, the discrimination of these pigments is possible from their reflectance spectra (section 5.1.1). The β -phase corresponds to a well-defined group in the score plot. Finally, PR9 is located close to PR112 and PR146, but this can be explained by the fact that their chemical structures are the same, as they all belong to the same class of Naphthol AS red pigments. The emission maxima of the pigments are summarised in Fig. 11 and their spectra are reported in Appendix A.

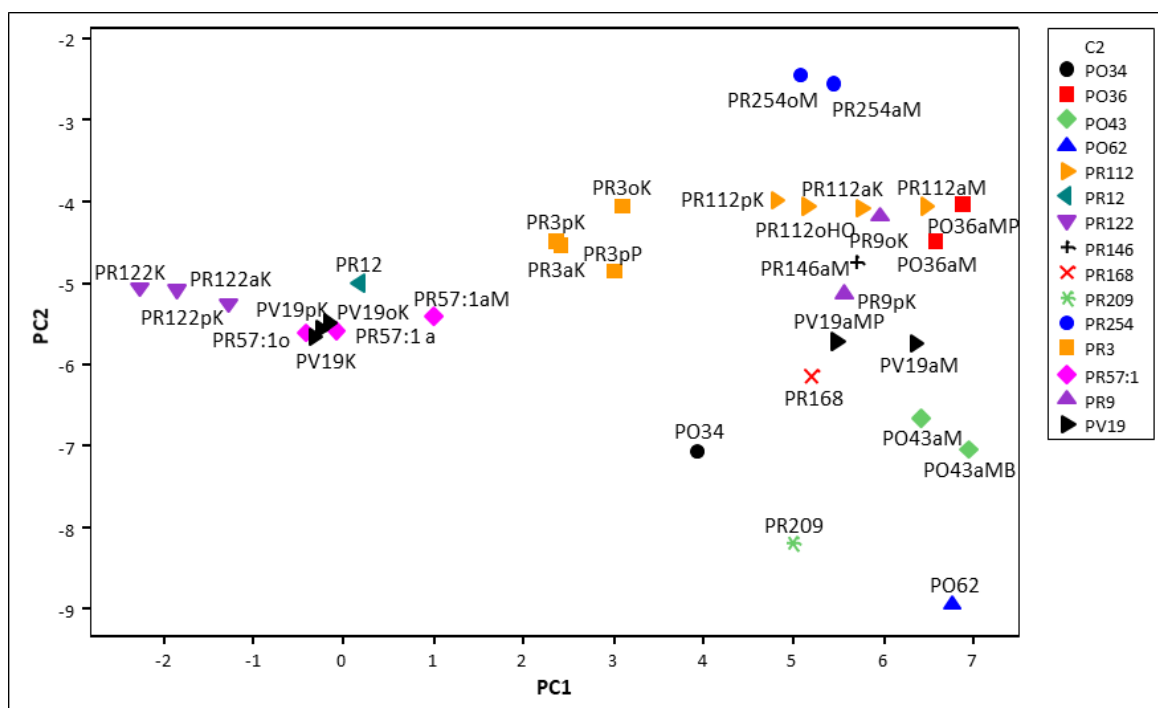


Figure 6. Score plot of the first two principal components of the emission spectra ($\lambda_{\text{exc}} = 435 \text{ nm}$) of red and orange pigments in painting mock-up samples on canvas.

5.2.2 Yellow pigments

Fluorescence emission of yellow pigments is generally close to that of pure binders (acrylic or oil), which give a spectrum characterised by a maximum around 520 nm (Appendix A). The emission due to the binding media can thus hide that of the pigments, making more complex

and sometimes preventing their identification. An exception is represented by PY139 and PY83, which show a maximum at 570 nm (Fig. 7). Indeed, they occupy in the score plot a well separated region from all other yellow pigments (graph shown in Appendix A). In addition, even if their spectra are very similar, these pigments can be easily distinguished considering that PY139 has a very intense fluorescence emission in contrast to PY83, whose response is significantly weaker.

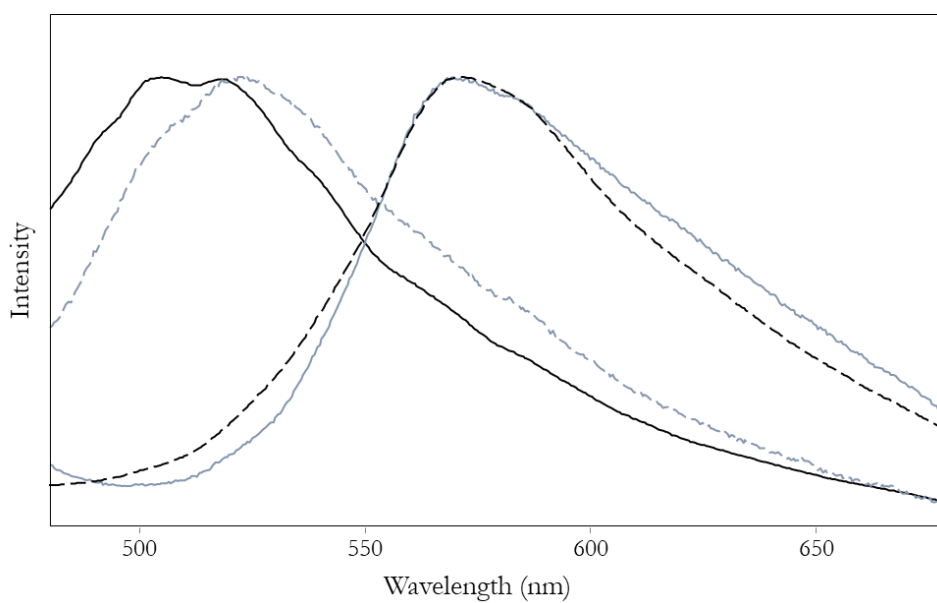


Figure 7. Emission spectra of acrylic binder (black line), PY3 (dotted grey line), PY139 (dotted black line) and PY83 (grey line). All the pigments are dispersed in acrylic.

PCA analysis was thus repeated excluding PY139 and PY83, in order to obtain a score plot where the different groups formed by the other yellow pigments could be more easily recognised (Fig. 8). The PY3 group is close to the binder group and indeed this pigment, as well as PY175, is only weakly fluorescent. This is especially true for the commercial formulations of PY3, in comparison with the painting samples obtained in the laboratory by mixing the pure pigment and the binders. Most probably, the pigment concentration in the industrial products is lower because of the presence of fillers and additives, which further decrease its already weak fluorescence. In the lower left part of the score plot, three pigments are located, specifically PY1, PY74 and PY97, all belonging to the same chemical family (mono-azo) and group (acetoacetylride). PY109 showed a weak fluorescence signal, with a low signal/noise ratio, justifying the random position of the corresponding painting samples in the multivariate hyperspace; anyway, its identification can be confirmed on the basis of its reflectance spectrum (section 5.1.2). Finally, PY110, which was not included in this PCA, is well identifiable from its

fluorescence emission because it is the only yellow pigment giving an emission maximum around 635 nm.

In conclusion, PCA analysis revealed that it is difficult to distinguish all the different yellow pigments, because their fluorescence emission is often weak and overlapped the one of binders. In any case, the multivariate approach allowed us to discriminate colourants belonging to the same chemical classes whose fluorescence emission is indeed similar. The emission maxima of these pigments are summarised in Fig. 11 and their spectra are reported in Appendix A.

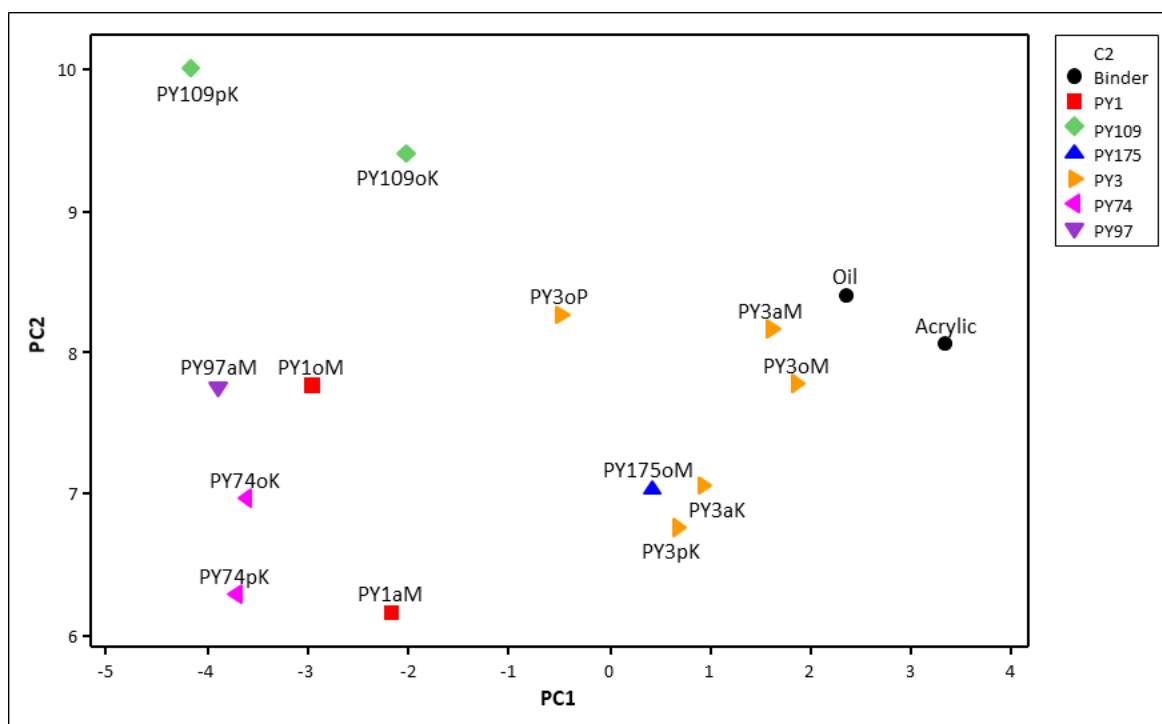


Figure 8. Score plot of the first two principal components of the emission spectra ($\lambda_{exc} = 435$ nm) of yellow pigments in painting mock-up samples on canvas.

5.2.3 Violet and blue pigments

All the violet pigments here analysed resulted to be fluorescent. PV19 showed a fluorescence emission when excited at 435 nm, therefore its spectrum was considered together with those of red and orange pigments (section 5.2.1). PV23 and PV37 are not fluorescent if excited at this wavelength, but they revealed characteristic emission bands (Fig. 9) that allowed their identification when excited at 562 nm. In particular, an emission maximum was observed around 743 nm for PV23 and at 786 nm for PV37. Given the limited number of pigments with such a hue, no multivariate analysis was performed on the corresponding spectral data. However, spectrofluorimetry demonstrated to be a powerful technique to distinguish PV23 and PV37, whose identification is not possible if based only on visible reflectance spectra. The emission maxima of these pigments are summarised in Fig. 11.

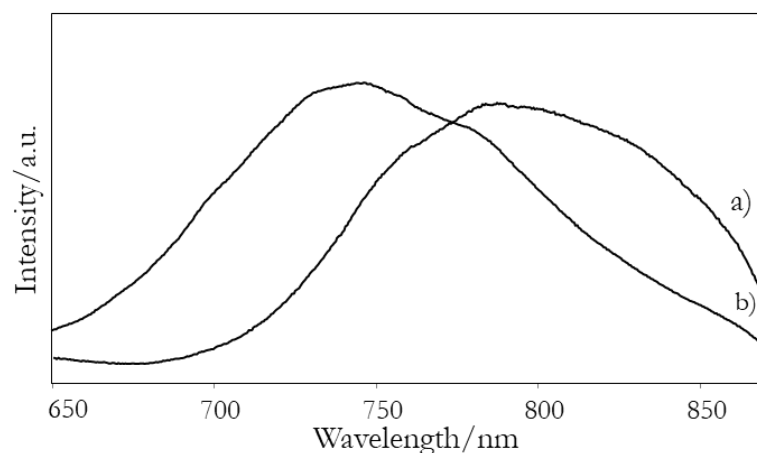


Figure 9. (a) Emission spectra ($\lambda_{\text{exc}} = 562 \text{ nm}$) of a) PV37 (a) and b) PV23 in painting mock-up samples on canvas (powder plus acrylic and commercial acrylic respectively).

Referring to blue organic pigments, only PB16 (phthalocyanine blue) exhibited a fluorescence emission upon excitation at 562 nm. In fact, this pigment, which is chemically a phthalocyanine, showed an emission band around 850 nm (Fig. 10).

PB15 is a phthalocyanine too, but it is not fluorescent, presumably due to the presence, in the centre of the porphyrin ring, of the paramagnetic copper (II) ion that quenches the emission. Both crystalline phases of such pigment, PB15:1 and PB15:3, showed the same behaviour, but they can be recognised on the basis of their reflectance spectra (section 5.1.3, [33])

PB60 belongs instead to a different chemical class, being an anthraquinone compound, and it did not show any fluorescence emission upon excitation at 562 nm. Anyway, its reflectance spectrum is different from those of PB15 making possible the distinction between these two non-fluorescent organic blue colourants. The results are summarised in Fig. 11 and their spectra are shown in Appendix A.

Moreover, spectrofluorimetry was proved suitable to recognise also one of the most important -in the past and nowadays- inorganic pigments, ultramarine blue (PB29), thanks to a fluorescence band whose maximum is around 680 nm. A similar orange fluorescence emission has already been observed in alkali glasses containing sulphur [34, 35], which have a composition analogous to this pigment.

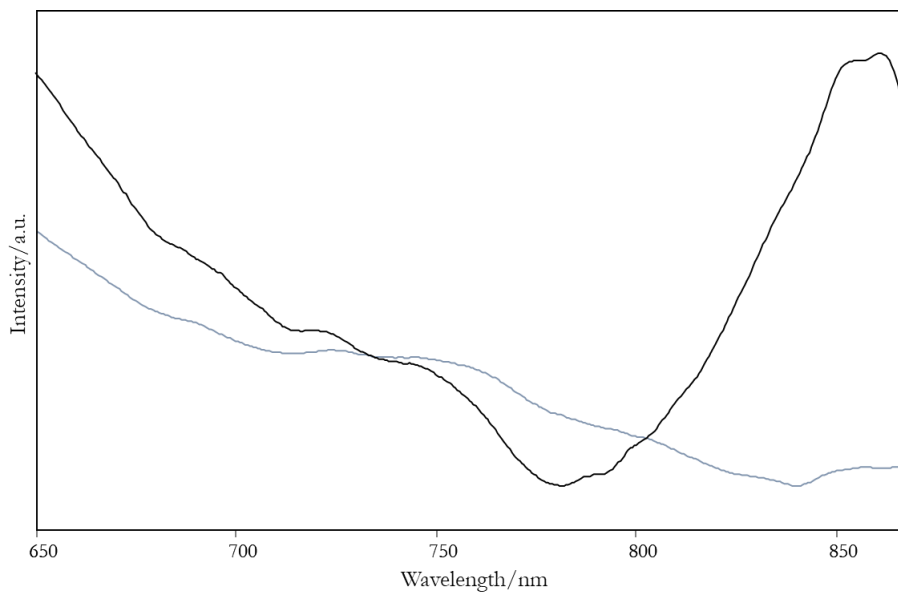


Figure 10. Emission spectra ($\lambda_{\text{exc}} = 562 \text{ nm}$) of PB16 (black line) and PB15 (grey line) in painting mock-up samples on canvas (powder plus oil binder).

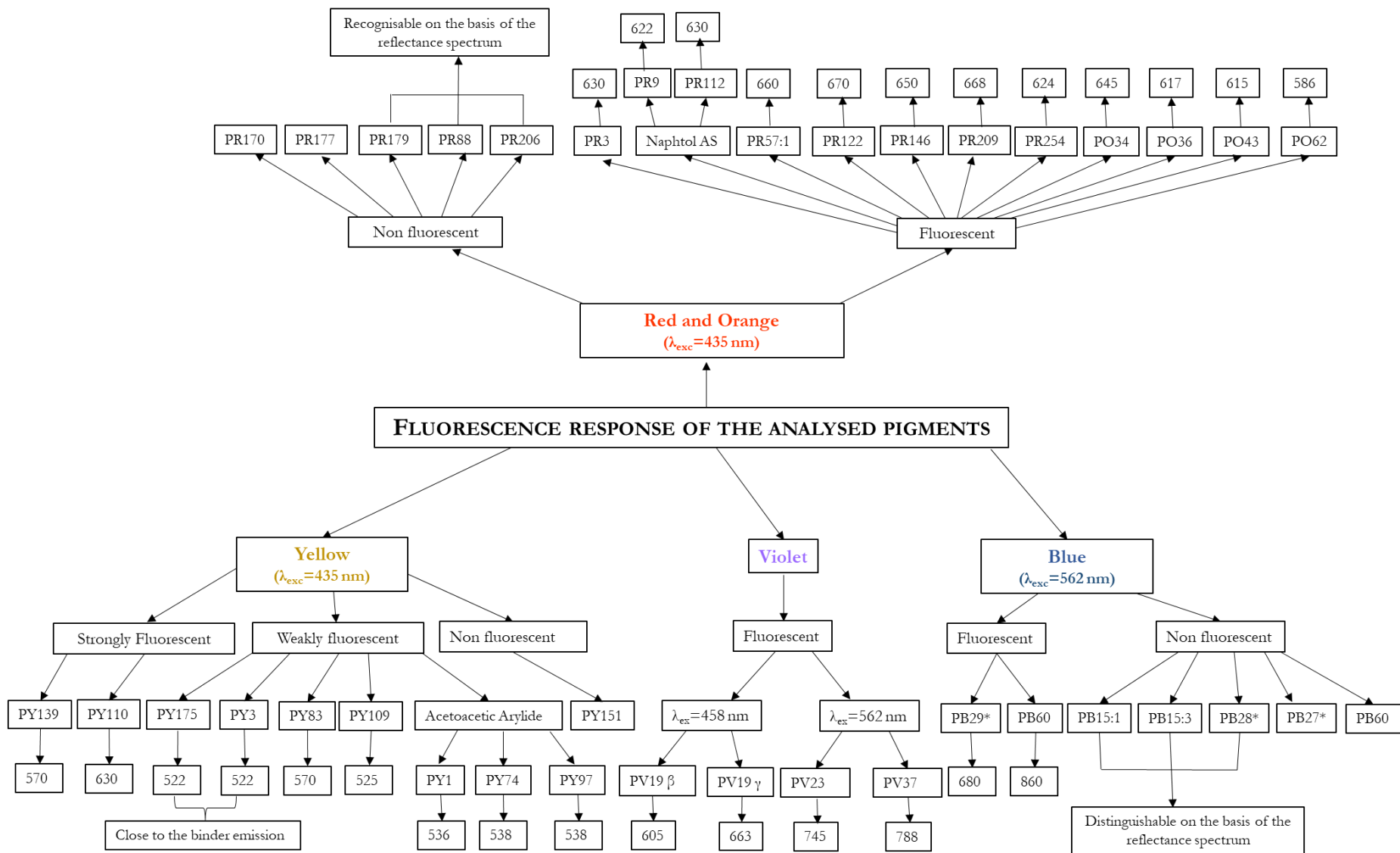


Figure 11. Scheme of the fluorescence response of the examined pigments. The wavelength of emission maxima is expressed in nanometres (nm). * = blue inorganic pigments.

5.2.4 Inorganic cadmium-based pigments

Besides organic pigments, spectrofluorimetry can be exploited also to identify the inorganic cadmium-based pigments, as already suggested in [33]. Cadmium yellow, orange and red are composed of cadmium sulphide (CdS) or cadmium selenium sulphide (CdS/CdSe) and their use is widespread in the artistic field. In the pure crystal form, they are not fluorescent, but the presence of a very small amounts of impurities can cause under UV light a fluorescence emission in the red and infrared region of the electromagnetic spectrum. From yellow to red, a shift of the band towards longer wavelengths is observed (Fig. 12 and [36]). In the present work the possibility of exciting the fluorescence of cadmium-based pigments also employing visible radiation ($\lambda_{exc} = 435$ nm) was demonstrated. Therefore, the interference filter centred at 435 nm was coupled with the dichroic one at 635 nm in order to collect the emission response in the 600-900 nm spectral range. The presence of these fluorescence bands was confirmed by the analysis of both pure powdered pigments, as such and mixed with binders, and commercial paints.

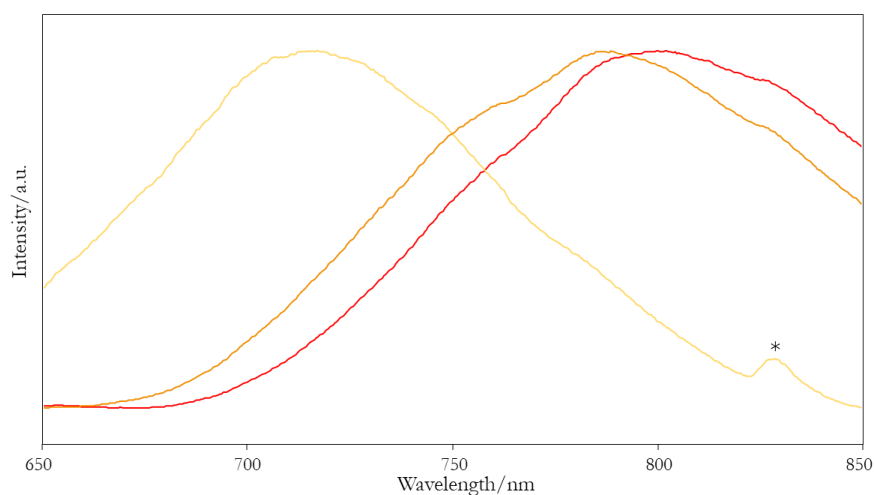


Figure 12. Emission spectra ($\lambda_{exc} = 435$ nm) of cadmium yellow PY35, cadmium orange PO20 and cadmium red PR108 in painting mock-up samples on canvas (powder plus oil). * = spurious band due to the dichroic filter.

5.2.5 Self-absorption correction applied to mixtures of pigments

The self-absorption correction described in section 4.4 was applied to binary mixtures of organic pigments. The identification of the substances composing a mixture is, in fact, an issue to take into account: often artist combined different colours to obtain particular hues and, in addition, a consistent number of commercial paints are actually a mixture. When two pigments are mixed together, the fluorescence spectrum is affected by the presence of both colouring substances. In particular, an apparent shift of the fluorescence band caused by the absorption due to the second component and a changing in fluorescence intensity can occur. Therefore, we investigated the possibility of identifying each component by applying the self-absorption

correction proposed in [28, 29]. For this purpose, three different kinds of mixtures were prepared by mixing two commercial acrylic paints and analysed:

- (i) Two fluorescent pigments with fluorescence emission of comparable intensity: PY139+PR122 (1:1)
- (ii) Two fluorescent pigments having complementary colours: PY139+PV23 (2:1)
- (iii) A fluorescent and a weakly fluorescent pigment: PR112 +PY3 (1:1)

Their reflectance and fluorescence spectra were acquired and the correction was performed. In order to investigate the possibility of recognising the two pigments composing each mixture, the corrected spectra were compared to those of the pure components, corrected as well for their self-absorption.

In case (i), the uncorrected spectrum showed a fluorescence band around 625 nm, corresponding to that of pure quinacridone magenta PR122. After the self-absorption correction, a broad band with three maxima appeared: the first two are attributable to PY139 (570 and 540 nm), the latter corresponds to the corrected spectrum of PR122 (614 nm). Therefore, the correction allowed the identification of the two fluorescent components of the mixture (Fig. 13).

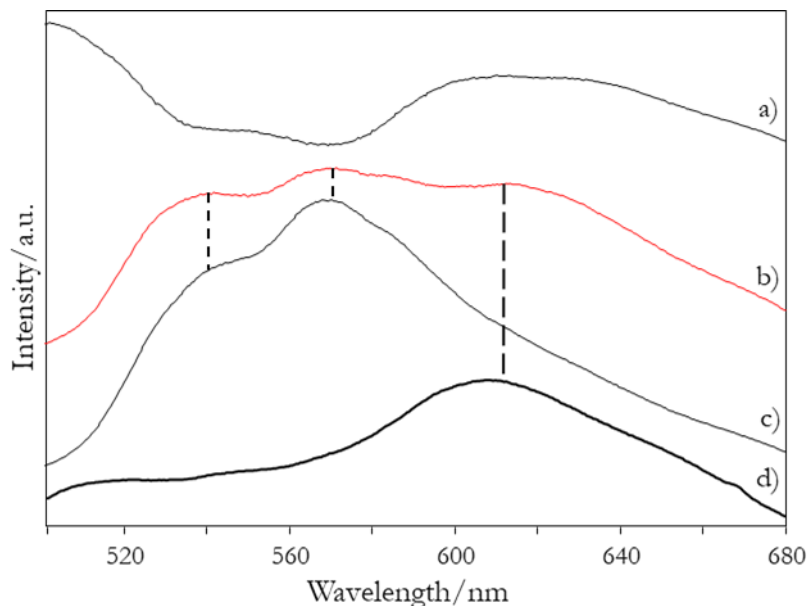


Figure 13. Emission spectra of a painting sample of the mixture PY139+PR122 ($\lambda_{exc} = 435$ nm), before (a) and after (b) correction for self-absorption. For comparison, also the corrected spectra of (c) PY139 and (d) PR122 are shown.

In case (ii), the analyses were performed with the two different combinations of filters (interference 435 nm/dichroic 458 nm and interference 562 nm/dichroic 635 nm) in order to verify if, by exciting separately the fluorescence of the two complementary pigments, their

identification in mixture is still possible. At $\lambda_{\text{exc}} = 435 \text{ nm}$, before the correction, the spectrum is characterised by two fluorescence bands (at 591 nm with two shoulders at 541 and 570 nm and at 668 nm) and apparently it is not attributable to any pigment. Once corrected, a single band at 568 nm with a shoulder at 540 nm appears and the spectrum becomes very similar to that of pure isoindoline yellow PY139, allowing us the identification of this component (Fig. 14). At $\lambda_{\text{exc}} = 562 \text{ nm}$, a spectrum characterised by a weak band is obtained. After the self-absorption correction, it shifts towards shorter wavelengths, but the identification of PV23 (dioxazine violet) is still impossible, probably due to the dilution of the pigment in the mixture.

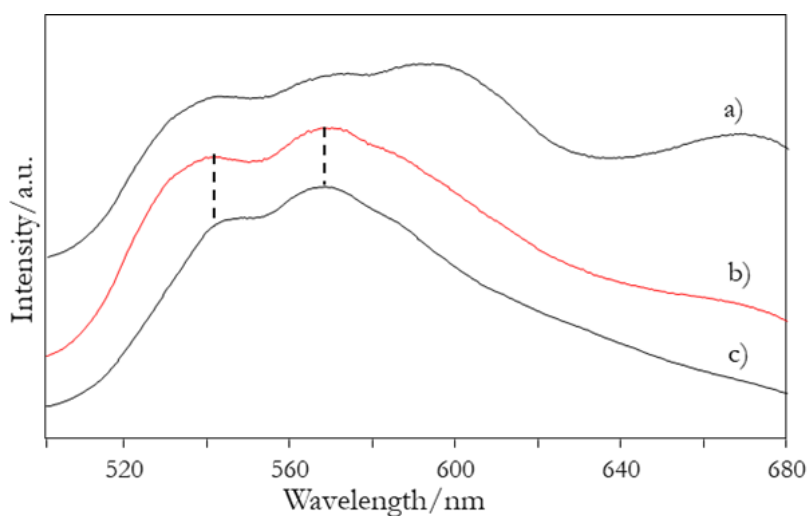


Figure 14. Emission spectra of a painting sample of the mixture PY139+PV23 ($\lambda_{\text{exc}} = 435 \text{ nm}$), before (a) and after (b) correction for self-absorption. For comparison, also the corrected spectrum of PY139 is shown (c).

In case (iii), the emission spectrum allowed us to recognise the fluorescent pigment PR112 in mixture with the weakly fluorescent pigment PY3 and the self-absorption correction worked as in the case of paint layers of different concentration [29]. In the solid state, a re-absorption of the emitted radiation by molecules of the same compound can occur, causing a quenching of the fluorescence and a shift of the band towards longer wavelengths. These phenomena are related to the concentration of the pigment: increasing it results in a reduction of the emission intensity and in a red shift of the emission maximum. Therefore, the emission spectrum of PR112 in mixture with PY3 is not immediately comparable with that of the pure reference pigment due to the different concentration. The correction for self-absorption shifted the emission maximum towards lower wavelengths, making the spectrum of the fluorescent pigment diluted in the mixture more similar to that of the pure one corrected as well (Fig. 15). It is worth noticing that the corresponding reflectance spectrum (datum non shown), which exhibits an edge at an intermediate wavelength between those of the two pure pigments, is of less use in identifying this component.

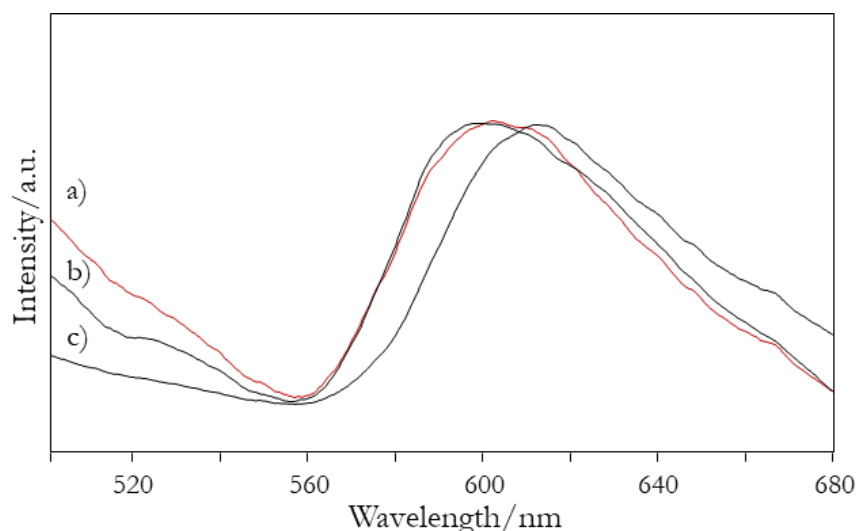


Figure 15. Emission spectra ($\lambda_{\text{exc}} = 435 \text{ nm}$) of a painting sample of the mixture PR112+PY3 (a) after and (c) before the correction for self-absorption. For comparison, also the corrected spectrum of PR112 is shown (b)

5.3 Case studies

The methodology proposed to identify the reference synthetic organic pigments on painting model samples was extended to real paintings, aiming to verify its validity in a complex system, where different pigments coexist and are often applied in mixture by the artists.

5.3.1 *Addetta near Zoate* by G. Faraone

The first paint under investigation was *Addetta near Zoate* by G. Faraone, dated 2011. During a previous campaign of scientific examinations [12], Raman analyses were carried out allowing the identification of the pigments employed by the artist. The analytical approach based on visible reflectance spectroscopy and visible-excited spectrofluorimetry was performed in order to confirm its potentiality, making a comparison with such previous experimental results. For this purpose, areas of different colours were examined and their spectra were compared to those of the reference pigments to identify the colorants employed (Fig. 16).

Green- In dark green areas corresponding to the trees in the background (area 5), a non-fluorescent pigment, supposed to be phthalocyanine green PG7 on the basis of its reflectance spectrum, was used. Moreover, the emission spectra obtained upon excitation at 435 nm and collecting the emission response in the range 600-900 nm demonstrated the use of PY35, cadmium yellow (Fig. 16 III) to lighten the colours in the light green details, such as grass (area 4) and willows (area 6). This information could be achieved only by spectrofluorimetry, as the reflectance spectrum is dominated by the response of the green pigment.

Red- The red colour is present in few details of the painting, namely some small flowers (point 2) and the artist's signature (area 1). Upon excitation at 435 nm, an emission band with

maximum at 597 nm was observed (Fig. 16 I). However, no correspondence was found with any of the red or orange pigments examined in the present work. Indeed, Raman analyses [12] demonstrated the use of a benzimidazolone pigment, possibly PO60, that was not available to us for comparison. Indeed, the benzimidazolone orange pigment analysed in the present work, PO36, shows an emission maximum at a higher wavelength. Finally, the possible presence of a cadmium pigment was ruled out due to the absence of the NIR emission band.

Pink- The pink colour used by the artist to paint the clouds (area 3) was probably a mixture of an orange together with a white or yellow pigment. The orange colourant could be identified by comparing its emission spectrum, corrected for self-absorption, with the spectrum of reference perinone orange PO43 (main band at 615 nm), corrected as well (Fig. 16 II). In this way the effect of the remarkably different concentration of the pigment in the light-coloured detail of the painting and in the reference mock-up sample was taken into account. Raman analyses confirmed the use of the perinone orange pigment [12], however the possible yellow component, suggested by the pattern of the emission band around 500 nm, where two other components (520 and 550 nm) besides that of the binder can be distinguished, was not recognised.

Violet- In the violet areas dioxazine violet PV23 was recognised (Fig. 16 IV). In particular, the flowers (area 8) were painted using this pure pigment, while in the violet brush strokes on the trees (area 7) it seems to be mixed with ultramarine blue (PB29), as the growing trend of the fluorescence spectrum around 650 nm suggests. The results achieved were confirmed by supplementary Raman analyses performed during this work (data non shown).

Blue- PCA did not allow us to recognise the blue pigments (area 9) in the paintings from their reflectance spectra. Upon excitation at 562 nm, fluorescence analyses revealed instead the presence of PB29, ultramarine blue. The previous Raman analyses confirmed the use of this pigment mixed with PB15:3 (phthalocyanine blue), which is not detectable by spectrofluorimetry, as discussed above (section 5.2.3).

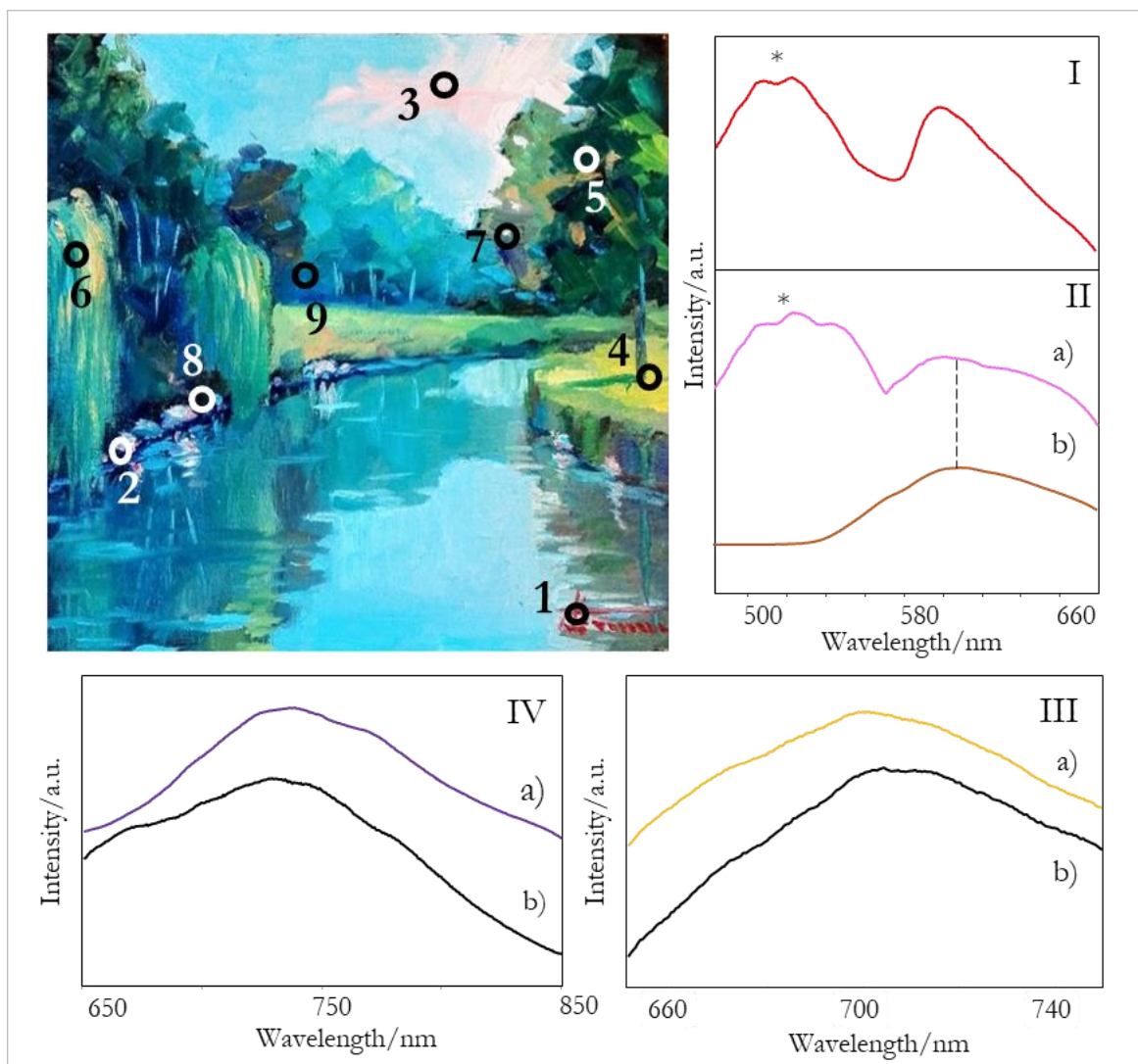


Figure 16. Measurement areas and emission spectra obtained on the painting *Addetta near Zoate* (G. Faraone, 2011). (I) emission spectrum ($\lambda_{exc} = 435$ nm) of area 1 (red); (II) emission spectrum ($\lambda_{exc} = 435$ nm) of a) area 3 (pink) after self-absorption correction, compared with that of the recognised reference pigments PO43 b); (III) emission spectrum ($\lambda_{exc} = 435$ nm) of (a) PY35 compared with that of (b) area 4 (light green); (IV) emission spectrum ($\lambda_{exc} = 562$ nm) of (a) PV23 compared with that of (b) area 7 (violet). * = band due to oil binder.

5.3.2 Paintings by S. Pasotti

Interesting results, underlining once again the effectiveness of the combined approach based on spectrofluorimetry and PCA, were obtained from the analysis of red and yellow pigments in *The monster* (1966) and in *The daily neo-mythology* (1966-1967) by S. Pasotti (Fig. 17 a and b). Also in this study, Raman analyses were available, making possible a cross-comparison of the results.



Figure 17. (a) *The monster* and (b) *Daily neo-mythology* by S. Pasotti (1966-1967).

Red- Two different synthetic organic pigments with this hue were used in the two paintings. The former is the β -naphthol PR3 in a red area of *The monster* (M14), but also in a red-purple detail of *The daily neo-mythology*: an emission maximum around 630 nm was in fact detected (Fig. 18 b and c), in accordance with what previously observed for the pure pigment (Fig. 18a). Moreover, an excellent correspondence was obtained in the score plot of the emission spectra of reference red and orange pigments between the area of the first painting and PR3. On the other hand, referring to *The daily neo-mythology*, the emission maximum is located around 630 nm (Fig. 18 d) too, in agreement with PR3, but an enlargement of the band towards 610 nm is also evident. Indeed, the red-purple hue of that measurement area NQ12 suggests a second pigment, possibly of violet colour, such as the β -form of PV19, which emission maximum is around 605 nm. The second red-orange pigment could not be identified by our method since, as demonstrated by Raman measurements, it did not belong to our database of reference materials. As a consequence, in the score plot it does not match with any of the reference colourants. It is a naphthol red PR10 or a naphthol orange PO38, belonging to the same chemical class and thus exhibiting similar Raman spectra.

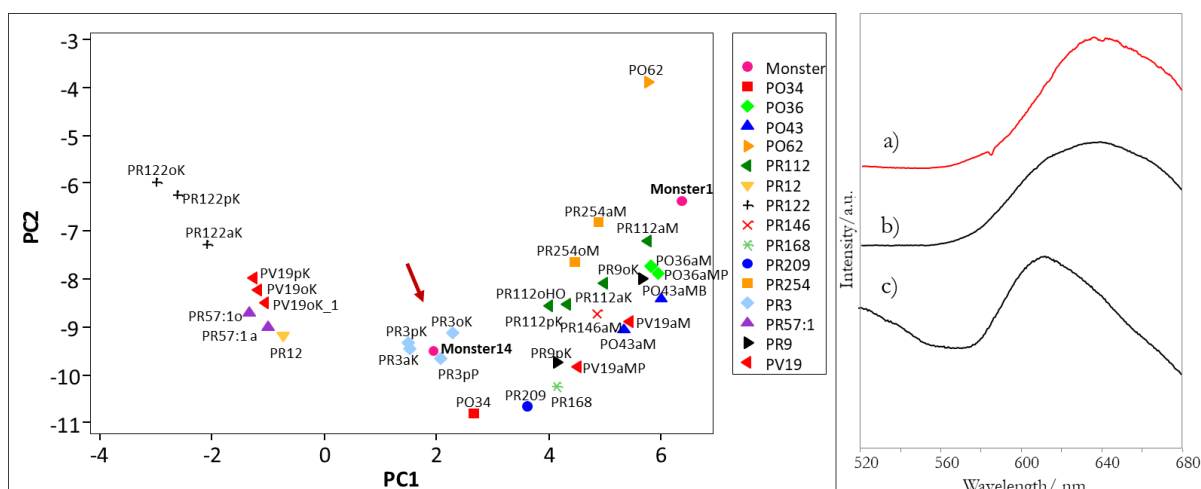


Figure 18. Left: score plot of the first two principal components of the emission spectra of red and orange pigments and painting areas ($\lambda_{exc} = 435$ nm). Right: emission spectra of: a) reference PR3; b) M14 c) NQ12.

Yellow- In *The monster*, a characteristic emission spectrum was recorded for both the yellow areas M10 and M20, having a maximum at 525 nm and shoulders at about 537, 560 and 582 nm (Fig. 19 b and c). Such pattern has a good correspondence with the fluorescence spectrum of the isoindole yellow PY109 (Fig. 19 a). The PCA of the emission spectra obtained on *The monster* compared with those of yellow synthetic organic pigments in painting mock-up samples shows nevertheless a certain distance in the space of the first two principal components between the spectra from the painting and those of the reference PY109 paints, that however do not form themselves a very close group. The possible identification of the pigment PY109 is of interest as it was introduced in the same years when Pasotti painted this artwork. Anyway, no Raman bands were observed for the yellow pigment in the yellow areas, so it was not possible to definitively confirm the hypothesis. For a yellow area of *The daily neo-mythology* (NQ7), the use of the arylide yellow PY1 was hypothesised on the basis of a good correspondence with the spectral pattern of the reference pigment (Fig. 19d), having an emission maximum situated around 540 nm, and PCA confirmed the attribution (Fig. 19e) as well as Raman measurements. Finally, in the green area NQ5, where the Raman spectrum of phthalocyanine green PG7 was obtained, the emission spectrum, with a maximum at 524 nm, suggest the presence a yellow component, reasonably the arylide yellow PY3 on the basis of PCA (Fig. 19).

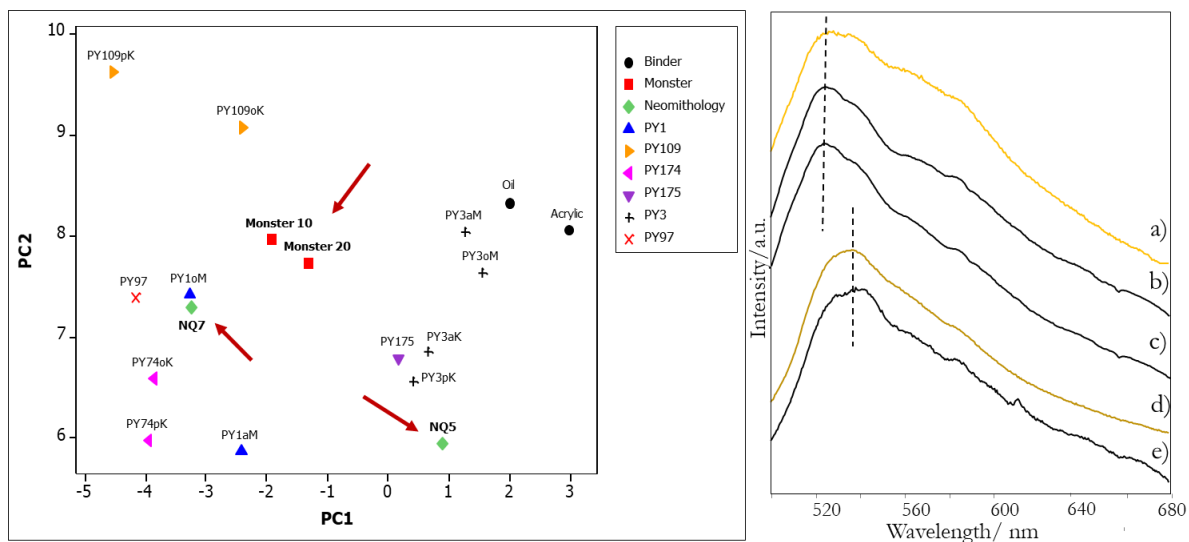


Figure 19. Left: score plot of the first two principal components of the emission spectra of yellow pigments and of painting areas ($\lambda_{exc} = 435$ nm). Right: emission spectra of: a) reference PY109; b) M10 c) M20, d) reference PY1 and e) NQ7.

5.4 UV-induced spectrofluorimetry

In this second part of the work, the possibility of exploiting an UV source (precisely emitting at 365 nm) to induce the fluorescence emission of synthetic organic pigments was confirmed. As discussed below, the results are perfectly in agreement with those obtained upon excitation at $\lambda_{exc} = 435$ nm range for yellow, orange and red pigments and at $\lambda_{exc} = 562$ nm for violet and blue ones. Indeed, a very good correspondence in terms of emission maximum and spectral pattern was observed. Moreover, also the inorganic cadmium-based pigments showed their peculiar emission band in the NIR range upon UV excitation, as already reported in the literature [33]. Also in this case, the emission spectra were processed by PCA. The resultant score plots reflect what previously observed, allowing once again the identification of most pigments or at least their chemical class. Since in the first part of the work a high degree of correspondence between different commercial paints containing the same pigment was found, only a lower number of reference samples was here investigated, more representative of the use of different binders (acrylic and oil) rather than of the various manufacturers.

5.4.1 Red and orange pigments

As previously observed, most red and orange pigments are fluorescent and occupy different areas of the corresponding score plot, allowing their identification and confirming the possibility of distinguishing the same colourant applied with different binders. For a more readable output, PCA was repeated after excluding four pigments, namely PV19 β , PO62, PR209 and PO34. They have peculiar spectra in terms of pattern (PO62) and red-shifted emission maxima (PV19 β ,

PR209 and PO34, whose representative points partially overlap, but can be distinguished considering their different colour). In Fig. 20, the score plot which does not include these substances is reported, while for the overall one the reader is referred to Appendix A. All the pigments can be recognised and there are only few overlaps: it is the case of PR3 in oil, which is slightly different from the acrylic formulation and is located near PR254. This effect is probably due to a different concentration of the pigments in the two formulations, which determines a higher self-absorption and, as a consequence, a red-shift of the emission maximum for the oil paint.

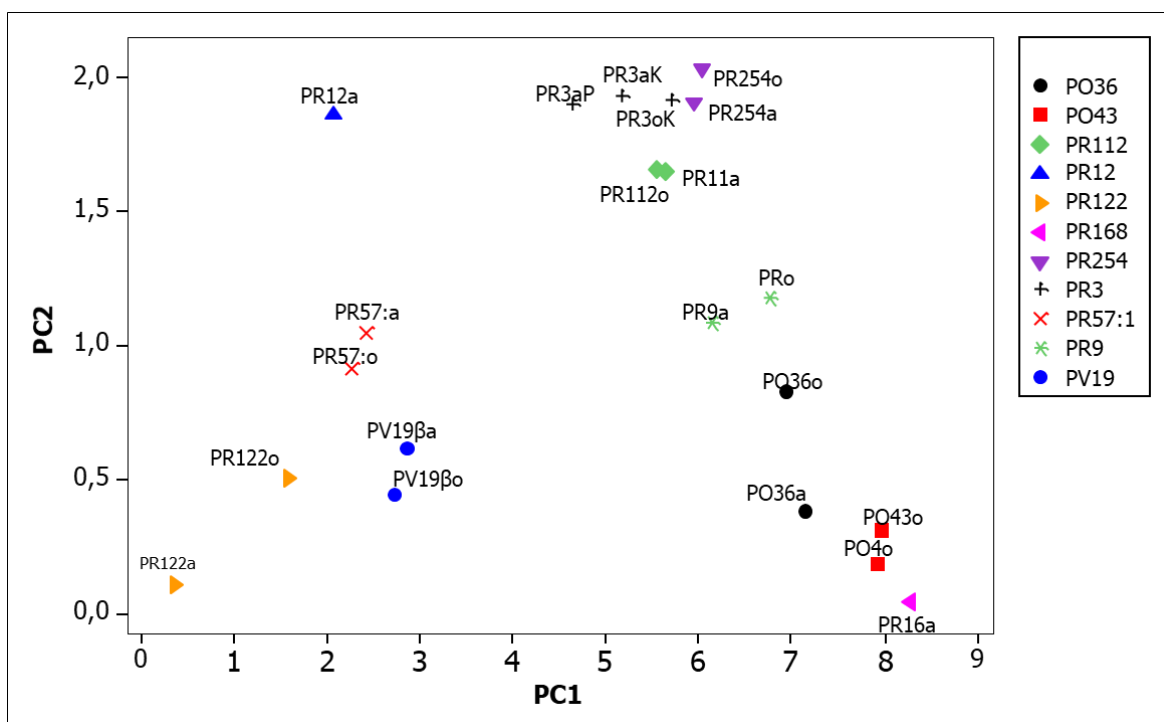


Figure 20. Score plot of the first two principal components of emission spectra of red and orange pigments ($\lambda_{exc} = 365$ nm). PO62, PR209, PV19 β and PO34 are not included.

5.4.2 Yellow pigments and binders

Also in the case of yellow pigments the results are in agreement with what was already observed upon 435-nm excitation: PY83, PY139 and PY110, having red-shifted emission maxima, occupy a separate region of the score plot (Appendix A); the other pigments, whose emission is closer to that of binders, are indeed located near to oil and acrylic resin. In respect of binding media, it is worth underlining that, if excited by an UV source, their emission is much more intense than when excited in the visible range. This drawback should be kept in mind to understand the results of imaging analyses. The score plot of yellow pigments is reported in Fig. 21: all the colourants can be distinguished, or at least their chemical class (e. g. PY1 and PY74 are close in the multivariate space, but they are both acetacetarylides, justifying this similarity). Once again,

the combination of spectrofluorimetry and PCA proved to be an effective approach for identification purposes.

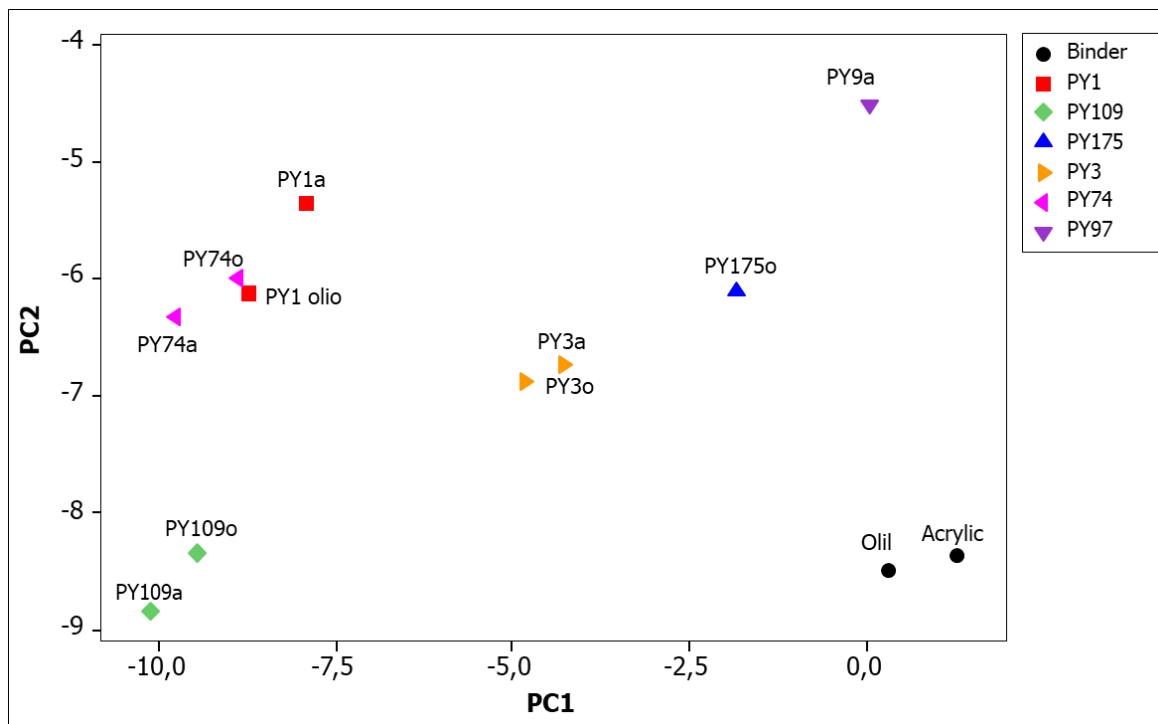


Figure 21. Score plot of the first two principal components of emission spectra ($\lambda_{exc} = 365$ nm) of yellow pigments.

5.4.3 Blue, green, violet and cadmium-based inorganic pigments

The behaviour of these pigments emitting in the NIR range upon visible excitation was verified too. They are PB16, PV23 and PV37 and the inorganic cadmium-based pigments. PB16 gave a weak emission at about 870 nm, confirming what observed upon visible excitation. On the other hand, no remarkable emission could be detected upon UV-excitation for the two dioxazine violets, differently from what reported for the same pigments excited at 562 nm. This fact was probably due also to the interference of the first overtone of the UV exciting radiation, located at 730 nm. Finally, both PG7 and PG8 are confirmed to be not fluorescent.

5.5 UV-imaging

The investigated synthetic organic pigments, spread on canvas in acrylic or oil binder, show different behaviours when irradiated with UV-light at 365 nm and analysed by the imaging technique. However, for the visible fluorescence observed in the UV-excited images (UVF), two aspects must be considered: the effect of the binder and the concentration of the pigments in the mock-up samples.

Acrylic and oil binder contributes in a different extent to the UVF images, as demonstrated by the corresponding details in Fig. 22. When excited at 365 nm, in fact, both binders exhibit a fluorescence emission maximum around 500-510 nm, but the intensity of the spectrum is significantly weaker for the synthetic binder in comparison with linseed oil (Fig. 22).

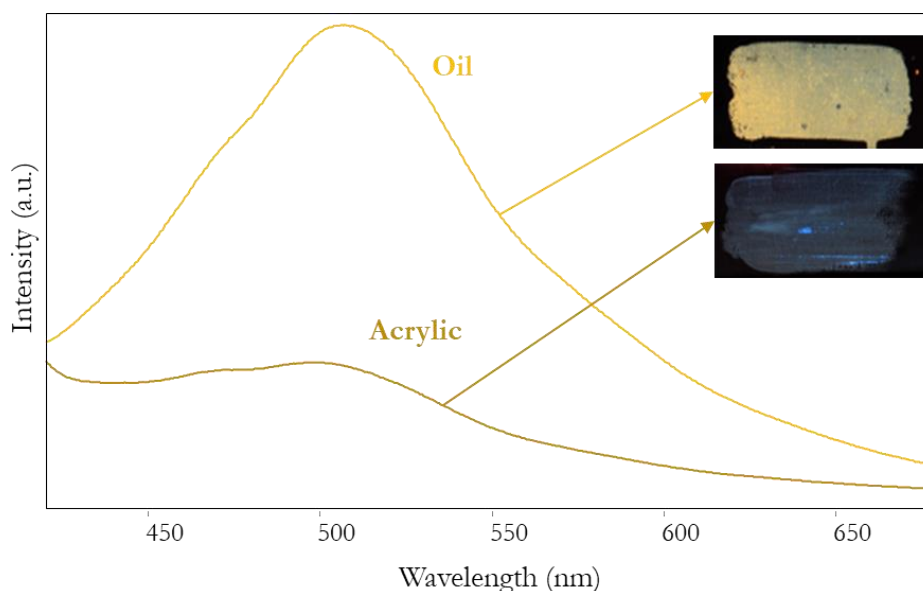


Figure 22. Emission spectra of linseed oil and acrylic resin spread on canvas and their UVF images.

Such emission adds up to that of the pigments and contributes to the fluorescence acquired in the UVF images, as demonstrated in Fig. 23 for the painting layer containing the strongly fluorescent pigment PR122. Therefore, the image obtained under UV light shows a considerable contribution of the yellowish emission of oil, superimposed on the red one due to the pigment (Fig. 23a). On the other hand, when the colourant is spread in acrylic, the binder, coherently with the weaker emission of the synthetic resin, has a less effect. Interestingly, the contribution of the binding media can be minimised in favour of the fluorescence emission of the pigment by choosing an excitation wavelength in the visible range, namely 420 nm, and acquiring the so-called visible fluorescence induced by visible radiation (VIVF) image (Fig. 23c). This happens because the absorption of the binders is centred in the near UV and, as a consequence, their fluorescence is more strongly induced upon that excitation wavelength.

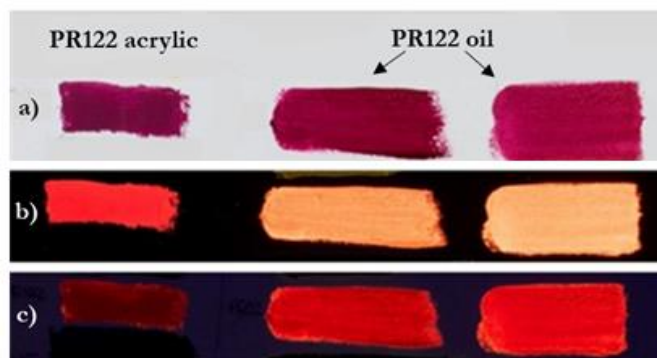


Figure 23. a) Visible image of painting layers on canvas containing PR122 in acrylic resin and linseed oil.; b) UVF image; c) VIVF image. For oil binder, the concentration of the pigment in the sample decrease from left to right.

Fig. 23 allows us to explain also the second aspect that must be taken into account: the concentration of the pigment. The emission intensity of fluorescent substances increases with increasing the concentration of the emitter, but this tendency can be inverted for higher concentration as the already described self-absorption phenomenon takes place [11]. This is exemplified by the two samples of PR122 in oil, whose concentration decrease from left to right: the intensity of the red fluorescence emission is, in fact, higher for the more diluted one (right column).

In the following sections, the preliminary results and some considerations based on the comparison between the images and the spectroscopic data will be presented.

5.5.1 Red, orange and yellow pigments

In UVF images, only the most fluorescent red and orange pigments, in accordance with the UV-induced spectrofluorimetric results, could be distinguished. They were PR57:1, PO43 and PR122, which show a characteristic colour corresponding to their emission maximum (Tab. 3). A weaker emission was observed for PR3, whereas, even if emitting between 630 and 638 nm, PR9, PR112 and PR254, have a weaker fluorescence intensity in comparison with that of the aforementioned pigments, preventing their detection because of the low intrinsic sensitivity of the imaging method. The remaining red and orange pigments did not yield any emission when excited at 365 nm, as expected from visible and UV-excited spectrofluorimetric data.

Referring to yellow pigments, in the UVF images (Tab. 3) a characteristic bright orange emission was observed for PY139, in agreement with its strong fluorescence band at 572 nm. PY83 and PY110 are weak emitters, as expected from the relative intensity of their emission bands (Fig. 24 and 25). Finally, PY1 and PY74, whose fluorescence is very weak, and PY151, which is not fluorescent, cannot be observed in UVF images.

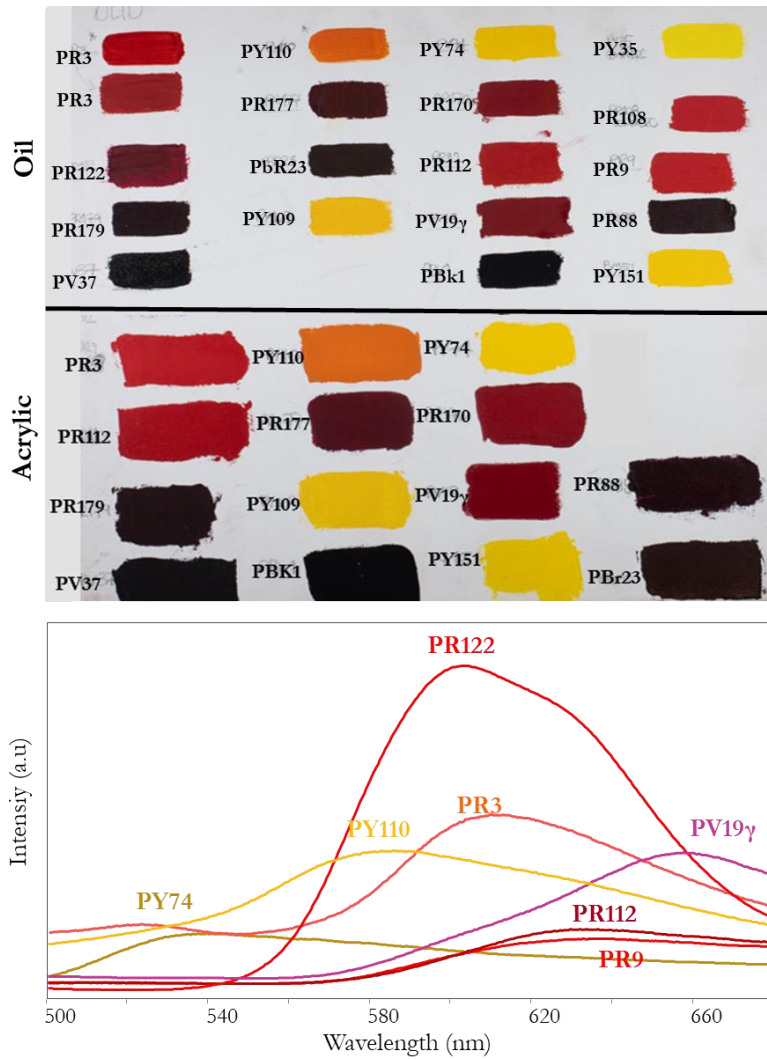


Figure 24. Bottom: emission spectra ($\lambda_{exc} = 365$ nm) of painting layers with PR3, PY110 and PV19 in linseed oil, PY74, PR9, PR122 and PR112 in acrylic resin. Top: visible image of the mock-up painting samples on canvas.

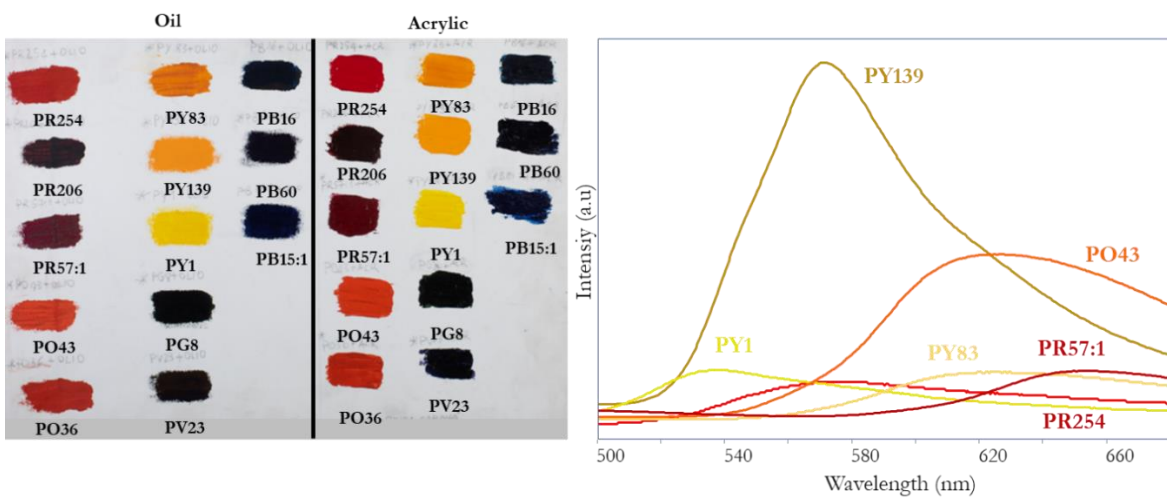


Figure 25. Right: emission spectra ($\lambda_{exc} = 365$ nm) of painting layers with PY1, PY83, PY139, PO43, PR57:1 and PR254 in linseed oil. Left: visible image of the mock-up painting samples on canvas.

5.5.2 Violet pigments

The quinacridone violet PV19 in the γ crystalline form exhibits a red-coloured fluorescence, consistent with the emission maximum at 665 nm (Fig. 25). Also the β form of this pigment, whose emission maximum is at 615 nm, can be distinguished thanks to a characteristic purple-red fluorescence (Tab. 3). Moreover, two mixtures, containing respectively PV19 with PR206 and PR254, were investigated. In both painting samples, only the emission due to quinacridone violet is observed, as the other two components are not, or just weakly, fluorescent, as already discussed for red pigments (Fig. 26).

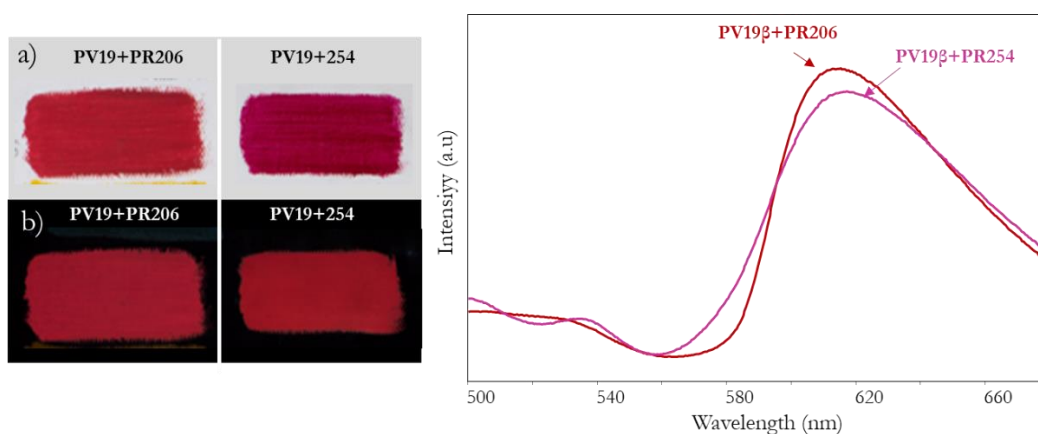


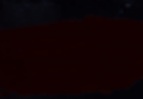






Figure 26. a) Visible images of two samples of commercial oil paints containing a mixture of PV19 and PR206 and a mixture of PV19 and PR254; b) UVF images; c) emission spectra ($\lambda_{exc}=365$ nm) of the corresponding samples.

Table 3. Emission maxima ($\lambda_{exc} = 365$ nm) and UVF images of the synthetic organic pigments dispersed in acrylic or oil binder.

Pigment	Binder	Emission maximum	UVF response
P3	Oil	618 nm	
	Acrylic	620 nm	
PR9	Oil	637 nm	
	Acrylic	632 nm	
PR57:1	Oil	657 nm	
	Acrylic	657 nm	

PR112	Oil	637 nm	
	Acrylic		
PR122	Oil	665 nm	
	Acrylic	670 nm	
PR254	Oil	630 nm	
	Acrylic	630 nm	
PO43	Oil	623 nm	
	Acrylic	623 nm	
	Acrylic	541 nm	
PY83	Oil	577 nm	
	Acrylic	573 nm	
PY110	Oil	635 nm	
	Acrylic		
PY139	Oil	571 nm	
		571 nm	

5.5.3 Blue and green pigments

Among the blue and green pigments analysed in this work, PB15:1, PB60 and PG8 did not yield any luminescence, in accordance with the results of UV-excited spectrofluorimetric analyses. Only a weak fluorescence emission was detected for PB16 at around 867 nm by UV-induced spectrofluorimetry, but it is not appreciable in VIL image. It is conceivable that the imaging technique is not sensitive enough to detect this very low-intensity emission.

5.5.4 Cadmium-based pigments

As already documented and observed by spectrofluorimetry, the inorganic cadmium pigments exhibit a fluorescence emission in the NIR region (Fig. 27). This can be detected also by the imaging technique and is particularly evident when illuminating the model paintings with a 420 nm light-source and filtering above 850 nm (Fig. 27c).

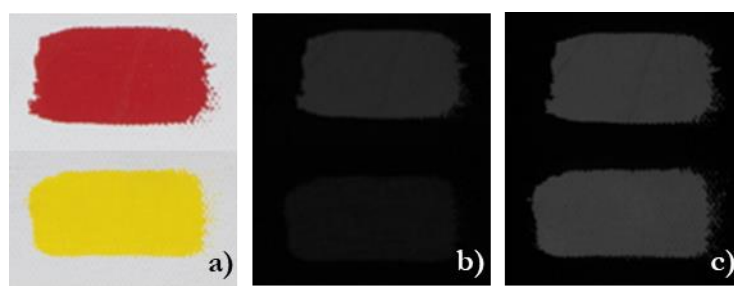


Figure 27: a) Visible image, b) VIL image with 365-nm illumination and c) VIVF image with 420-nm illumination.

5.6 Case study

To test both UV-excited spectrofluorimetry and UV-imaging on a real case of study, both the analyses were performed on the already examined oil painting *Addetta near Zoate* by G. Faraone. Referring to UV-induced spectrofluorimetry, the results correspond to those provided by the same method upon visible excitation: no emission was observed for blue and green pigments, while for the red details a spectrum showing a maximum at 600 nm was obtained. It is worth underlining a peculiar result in the spectrum acquired on the pink areas corresponding to clouds, where the colour was attributed to a mixture of PO43 and an unidentified yellow component by exciting at 435 nm (section 5.3.1). The spectrum obtained upon UV excitation, however, shows a completely different pattern: beside the emission at 510 nm due to oil binder, there is a second band around 560 nm, which have an high degree of correspondence with PY139 (Fig. 28a). UV excitation seems to favour the response of the yellow pigment in comparison with the orange one, whose fluorescence instead prevails with visible excitation. Indeed, under UV

excitation the emission of PY139 results significantly more intense than that of the same colourant excited by visible light at 435 nm (Fig. 28b)); the emission of PO43, on the other hand, has an intensity comparable in both experimental conditions. The information obtained with the two excitation wavelengths is therefore complementary and confirms a mixture of PO43 and PY139, which, quite interestingly, is a commercially available formulation.

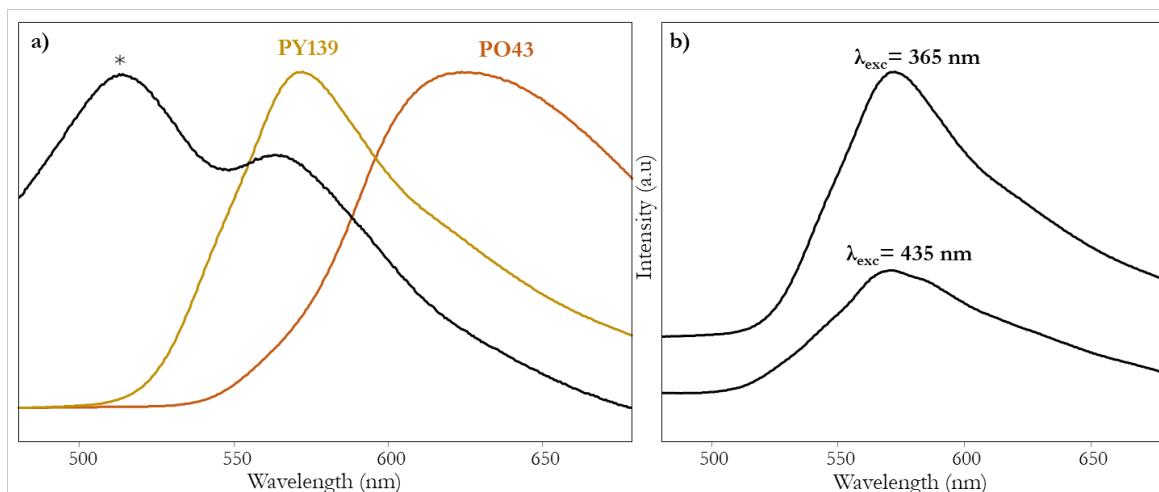


Figure 28. a) Comparison between the spectra of the reference pigments PO43 and PY139 ($\lambda_{exc} = 365$ nm) and the spectrum of pink clouds in the painting; b) comparison between the emission of intensity of PY139 under the two different excitation wavelengths. Legend: * = band due to the oil binder.

The image obtained by illuminating at 365 nm shows a diffuse luminescence (Fig 29 b) on all the pictorial surface, possibly attributable to the oil binder (its significant contribution is confirmed by emission spectra, where the oil band at 520 nm is always observed together with the one corresponding to pigments). When illuminating at 420 nm and filtering from 480 nm, the significant emission of the oil binder can be reduced and the image (Fig 29 c) shows a marked red-coloured fluorescence in the detail of the clouds, in agreement with the presence of PO43. Finally, in the image resulting from illumination at 420 nm and filtering above 850 nm, the presence of cadmium yellow (PY35) is highlighted in the light-coloured areas of the paintings, such as the lawn, the willows and their shadows on water (Fig. 29d).



Figure 29. a) Visible image of the painting *Addetta near Zoate* by G. Faraone; b) UVF image; c) VIVL image (excitation source 420 nm); d) VIL image (excitation source 420 nm).

6. Conclusions

In this chapter it was demonstrated that the use of spectrofluorimetry, possibly integrated by that of visible reflectance spectroscopy and combined with multivariate analysis of spectral data, is an effective method for the identification of synthetic pigments, in spite of the broad bands that usually characterise electronic spectra. The main advantage of the present method lies of course in the possibility of applying it in a non-invasive manner and *in situ* by means of portable instrumentation, thus obtaining complementary information to that supplied by other non-destructive techniques.

Most red, orange and yellow pigments turned out to exhibit an appreciable fluorescence emission upon visible excitation, allowing their identification, or at least to recognise the chemical class to which they belong. Almost all the non-fluorescent ones could be instead recognised by their visible reflectance spectra. The two dioxazine violets and the inorganic

cadmium pigments exhibited a characteristic fluorescence band in the NIR range. Moreover, the Kubelka-Munk correction of emission spectra for self-absorption was successfully applied to recognise fluorescent pigments in binary mixtures. This method was finally tested on three real contemporary paintings, leading to the successful identification of most pigments (pure or in mixtures) employed by the artists.

As a further step, a proof of concept of the applicability of UV-imaging methods for the identification of some synthetic organic pigments and the cadmium-based inorganic ones by their characteristic luminescence was demonstrated both on reference mock-up samples and on the contemporary painting *Addetta near Zoate*. The results are consistent with spectrofluorimetric analyses upon UV-excitation, although the imaging technique is certainly affected by an intrinsically lower sensitivity. In addition, the use of a different excitation wavelength, in particular a visible one was proved advantageous to reduce the strong contribution of the binder, especially if oil, to the luminescence observed in the image, thus promoting the response of the pigment. This is an interesting result as most imaging analyses are conventionally performed only by UV-excitation

References

- [1] S. Q. Lomax, T. Learner, *J. Am. Inst. Conservat.* 2006, 45, 107-125.
- [2] G. A. Milovanovic, M. Ristic-Solajic, T.J Janjic, *J. Chromatogr.* 1982, 249, 149-154.
- [3] G. Massonnet, W. Stoecklein, *Sci. Justice* 1999, 39, 128-134.
- [4] J.W. Wegener, J.C. Klamer, H. Govers, U. A.Brinkman, *Chromatographia* 1987, 24, 865-875.
- [5] J. Russell, B. W. Singer., J. J. Perry, A. Bacon, *Anal. Bioanal. Chem.* 2011, 400, 1473-1491.
- [6] J. Jonsson, T. Learner, *Separation of acrylic paint components and their identification with FTIR spectroscopy*. Proceedings of the 6th Infrared and Raman Users Group (IRUG 6). Ed. M. Picollo. Florence: Il Prato, 58-63. 2004.
- [7] M. Longoni, S. Bruni, *J. Chem. Educ.* 2021, 98, 966-972
- [8] M. Gulmini, A. Idone, E. Diana, D. Gastaldi, D. Vaudan, M. Aceto, *Dyes Pigm.* 2013, 98, 136-145.
- [9] C. Zaffino, M. Bertagna, V. Guglielmi, M. V. Dozzi , S. Bruni, *Microchem. J.* 2018, 139, 77-82.
- [10] M. Bacci, *UV-VIS-NIR, FT-IR, and FORS spectroscopies*, in Ciliberto E., Spoto G. (eds.) *Modern Analytical Methods in Art and Archaeology*, J. Wiley & Sons, New York, 2000, p. 343.
- [11] D. A. Skoog, F. J. Holler, S. R. Crouch, *Principles of Instrumental Analysis* 7th edition. Cengage, Boston, USA, 2018, p. 369.

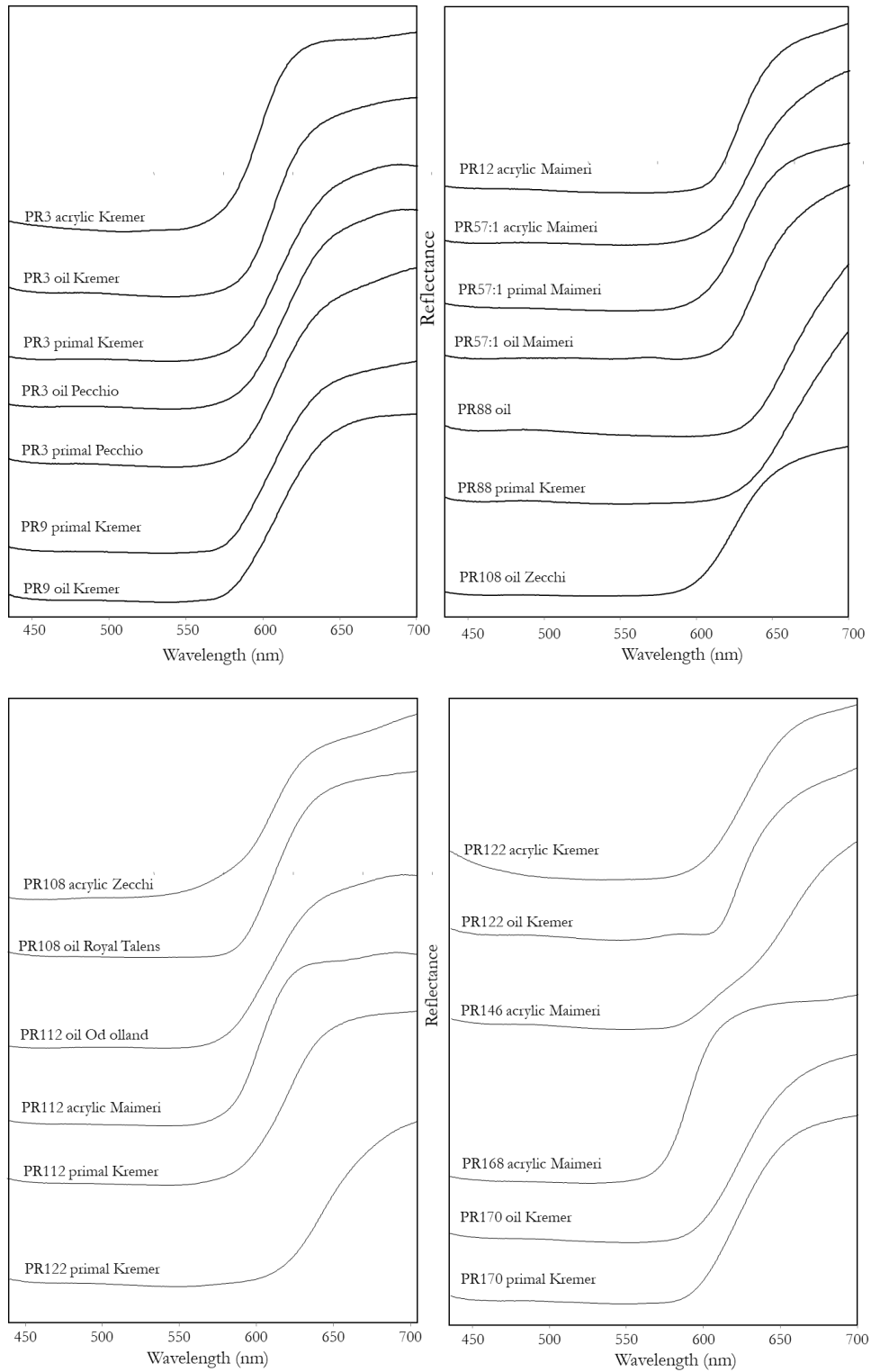
- [12] S. Bruni, V. Guglielmi, *Raman Spectroscopy for the Identification of Materials in Contemporary Painting*, in Vandenberghe P., Edwards H. (eds.), *Raman Spectroscopy in Archaeology and Art History* (Vol.2), The Royal Society of Chemistry, 2019, p.168.
- [13] J. J. Rorimer, *Ultra-Violet Rays and Their Use in the Examination of Works of Art*, Metropolitan Museum of Art, 1931.
- [14] R. A. Lyon, *Ultra-violet rays as aids to restorers*, *Technical Studies in the Field of Fine Arts*, 1934, 153–157.
- [15] J.D. Winefordner, *Practical fluorescence: theory, methods, and techniques*, 1974.
- [16] D. C. Creagh, D. A. Bradley, *Radiation in Art and Archeometry*, Elsevier, 2000.
- [17] A. Pelagotti, Pezzati, L. Bevilacqua, N. Vascotto, V. Reillon, C. Daffara, *A study of UV fluorescence emission of painting materials*, in: *Art '05–8th International Conference on Non-Destructive Investigations and Microanalysis for the Diagnostics and Conservation of the Cultural and Environmental Heritage*. Lecce, Italy, 2005: p. A97
- [18] D. Comelli, G. Valentini, A. Nevin, A. Farina, L. Toniolo, R. Cubeddu, *Rev. Sci. Instrum.* 2008, 79, 086112.
- [19] Daniela Comelli, Gianluca Valentini, Rinaldo Cubeddu, Lucia Toniolo, *Multi-spectral fluorescence imaging for cultural heritage*, *Proceedings Volume 6618, O3A: Optics for Arts, Architecture, and Archaeology*, 2007, 66180M.
- [20] R. Kellner, J. M. Mermet, M. Otto, H. Widmer, *Chimica Analitica*, Edises, 2003.
- [21] S. Schlucker ed., *Surface Enhanced Raman Spectroscopy: Analytical Biophysical and Life Science Applications*, Wiley-VCH, Weinheim, Germany, 2011.
- [22] M. Milazzo, N. Ludwig, *Misurare l'arte. Analisi scientifiche per lo studio dei beni culturali*, Bruno Mondadori Ed., Milano, 2010.
- [23] M. Hain, J. Bartl, V. Jacko, *Meas. Sci. Rev.* 2003, 3, 9-12.
- [24] G. Poldi, G. C. F. Villa, *Dalla conservazione alla storia dell'arte. Riflettografia e analisi non invasive per lo studio dei dipinti*, Edizioni della Normale, Pisa, 2007.
- [25] A. Aldrovandi, E. Buzzegoli, A. Keller, D. Kunzelman, *Investigation of painted surfaces with a reflected UV false color technique*, in *Proceedings of 8th International Conference On Non-Destructive Investigations and Microanalysis for the Diagnostics And Conservation of the Cultural and Environmental Heritage*, Lecce, 2005.
- [26] F. Mairinger, *Ultraviolet and fluorescence study of paintings and manuscripts*, in *Radiation in Art and Archeometry*, curated by di D.C. Creagh, D.A. Bradley, Amsterdam 2000, 56-75.
- [27] <http://www.webexhibits.org/pigments/intro/uv.html>
- [28] C. Clementi, C. Miliani, G. Verri, B. G. Brunetti, A. Sgamellotti, *Appl. Spectrosc.* 2009, 63, 1323-1330.
- [29] G. Verri, C. Clementi, D. Comelli, S. Cather, F. Piqué, *Appl. Spectrosc.* 2008, 62, 1295-1302.
- [30] E. F. Paulus, F. J. J. Leusen, M. U. Schmidt, *CrystEngComm* 2007, 9, 131-143.
- [31] C. Binant, B. Guineau, A. Lautié, *J. Soc. Dyers Colour.* 1990, 106, 187-191.
- [32] <https://www.handprint.com/HP/WCL/pigmt1d.html>

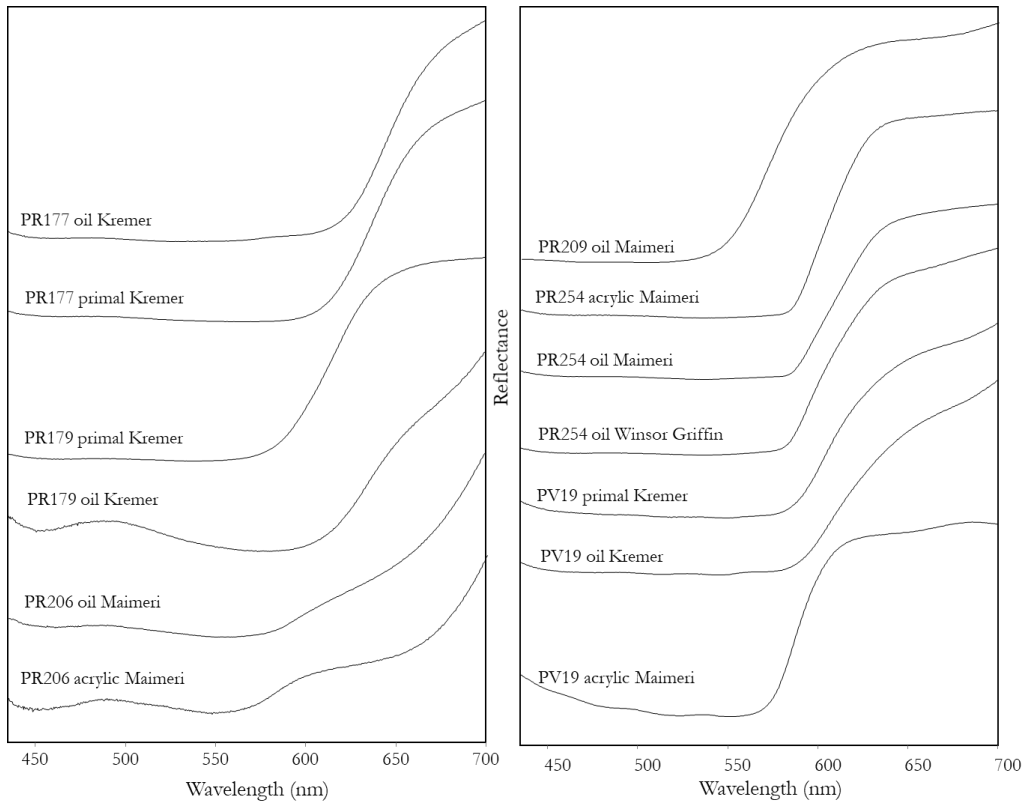
- [33] G. Poldi G., S. Caglio, *Opt. Spectrosc.* 2013, 114, 929–935.
- [34] A. Paul, A. Ward, S. Gomolka, *J. Mater. Sci.* 1974, 9, 1133-1138.
- [35] W. Giggenbach, *Inorg. Chem.* 1971, 10, 1308-1311.
- [36] E. Rene de la Rie, *Stud. Conserv.* 1982, 27, 1-7.

Appendix A

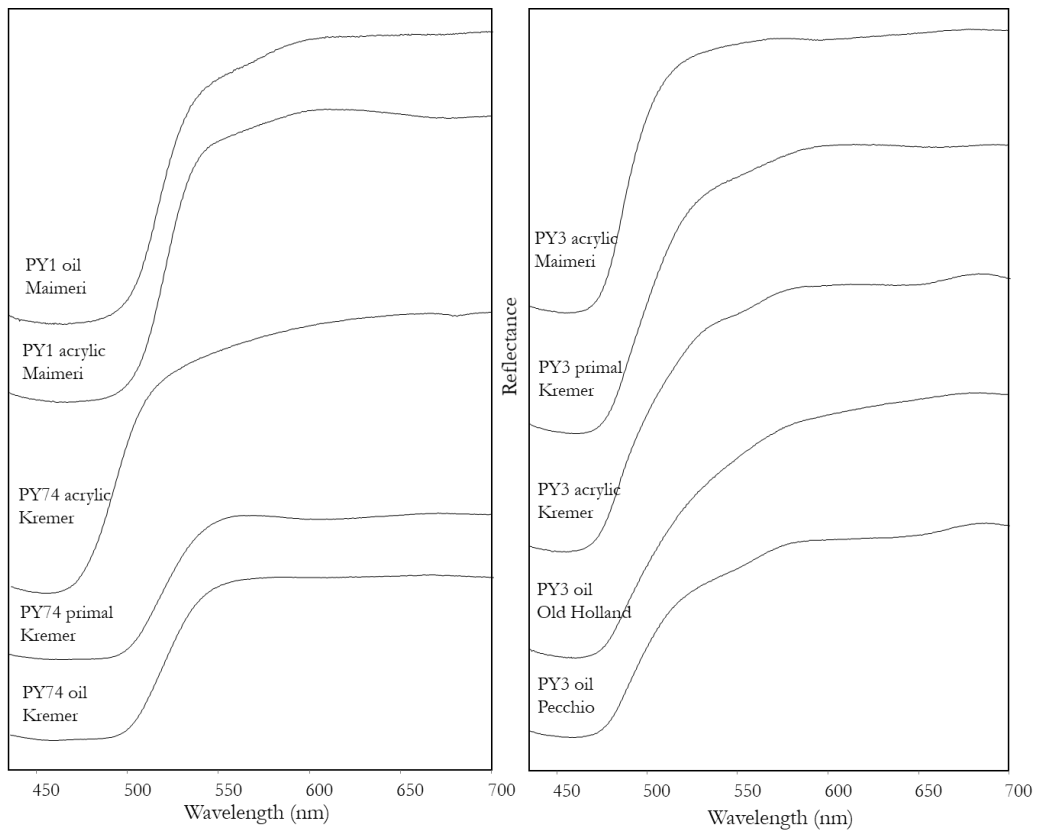
1. Reflectance and emission spectra

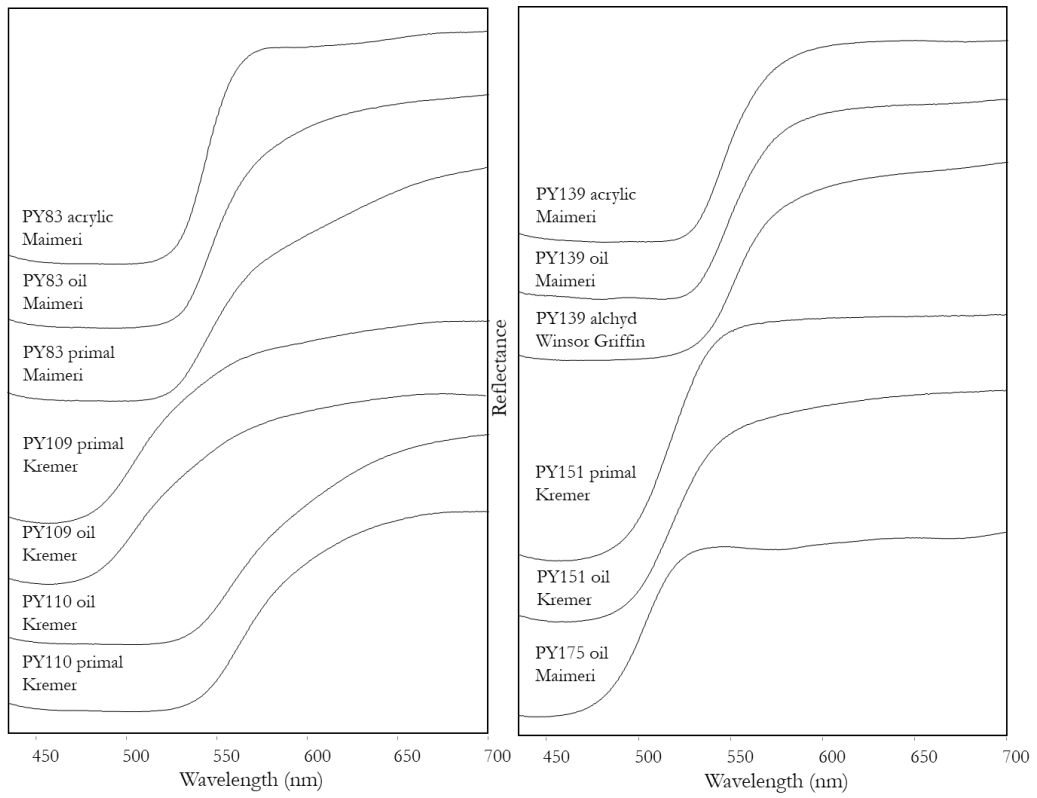
Visible reflectance spectra of red pigments



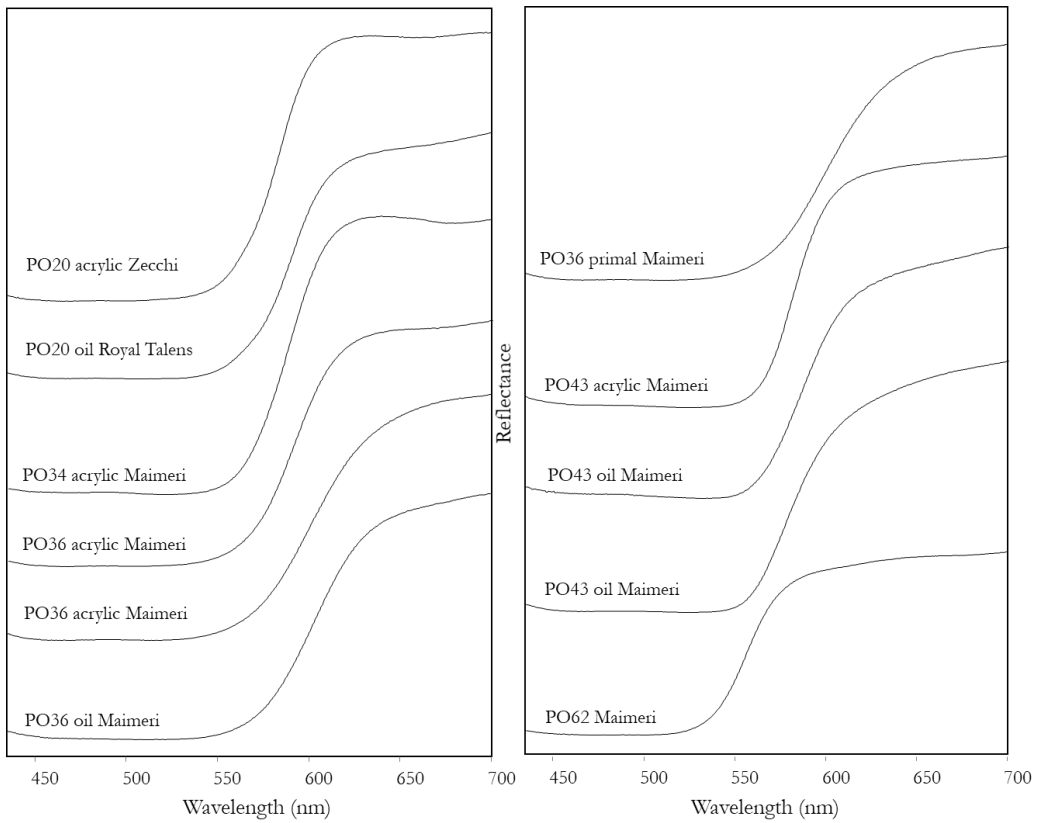


Visible reflectance spectra of yellow pigments

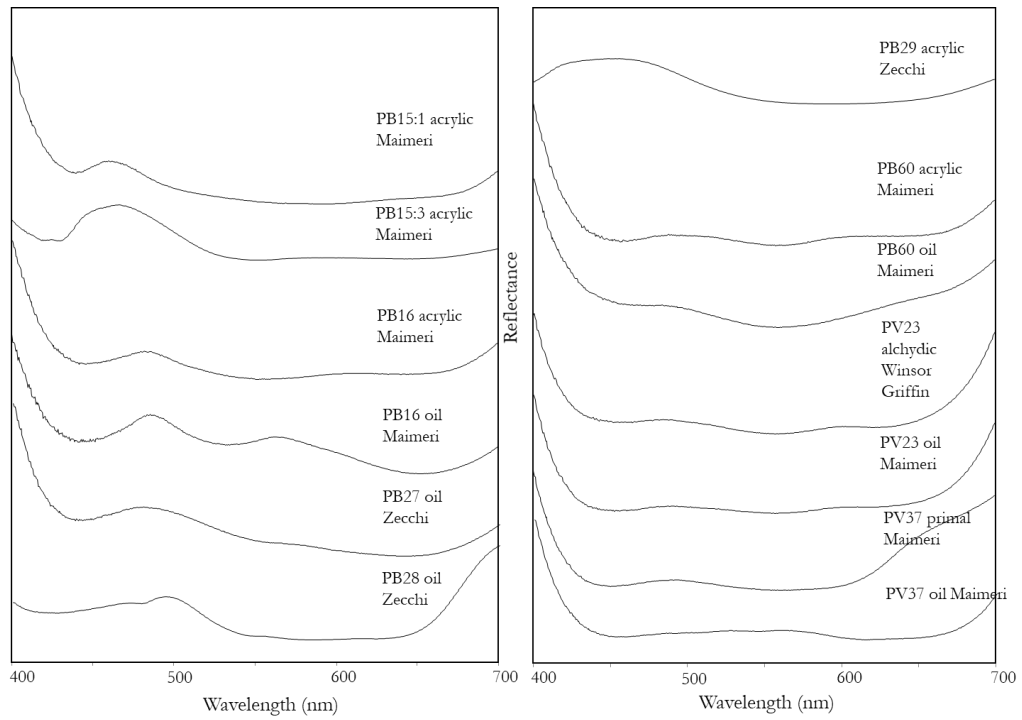




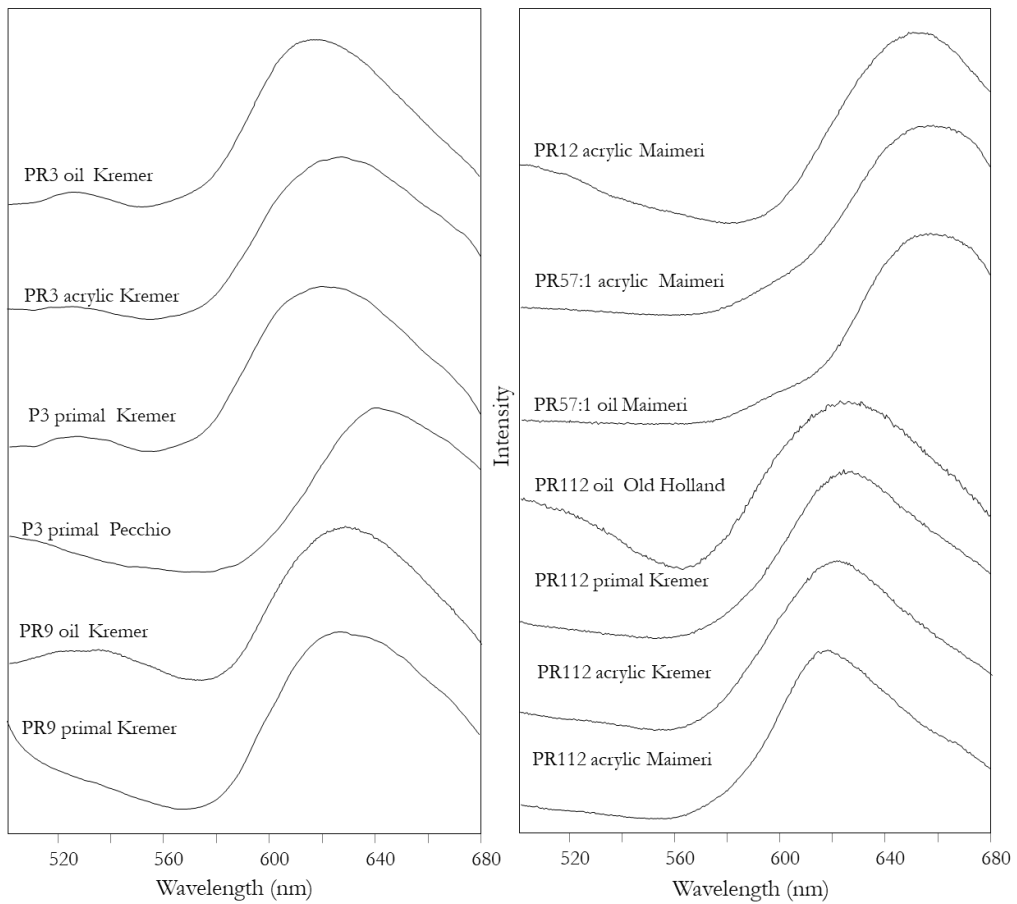
Visible reflectance spectra of orange pigments

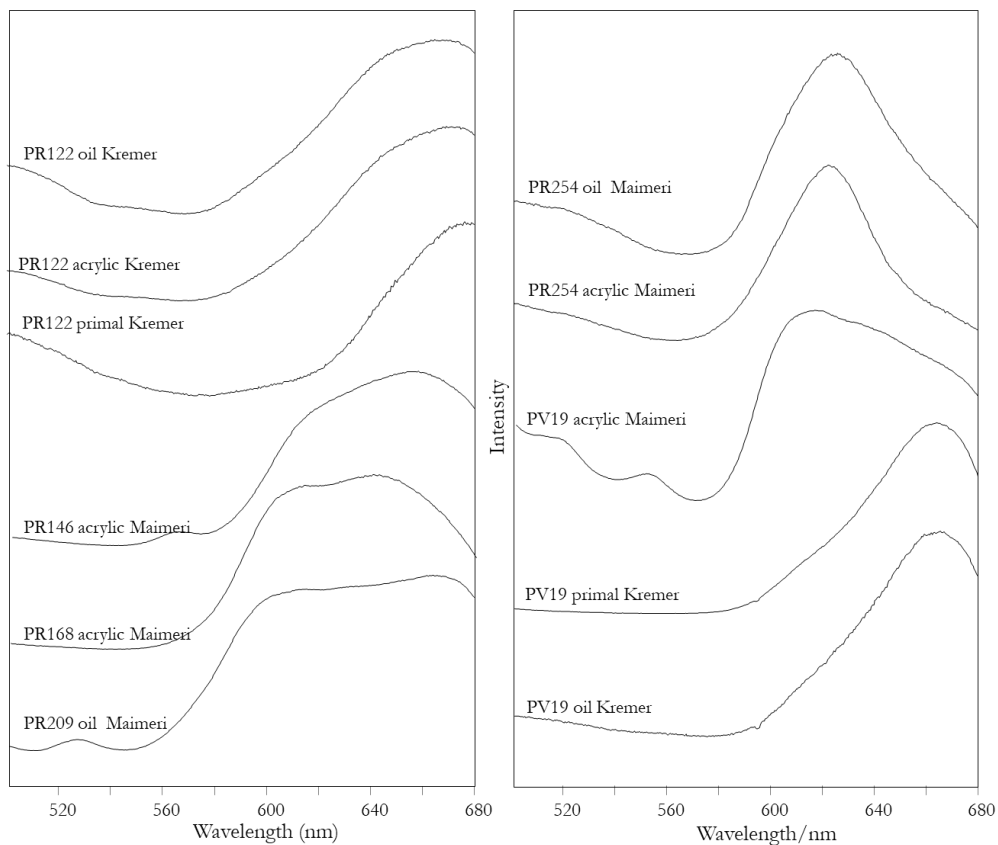


Visible reflectance spectra of blue and violet pigments

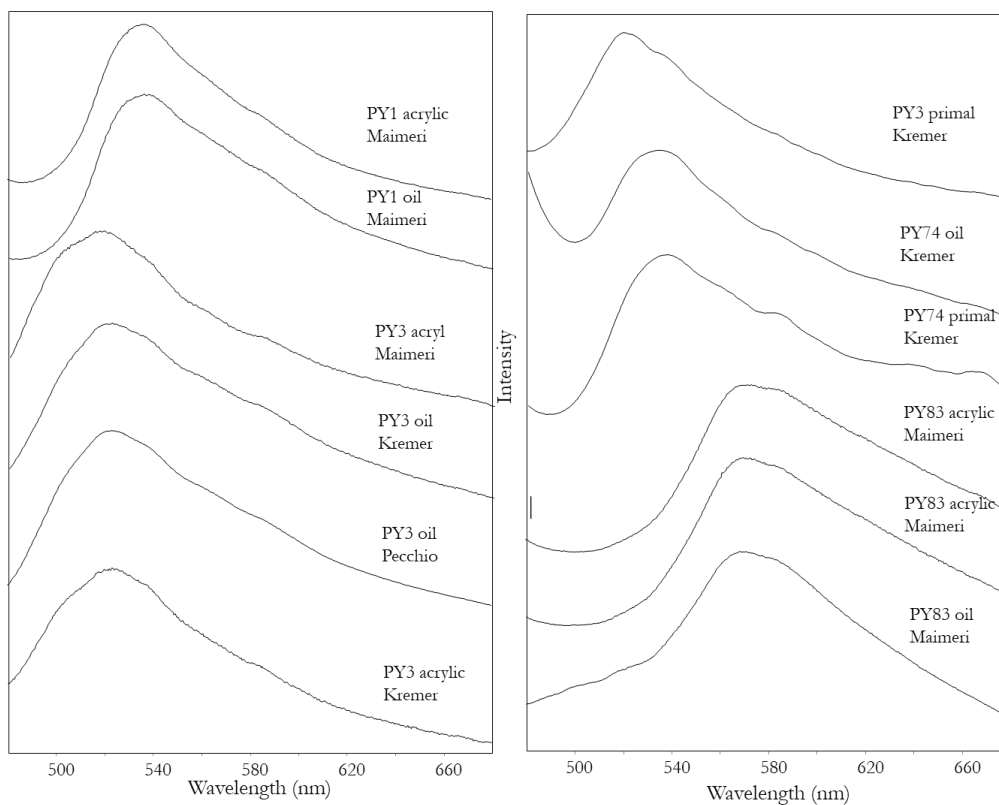


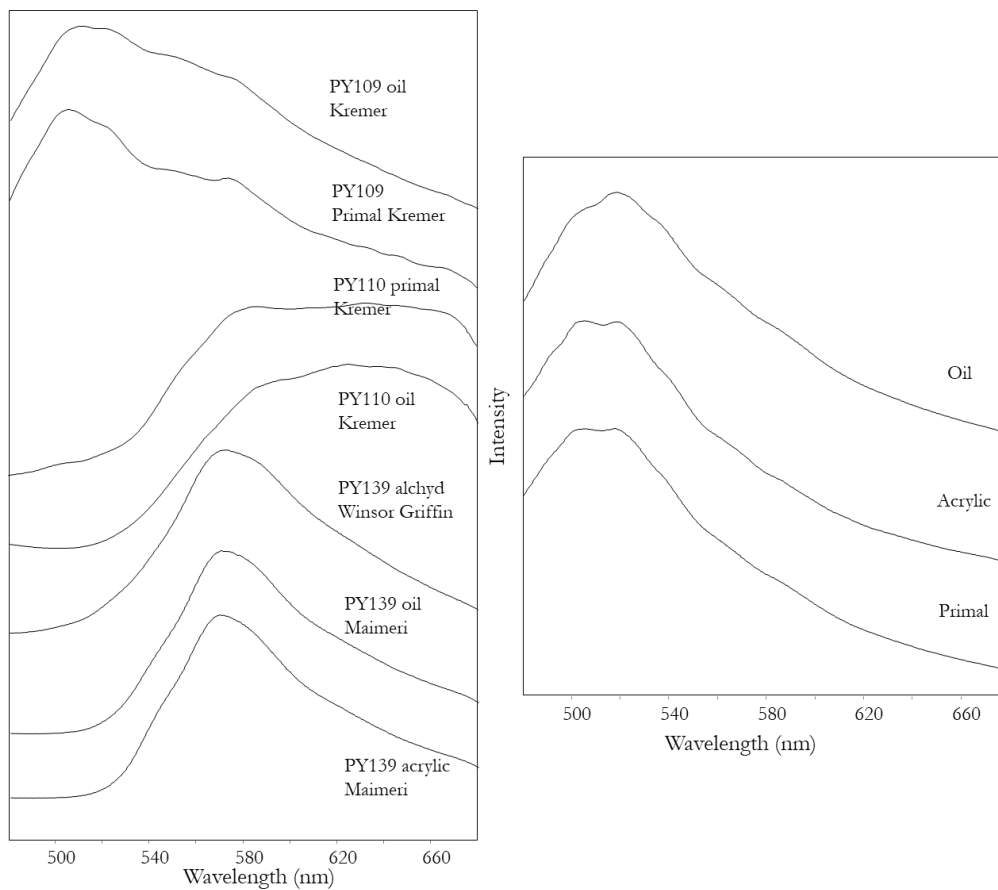
Visible-excited emission spectra of red pigments ($\lambda_{exc} = 435 \text{ nm}$)





Visible-excited emission spectra of yellow pigments and binders ($\lambda_{exc} = 435 \text{ nm}$)





Visible-excited emission spectra of orange pigments ($\lambda_{exc} = 435 \text{ nm}$)

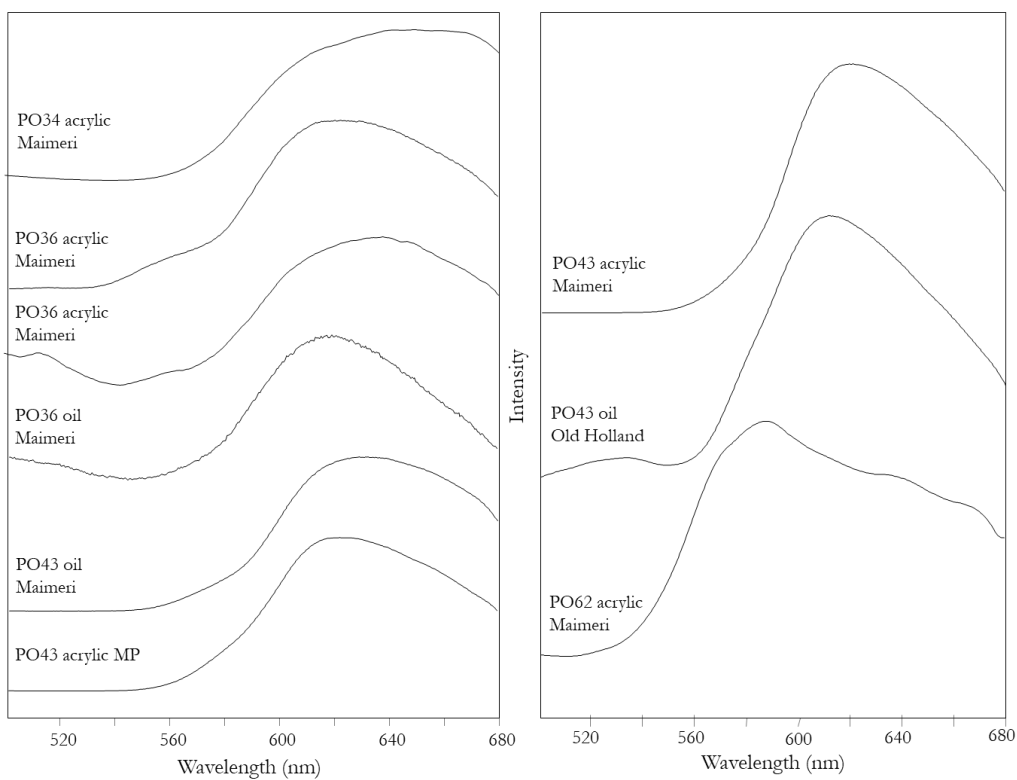


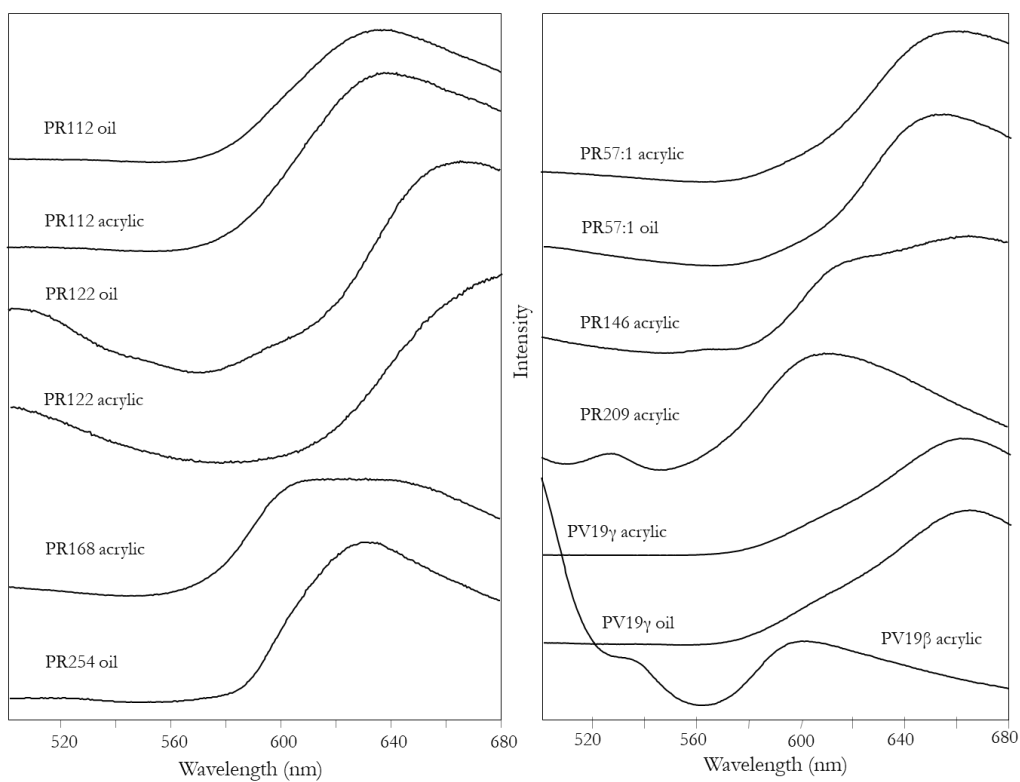
Table 1. Visible-excited fluorescence emission maxima of the analysed pigments. Not-fluorescent ones are not included.

Pigment	Emission maximum
Yellow	
PY1 oil Maimeri	536 nm
PY1 acrylic Maimeri	536 nm
PY3 acrylic Maimeri	524 nm
PY3 acrylic Kremer	522 nm
PY3 oil Old Holland Classic	522 nm
PY3 oil Pecchio	522 nm
PY3 primal Pecchio	521 nm
PY35 oil Zecchi	740 nm
PY35 oil Royal Talens	716 nm
PY74 oil Kremer	538 nm
PY74 primal Kremer	538 nm
PY83 acrylic Maimeri (com)	570 nm
PY83 acrylic Maimeri	570 nm
PY83 oil Maimeri	570 nm
PY97 acrylic Maimeri Brera	538 nm
PY109 oil Kremer	525 nm/586 nm (sh)
PY109 primal Kremer	522 nm/586 nm (sh)
PY110 oil Kremer	635 nm
PY110 primal Kremer	630 nm
PY139 alchyd Winsor & Griffin	570 nm
PY139 acrylic Maimeri	570 nm
PY139 oil Maimeri	570 nm
PY175 oil Maimeri Classic	522 nm
Binders	
Acrylic	518 nm/502 nm (sh)

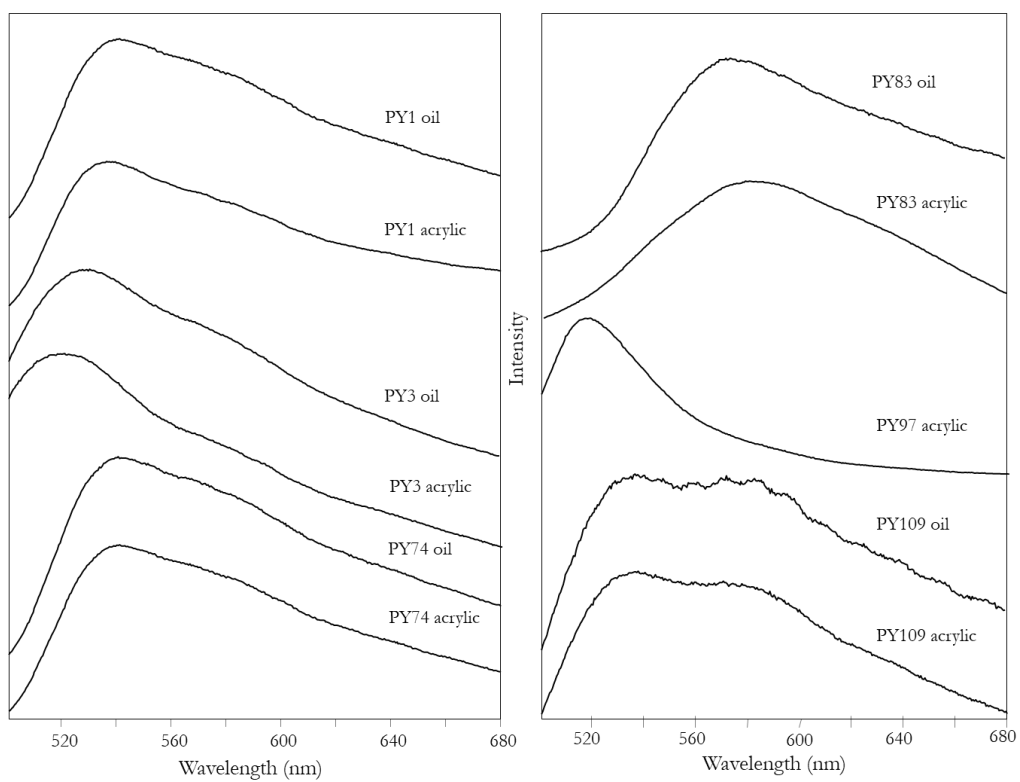
Oil	520 nm/502 nm (sh)
Primal	518 nm/ 502 nm (sh)
Orange	
PO20 acrylic Zecchi	790 nm
PO20 oil Zecchi	790 nm
PO20 oil Royal Talens	760 nm
PO34 acrylic Maimeri	645 nm
PO36 acrylic Maimeri	616 nm
PO36 oil Maimeri	617 nm
PO36 acrylic Maimeri PC	618 nm
PO43 acrylic Maimeri	615 nm
PO43 acrylic Brera Acrylyc	611 nm
PO43 oil Maimeri	625 nm
PO43 oil Maimeri	604 nm
PO62 acrylic Maimeri PC	586 nm
Red	
PR3 oil Kremer	617 nm
PR3 acrylic Kremer	620 nm
PR3 primal Pecchio	640 nm
PR3 oil Kremer	626 nm
PR9 oil Kremer	621 nm
PR9 primal Kremer	623 nm
PR12 acrylic Maimeri	652 nm
PR57:1 acrylic Maimeri	660 nm
PR57:1 oil Maimeri	661 nm
PR108 ((ilght) oil Zecchi	796 nm
PR108 (dark) oil Zecchi	801 nm
PR108 oil Royal Talens	801 nm

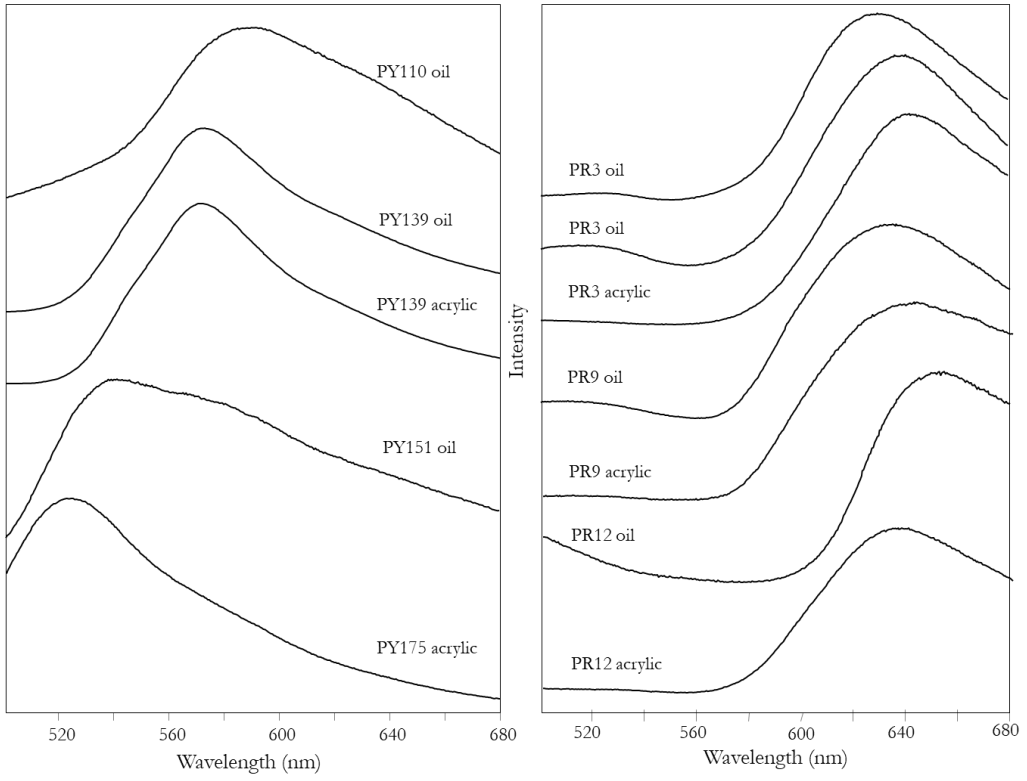
PR112 acrylic Maimeri	621 nm
PR112 oil Old Holland	623 nm
PR112 oil Kremer	628 nm
PR112 primal Kremer	630 nm
PR122 oil Kremer	665 nm
PR122 acrylic Kremer	670 nm
PR122 primal Kremer	670 nm
PR146 acrylic Maimeri	650 nm (broad)
PR168 acrylic Maimeri	640 nm (broad)/613 nm (sh)
PR209 oil Maimeri	668 nm (broad)/608 nm (sh)
PR254 oil Maimeri	624 nm
PR254 acrylic Maimeri	624 nm
Violet	
PV19 primal Kremer	662 nm
PV19 oil Kremer	663 nm
PV19 acrylic Maimeri	605 nm
PV23 alchidic Winsor Griffin	788 m
PV37 acrylic Maimeri	745 nm
Blue	
PB16 oil Maimeri	860 nm
PB29 oil Zecchi	680 nm

UV-excited emission spectra of red pigments ($\lambda_{exc} = 365\text{ nm}$)



UV-excited emission spectra of yellow pigments ($\lambda_{exc} = 365\text{ nm}$)





UV-excited emission spectra of orange pigments and binders ($\lambda_{exc} = 365 \text{ nm}$)

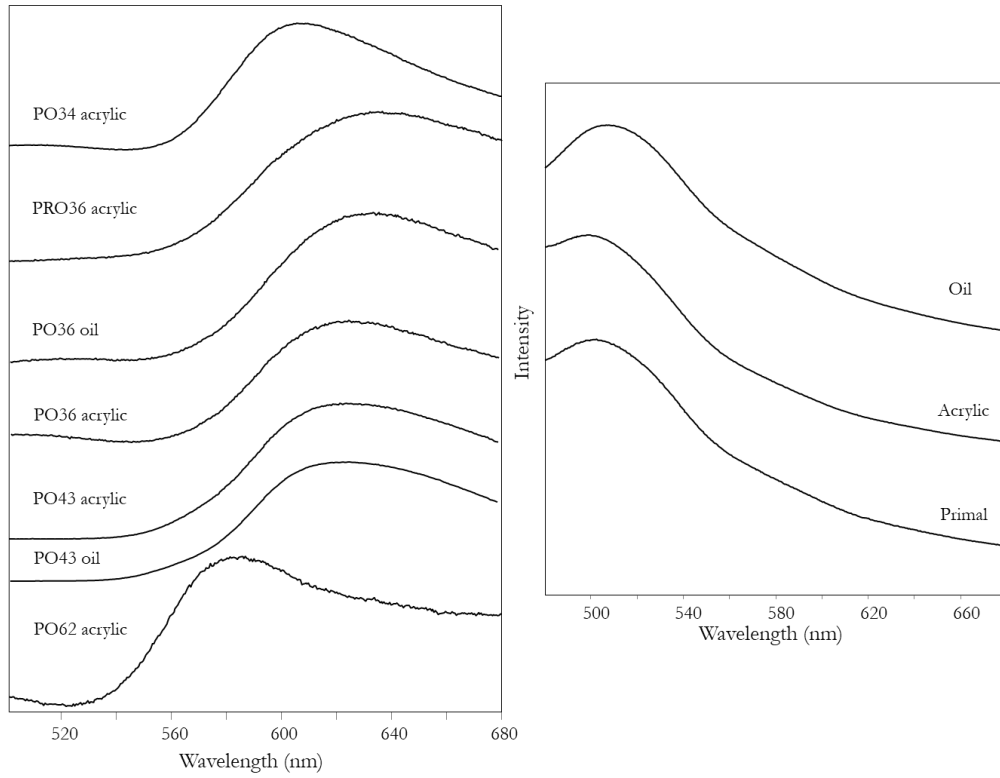


Table 2. UV-excited emission maxima of the analysed pigments. The non-fluorescent ones are not included. n.d. = not determined because of the superimposition of the 1st overtone of the exciting radiation at 730 nm.

Pigments	Emission maximum
Yellow	
PY1 acrylic Maimeri	539 nm
PY1 oil Maimeri	537 nm
PY3 primal Pecchio	525 nm
PY3 oil Pecchio	528 nm
PY3 acrylic Maimeri	516 nm
PY35 acrylic	690 nm
PY35 oil Zecchi	690 nm
PY74 oil Kremer	540 nm
PY74 primal Kremer	541 nm
PY83 acrylic Maimeri	573 nm
PY83 oil Maimeri	577 nm
PY97 acrylic Maimeri	517 nm
PY109 oil Kremer	535 nm / 580 nm (sh)
PY109 primal Kremer	535 nm / 580 nm (sh)
PY110 oil Kremer	588 nm / 630 nm (sh)
PY139 acrylic Maimeri	571 nm
PY139 oil Maimeri	571 nm
PY151 oil	538 nm
PY175 oil Maimeri	522 nm
Binders	
Oil	507 nm
Acrylic	498 nm
Vinavil	493 nm
Orange	
PO20 acrylic Zecchi	790 nm

PO20 oil Zecchi	790 nm
PO34 acrylic Maimeri	606 nm
PO36 acrylic Maimeri	623 nm
PO36 oil Maimeri	630 nm
PO36 acrivinylic Maimeri	630 nm
PO43 acrylic Maimeri	623 nm
PO43 oil Maimeri	623 nm
PO62 acrylic Maimeri PC	581 nm
Red	
PR3 oil Kremer	628 nm
PR3 primal Pecchio	640 nm
PR3 acrylic Kremer	587 nm
PR9 oil Kremer	616 nm
PR9 primal Kremer	640 nm
PR12 acril Maimeri	650 nm
PR57:1 acrylic Maimeri	657 nm
PR57:1 oil Maimeri	657 nm
PR108 acrylic Kremer	n.d.
PR108 oil Zecchi	n.d.
PR112 oil Kremer	637 nm
PR112 primal Kremer	638 nm
PR122 oil Kremer	665 nm
PR122 primal Kremer	670 nm
PR122 acrylic Kremer	674 nm
PR146 acrylic Maimeri	650 nm
PR168 acrylic Maimeri Brera	624 nm
PR206 acrylic Maimeri	610 nm
PR254 oil Maimeri	630 nm
PR254 acrylic Maimeri	630 nm
Blue	
PB16 acrylic Maimeri	n.d.
PB16 oil Maimeri	n.d.
PB29 acrylic Zecchi	680 nm
PB29 oil Zecchi	680 nm
Violet	
PV19 γ oil Kremer	664 nm

PV19 γ primal Kremer	663 nm
PV19 β acrylic Maimeri	600 nm
PV23 acrylic	n.d.
PV37 oil Maimeri	n.d.
PV37 acrylic Maimeri	n.d.

2. Score plots from PCA of emission spectra of reference samples

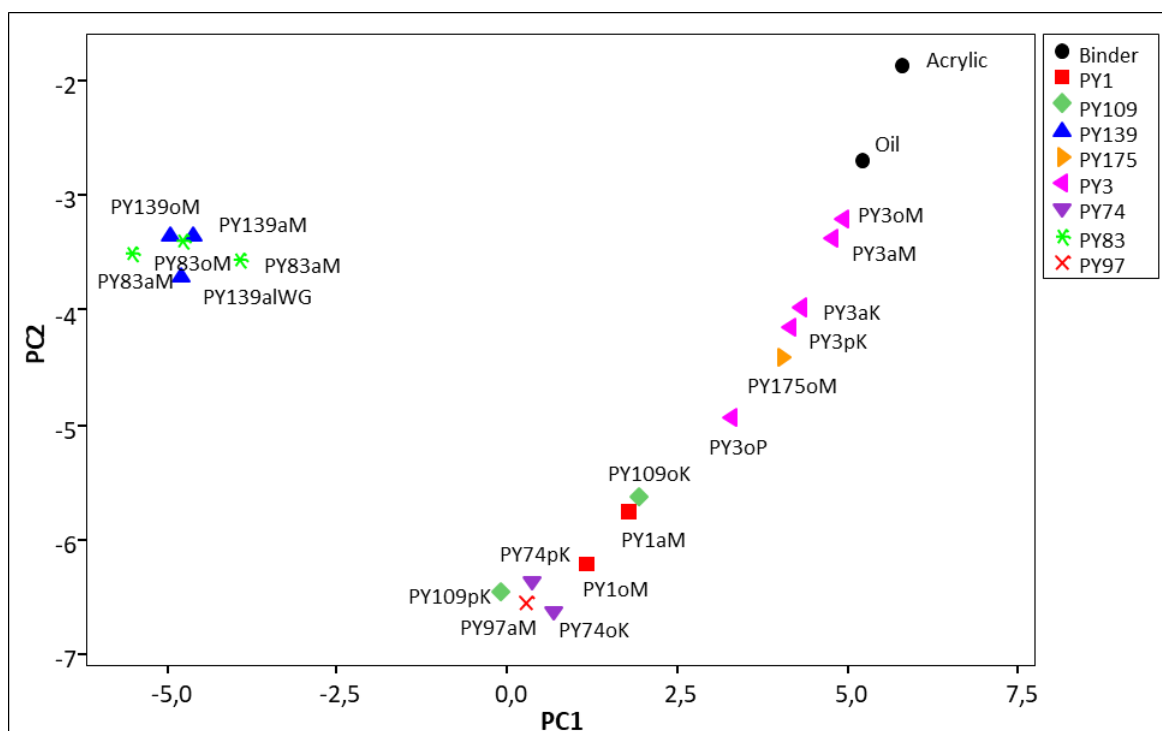


Figure 1. Score plot of the first two principal components of the emission spectra ($\lambda_{exc} = 435$ nm) of yellow pigments in painting mock samples on canvas including PY139 and PY83.

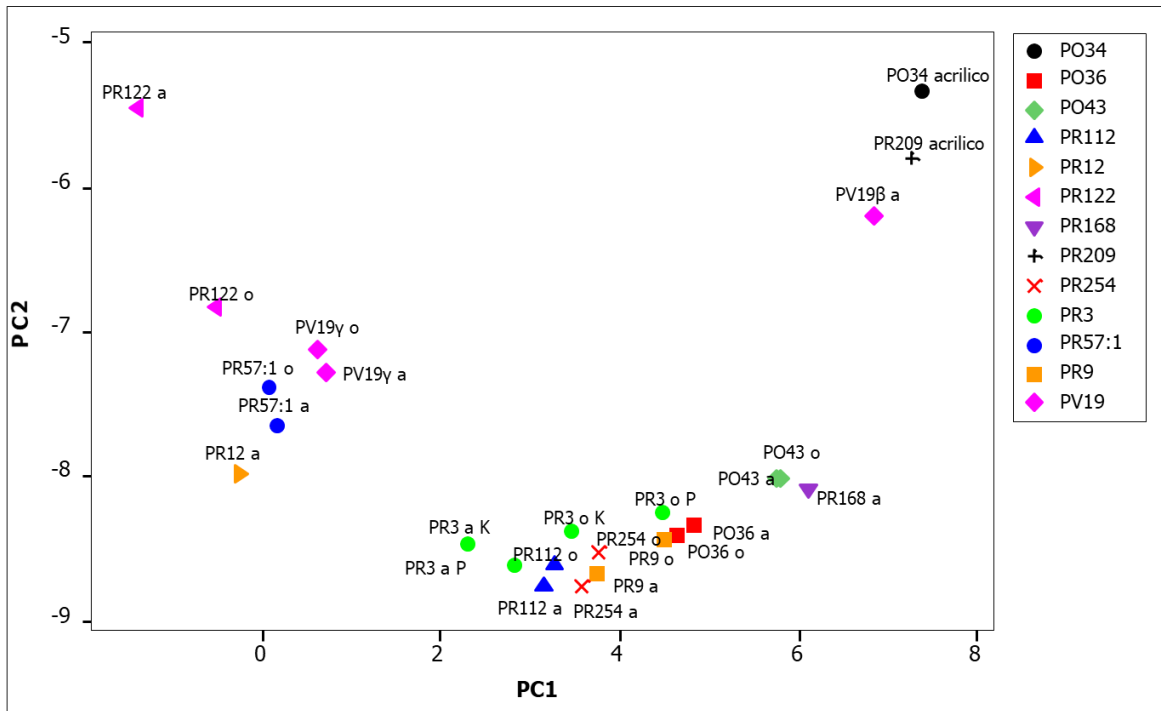


Figure 2. Score plot of the first two principal components of emission spectra ($\lambda_{exc} = 365 \text{ nm}$) of red pigments in painting mock samples on canvas including PO34, PR209 and PV19 β .

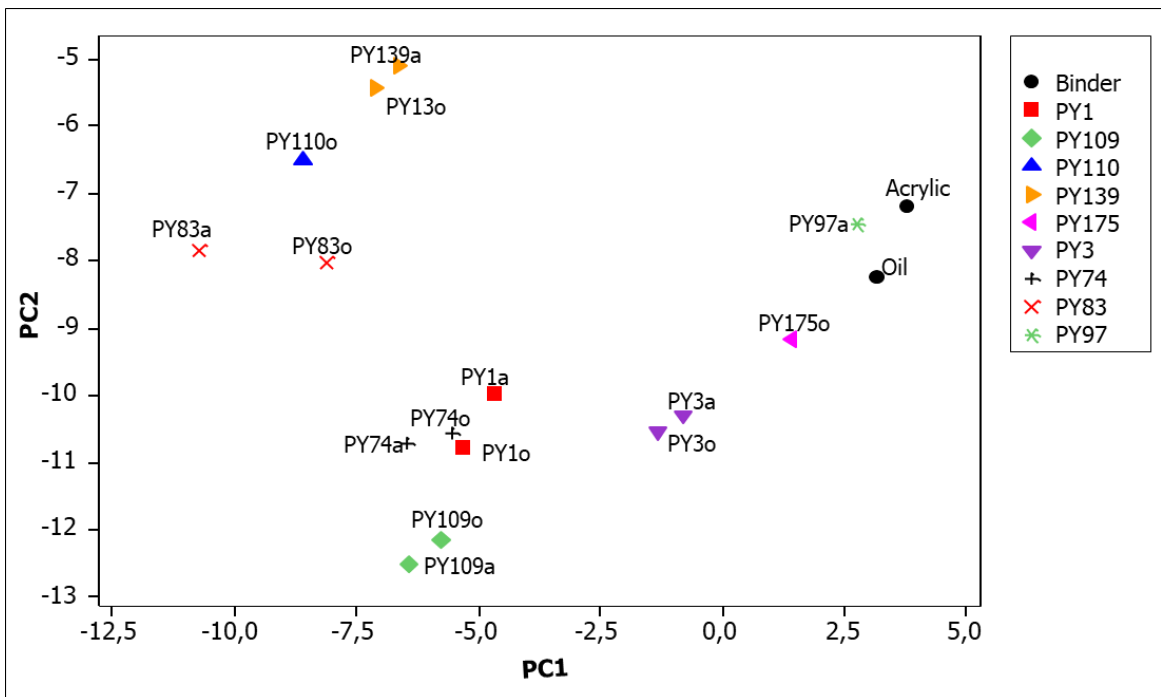


Figure 3. Score plot of the first two principal components of emission spectra ($\lambda_{exc} = 365 \text{ nm}$) of yellow pigments in painting mock samples on canvas including PY83, PY110 and PY139.

APPENDIX B

Identification of quinacridone pigments in artists' paints by micro-invasive IR and Raman methods

Abstract

During the first part of the work concerning spectrofluorimetry, two different commercially available PV19 and three PR122 pigments were examined and, despite what expected, they showed different emission spectra. A multi-analytical study combining IR and Raman methods with a suitable sample treatment to eliminate binders and inorganic fillers was therefore performed in order to understand the dual behaviour in fluorescence emission of these organic colourants.

1. Introduction

Quinacridones are high-performance pigments extensively used in the paint industry, in printing inks and for the coloration of plastics and textiles. They are very stable to light, heat, acids, alkali and solvents and, thanks to their brightness and high tinting strength, are really appreciated in the artistic field. Moreover, as already described in section 2.1.2.2 of chapter 2, methylation or halogenation of the quinacridone rings leads to different shades, from bluish-red to magenta-yellow. Pigment Violet 19 (PV19) and Pigment Red 122 (PR122) are among the most currently employed quinacridone pigments. The former (Fig. 1a), characterised by a red-violet shade, is the linear trans-quinacridone (QA), which exists in two different crystalline forms, the reddish γ -phase and the violet β -phase. The latter (Fig. 1b) is the 2,9-dimethylquinacridone (DMQA), whose colour is shifted to magenta-yellow by the presence of two methyl groups. [1]

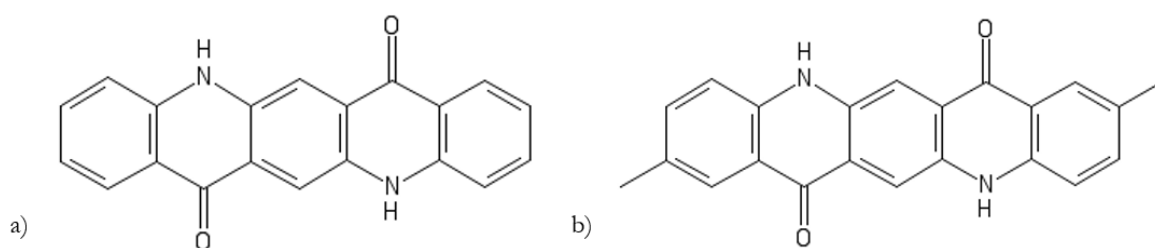


Figure 1. Chemical structure of a) PV19 and b) PR122

Until now, many analytical techniques have been applied for the characterisation of pure quinacridone pigments. X-ray diffraction (XRD) [2], Fourier-transform infrared (FTIR) [3, 4] and Raman spectroscopies [5, 6] allowed not only the identification of these colouring compounds, but also to understand their crystalline structure. However, when dealing with the commercial paints used by artists, the presence of additional components must be taken into account. Inorganic fillers (gypsum, calcite and silica) and/or binders (acrylic or oil) give strong signals which can hide the weaker ones due to the pigments. The commercial PV19 and PR122 pigments and paints were here examined by XRD, FT-IR and FT-Raman spectroscopies. The final aim is to identify the pigment molecules and to correlate this information to the different pattern of their emissions spectra. In particular, in the case of PR122, the powdered pigment spread in acrylic binder exhibited an emission maximum at 675 nm, while the commercial acrylic and oil formulations gave an absorption band shifted at 665 nm and 630 nm respectively. Referring to PV19, the pure colourant spread in acrylic showed an emission maximum at 605 nm, whereas the commercial formulation with the same binder at 662 nm (Fig. 2).

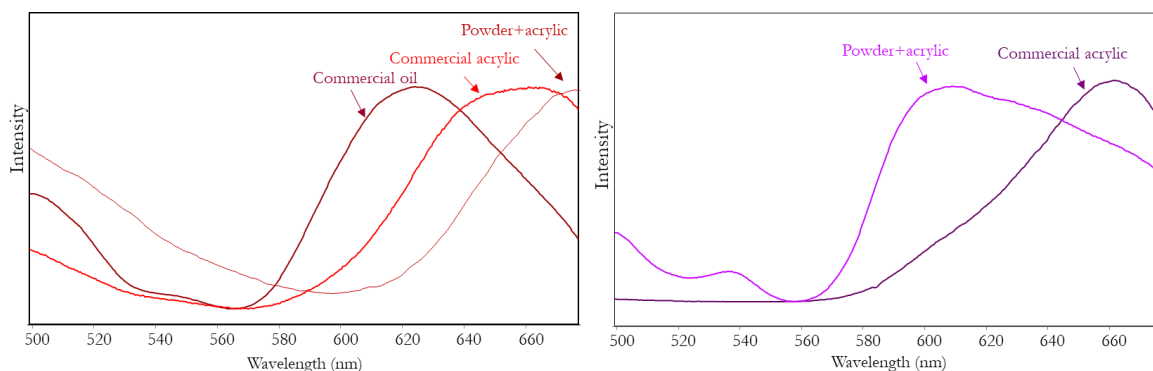


Figure 2. Emission spectra ($\lambda_{exc} = 435$ nm) of different commercially available PR122 (left) and PV19 (right).

To reach the goal of identifying the molecules responsible for the colour in the commercial paints, the main challenge was the at least partial removal of the fillers and/or binders.

2. Material and methods

2.1 Materials

Pure PV19 and PR122 powders were purchased from Kremer Pigmente, the acrylic paints containing respectively PV19 and PR122 were two products of the Maimeri Polycolor series and finally the oil-based PR122 was a Maimeri Classic Oil formulation.

Among the chemicals, hydrochloric acid min. 37% was obtained from Riedel-de Haën, methanol (assay, $\geq 99.9\%$), chloroform and ethyl acetate were purchased from Sigma-Aldrich.

2.2 Sample treatment

For pure powdered PV19 and PR122, all the analyses were performed directly on the pigments, without any treatment. On the other hand, the industrial paints were treated in order to partially eliminate the binders and the inorganic fillers.

In the case of the Maimeri acrylic formulation containing PV19 or PR122, the paints were first washed twice with ethyl acetate in order to partially dissolve the acrylic resin. The solvent was chosen considering that acrylic binders are presently based on copolymers between methyl methacrylate and another acrylate such as the *n*-butyl one [6]. Indeed, in a literature study on the solubility of poly(methyl methacrylate) [7], ethyl acetate appeared to be one of the most effective solvents. Afterwards, a 1% HCl aqueous solution was dropped to partially remove the calcite filler previously identified by FT-IR and XRD (section 3). When a further treatment with HCl proved to be necessary, it was performed by means of a 15% HCl aqueous solution. For the PR122 commercial oil paint, a 2:1 CH₃OH : CHCl₃ mixed solvent was used for the dissolution of the lipidic binder.

2.3. Instrumentation

FT-IR analyses were performed by a Jasco FTIR-620 spectrophotometer. All the samples were previously ground and dispersed in KBr to obtain pellets. The spectra were recorded as a sum of 16 scans with a 4 cm⁻¹ resolution.

FT-Raman spectra were recorded between 4000 and 200 cm⁻¹ by an RFT-600 Jasco FT-Raman spectrometer using for excitation the 1064 nm emission of a Nd:YAG laser. The output laser power was kept at 176 mW. A different number of scans according to the sample (between 100 and 300) was acquired. The resolution was 4 cm⁻¹.

For Raman analyses, a micro-Raman spectrometer equipped with a Jasco RPM-100 probe, provided with a notch filter and an Olympus 50x objective and interfaced by optical fibres to the laser and to a Lot-Oriel MS125 spectrometer, was used. The Andor CCD detector (1024 × 128 pixels) was cooled by means of a Peltier device. Two sources were employed to test different excitation wavelengths: a frequency-doubled Nd:YAG laser emitting at 532 nm and a diode laser emitting at 785 nm. Raman spectra were obtained by collecting 60 scans, with an exposure time of 2 s. In both cases an incident laser power of few milliwatts was used.

XRD analyses were performed by means of a Philips PW 1820 diffractometer with vertical scan. The instrument was equipped with collimator plates (Soller's slits), a single crystal graphite monochromator and a Na(Tl)I scintillation counter with impulse height amplification. The

incident radiation corresponded to Cu K α (1.5418 Å) (settings HV: 40 KV and 40 mA) and the acquisition was run at room temperature in the range 5°-65°.

3. Results and discussion

Preliminarily, all the quinacridone pigments were characterised by XRD. Apart from the pure powders, where the typical diffraction patterns of the PV19 (γ -phase) and PR122 crystalline structures were recognised (Fig. 3 a and c), the inorganic fillers prevented the identification of the colouring molecules. In the case of acrylic formulations, in fact, both for QA and DMQA, only calcite was detected (Fig. 3 b and d), while in the oil paint the pattern is dominated by a broad peak due to an amorphous component (datum non shown).

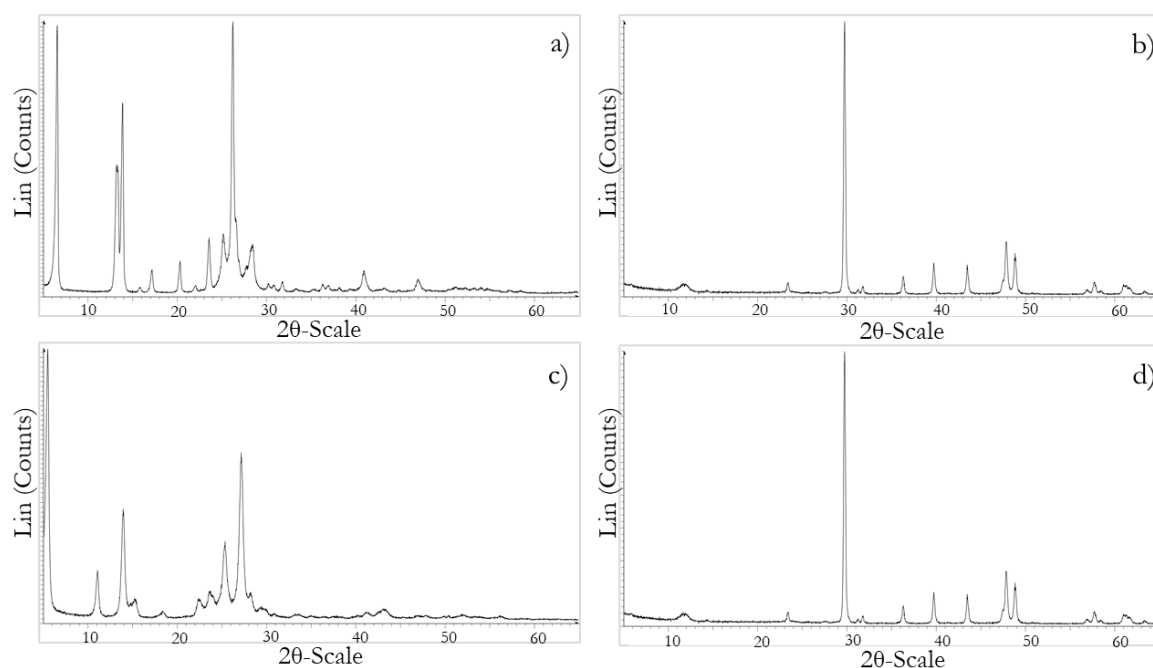


Figure 3. XRD patterns of PV19 (a) pure pigment, (b) acrylic paint and of PR122 (c) pure pigment; (d) acrylic paint. In both acrylic paints the observed peaks are due to calcite.

Subsequently, FT-IR analyses were performed on all the samples. Considering the interference of the inorganic components and/or of the binders, commercial paints were at first treated for their at least partial removal (See section 2.2). Concerning the two paints containing PR122, as shown in Fig. 4 and in agreement with what observed by XRD, even after sample treatment the prevailing signals in the FT-IR spectrum were those due to calcite for the acrylic paint and to amorphous silica for the oil one. In fact, CO₃²⁻ anions and Si-O bonds have very high absorption coefficients, thus their bands are largely predominant in the IR spectrum in comparison with those of any organic component. Nevertheless, some very weak bands due to DMQA were recognisable between 830 and 500 cm⁻¹ (box in Fig. 4 and Tab. 1). Similarly, for the paint

containing PV19 the main signals of QA could be observed as minor features between 1100 and 400 cm^{-1} (box in Fig. 4 and Tab. 1).

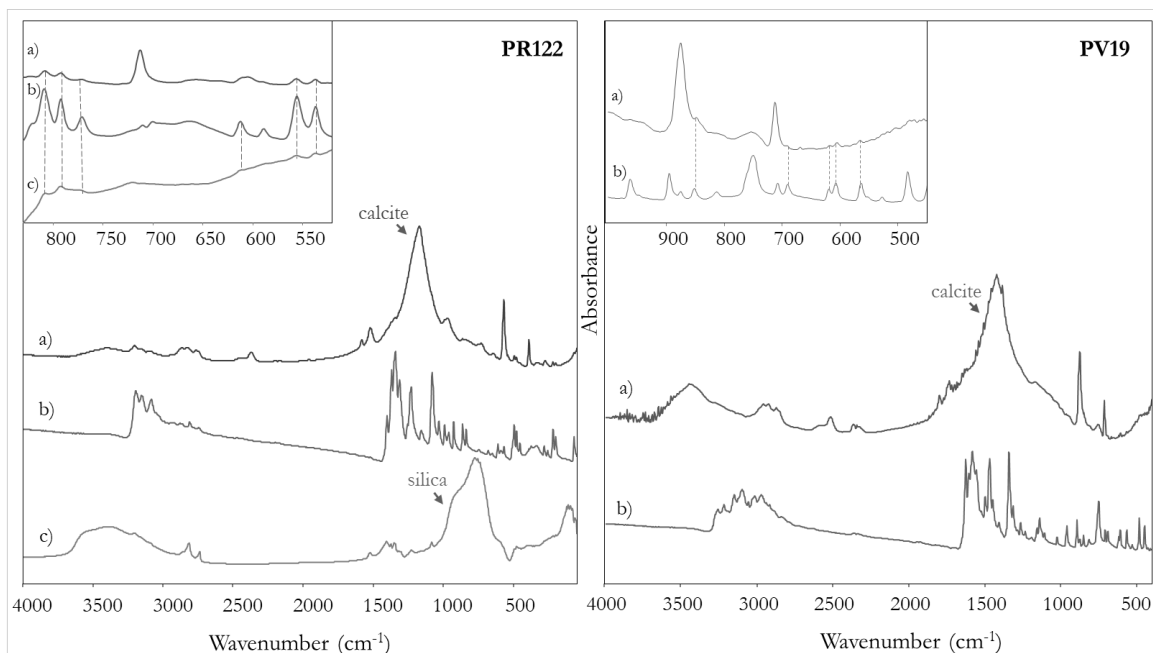


Figure 4. FT-IR spectra of the analysed PR122 and PV19 pure pigments and pre-treated paint samples: a) acrylic paint; b) pure powder; c) oil paint. The regions where the spectra of the paints show weak bands due to the pigments are enlarged in the boxes.

Table 1. FT-IR bands of PR122 and PV19 as pure pigments and acrylic and oil paint after treatment. * = bands due to calcite; ° = bands due to silica.

		<i>FTIR bands (cm⁻¹)</i>
PR122	Pure powder	3265, 3226, 3164, 2979, 2914, 2856, 1635, 1604, 1578, 1553, 1476, 1412, 1340, 1296, 1260, 1234, 1201, 1143, 1119, 1035, 976, 950, 915, 873, 808, 792, 771, 710, 700, 663, 612, 588, 555, 536
	Acrylic paint	3272, 3231, 3170, 2963, 2915, 2874, 2514, 1797*, 1741, 1424*, 1242, 1144, 1021, 946, 875*, 808, 792, 712*, 604, 555, 537
	Oil paint	3273, 3162, 2919, 2850, 1744, 1636, 1606, 1583, 1553, 1471, 1343, 1061°, 792, 466°
PV19	Pure Powder	3258, 3219, 3150, 3097, 3058, 3015, 2973, 2941, 2919, 2842, 1626, 1604, 1582, 1554, 1523, 1498, 1469, 1448, 1407, 1341, 1313, 1264, 1235, 1193, 1155, 1138, 1107, 1023, 961, 894, 874, 851, 813, 749, 707, 690, 69, 607, 564, 527, 483, 447
	Acrylic paint	2959, 2921, 2874, 2515, 2365, 2344, 1420*, 1166, 875*, 847, 712*, 668, 617, 605, 564, 527, 418

On the other hand, Raman spectroscopy, when applied to the paints, gave spectra dominated by an intense fluorescence background due to the binders and to the pigments themselves, both using a 532 and a 785 nm excitation wavelength.

As a consequence, FT-Raman analyses were performed, as the excitation in the near-infrared region (1064 nm), where most materials do not absorb, allows the quenching of the fluorescence emission.

Concerning PR122, the analyses made directly on the paint layers allowed us to detect only fluorescence for the oil paint and the presence of calcite in the case of the acrylic one. Small samples were thus taken and treated as described in section 2.2 to remove the oil binder in the first case and part of the acrylic binder and most of the calcite filler in the second one. In this way the signals due to DMQA became evident in the commercial formulations (Fig. 5 and Table 2). Referring to the acrylic paint, in order to further highlight the colourant molecules, a supplementary treatment with an HCl 15 % aqueous solution was performed. Similarly, for the paint containing PV19, before the partial elimination of calcite, only this compound was detectable in the FT-Raman spectrum, but after repeated washing with aqueous HCl the bands due to the pigment were evidenced (Fig. 5 and Tab. 2). It is worth noticing in the same spectrum the presence of intense bands due to the acrylic binder (Fig. 5 and Tab. 2) [8], which was only partially dissolved by ethyl acetate.

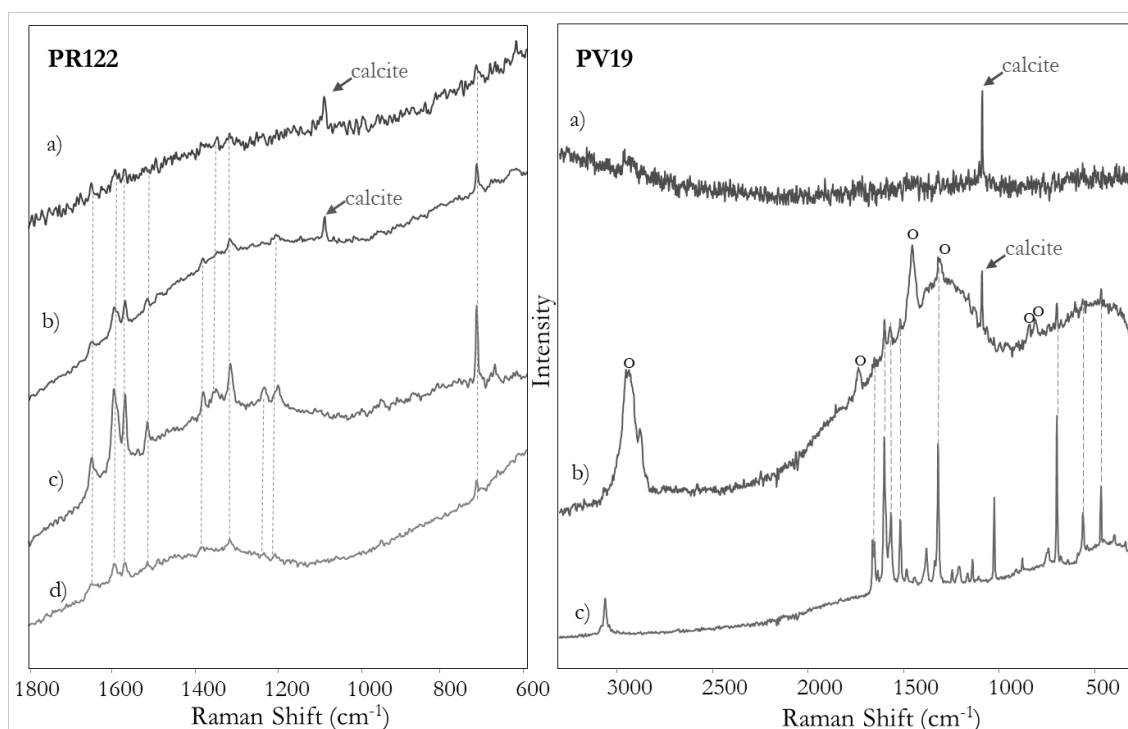


Figure 5. FT-Raman spectra of the analysed PR122 and PV19 pure pigments and paints: a) untreated acrylic paint; b) treated acrylic paint; c) pure powder; d) treated oil paint. Legend: o= band due to acrylic resin.

Table 2. FT-Raman bands of pure PR122 and PV19, acrylic and oil paint after treatment. * = bands due to calcite; ° = bands due to acrylic resin [8].

		<i>FT-Raman bands (cm⁻¹)</i>
PR122	Pure powder	1647, 1593, 1567, 1536, 1513, 1379, 1348, 1334, 1314, 1231, 1198, 721, 677, 537
	Acrylic paint	1648, 1593, 1567, 1511, 379, 1314, 1087*, 720
	Oil paint	1648, 1593, 1567, 1511, 1314, 720
PV19	Pure Powder	3060, 1660, 1651, 1628, 1598, 1563, 1514, 1481, 1440, 1243, 1208, 1162, 1137, 1023, 876, 739, 695, 558, 464
	Acrylic paint	2935, 2876, 1731°, 1598, 1565, 1512, 1452 °, 1311°, 1082*, 842°, 806°, 695

On the basis of these results, it was possible to conclude that the different fluorescence emission for PV19 can be attributable to two different crystalline forms of the unsubstituted quinacridone: as the γ form was confirmed by XRD analysis on the powdered pigments, the use of the β form is supposed for the commercial paint. On the other hand, in all the red paints analysed 2, 9-dimethyl quinacridone turned out to be the colouring molecule and no differences in the chemical structure or in the crystalline phase could be detected. In the light of this information, it was concluded that the origin of the observed shifts of the emission bands are related to the self-absorption phenomenon, and thus depend on the concentration of the pigment in the paints. As a matter of fact, when dealing with the pure powdered directly spread in the binders, the concentration of quinacridones is certainly higher than in the case of the commercial formulation, where the colourants are diluted in inorganic fillers. Therefore, a higher self-absorption takes place in the former case, determining an apparent shift of the emission band towards longer wavelengths.

4. Conclusion

The combination of micro-invasive IR and Raman methods led to the successful identification of the two quinacridone pigments PR122 and PV19 in acrylic and oil paints. Although these substances provide well-defined FT-IR and FT-Raman spectra when pure, the presence of additives and/or binders prevents their identification in commercial formulations. To this aim, a preliminary sample treatment was successfully applied in order to partially remove binders and inorganic fillers, highlighting the presence of DMQA and QA molecules in the FT-IR and, especially, FT-Raman spectra of both acrylic and oil formulation. Based on the obtained results,

it was possible to conclude that the difference in the emission spectra of the violet pigment PV19 is due to two different crystalline forms of the unsubstituted quinacridone, while for PR122 it was related to the self-absorption phenomenon determined by the concentration of the pigment itself in the different mock-up painting samples.

References

- [1] L. S. Quillen, *Reviews in Conservation* 2005, 6, 19-29.
- [2] L. S. Quillen, *J Coat Technol Res* 2010, 7, 331-346.
- [3] C. Binant, B. Guineau, A. Lautié, *J. Soc. Dye. Colour.* 1990, 106, 187-191.
- [4] G. Massonnet, W. Stoecklein, *Sci. Justice* 1999, 39, 135-140.
- [5] G. Massonnet, W. Stoecklein, *Sci. Justice* 1999, 39, 181-187.
- [6] T. Learner, Modern Paints in J. H. Stoner, Rushfield R. (eds.) *The Conservation of Easel Paintings*, Routledge, Oxon, 2012, 247.
- [7] I. Y. Evchuk, R. I. Musii, R. G. Makitra, R. E. Pristanskii. *Russ. J. Appl. Chem.* 2005, 78, 1576-1580.
- [8] G. Ellis G., M. Claybourn, Richards, *Spectrochim. Acta A* 1990, 46A, 227-241.

Chapter 3

FT-NIR Spectroscopy for the non-invasive study of binders and multi-layered structures in paintings

Abstract

This chapter is dedicated to the identification of natural binders and to the study of the complex stratigraphy in paintings by means of FT-IR spectroscopy. In particular, the potentiality of the near-infrared (NIR) region of spectra, dominated by the absorption bands due to CH, CO, OH and NH functional groups, is successfully exploited to distinguish a lipidic from a proteinaceous binder, as well as the coexistence of the two media in laboratory-made model samples simulating the complex multi-layered structure of a painting. The combination with multivariate analysis methods or with the calculation of indicative ratios between the intensity values of characteristic absorption bands are proposed to facilitate the interpretation of the spectral data. Moreover, the deeper penetration depth of the NIR radiation is exploited to have information about the inner layers of the paintings, in particular focusing the attention on the preparatory coatings of the supports. Finally, as a proof of concept, FT-NIR analyses are carried out on eight ancient paintings, dating to different centuries (from the end of the 15th to the end of the 18th) and exemplifying different artistic techniques.

1. Introduction

The analysis of binders, i.e. the media where pigments are dispersed to be spread on painting supports, is a relevant but challenging task in the field of conservation science.

Over the centuries, artists used a wide range of materials - siccative oils, natural gums and proteinaceous substances as egg, animal glue or milk derivatives -, associated with different painting techniques. Since antiquity, proteinaceous tempera based on water-diluted egg yolk was employed in painting, while egg white, vegetable gums and animal glues were preferred, separately or in mixture, to create illuminated manuscripts. In the Renaissance the use of siccative oils spread in European painting and they became progressively one of the most employed binding media during the Modern age. Moreover, artists experimented recipes based on mixed binders to improve and modify the painting properties or to obtain particular chromatic effects by combining their different features. This was, for example, the case of

tempera grassa, an emulsion of oil and egg or, sometimes, oil and casein. [1] In addition, also the preparatory layers, i.e. the coating spread on the support (typically a wooden panel or a canvas) before applying the subsequent layers, represent an important aspect in the investigation of a painting. They were traditionally made of white mineral substances mixed with an adhesive, usually animal glue. Gypsum ($\text{CaSO}_4 \cdot 2\text{H}_2\text{O}$) or calcite (CaCO_3) were the main raw materials, according to the geographical area of origin: the former was mostly adopted by artists from Mediterranean countries, the latter was typical of central and northern Europe [2].

In this scenario, the identification of binders is of major interest both for the restoration and conservation of paintings, as well as from an historical and artistic point of view. Until now, the analytical technique commonly employed for their investigation is gas chromatography, often coupled with mass spectrometry (GC/MS) [3-7]. Anyway, despite being a very sensitive and specific method, it suffers from the main disadvantage of being destructive and sample-requiring. A completely non-invasive approach should be instead highly recommended in the field of cultural heritage. Anyway, in comparison with inorganic pigments and fillers, the detection of binders represents a difficult task as they are present inserted in a complex system and more prone to chemical alterations. On the other hand, referring to the study of the composition of preparatory layers, it is achievable only when a sample containing the whole stratigraphy is available. The destructive methods (i.e. GC/MS), in fact, do not allow the discrimination of the layers, while the non-invasive ones generally enable the investigation of only the most superficial substances.

Among spectroscopic techniques traditionally employed for the non-invasive analysis of works of art, FT-IR spectroscopy has gained a key role thanks to the development of portable and compact instrumentation suitable for non-invasive *in-situ* analyses in reflection mode. Nevertheless, the mid-infrared (MIR) region ($4000\text{-}400\text{ cm}^{-1}$), which is commonly studied to characterise materials, is dominated by the strong absorption bands of the pigments or, in general, of the substances composing the surface layer of the painting, i.e. protective varnishes. On the other hand, the interval from $7500\text{ to }4000\text{ cm}^{-1}$ of the near-infrared (NIR) region shows interesting features for the identification of organic compounds. This spectral range is indeed dominated by overtone and combination bands, whose wavenumbers are multiples or sums of those of fundamental bands - due to stretching or bending vibrations - occurring in the MIR. These absorption bands are broader and less resolved than the fundamental ones, but, being orders of magnitude weaker, allow the acquisition of reflection spectra that do not require any spectral processing (for example Kramers-Kronig transform). Especially bands due to functional groups containing hydrogen atoms (e.g. OH, CH, NH) are located in the NIR part

of the spectrum and can be exploited to identify organic binders, although their broadness may cause overlapping in the case of mixtures and superimpositions. Moreover, the lower absorption coefficient and the higher energy of the NIR radiation enable a deeper penetration in comparison with the MIR one. This is a main advantage as, in principle, allows one to obtain compositional information about the layers below the surface.

For all these reasons, NIR spectroscopy has already been proposed for the identification of artistic binders, focusing in particular on pure substances [8, 9]. The work reported in this chapter aimed instead to investigate the possibility of exploiting FT-NIR spectroscopy to recognise binders in complex systems, as real paintings are. Moreover, the potential usefulness of the deeper penetration power of the NIR radiation to gain information about the inner layers of a painting was also considered. To this aim, mock-up painting samples were first of all realized in the laboratory following ancient recipes and using different binders to spread pigments in single or multiple layers on wood panels. In particular, inorganic pigments showing absorption bands in the NIR region were chosen in order to evaluate how they can affect the identification of the binders. Two different ground layers, respectively made of calcite or gypsum mixed with animal glue, were used for the models, considering that, differently from calcite, gypsum displays characteristic absorptions in this spectral region. Finally, a multivariate approach based on principal component analysis (PCA) of spectral data was also investigated as a possible tool to differentiate binders.

As a proof of concept, FT-NIR analyses were then carried out on ancient paintings, dating from the end of the 15th to the end of the 18th century and created on different supports with different techniques, to gain a wider insight on the applicability of this method for the non-invasive detection of binders and the stratigraphic study of paintings.

2. Objects of study

2.1 Artistic binders

Organic binders provide a matrix capable of adhering to the ground layer and suspending pigments. Specific materials were needed to form stable films with suitable physical (viscosity, adhesion, cohesion), chemical (stability and lightfastness) and optical (transparency) properties. During the centuries, painters experimented with a variety of materials as paint media, anyway the requirements for an appropriate binder strongly limited the choice. As a result of this centuries-old experimentation, siccative oils and proteinaceous materials such as egg, and to a lesser extent casein and animal glue, and polysaccharides became the most used binding media.

Indeed, these different materials are at the basis of the distinction between oil and tempera painting technique.

The term *tempera* generically refers to binders which are used in aqueous dispersion. According to their nature, two kinds of tempera can be identified: the one obtained from animal proteins such as egg, casein and glue and the one having a polysaccharide component of vegetable origin (i.e. Arabic gum, dammar). During the Medieval and Renaissance period, egg tempera was extensively used to create paintings on panel or polychrome sculptures. The most common recipe involved the use of yolk diluted in water and mixed with a small amount of vinegar to prevent fermentation processes. This mixture was then kneaded with powdered pigments, in different amounts according to the nature of the colourant itself and the taste of the artist: an excess of yolk leads to a “fat” and slow-drying pictorial film, a defect to an inhomogeneous surface, with lacklustre colours. On the other hand, egg white was largely employed in illuminations and decorated manuscripts, often in mixture with honey or sugar to confer flexibility to the film. [1, 10]

Since the 15th century, the use of siccative oils became common practice. Even if their application as binding medium was already reported from Greek and Romans historians, oil paint established itself in this period in the Flemish environment, where it was introduced by Jan Van Eyck. Subsequently, in the last decades of the same century, it arrived to Italy thanks to the activity of Antonello da Messina and widespread all over Europe. [1, 11] From the Renaissance to the 20th century, when synthetic materials appeared, oil was the most popular binder in artists’ workshops. However, it should be remarked that the transition between oil and tempera gave rise to mixed techniques, where the two binders were used in mixture. It is the case of the so-called *tempera grassa*, where oil was emulsified with a proteinaceous component, such as egg, glue, milk or casein. Among the greater masters, Leonardo da Vinci himself used to employ such method in painting. The superimposition of oil and tempera layers to create peculiar effects and shades was documented too. Siccative oils were really appreciated as their chemical structure, rich in long unsaturated chains of fatty acids, easily oxidises in the air, starting a polymerisation reaction from which solid consistence films were obtained. Linseed oil was the most used, as its structure gives painting films characterised by cohesion, resistance and elasticity. Anyway, it is prone to yellowing with time and for this reason sometimes it was replaced or mixed with other oils, such as poppy or walnut oil. They are less resistant and their filming properties are not comparable to those of linseed oil, but exhibit better optical properties. As a consequence, they were often used, pure or in mixture with linseed oil, to disperse white pigments [1].

2.2 Preparatory layers

The term preparatory or ground layer refers to the overall layers applied to the support (panel or canvas) before paintings are executed. The application of this coating is important to obtain a smooth and homogeneous surface, suitable to receive pigments. Its function is, in fact, to make the support less absorbent and brighter. The layer(s) applied should adhere to the support, be compatible with the subsequent paint layers and must remain stable over time. Because of its function, the ground layer cannot be considered an isolated one, but must always be related to the full stratigraphy of the painting. Features such as thickness, texture, degree of absorption and colour are part of the artistic technique: over the centuries, stylistic developments went hand-in-hand with changes in the materials.

Documentary research and analyses suggest that both for tempera and oil paintings on panel, grounds were generally bound with animal glue (often skin or parchment based), prepared by boiling the shredded material in water and using the filtered liquid.[13] Glue-bound grounds typically contained chalk or gypsum. Generally, chalk (CaCO_3) was predominant north of the Alps, while gypsum ($\text{CaSO}_4 \cdot 2\text{H}_2\text{O}$) was in use in the southern regions, probably due to local availability. With only a few exceptions, gypsum was the most common filler in Italy [2, 13].

Whereas the transition to oil painting during the 15th century did not result in changes in panel ground composition, it had its effect on the importance and meaning of insulating layers. An insulating layer applied to the ground, called *imprimitura* (primer or priming layer), became an indispensable feature since it prevented uneven absorption of the oil binder into the support. In addition to glue, unpigmented oil or oil-resin layers having such a function were identified. While the importance of the insulating layer increased, it became more diverse in both material composition and colour. Lead white is the main pigment found in such pigmented layers up to the 15th century [13], while coloured priming layers became a regular feature of Italian panel grounds towards the end of the same age [11]. Such thin, sometimes rather transparent priming layers consisted of lead white in oil, tinted with blacks, red or yellow earth pigments and sometimes minor additions of other pigments. In some cases, they were applied very diluted and simply toned.

Since the second half of the 15th century, the use of canvas instead of panel as painting support became common. This did not lead to significant variations in preparatory layers, unless for the lack of the thick gypsum coating that was applied to confer homogeneity and smoothness to the wooden support. The thickness of the preparatory layer became, in fact, extremely small (less than 100-150 μm), often to leave the texture of the canvas intentionally visible. During the

16th century, the use of a mixture of pigments and oil spread on canvas to reduce its porosity and to limit the absorption of oil binder became common practice because of its higher flexibility in comparison with gypsum. For example, canvas was often covered by a thin layer of animal glue mixed with white materials, such as chalk and lead white. Lately, from the second half of the 16th century and mainly during the 17th and 18th centuries, artists began to use dark-coloured primer layer, obtained by dispersing in oil earth pigments such as yellow and red ochre. [2]

3. Near-infrared (NIR) spectroscopy

Fourier-transform infrared spectroscopy (FT-IR) is a well-established analytical technique in the field of cultural heritage diagnostics. This vibrational spectroscopic analysis, in fact, provides information at the molecular level which results in the unambiguous identification of a wide range of organic and inorganic substances. Moreover, the recent technology led to the development of compact and portable instruments, suitable for measurements in reflection mode and thus allowing non-invasive analyses directly on the artistic objects in their place of conservation.

The mid-infrared (MIR) region, ranging from 4000 to 400 cm^{-1} , is most commonly studied as it hosts the fundamental vibration modes (stretching and bending) of molecules. In particular, two different parts can be distinguished in the spectrum, the functional groups and the fingerprint region, whose combined interpretation is uniquely associated with a specific compound [13, 14].

In the artistic field, infrared spectroscopy has been extensively employed for the examination of paintings and a consistent number of spectral databases and reference data are reported in the literature [15-19], allowing the identification of a wide range of compounds. However, it is worth noticing that this method is especially suitable for the identification of the substances in the most superficial layers of paintings. In particular, its main application is the identification of inorganic pigments, whose absorption bands are strong and intense in the MIR region. Otherwise, when there is a final layer of varnish on the surface of the artistic object, FT-IR spectroscopy enables its certain detection. Information about the composition of the different layers of a painting can be obtained analysing a cross section of a sample by the micro-FT-IR technique [20]. In this case, however, the non-invasive applicability of the method is intrinsically compromised by the need of a sample.

In recent years, the near-infrared (NIR) region has become object of research also in the diagnostics field and the potentiality of this part of the electromagnetic spectrum (in particular the interval 6500-4000 cm^{-1} , also referred as SWIR) has been studied. This spectral range,

corresponding to the first non-visible part and ranging from 13000 to 4000 cm^{-1} , was firstly discovered by Frederik William Herschel in 1800 [21]. However, during the 150 years after, it was neglected by scientists in favour of analytical methods providing more unambiguous results and because of the limited availability of suitable instrumentation. The situation radically changed in the second half of the 20th century when Karl Norris [22] conceived the modern NIR spectroscopy and Phil Williams introduced the application of this method for the analysis of protein and moisture content in wheat. Nowadays, NIR spectroscopy is considered of equal importance among the major analytical techniques and is currently applied for quality control in various fields, ranging from agriculture, food and cosmetics to pharmaceuticals. Indeed, it is a rapid, easy-to-use, chemical-free and non-destructive method allowing *in-situ* detection of substances directly in their packaging. [23]

NIR spectra comprise overtone and combination bands resulting from bond vibrations (stretching and bending) whose fundamental bands occur in the MIR region. These signals have a lower absorption coefficient, allowing for this reason the acquisition of spectra in reflection mode without distortions and possibly without requiring processing (such as the Kramers-Kronig transform). [24, 25]

The NIR spectral range is dominated by vibrational bands mainly associated with NH, CH and OH (together with CC) functional groups. NIR spectra result generally quite complex and characterised by broad and scarcely resolved signals. This can cause overlapping of the bands themselves, making it difficult to interpret the spectra as well as to extract information about a specific chemical component. In this respect, a multivariate approach is often adopted for a better understanding of the analytical results. [9, 25]

The functional groups showing signals in the NIR region, however, can be of great interest for the detection of artistic binders and natural varnishes. These substances, in fact, as already exposed in chapter 1, are characterised by functional groups (i.e. carboxyl and amino), which allow the distinction between a lipidic and a proteinaceous compound. In this respect, the exploitation of NIR spectroscopy for their identification has been already proposed, but mainly referring to the study of pure reference materials [8, 9]. Moreover, the higher energy and the lower absorption coefficient of NIR radiation, allows a deeper penetration [8], making possible, in principle, to reach the inner layers and detecting their composition (Fig. 1).

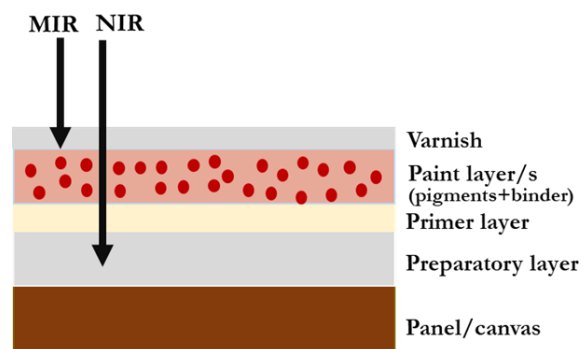


Figure 1. Schematic representation of the complex stratigraphy of a painting. NIR radiation is able to penetrate through the most superficial layer, in comparison with the MIR one.

4. Materials and methods

4.1 Materials

Pure reference materials were purchased from Maimeri and from local paint shops, while the inorganic pigments (lead white, azurite, yellow ochre and hematite) were from Zecchi. Gypsum and calcite were commercialised by Sigma-Aldrich. For the synthesis of lead palmitate, methanol, palmitic acid and lead nitrate were from Sigma Aldrich and ethanol from Fluka. For cross sections, the Struers Epofix Kit, containing Epoxy resin and Epofix hardener, was used.

4.2 Instrumentation

A FT-IR spectrophotometer Bruker Alpha was used for non-invasive analyses in reflection mode. The instrument is equipped with a reflection module for contactless measurements and a deuterated triglycine sulphate (DTGS) detector, operating at room temperature and ensuring a linear response in the spectral range between 7500 and 375 cm^{-1} . The FT-IR spectrophotometer collects spectra from a sample area with a diameter of around 6 mm and with a resolution of 4 cm^{-1} . An integrated video camera allows the operator to select the area to be measured. FT-IR spectra were recorded as sum of 200 scans after the acquisition of the background spectrum on a golden mirror. Reflection spectra in the MIR region were processed by Kramers–Kronig transform using Bruker OPUS software. In the NIR range they were instead transformed in pseudo-absorbance $\log(1/R)$.

4.3 Sample preparation

4.3.1 Pure reference materials

Pure reference substances were spread directly on glass slides and allowed to dry in the air or, especially in the case of drying oils, in an oven set at $\approx 50^\circ \text{C}$ to speed up the polymerisation

process. In particular the reference materials were: siccative oils (linseed, poppy and walnut), egg (white and yolk), animal glue, gum Arabic and dammar varnish.

4.3.2 Mock-up painting samples

Mock-up samples, simulating the complex layered structure of a real painting, were prepared on the basis of historical treatises and scientific reports [10-12]. They were painted on a wooden panel employing two different preparatory layers commonly adopted by artists, calcite and gypsum-based respectively.

In the first case, a ground layer made of calcium carbonate (CaCO_3) mixed with rabbit skin glue (ratio 1:7) was first applied on the wooden support. The mock-up samples were then prepared according to the stratigraphy reported in Tab. 1. The selected inorganic pigments were yellow ochre $\text{FeO}(\text{OH}) \cdot n\text{H}_2\text{O}$, azurite $2\text{Cu}(\text{CO}_3) \cdot \text{Cu}(\text{OH})_2$ and lead white $2\text{PbCO}_3 \cdot \text{Pb}(\text{OH})_2$, all showing absorption bands in the NIR region, which could overlap those of the binders. The chosen binding media were linseed or walnut oil, egg (whole or yolk) and a mixture of the two materials to obtain the so-called *tempera grassa*. Two identical series of samples were prepared and on one of them a final layer of dammar resin was applied as varnish.

For the second set of models, a preparatory layer made of gypsum ($\text{CaSO}_4 \cdot 2\text{H}_2\text{O}$) mixed with rabbit glue (ratio 2:1) was first applied on the wooden panel, followed by a second one (ratio 1:1). On this coating, two different pigments (lead white and hematite Fe_2O_3) were then applied with different binders, pure, in mixture or in multiple layers (see Tab. 1).

Table 1. Stratigraphy of the mock-up samples prepared on a wooden panel.

Preparatory layer	Priming layer	Binders	Pigments
CaCO_3 + animal glue	Animal glue	Tempera	Yellow ochre Lead white Azurite
		<i>Tempera grassa</i>	
		Linseed oil on tempera	
	Walnut oil + lead white	Linseed oil	
Walnut oil + lead white + red lead + lead tin yellow			
$\text{CaSO}_4 \cdot 2\text{H}_2\text{O}$ + animal glue	-	Linseed oil	Hematite Lead white
		Walnut oil	
		Tempera	
		<i>Tempera grassa</i>	
		Tempera on walnut oil	
		Tempera on linseed oil	

4.4 Preparation of cross sections

Cross sections were prepared from the mock-up samples to evaluate the thickness of the painting layers and to correlate it to the penetration depth of NIR radiation. For each sample, a

small fragment containing all the layers was carefully collected by a scalpel and placed into a silicon mould on an already hardened layer of the embedding resin. The latter was prepared by mixing Struers Epoxy resin and Epofix hardener in a 15:2 ratio and stirring until the mixture was completely homogenous. The sample was then covered with a second layer of resin and left to cure overnight. The cross sections were polished manually employing a lapping machine Struers Labopol-1 equipped with a magnetic rotating disk. Different silicon carbide abrasive papers with decreasing granulometry were used in succession, until the surface of the sample emerged from the resin block. Afterwards, a 6 μm DP-Struers diamond paste was used to obtain a perfectly smooth surface. Finally, the cross sections were observed and photographed by means of an Olympus optical microscope.

4.5 Multivariate analysis of data

FT-NIR spectra were processed by principal component analysis (PCA), performed by MINITAB 14 software. The spectra were first truncated between 6000 and 4000 cm^{-1} and normalised between 0 and 1. Afterwards, they were transformed into the corresponding 1st derivatives using GRAMS AI software (Thermo Fisher Scientific) and the Savitsky-Golay algorithm (2nd degree polynomial and 31 points), to eliminate the contribution of the baseline slope and to emphasise the differences among the spectra. In this case, the original variables of PCA analysis are the $dA/d\nu$ values in the range 6000-4000 cm^{-1} , while the samples are the spectra of the different mock-ups or of pure binders. The covariance matrix was used in order to give less weight to baseline points in the calculation.

4.6 Ratio calculation

To calculate ratios between band intensities, the baseline was subtracted from the spectrum and band heights were evaluated by using Grams/AI software. Absorption bands typical of oil or egg yolk respectively were chosen to exploit the ratio as discriminating value between the two binders (see section 5.3 for more details). When bands due to the gypsum ground layer were detected in the NIR spectrum, the contribution of calcium sulphate dihydrate was subtracted using the same software.

4.7 Synthesis of lead palmitate

Lead palmitate was synthesised following the procedure reported in [29]. 30 mL of a 0.02 M Pb $(\text{NO}_3)_2$ solution were prepared by dissolving 0.199 g of the lead salt in ethanol, water and methanol in proportions 5:5:2. A second solution of palmitic acid 0.02 M in methanol was then prepared by dissolving 0.064 g palmitic acid in 12.5 mL methanol. To promote the dissolution

of the acid, the solution was sonicated for several minutes, until it became clear and transparent. The two solutions were then mixed into a flask and left to react under sonication for 30 minutes. A dense, white suspension was thus obtained and filtered. The collected product was washed with hot water, ethanol and ether to eliminate any residual reagent and finally dried overnight. The next day, the remaining white powder was scraped off the filter paper and placed on a Petri dish in an oven at 50° C for about 2 hours, in order to evaporate all the residual water. Before performing FT-NIR analyses in reflection mode, the lead palmitate was analysed in transmission mode by FT-IR bench instrumentation to verify that the synthesis was successful. The acquired spectrum confirmed the nature of the product (data non shown).

4.8 Ancient paintings

In the present work, different paintings from the 15th to the 18th centuries were studied by FT-NIR spectroscopy. Three of the artworks under investigation belong to Leonardo's school and were painted in the last two decades of the 15th century. They are *The Virgin and Child (The Madonna of the Rose)* by Giovanni Antonio Boltraffio and *The Virgin feeding the Child* by an unknown painter of the Lombard school, all exposed by Poldi Pezzoli Museum in Milan (Italy), and *The Virgin and Child* by Francesco Galli, known as Francesco Napoletano, kept by Pinacoteca di Brera in Milan.

St. Augustine and St. Jerome was painted by the Lombard artist Ambrogio da Fossano, called Bergognone, at the end of the 15th century. The support is a wooden panel and it seems that originally this painting was part of a polyptych. Today it is stored in the Church of *the Certosa delle Grazie* in Pavia (Italy).

St. John the Baptist was represented by the Milanese artist Bernardo Zenale at the beginning of the 16th century. It is painted on a wooden panel and nowadays it belongs to a private collection. The painting on canvas *Porter boy sitting on a basket* is a work by the Italian artist Giacomo Ceruti, known as Pitocchetto ("the little beggar"), dating to ca. 1735. The painting, belonging to the Milanese Pinacoteca di Brera, is documented as an oil on canvas.

The masterpiece *Napoleon* is one of the several versions of Napoleon's portraits represented by Andrea Appiani. It dates back to the second half of the 18th century and it is described as an oil painting on canvas. It belongs to a private collection.

Finally, a peculiar case is represented by the work *Ecce homo* made by Andrea Solario on a paper support at the beginning of the 16th century. The artwork is exposed at the Accademia Carrara Art Gallery in Bergamo (Italy).

5. Results and discussion

5.1 Pure reference materials

NIR infrared spectra of siccative oils, proteinaceous substances, natural resins and some inorganic pigments commonly employed for preparatory layers were first acquired on pure reference materials.

Concerning drying oils, FT-NIR spectra are dominated by the absorption bands due to the combination of C–H stretching and bending, the first and second overtones of CH₂ stretching, the first overtone of ester carbonyl stretching mode and the combination of C=O and C–H stretching modes. The assignments for the main NIR bands are reported in Tab. 2 [8, 30]. The spectra acquired from different siccative oils, namely linseed (raw and heated), poppy and walnut oil, do not show significant differences in terms of shape and position of the bands (Fig. 2 and Tab. 2). As reported by [8], further considerations about the nature of this lipidic substances can be made on the basis of the first derivatives of the spectra. In fact, in the range between 4600 and 4000 cm⁻¹ the bands of the derivatives spectra have different relative intensities and wavenumber shifts, which can be helpful for identification purposes.

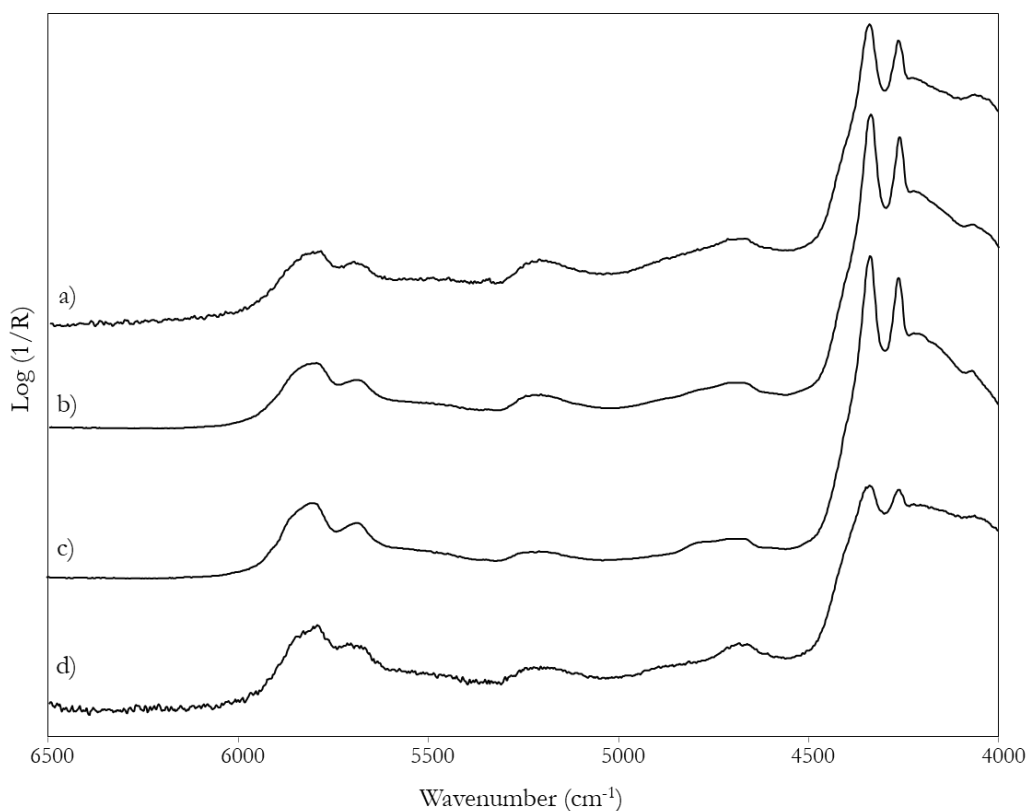


Figure 2. FT-NIR spectra of a) heated linseed oil b) raw linseed oil, c) poppy oil and d) walnut oil.

Table 2. Wavenumbers (cm⁻¹) of NIR bands of oils and tentative assignment [8, 30].

	Wavenumber (cm⁻¹)	Band assignment
Linseed oil (raw)	4259	$\nu_s(\text{CH}_2) + \delta(\text{CH}_2)$
	4333	$\nu_a(\text{CH}_2) + \delta(\text{CH}_2)$
	4686	$\nu_a(\text{CO}) + \nu_a(\text{CH}_2)$
	5208	2nd overtone $\nu(\text{C}=\text{O})$ ester
	5698	1st overtone $\nu_s(\text{CH}_2)$
	5805	1st overtone $\nu_a(\text{CH}_2)$
Linseed oil (heated)	4261	$\nu_s(\text{CH}_2) + \delta(\text{CH}_2)$
	4340	$\nu_a(\text{CH}_2) + \delta(\text{CH}_2)$
	4683	$\nu_a(\text{CO}) + \nu_a(\text{CH}_2)$
	5210	2nd overtone $\nu(\text{C}=\text{O})$ ester
	5696	1st overtone $\nu_s(\text{CH}_2)$
	5803	1st overtone $\nu_a(\text{CH}_2)$
Poppy oil	4260	$\nu_s(\text{CH}_2) + \delta(\text{CH}_2)$
	4341	$\nu_a(\text{CH}_2) + \delta(\text{CH}_2)$
	4675	$\nu_a(\text{CO}) + \nu_a(\text{CH}_2)$
	5216	2nd overtone $\nu(\text{C}=\text{O})$ ester
	5695	1st overtone $\nu_s(\text{CH}_2)$
	5803	1st overtone $\nu_a(\text{CH}_2)$
Walnut oil	4239	$\nu_s(\text{CH}_2) + \delta(\text{CH}_2)$
	4341	$\nu_a(\text{CH}_2) + \delta(\text{CH}_2)$
	4683	$\nu_a(\text{CO}) + \nu_a(\text{CH}_2)$
	5204	2nd overtone $\nu(\text{C}=\text{O})$ ester
	5698	1st overtone $\nu_s(\text{CH}_2)$
	5803	1st overtone $\nu_a(\text{CH}_2)$

Referring to proteinaceous materials, they are characterised by the combination of amide II band and the first overtone of carbonyl stretching mode, together with the combination bands of N–H stretching and bending modes. The discrimination among the different proteinaceous substances is rather challenging, with the exception of whole egg and, in particular, yolk. In fact, having yolk a lipidic component, its spectrum shows C–H combination and overtone bands which are much more intense than the other proteins [8, 31]. FT-NIR spectra of proteinaceous materials and the assignment of their bands are reported in Fig. 3 and Tab. 3 respectively.

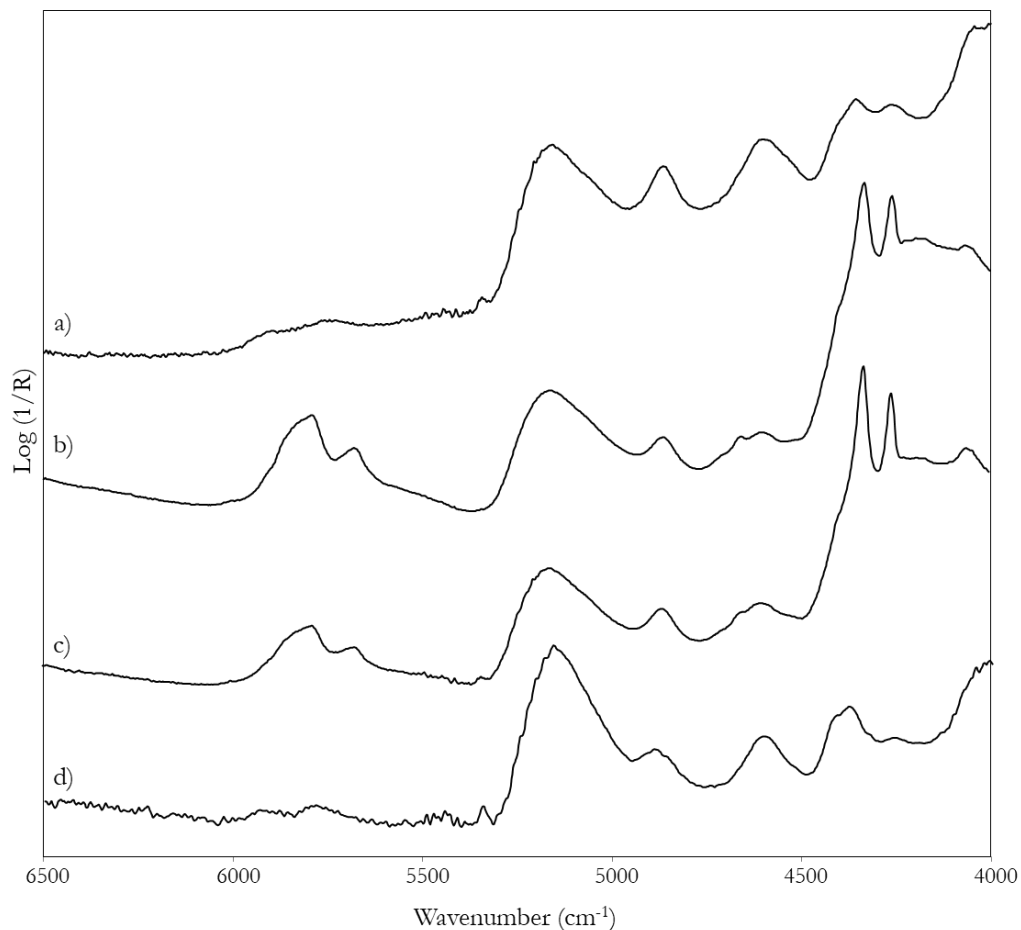


Figure 3. FT-NIR spectra of a) egg white b) egg yolk, c) yolk and d) animal glue.

Table 3. Wavenumbers (cm^{-1}) of NIR bands of proteinaceous materials and tentative assignment [8, 31].

	Wavenumber (cm^{-1})	Band assignment
Egg	4258	$\nu_s(\text{CH})+\delta(\text{CH})$
	4331	$\nu_a(\text{CH}_2)+\delta(\text{CH}_2)$
	4602	1st overtone $\nu(\text{CO})$ amide I+amide II
	4660	-
	4865	$\nu(\text{NH})+\delta(\text{NH})$
	5165	$\nu(\text{OH})+\delta(\text{OH})$
	5678	1st overtone $\nu_s(\text{CH}_2)$
	5794	1st overtone $\nu_a(\text{CH}_2)$
Yolk	4258	$\nu_s(\text{CH})+\delta(\text{CH})$
	4331	$\nu_a(\text{CH}_2)+\delta(\text{CH}_2)$
	4602	1st overtone $\nu(\text{CO})$ amide I+amide II
	4660	-
	4865	$\nu(\text{NH})+\delta(\text{NH})$
	5165	$\nu(\text{OH})+\delta(\text{OH})$
	5680	1st overtone $\nu_s(\text{CH}_2)$
	5793	1st overtone $\nu_a(\text{CH}_2)$

Egg white	4262	$\nu_s(\text{CH}_2)+\delta(\text{CH}_2)$
	4602	1st overtone $\nu(\text{CO})$ amide I+amide II
	4864	$\nu(\text{NH})+\delta(\text{NH})$
	5162	$\nu(\text{OH})+\delta(\text{OH})$
	5750	1st overtone $\nu_s(\text{CH}_2)$
Animal glue	4257	$\nu_s(\text{CH}_2)+\delta(\text{CH}_2)$
	4381	$\nu_a(\text{CH}_2)+\delta(\text{CH}_2)$
	4604	1st overtone $\nu(\text{CO})$ amide I+amide II
	4893	$\nu_s(\text{NH})+\delta(\text{NH})$
	5157	$\nu(\text{OH})+\delta(\text{OH})$
	5786	1st overtone $\nu(\text{CH}_2)$

Referring to natural varnishes, the NIR spectrum of dammar resin (Fig. 4b) shows the characteristic pattern of a triterpene resin, where the signals of the stretching and bending overtone bands are not resolved and result in a single broad band. A different case is represented by gum Arabic (Fig. 4a): being a polysaccharide its spectrum exhibits typical bands due to the combination of O–H stretching and bending modes, to the combination of C–H stretching and CH_2 bending and finally to the combination of C–H and C–C stretching modes (Tab. 4) [8].

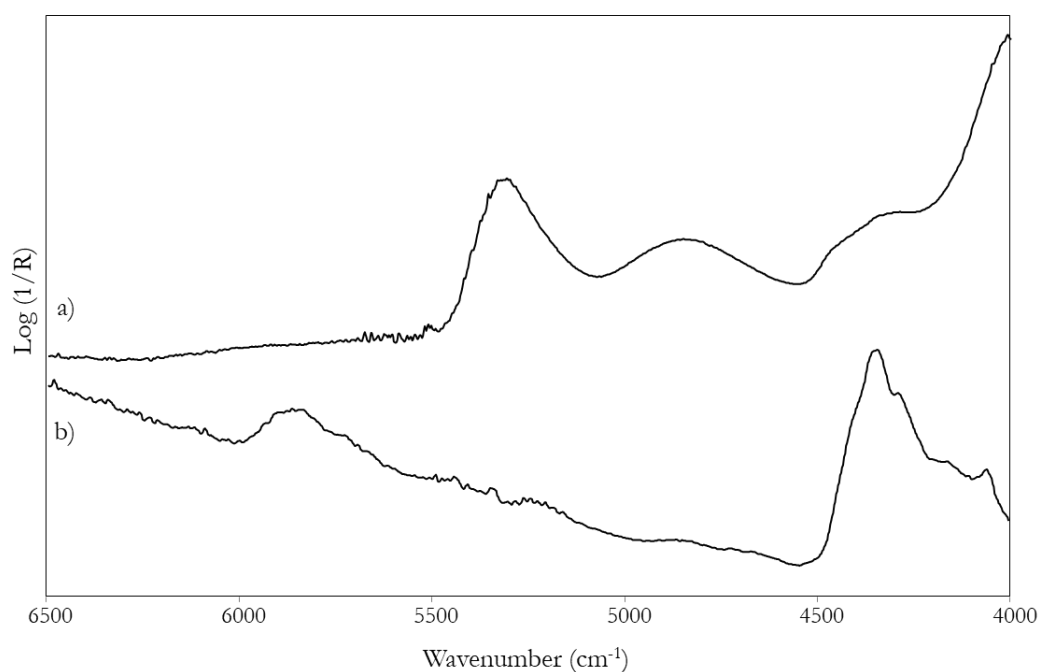


Figure 4. FT-NIR spectra of a) Arabic gum and b) dammar resin.

Table 4. wavenumbers (cm^{-1}) of NIR bands of gum Arabic and dammar and tentative assignment [8].

	Wavenumber (cm^{-1})	Band assignment
Gum Arabic	4260	$\nu_s(\text{CH})+\nu(\text{CC})$
	4300	$\nu(\text{CH})+\delta(\text{CH}_2)$
	4750	$\nu_a(\text{CH})+\nu(\text{CC})$
	5160	$\nu(\text{OH})+\delta(\text{OH})$

Dammar	4057	3rd overtone $\delta(\text{CC})$
	4164	$\nu_s(\text{CH}_2)+\delta(\text{CH}_2)$
	4345	$\nu_a(\text{CH}_2)+\delta(\text{CH}_2)$
	4632	1st overtone $\nu(\text{CO})$ amide I+amide II
	4830	$\nu(\text{CO})+\nu(\text{OH})$
	5190	$\nu(\text{OH})+\delta(\text{OH})$
	5737	1st overtone $\nu_s(\text{CH}_2)$
	5864	1st overtone $\nu_a(\text{CH}_2)$

Obviously, all the examined binders show peculiar features also in the MIR region (Fig. 5). In particular, oil and egg (especially yolk) exhibit a narrow band at 1740 cm^{-1} , due to the C=O stretching mode of the lipidic component (Fig. 5 a and b). On the other hand, the proteinaceous materials show the bands typical of amide bonds, such as the C–N–H stretching band around 1650 cm^{-1} (Fig. 5 b for egg and c for animal glue). Referring to gum Arabic, its spectrum (Fig. 5e) is dominated by the bands due to hydroxyl group. The band assignments are reported in Tab. 5. However, it is worth remembering that these spectral features are well recognisable studying pure reference materials, but when dealing with complex systems such as a painting, the signals due to those inorganic pigments that absorb in MID-IR prevail, strongly limiting the possibility of identifying the binding media.

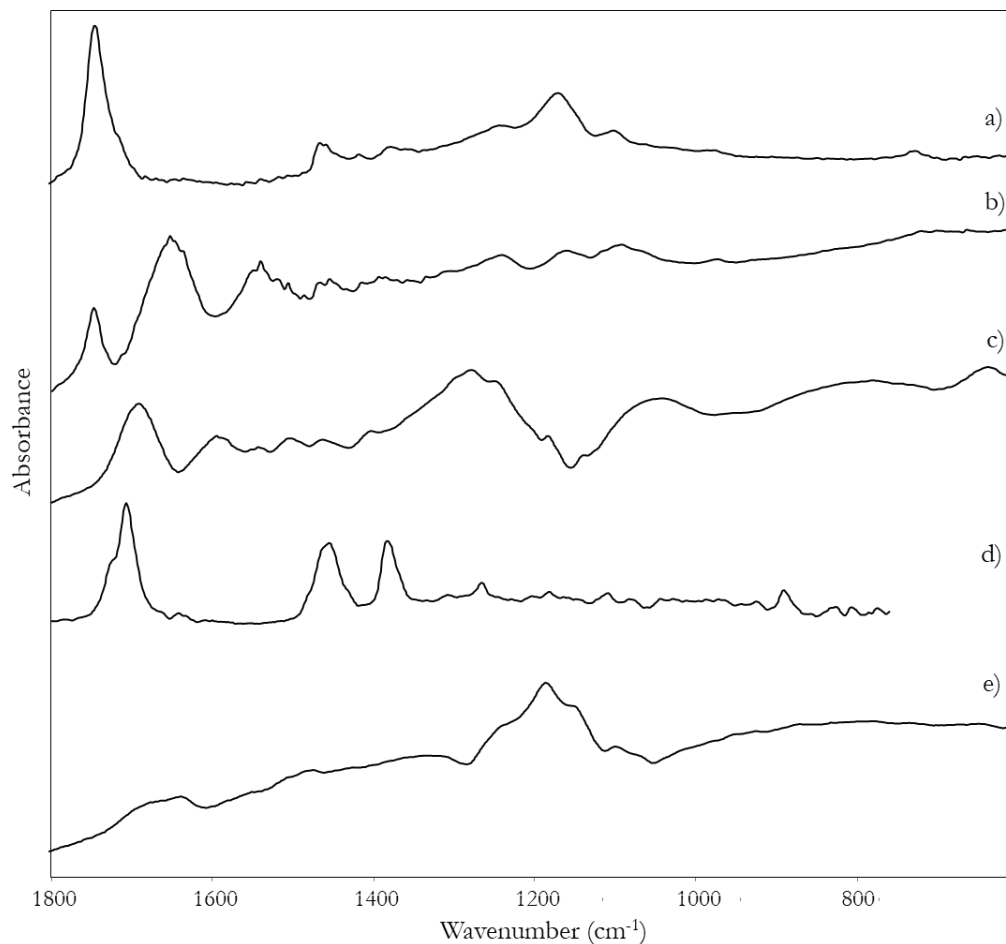


Figure 5. FT-NIR spectra of a) linseed oil, b) egg, c) animal glue, d) dammar and e) gum Arabic.

Table 5. Wavenumbers (cm^{-1}) of NIR bands of binders and natural varnishes and tentative assignment [32].

	Wavenumber (cm^{-1})	Band assignment
Oil	1750-1730	C=O stretching band
	1480-1300	C-H bending bands
	1300-9900	C-O stretching bands
	750-700	C-H torsion band
Yolk	1750-1600	C=O stretching bands
	1565-1500	C-N-H bending band
	1480-1300	C-H bending band
Animal glue	1660-1600	C=O stretching band
	1565-1500	C-N-H bending band
	1480-1300	C-H bending band
Arabic gum	1650	O-H bending bands
	1480-1300	C-H bending bands
	1300-900	C-O stretching bands
Dammar	1740-1640	C=O stretching band
	1650-1600	O-H bending band
	1480-1300	C-H bending band
	1300-900	C-O stretching bands

In addition, also some inorganic pigments that are commonly used in preparatory or priming layers can show absorption bands in the NIR region. This is the case of gypsum $\text{CaSO}_4 \cdot 2\text{H}_2\text{O}$ and lead white $2\text{Pb}(\text{CO}_3)_2 \cdot \text{Pb}(\text{OH})_2$, whose chemical structure is characterised by the presence of water molecules or hydroxyl groups. On the other hand, calcite CaCO_3 , another mineral substance historically employed to prepare canvases and panels, does not show significant absorption bands in this spectral range. NIR spectra and band assignments of these substances are reported in Fig. 6 and in Tab. 6. In particular, lead white (Fig. 6b) shows signals due to the combination of O–H stretching and the deformation modes of Pb–OH [8, 33, 34], while gypsum (Fig. 6a) those due to the combination of the stretching and bending modes of hydroxyl group [8, 34-36].

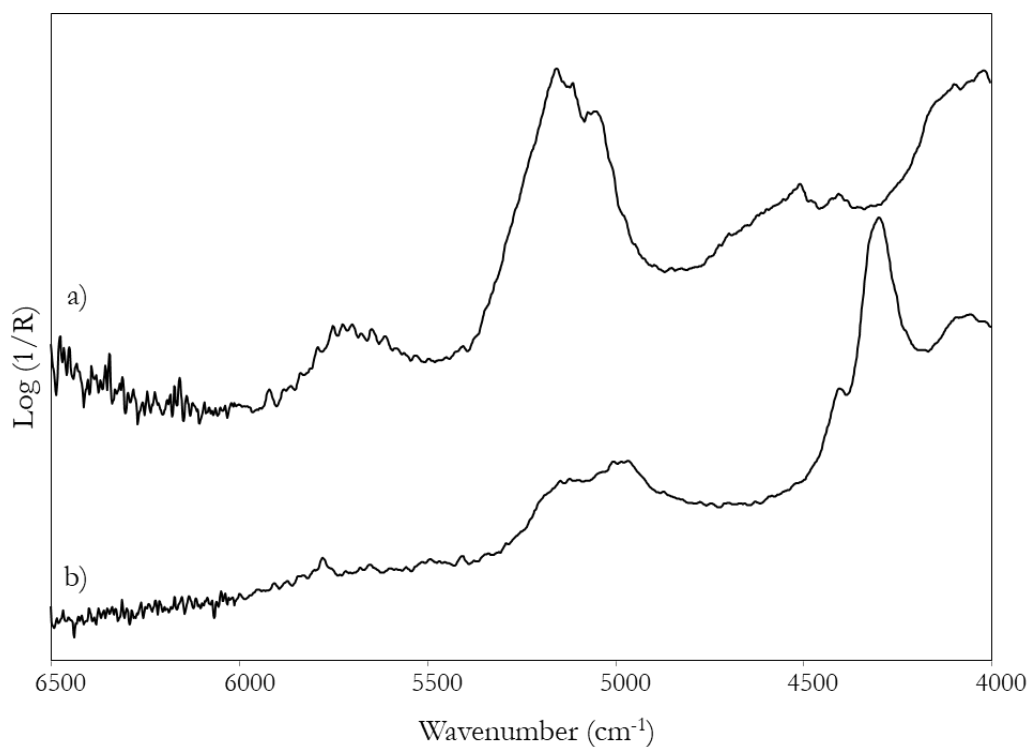


Figure 6. FT-NIR spectra of a) gypsum and b) lead white.

Table 6. Wavenumbers (cm^{-1}) of NIR bands of gypsum and lead white and tentative assignment [8].

	Wavenumber (cm^{-1})	Band assignment
Gypsum	4401	-
	4506	$\nu_s(\text{OH})+\delta(\text{OH})$
	5051sh	-
	5150	$\nu_a(\text{OH})+\delta(\text{OH})$
	5726	-

Lead white	4300	$\nu(\text{OH})$ +deformation modes (Pb-OH)
	4403	$\nu(\text{OH})$ + $\nu(\text{CO})$
	4988	-
	5135	-

Finally, also the possible interference of degradation products, i.e metal soaps and calcium oxalates, was taken into account. The presence of metal soaps in the layers of oil paintings is, in fact, an important issue to be considered in the context of conservative studies. These compounds are formed as a result of the interaction between free fatty acids in the degraded oil (but also egg) binder and heavy metal ions deriving from inorganic pigments such as lead white, lead tin yellow and zinc white, commonly used in preparatory and colour layers. Anyway, the mechanism of their formation is not completely clear and still under investigation [37-40]. In this work lead palmitate, a typical metal soap deriving from the reaction between palmitic acid and Pb ions, was synthesised (section 4.7) and its NIR spectrum was investigated. It shows the typical bands due to the stretching and bending of C-H bonds, but also a characteristic signal at 4190 cm^{-1} (Fig. 7b). Another degradation product, already extensively studied in the NIR region, are oxalate salts [41]. Although they have been the subject of extensive research as alteration products on calcareous substrates (i. e. stone and fresco) [36, 42], oxalates can be detected also on painting surfaces where they can be responsible for significant changes in the surface appearance, posing challenges for the visual interpretation [43, 44]. The oxalate salts of calcium, whewellite (calcium oxalate monohydrate) and weddellite (calcium oxalate dihydrate), are those most commonly encountered on painted surfaces [45] and various mechanisms (biological and chemical) have been proposed for their formation on artworks [46]. The NIR spectra of calcium oxalates are dominated by the overtones and/or combination bands of the O-H and C-O vibrational modes (Tab. 7 and [45]). In particular, weddellite was analysed in the present work (Fig. 7a), while the NIR spectrum of whewellite is reported in [45]

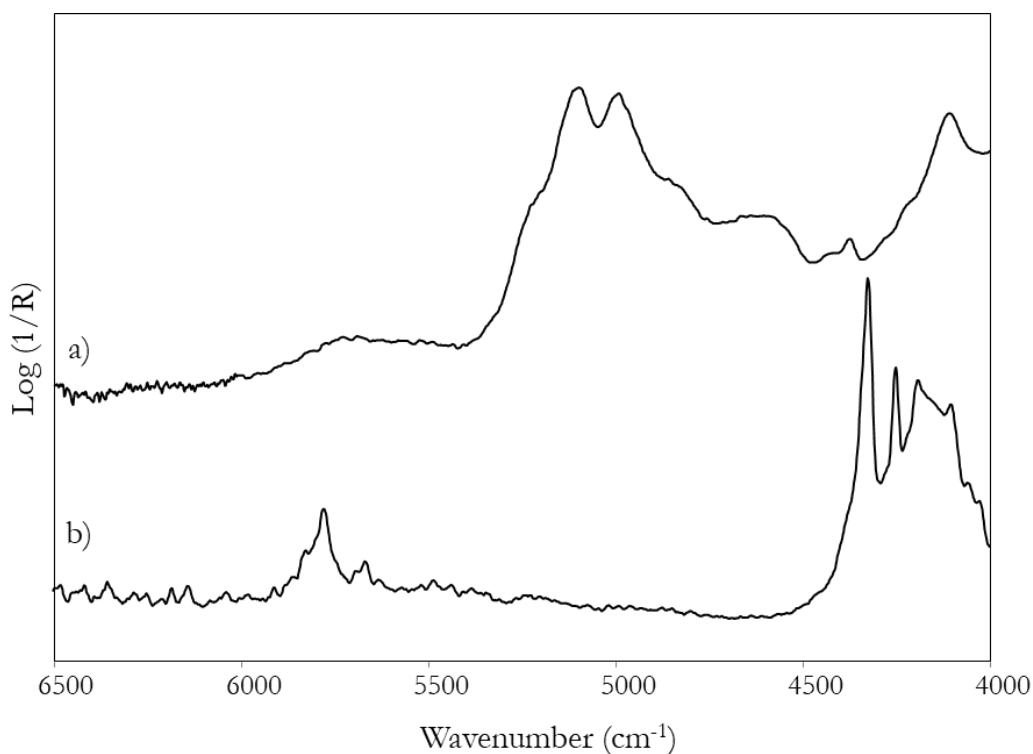


Figure 7. FT-NIR spectra of a) lead palmitate and b) weddellite.

Table 7. Experimental NIR wavenumber (cm^{-1}) of gypsum and lead white and tentative assignment [].

	Wavenumber (cm^{-1})	Band assignment
Pb palmitate	4192	-
	4252	$\nu_s(\text{CH}_2)+\delta(\text{CH}_2)$
	4325	$\nu_a(\text{CH}_2)+\delta(\text{CH}_2)$
	5670	-
	5777	-

5.2 Model samples with CaCO_3 preparatory layer

The first mock-up samples under investigation were those having a preparatory layer made of calcite. Below, the spectra corresponding to the different samples will be discussed in detail. First, the case of tempera, *tempera grassa* and oil on tempera on a preparatory layer made of calcite and animal glue will be examined, followed by the one of a linseed oil painting layer applied on two different walnut oil priming layers. Three different inorganic pigments traditionally employed by artists, namely yellow ochre, azurite and lead white, were chosen, as they have characteristic absorption bands in the NIR region because of the presence of hydroxyl groups in their chemical structure.

Preparatory layer - Calcium carbonate is a material which does not show absorption bands in the NIR region, so the only signals observed in this range for the spectrum of the ground layer are

due to the animal glue used to prepare it, evidenced by Fig. 8. In particular, the bands of animal glue at 4370, 4610, 4900 and 5142 cm^{-1} are well evident in the spectrum of the preparatory layer.

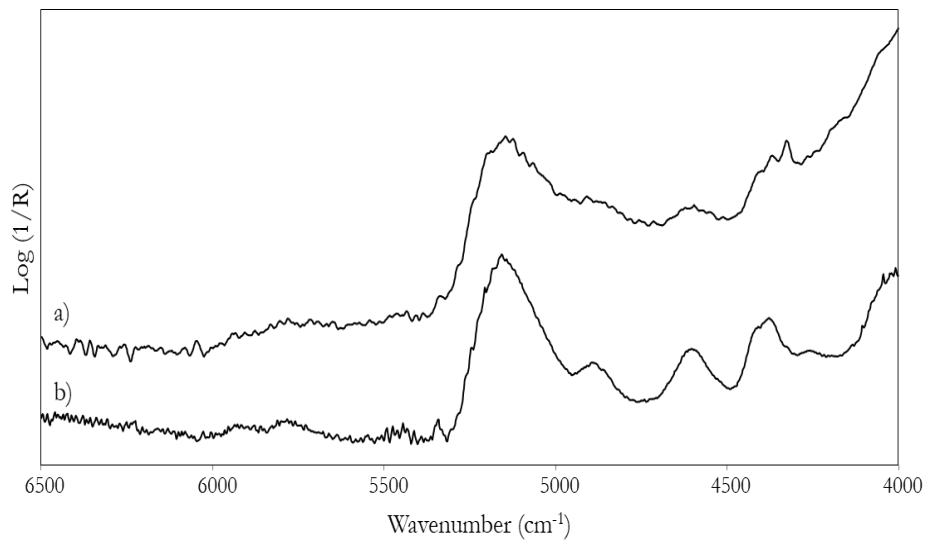


Figure 8. Comparison between FT-NIR spectra of a) calcite preparatory layer and b) pure animal glue.

In the following, the NIR spectra obtained for the different model painting samples (Figg. 9 and 10) will be discussed in detail.

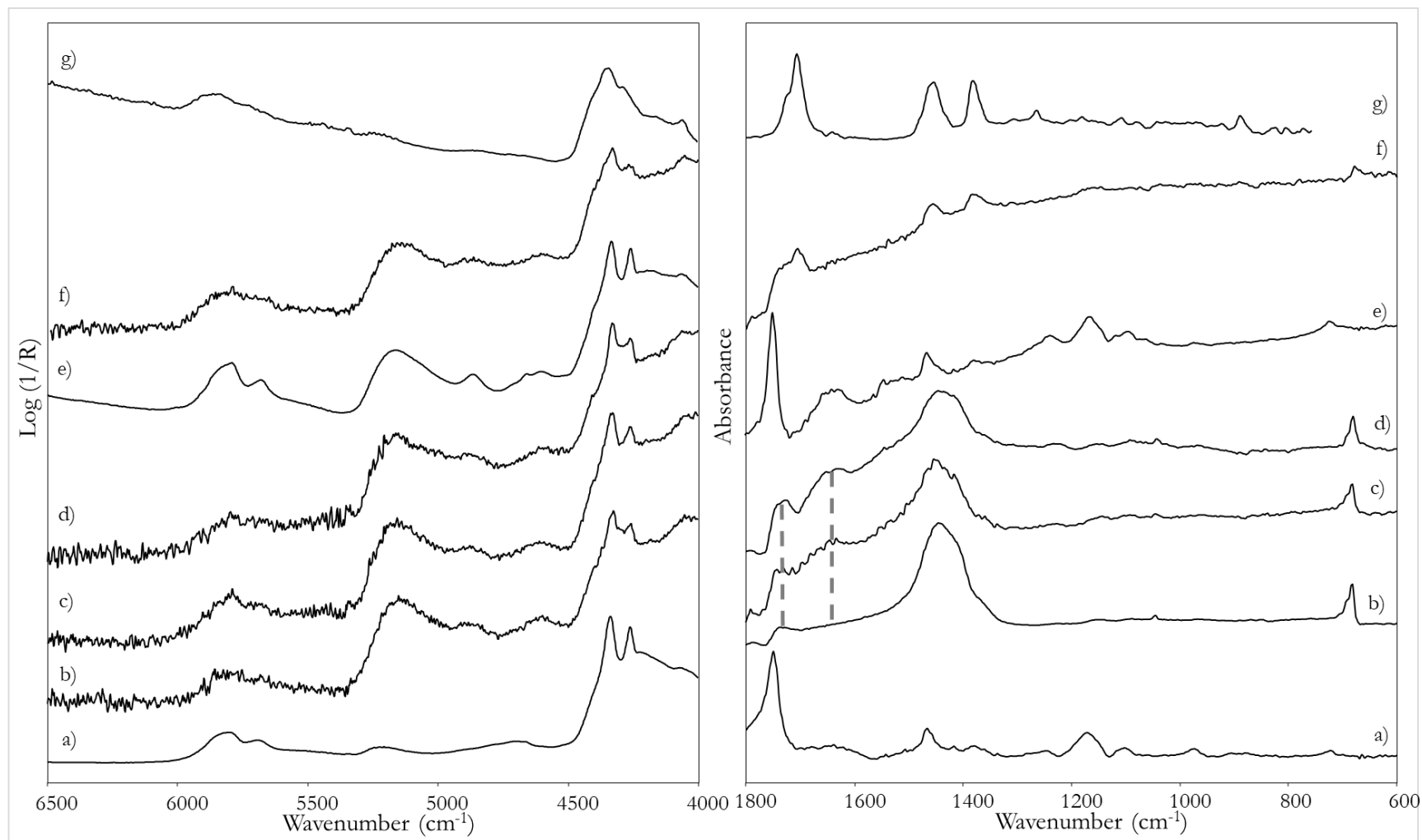


Figure 9. FT-NIR (left) and FT-MIR (right) spectra of: a) linseed oil; b) model painting sample of linseed oil on tempera; c) model painting sample of *tempera grassa*; d) model painting sample of tempera; e) yolk; f) model painting sample of *tempera grassa* with dammar varnish; g) dammar varnish. All model samples contained lead white as pigment. All spectra of reference materials and model painting samples were acquired in reflection mode, except for the MIR spectrum of dammar that was acquired in transmission mode.

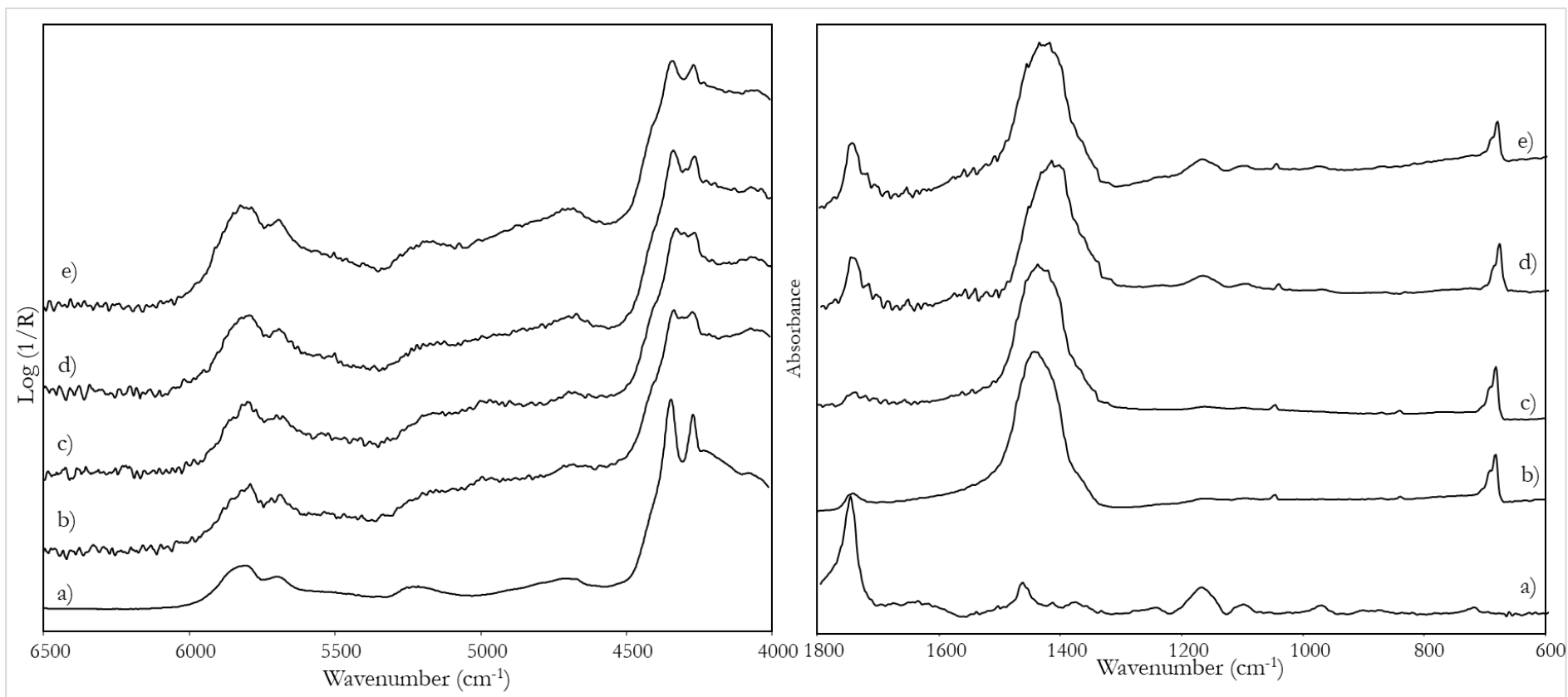


Figure 10. FT- NIR (left) and FT-MIR (right) spectra of: a) linseed oil, b) white priming layer, c) pink priming layer, d) lead white in linseed oil on white priming layer, e) lead white in linseed oil on white pink priming layer. All spectra of reference materials and model painting samples were acquired in reflection mode.

Tempera - The NIR spectra of the tempera mock-up sample (Fig. 9d) allow the identification of the proteinaceous binder from the characteristic bands at 5150, 4860, 4604, 4330 and 4258 cm^{-1} , clearly recognisable in the spectrum of pure yolk (Fig. 9e). All the used inorganic pigments show signals in this spectral range, because of the presence of OH groups in their chemical structure. In particular, lead white is recognisable from the band at 4275 cm^{-1} , azurite from those at 4370 and 4245 cm^{-1} and yellow ochre at 4526 cm^{-1} . In Fig. 9 only the spectra referring to the painting layers containing lead white are presented (see Appendix A for the other pigments). Moreover, some minor spectral features suggest a contribution of the glue from the preparatory and the priming layers: the slight broadening of the band at 4860 cm^{-1} , the shoulder at 4400 cm^{-1} and the intensity ratio of the bands at 5790 cm^{-1} and 5674 cm^{-1} , lower than in pure yolk. In these samples, in fact, the thickness of the painting layer is only 30 μm , as demonstrated by the cross section obtained from the mock-up sample of ochre in tempera (Fig. 11), allowing the NIR radiation to reach the ground layer.

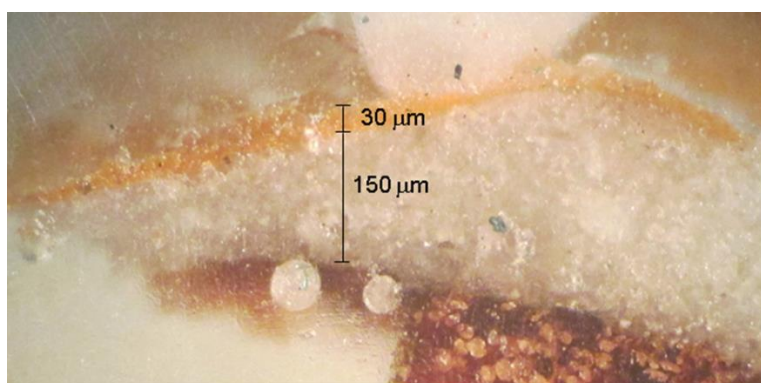


Figure 11. Cross section of the mock-up sample of yellow ochre in tempera.

The MIR region of the spectra is dominated by the signals of the inorganic pigments (for lead white at 1443 and 683 cm^{-1} [47]), while the binder is suggested only by the bands at 1650 and 1740 cm^{-1} , respectively due to the proteinaceous and lipidic components of yolk. It must be remembered that in the MIR region the absorptions due to the pigments are the prevailing ones (Fig. 9, box on the right).

Tempera grassa - When the binder is a mixture of yolk and a lower amount of linseed oil, the NIR spectrum (Fig 9c) is dominated by the signals due to yolk. Anyway, in comparison with egg tempera, in the spectrum of *tempera grassa* layers there is an increase of the signals at 4330 cm^{-1} and 4258 cm^{-1} due to the stretching of C-H bonds, typical of the lipidic component (Fig. 12) [8]. Moreover, also in the MIR region the relative intensity of the broad band at 1650 cm^{-1} , characteristic of a proteinaceous material, and of the signal at 1740 cm^{-1} is slightly higher in the

case of the pure egg-based binder rather than for the mixture with oil (see dotted line in Fig. 9 c and d, right box).

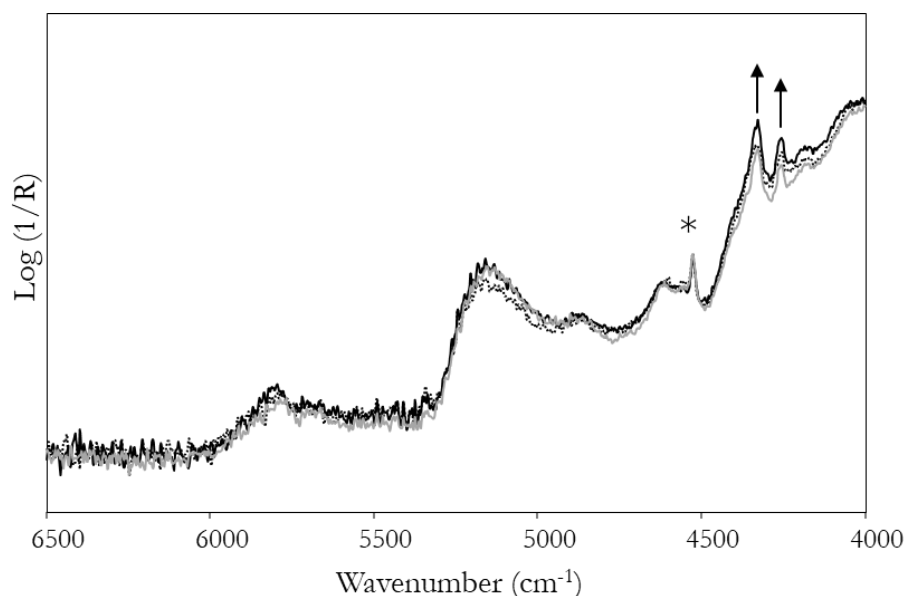


Figure 12. Comparison of NIR spectra of egg tempera (grey line) and *tempera grassa* with linseed (dotted line) and walnut (black line) oils with yellow ochre (* = band of the pigment). The arrows indicate the signals of the lipid component, which increase in intensity in the mixed binders.

Principal component analysis applied to the NIR spectra in the 6000-4000 cm^{-1} region of pure binding media (alone or in mixture) and of the tempera painting models, demonstrated that they belong to the group of the egg-based binder (egg and egg yolk), but are shifted towards the symbol representing the spectrum of the ground layer (see score plot in Fig. 13). To give more consistence to the statistical analysis, poppy and walnut oils were also included in the PCA besides linseed oil, both as pure binders and/or in the painting models. Indeed, as discussed before, in the mock-ups the colour layer is thin enough to allow NIR radiation to penetrate and reach the preparatory layer. It worth noticing that, because of the choice of three pigments which absorbs in the NIR region, in multivariate analysis the comparison must be done between spectra from paint layers obtained with the same pigment. Anyway, the three colouring materials gave analogous results in the PCA. In the following the case of lead white will be shown (for the score plots with the other pigments refer to Appendix A).

Oil on tempera - These mock-up samples were prepared to evaluate the possibility of discriminating among the coexistence of oil and egg in the same layer rather than the superimposition of a tempera on an oil layer. The spectrum of the oil-on-tempera superimposed layers (Fig. 9 b) is very similar to those of *tempera grassa* in the NIR region, as confirmed by PCA. In fact, as showed in the score plot for the painting layer with lead white (Fig. 13), when there is a coexistence of oil and tempera, the symbol corresponding to the spectrum matches with the

group of the mixed binders. Anyway, focusing again on the MIR, the band at 1650 cm^{-1} disappears while the one at 1740 cm^{-1} , which is typical of siccative oils, arises (see dot lines in Fig. 9 b, right box). Therefore, combining the information from the NIR and the MIR, it is possible to distinguish a mixture from a superimposition of the two binders.

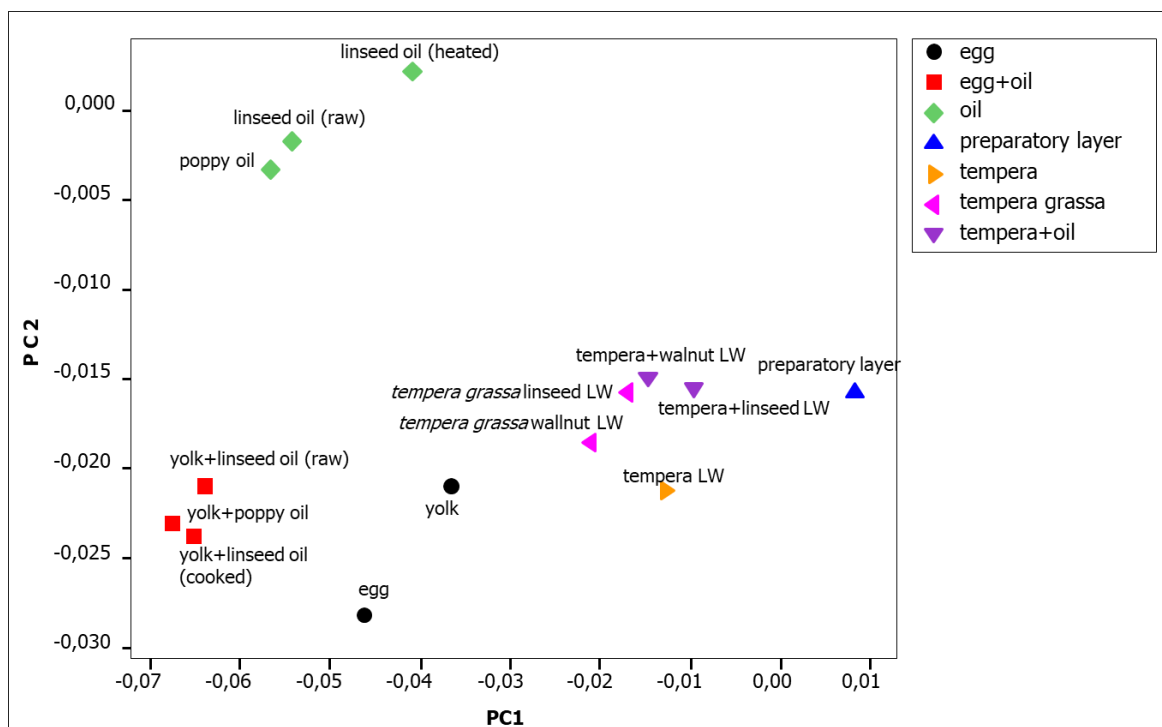


Figure 13. Score plot of the first two principal components of the NIR spectra (6000-4000 cm^{-1}) of pure oil and egg-based binders and of model painting samples of tempera, *tempera grassa* and oil on tempera on calcite ground layer. In the model samples, lead white (LW) was used as pigment.

Dammar varnish on “tempera grassa” - When a layer of dammar resin is applied as varnish on the painting samples, the MIR spectrum is dominated by its signals (at $1705, 1455, 1380\text{ cm}^{-1}$) that hide those of the inorganic pigments, as shown in Fig. 9f for a *tempera grassa* sample. On the other hand, in the NIR range, the spectral trend remains substantially unvaried, still allowing the identification of the binder. This fact is, again, explained by the higher penetration depth of the NIR radiation which is able to pass through the most superficial layers. The cross section prepared from a small fragment of the varnished mock-up sample allowed us to estimate a thickness of $80\text{ }\mu\text{m}$ for the surface coating (Fig. 14).

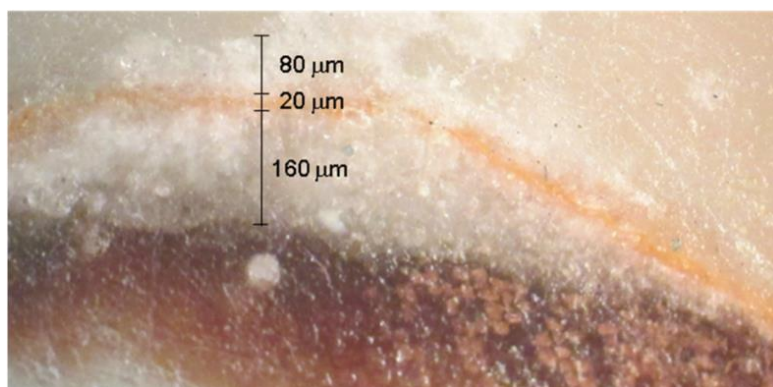


Figure 14. Cross section of the mock-up sample of yellow ochre oil paint with a surface layer of dammar varnish.

Oil on priming layer- The NIR spectra acquired from these mock-up samples clearly demonstrate the presence of a siccative oil as a binder. The bands at 5810, 5690, 5180, 4690, 4340 and 4260 cm^{-1} are, in fact, typical of this lipidic substance. The spectra of the two priming layers are very similar to each other (Fig. 10 c and b), confirming that the presence of the two inorganic pigments (red lead and lead tin yellow) in the pink sample do not affect the spectrum in the NIR region. In both cases, the already mentioned signals at 4275 and a weaker one at 5150 cm^{-1} are due to lead white. It is worth underlining that such signals are less evident when a painting layer, even containing the same pigment, is applied on the primer, as the latter contains a higher pigment:oil ratio in comparison with the former. The MIR region is on the other hand dominated by the signals due to the inorganic pigment, associated to the characteristic band of oil at 1740 cm^{-1} (Fig. 10, right box). The cross section of the azurite oil paint layer on white priming layer is shown in Fig. 15.

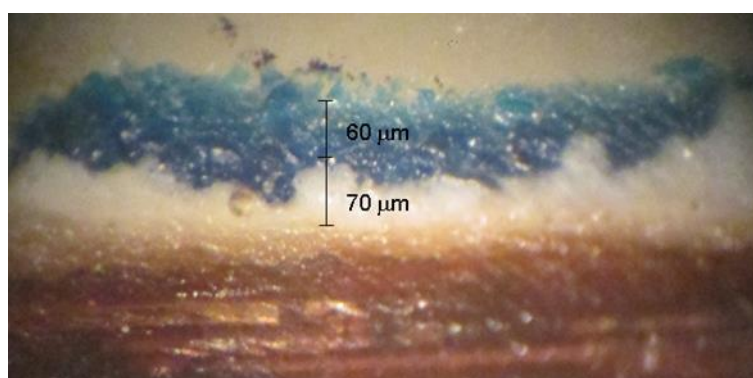


Figure 15. Cross section of the mock-up sample of azurite in oil on white primer layer.

The presence of oil as binder is confirmed by PCA. In fact, both priming layers (white and pink), with or without a superimposed layer of lead white in oil, occupy the region corresponding to the group of pure oils in the score plot (Fig. 16).

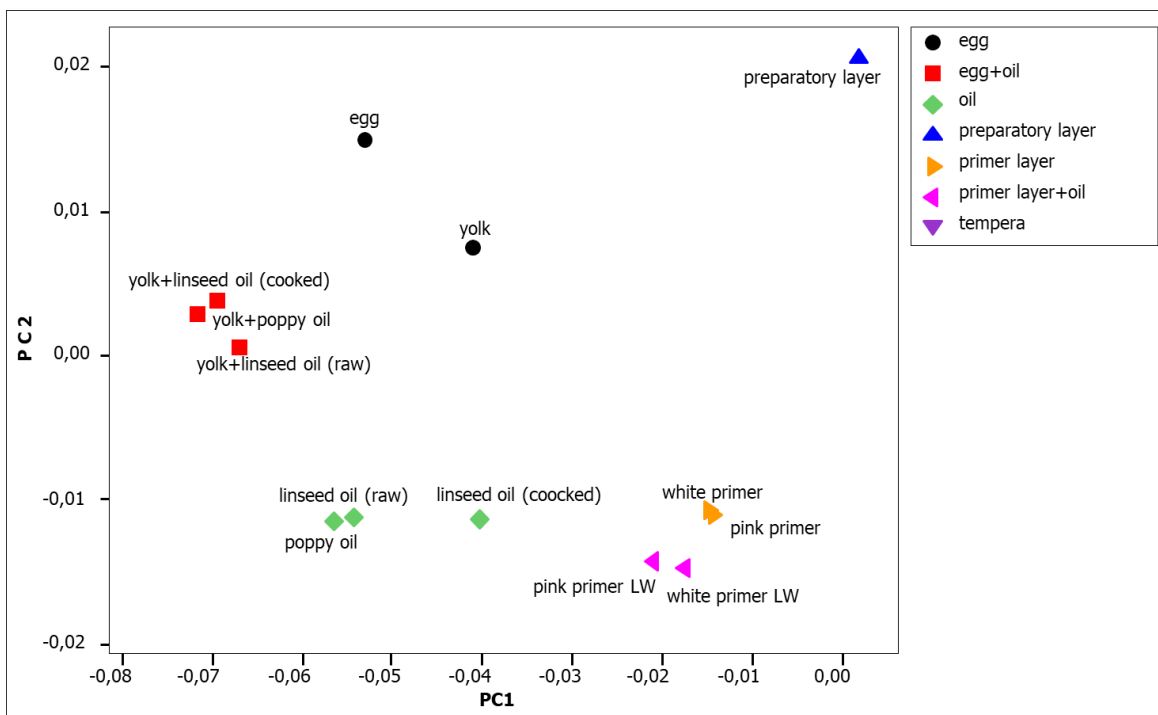


Figure 16. Score plot of the first two principal components of the NIR spectra ($6000\text{-}4000\text{ cm}^{-1}$) of pure oil and egg-based binders and of model painting samples of pink and white priming layers, with and without a superficial hand of lead white (LW) in linseed oil.

In addition, the possibility of recognising the coexistence of two different siccative oils, i.e. linseed and walnut oil, by studying the 1st derivatives of their spectra (Fig. 17) was considered. In particular, in our previous study [48] it was highlighted a diagnostic difference in the shift of the minimum of the derivative pattern of the spectrum from 4430 cm^{-1} for walnut oil to 4418 cm^{-1} for linseed oil [48]. By applying the same criterium to the spectra acquired from the mock-up samples, a better correspondence was found with walnut oil, although both of the binders are present. However, especially referring to yellow ochre paint layers, the presence of linseed oil seems to influence the position of this minimum, shifting it towards shorter wavenumbers.

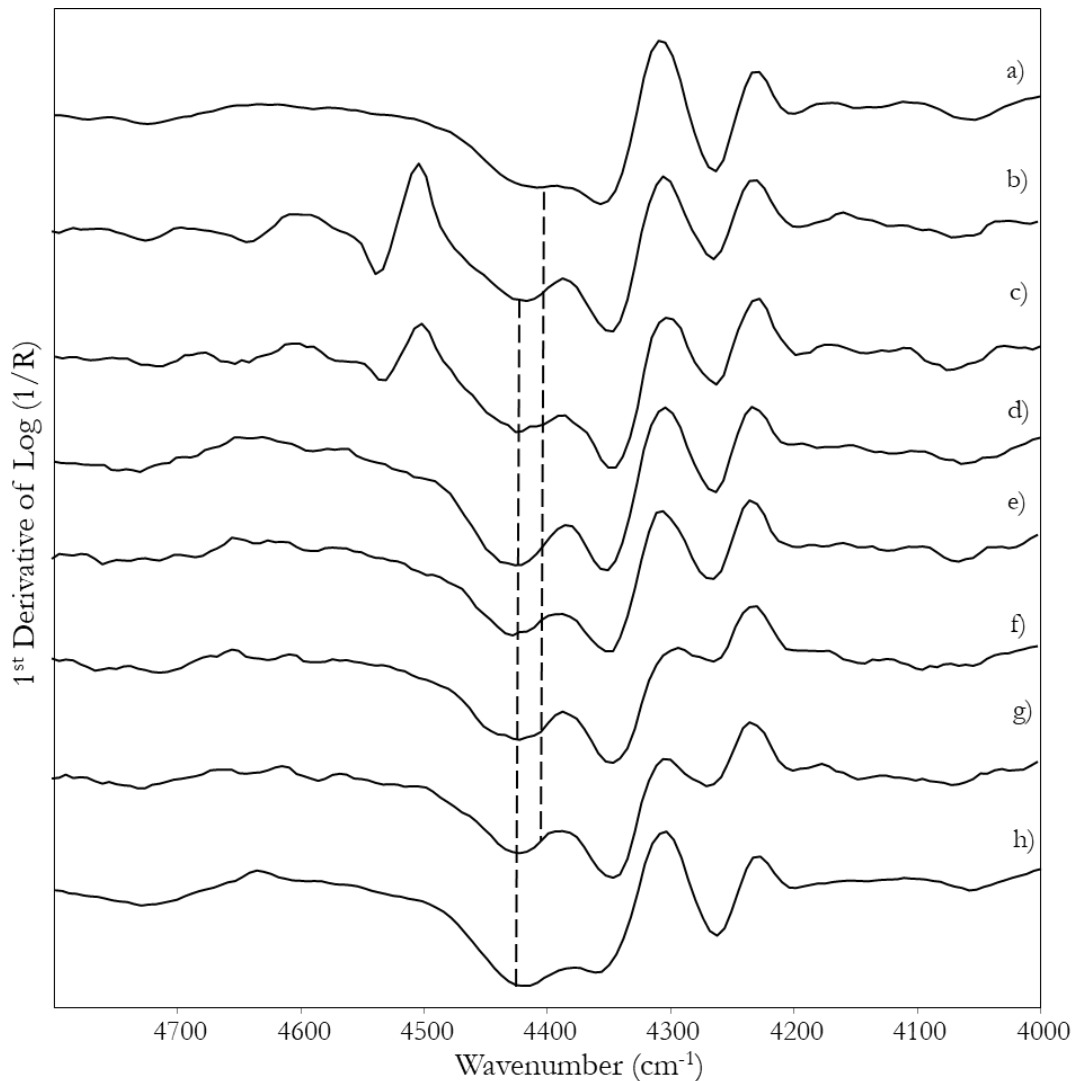


Figure 17. 1st derivatives of NIR spectra of a) linseed oil, b) yellow ochre paint layer on pink primer, c) yellow ochre painting layer on white primer, d) lead white painting layer on pink primer layer, e) lead white painting layer on white primer, f) pink primer, g) white primer, h) walnut oil.

Finally, also the possibility of exploiting the multivariate approach to distinguish simultaneously the tempera mock-up samples from those having an oil priming layer was successfully tested. As showed in the upper part of the total score plot (Fig. 18), when there is a coexistence of oil and tempera, the spectra match with the group of the mixed binders, even if with a shift towards the symbol corresponding to the ground layer as already observed.

On the other hand, both the priming layers (white and pink), with or without a superimposed layer of lead white in oil, occupy the region corresponding to the group of pure oils in the graph. It can be assumed that PCA is a powerful method to highlight even slight differences among these spectra.

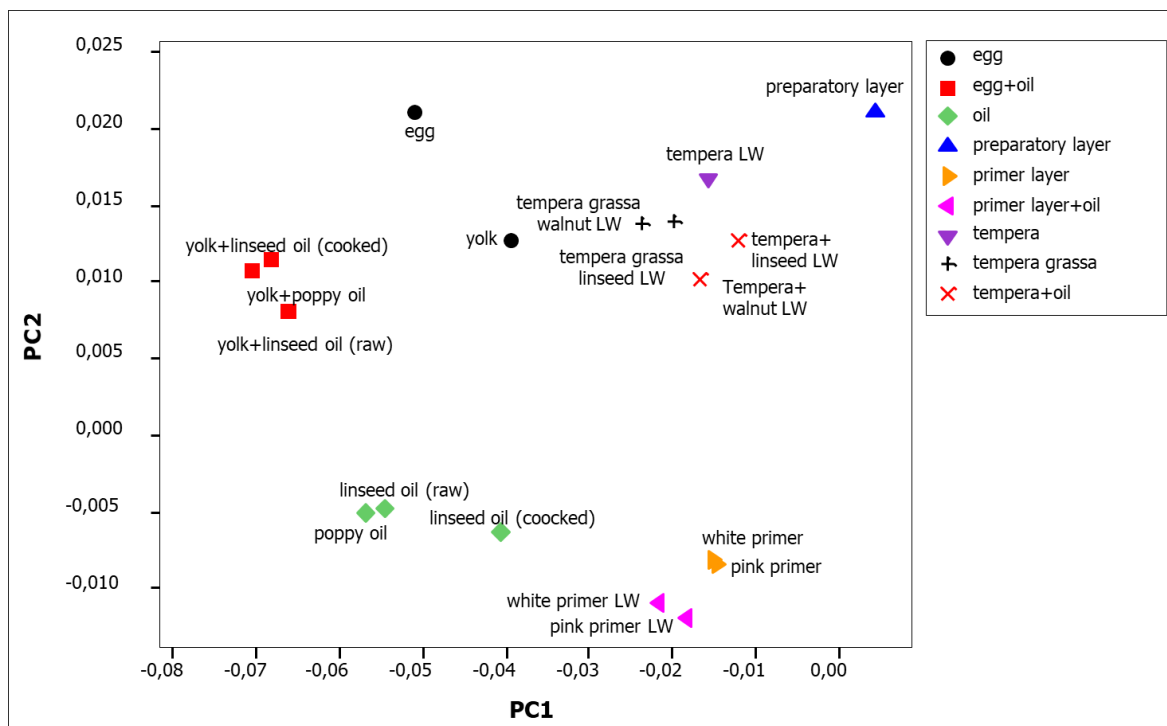


Figure 18. Score plot of the first two principal components of the NIR spectra (6000-4000 cm^{-1}) of pure binders and of all the model painting samples on calcite ground layer. In the model samples lead white (LW) was used as pigment.

5.3 Model samples with $\text{CaSO}_4 \cdot 2\text{H}_2\text{O}$ preparatory layer

A further step was the study of the influence on the NIR spectra of a preparatory layer made of gypsum. As already discussed, this material, in fact, is characterised by an intense absorption band [8, 34-36] in this region due to the two water molecules in its chemical structure. Therefore, the possibility of identifying the binder through the NIR spectrum even in the presence of gypsum was investigated and the information was correlated with the thickness of the painting layers as estimated from the corresponding cross sections. In this respect, the prepared mock-up samples differ not only for the binder/s, but also for the number of colour layers spread on the gypsum coating, and thus for the total thickness of the superficial layer.

Fig. 19 shows the FT-NIR spectra obtained from the different mock-up samples for lead white paint layers (for the hematite ones refer to Appendix A) and the results are discussed below.

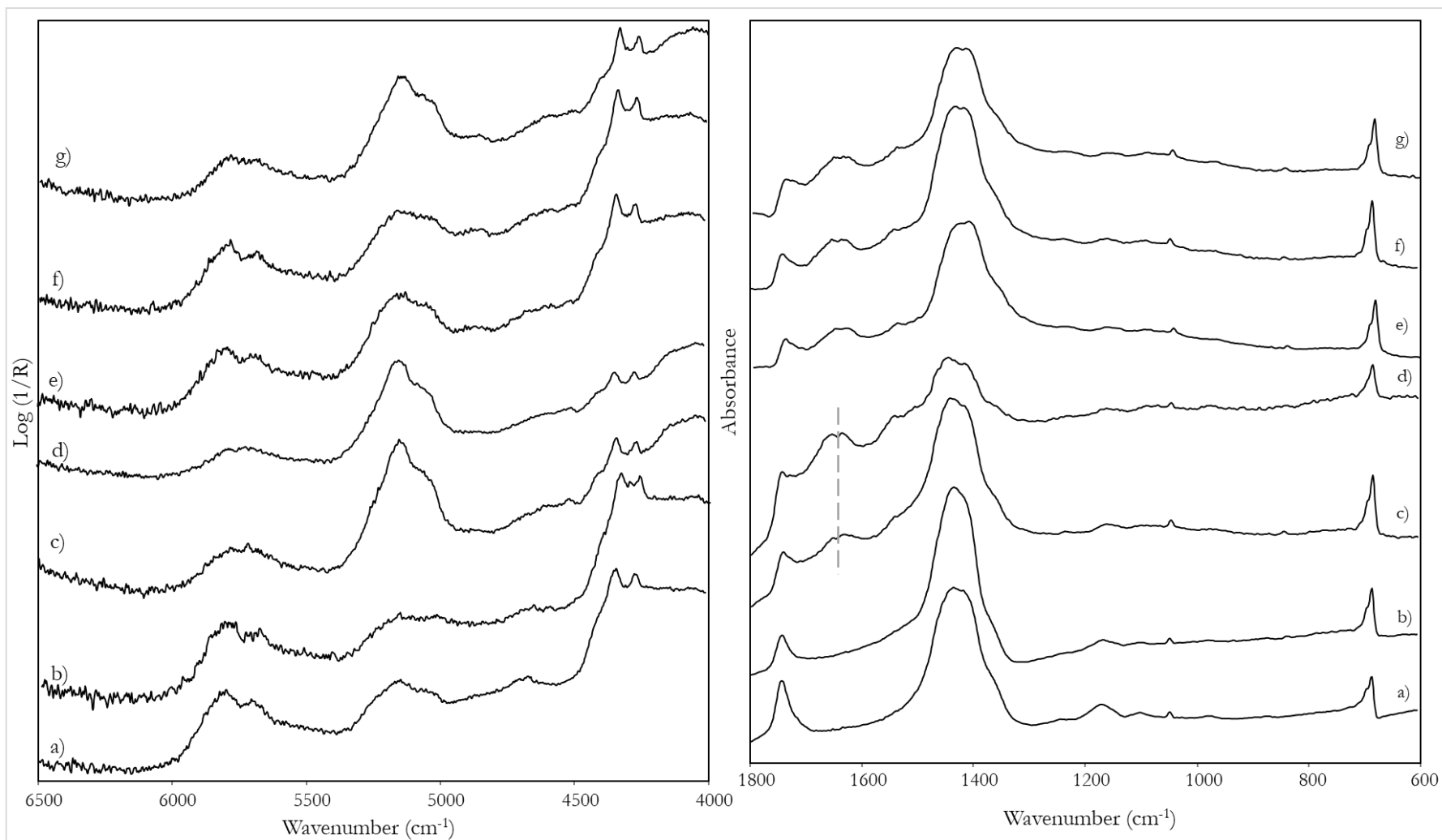


Figure 19. FT- NIR (left) and FT-MIR (right) spectra of model painting samples where the binder is a) linseed oil, b) walnut oil, c) *tempera grassa* with linseed oil, d) *tempera grassa* with walnut oil, e) one layer of tempera on linseed oil, f) one layer of tempera on walnut oil, g) egg tempera.

Preparatory layer - The NIR spectrum (Fig. 20 left) obtained from the preparatory layer of the panel shows the peculiar band of gypsum ($\text{CaSO}_4 \cdot 2\text{H}_2\text{O}$) at 5150 cm^{-1} , associated with those at 4510 and 4105 cm^{-1} [8, 35]. The signals due to animal glue are instead hidden by the inorganic component. Also the MIR spectrum is dominated by the contribution of calcium sulphate dihydrate with the intense band of silicates at 1160 cm^{-1} accompanied by signals at approximately 1680 , 1620 , 670 and 600 cm^{-1} (Fig. 20 right) [19].

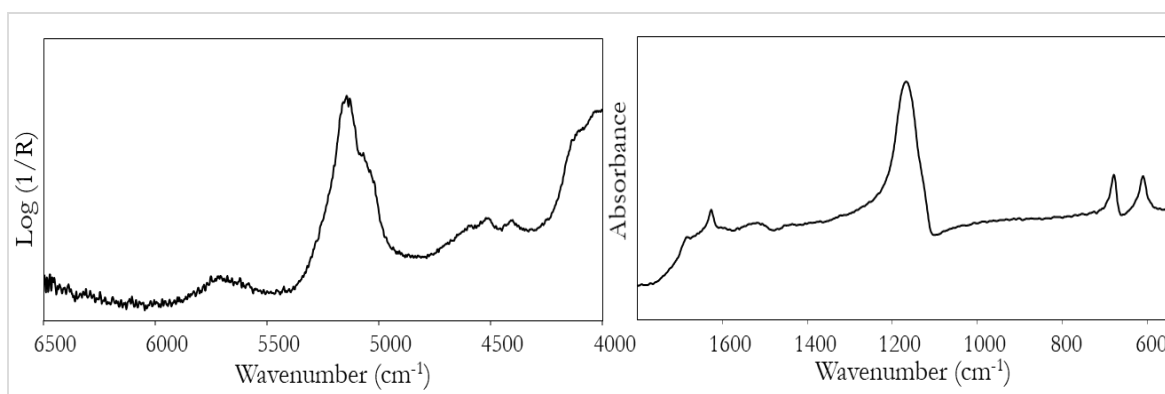


Figure 20. FT-NIR (left) and MIR (right) spectra of the gypsum preparatory layer.

Tempera - The NIR spectrum (Fig. 19g, left box) of this painting layer clearly allows the identification of egg yolk as a binder thanks to the characteristic bands at 5160 , 4867 , 4604 , 4330 and 4258 cm^{-1} . Referring to the MIR spectrum, the signals of the inorganic pigments (lead white in Fig. 19, right box, and hematite in Appendix A) are the predominant ones, while the presence of yolk is suggested only by the broad and relatively weak bands at 1740 cm^{-1} , due to the C=O ester bond of the lipid component, and 1650 cm^{-1} , associated with the proteinaceous one.

Oil - Oil paint layers are characterised by NIR spectra (Fig. 19) showing the signals due to the lipidic binder: the pair of narrow bands at 4330 and 4260 cm^{-1} , the broad band at 4670 cm^{-1} and those at 5670 and 5807 cm^{-1} . On the other hand, the typical band of a siccativ oil around 5200 cm^{-1} is hidden by the band of gypsum when the thickness of the paint layer is thin enough to allow the passage of near-infrared radiation through it. In this respect, mock-up samples having colour layers of different thickness were analysed and the influence of thickness on the gypsum rather than the oil band was studied. The spectral modifications as a function of thickness are evidenced by comparing the spectra of the gypsum-based preparatory ground and of pure oil with those of the single and double layered model samples (Fig. 21). In general, when a single colour layer is applied, the NIR spectrum is dominated by gypsum, preventing the identification of the binder. We observed in the cross section that in this case the thickness of the painting layer is around $60 \mu\text{m}$ (Fig. 21 bottom photo), so NIR radiation is able to pass through it and

reach the preparatory layer. When a second layer of colour is applied, for an overall thickness of about 150 μm (Fig. 21 top photo), the contribution of calcium sulphate dihydrate decreases and that of the binder becomes more evident. In the MIR, the characteristic signals of each pigment are observed, associated with the band at 1740 cm^{-1} typical of the lipid binder.

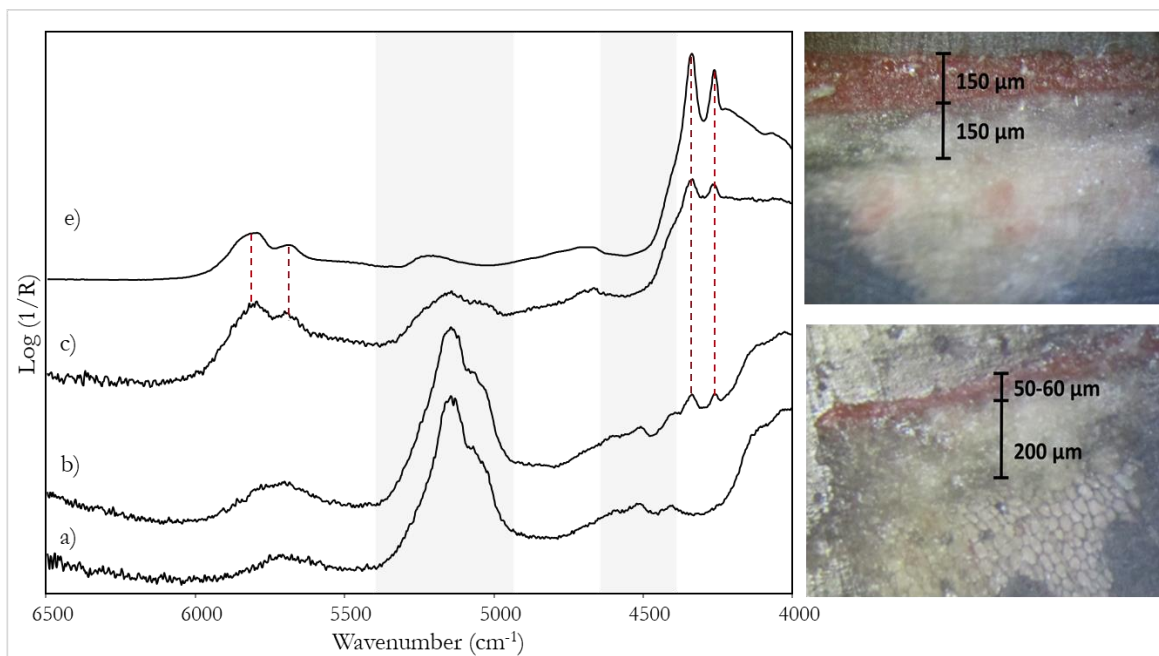


Figure 21. NIR spectra of: a) gypsum preparatory layer, b) one oil colour layer on gypsum, c) two oil colour layers on gypsum, d) linseed oil; the bands due to gypsum are highlighted. Cross sections of mock-up samples corresponding to b) (bottom) and c) (top) respectively are also shown.

Again, the 1st derivatives of the spectra were considered to investigate the possibility of distinguishing linseed from walnut oil. Also for these models, a slight shift of few wavenumbers of the minimum of the derivative pattern of the spectrum for walnut oil in comparison with linseed oil was observed (Fig. 22).

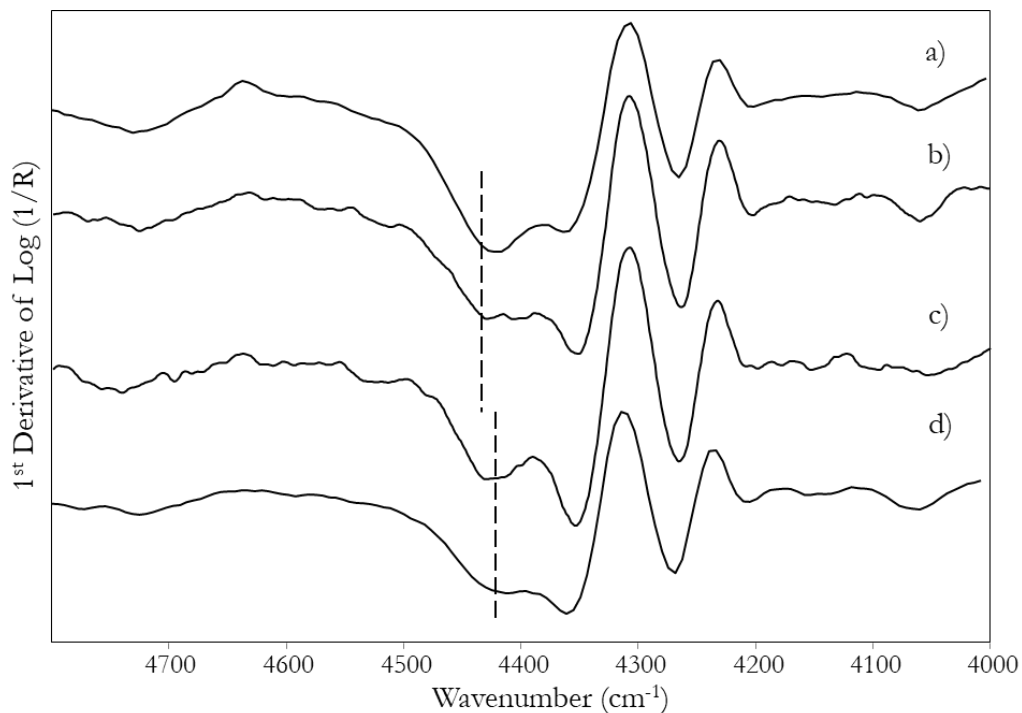


Figure 22. 1st derivatives of NIR spectra of reference a) walnut and d) linseed oils and model paintings of hematite in b) walnut oil and c) linseed oil.

Tempera grassa - Referring to the *tempera grassa* paint layers, both in linseed and walnut oil, NIR spectra are dominated by the signals due to the gypsum coating (Fig. 19 c and d), again due to the small thickness of the colour layer (around 60 μm , as demonstrated by the corresponding cross section in Fig. 23).

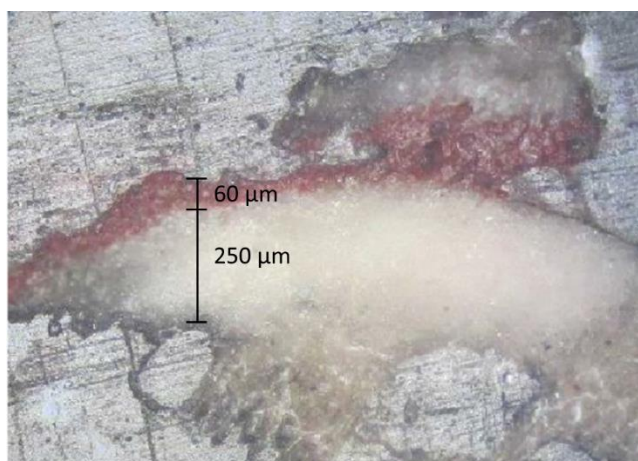


Figure 23. Cross section of the mock-up sample of haematite in *tempera grassa*.

The presence of the proteinaceous component in this mixed binder is however suggested by the presence of the shoulder at approximately 4610 cm^{-1} and by a hint of the second peculiar band at 4865 cm^{-1} . In the MIR region, it is still possible to appreciate a slightly higher intensity for the band of the protein component at 1650 cm^{-1} in pure tempera compared to *tempera grassa*,

since in the former there is obviously a higher lipid : protein ratio. Moreover, the band at 1740 cm^{-1} due to the lipidic components rises because of the presence of oil. The effect is certainly less remarkable than that observed in the NIR region.

Superimposed layers: tempera on oil - When a layer of tempera paint is spread on an oil one, the thickness of the coloured layers (Fig. 24) is sufficient to considerably reduce the contribution of the underlying gypsum ground layer. In the NIR spectral region, in the case of tempera on oil it is possible to recognise the characteristic bands of protein at 4665 and 4850 cm^{-1} (Fig. 19 e and f, left). Even in the MIR the band at 1650 cm^{-1} is clearly recognisable, although the prevailing signals are always those due to inorganic pigments ¹ (Fig. 19 e and f, right).

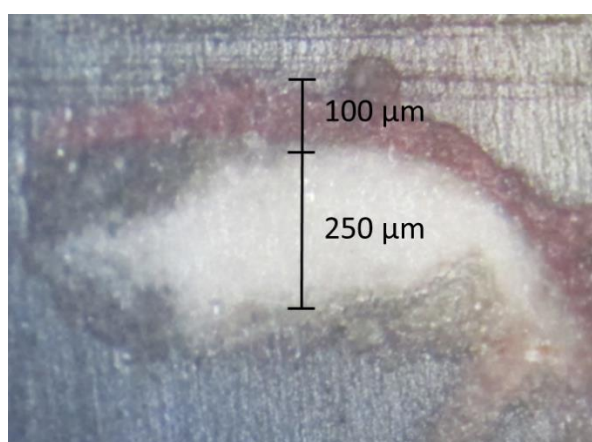


Figure 24. Cross section of the multi-layered mock-up sample of haematite tempera on a layer of hematite in linseed oil).

These differences between the spectra are evidenced by the score plot obtained from PCA of the NIR spectra in the range $6000\text{-}4000\text{ cm}^{-1}$ of the considered model samples (Fig. 25). It should be emphasised that in all the samples in the score plot the thickness of the colour layer was similar, so that also the contribution of the gypsum bands to the spectra was comparable. To appreciate the effect of this contribution, it can be observed that in the plot the points associated with the layers with a mixed binder are shifted along the first component towards the symbol of the ground layer spectrum, dominated by the bands due to gypsum. Indeed, in those models the thickness of the colour layer is slightly lower ($50\text{-}60\text{ μm}$) than in the painting mock-ups where two layers with different binders were superimposed.

The reported score plot refers to painting layers with lead white, but similar results were obtained for hematite (Appendix A).

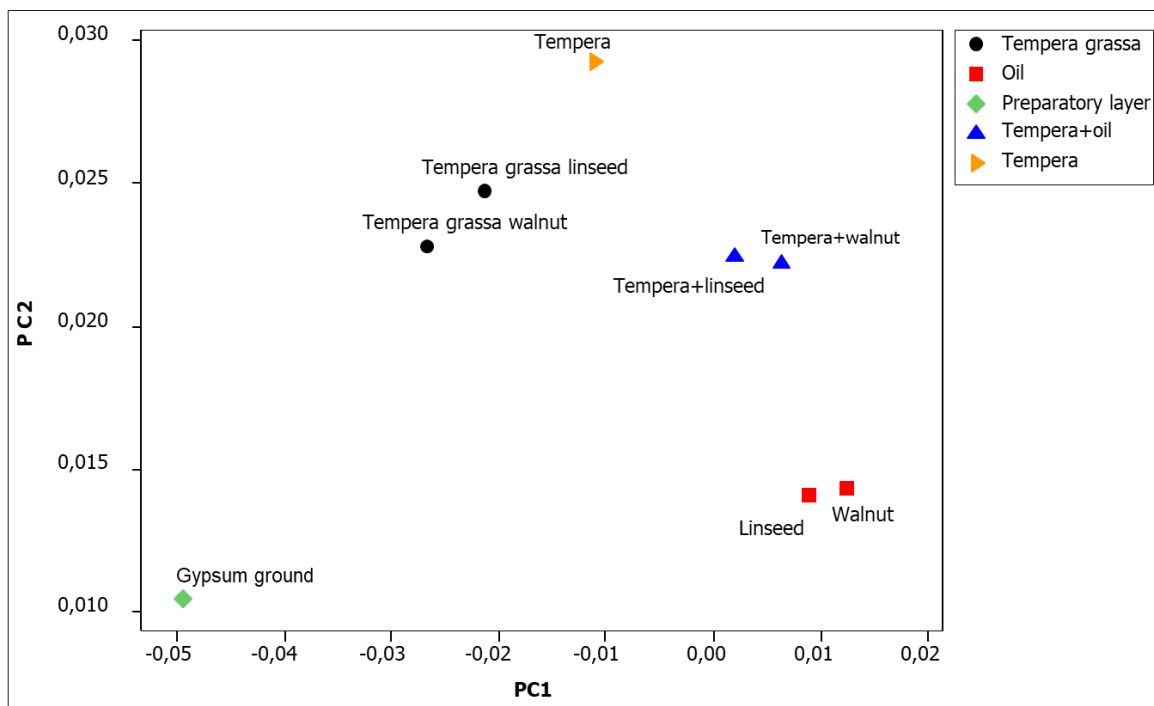


Figure 25. Score plot of the first two principal components of the NIR spectra (6000-4000 cm^{-1}) of model painting samples on gypsum ground layer. The binder are tempera and oil (linseed and walnut), pure in mixture or in superimposed layers. The pigment is lead white.

In summary, the higher penetration depth of NIR radiation allows the identification of gypsum in the preparatory layer, as already well known [8, 35]. On the other hand, the bands due to gypsum can have variable intensities in the spectra depending on the thickness of the superimposed colour layers. In principle, this fact could hinder the application of PCA analysis of spectral data in the 6000 - 4000 cm^{-1} region to the identification of binders and of their mixtures.

Anyway, it should be considered that, when dealing with real paintings, the situation is more challenging than in mock-up samples: the impossibility of predicting the stratigraphy, both in terms of composition and thickness of the layers, and the possible presence of degradation products make the situation more difficult. Calcium oxalates and metal soaps, for example, are typical by-products formed by the interaction between a siccative oil (but also the lipidic component of egg) and metal ions, i.e Ca, Pb or Zn, coming from pigments. As demonstrated in section 5.1, these compounds are both characterised by absorption bands in the NIR range that can interfere with those of the binder. Moreover, the natural ageing which can affect organic materials used as binders must be considered as it may induce important compositional changes reflecting on their FT-IR spectra. In fact, although proteins are quite stable and only small modification in the MIR region were detected [50, 51], siccative oils can be strongly affected by oxidative degradation processes [51]. Ageing could therefore induce slight variations in the

relative intensity of the MIR spectral bands which are even more pronounced in the presence of some inorganic pigments [50]. However, it is worth underling that the variations occurring in the NIR region, apart from a worsening of noise, are not so evident, as already observed in [8] and confirmed in the present work. Indeed, Fig. 26 shows a comparison between the spectrum of fresh linseed oil and those of the same oil heated in an oven at 100° C for 72 hours and irradiated for 6.5 hours by an Osram Powerstar lamp (150 W nominal power and emission between 390 and 600 nm). The aim was to simulate both a thermal and a UV-induced ageing. The spectra are rather similar and this is mainly due to the limited specificity of NIR spectroscopy that makes this technique less sensitive to structural changes in comparison with MIR spectroscopy [8]. This intrinsic limit of the NIR spectral range can however be exploited to investigate ancient painting materials also using non-aged samples.

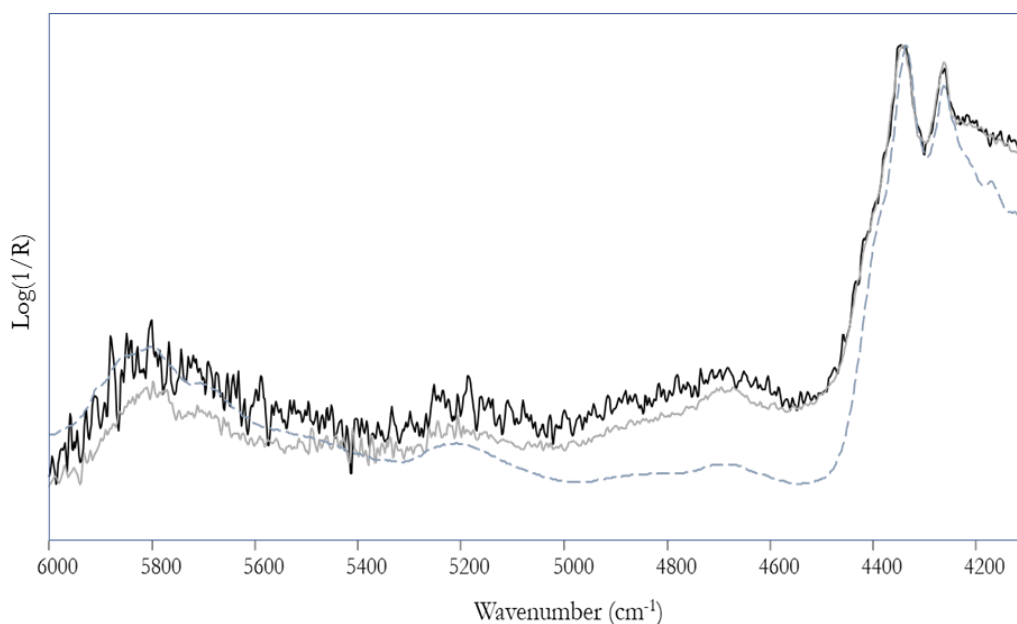


Figure 26. Comparison between the spectrum of fresh linseed oil (dotted line) and those of a thermal (grey line) and UV-aged (black line) sample respectively.

Nevertheless, and because of the uncontrollable factors described above, the use of PCA for the identification of binders in ancient paintings failed. In fact, being really sensitive, this method of data analysis is strongly affected even by subtle differences among the spectra. For these reasons, an alternative method which can be combined with the direct observation of the spectral data was proposed. It is based on the calculation of the ratio between the absorbance values at 4694 and 5160 cm^{-1} , where bands univocally typical of oil and egg respectively can be found (see Tab. 8 and Fig. 27). This approach can be successfully applied also to discriminate an egg tempera from a *tempera grassa* (or a super imposition of tempera on oil). In particular, the

ratio of their values proved to be in the range 0.2-0.5 for pure tempera, between 0.5 and 0.8 when the two binders are in mixture or in multiple layers and greater than 1 for pure oil (Fig. 28).

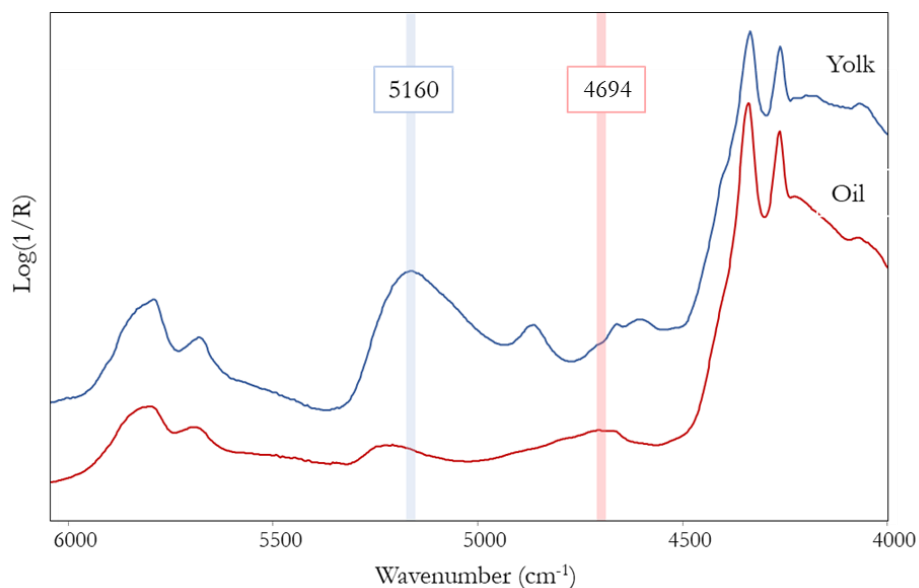


Figure 27. Highlighting of the absorption bands at 4194 and 5160 cm^{-1} uniquely typical of oil and egg respectively

Table 8. Relative absorbance values observed for bands of egg (characteristic bands in blue) and oil (characteristic bands in red).

Wavenumber (cm^{-1})	Linseed oil (heated)	Linseed oil (raw)	Poppy oil	Yolk	Egg
5797	0,037	0,11	0,11	0,2	0,056
5685	0,022	0,066	0,063	0,12	0,035
5203	0,02	0,036	0,019	0	0
5160	0	0	0	0,26	0,13
4865	0	0	0	0,11	0,074
4757	0	0	0	0	0
4694	0,029	0,05	0,034	0	0
4608	0	0	0	0,083	0,055
4334	0,2	0,6	0,55	0,63	0,29
4262	0,18	0,54	0,5	0,58	0,24

The effectiveness of the method, successfully verified for the mock-up samples, was then applied to the case studies, as will be explained below.

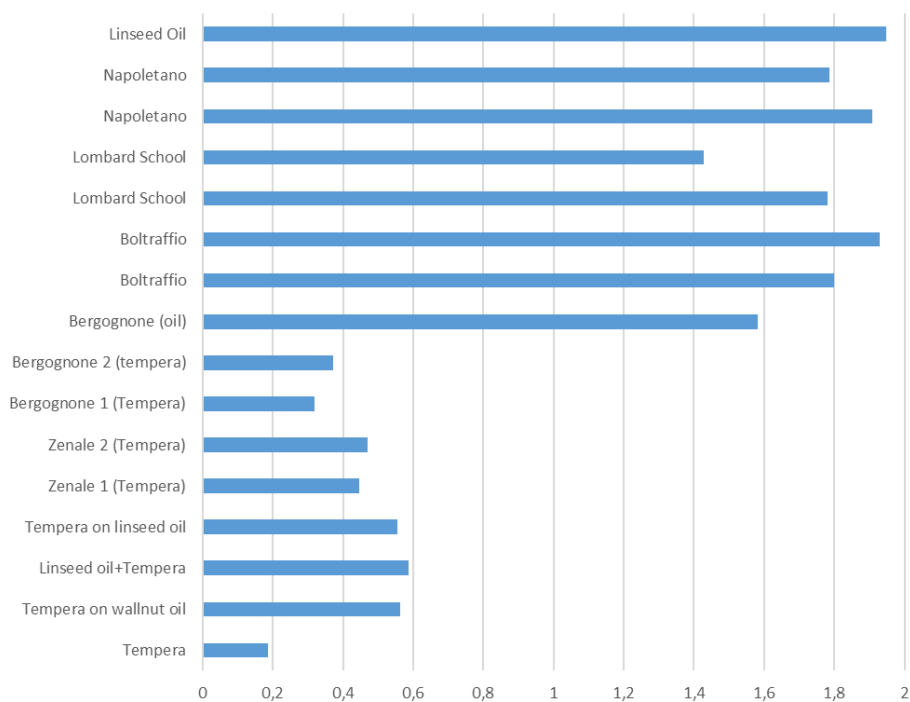


Figure 28. Histogram resuming the ratio between the absorbance values at 4964 and 5160 cm^{-1} calculated for reference samples and for the examined ancient paintings.

5.4. Case studies

5.4.1 Paintings of the Lombard Renaissance (late 15th - early 16th century)

The first three paintings here discussed are artworks by Leonardo's pupils in Milan and were investigated inside the museums in the scope of the project "Leonardesque artists beyond the visible" coordinated by the Italian *Consiglio Nazionale delle Ricerche* (CNR) and the University of Milano-Bicocca. The project included an extensive campaign of imaging and spectroscopic analyses [48]. The results of the investigation by NIR spectroscopy will be here discussed in detail. The other two coeval paintings on wood panel, by Bergognone and Zenale, as well as the painting on paper by Solario, were instead non-invasively analysed in the studio of restorer Carlotta Beccaria (Milan), who is acknowledged for offering the opportunity to test the proposed methodology on ancient artworks. It should be emphasised that Italian paintings of the considered period are of special interest both from the point of view of the transition from tempera to oil binder and of the possible use of different siccative oils, particularly by artists of Leonardo's school (see section 2.1). Also the possibility of recognising the presence and the composition of the ground layer (see section 2.2) could supply valuable information about the painting technique. With the exception of the painting by Solario, the other four artworks had been already restored when NIR measurements were performed, therefore presenting a finishing layer of synthetic varnish. In principle, as already demonstrated for dammar varnish

(see section 5.2), this fact should not prevent obtaining NIR spectra of the underlying painting layers, as further evidenced by the comparison shown in Fig. 29 between the NIR spectrum of an oil layer as such on a glass slide and of an oil layer on which a layer of synthetic varnish was applied.

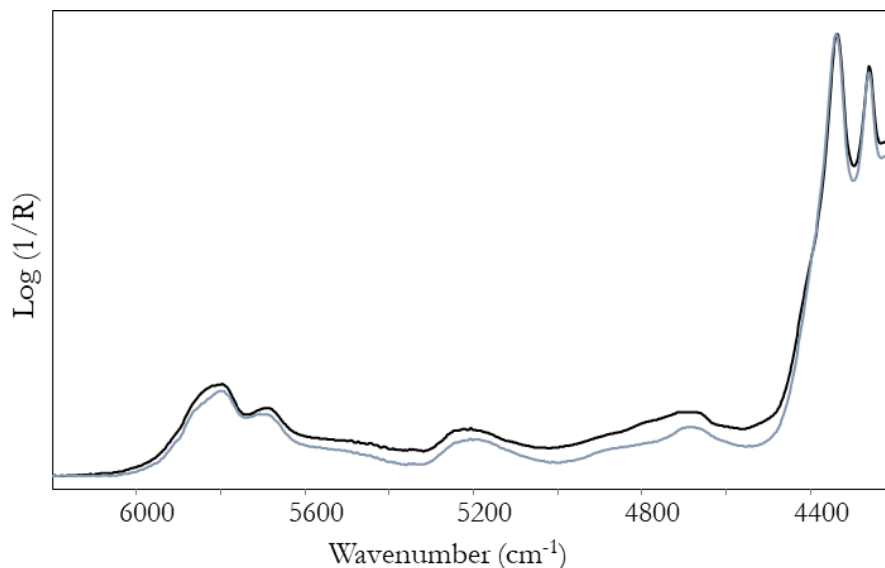


Figure 29. Comparison between the FT-NIR spectrum of an oil layer as such on a glass slide (black line) and that of an oil layer on which a layer of synthetic varnish was applied (grey line).

5.4.1.1 Paintings by Leonardo's pupils

Referring to the *Virgin and Child (The Madonna of the Rose)* by Giovanni Boltraffio, the MIR region of the spectra obtained from 15 different areas of the painting invariantly show the signals due to the materials applied during the restoration works (synthetic varnishes and a consolidant product). Moreover, some signals due to pigments were recognisable, such as lead white and azurite [47]. More information can be achieved from NIR spectra (Fig. 30), which allow the investigation of the inner layers of the painting. In particular, the presence of gypsum, presumably associated with the ground layer, was detected by the typical signal at 5150 cm^{-1} , as well as the use of a siccative oil as binder, also supported by a calculated ratio between the absorbance values of the bands at 4694 and 5160 cm^{-1} around 1.8 (Fig. 28).

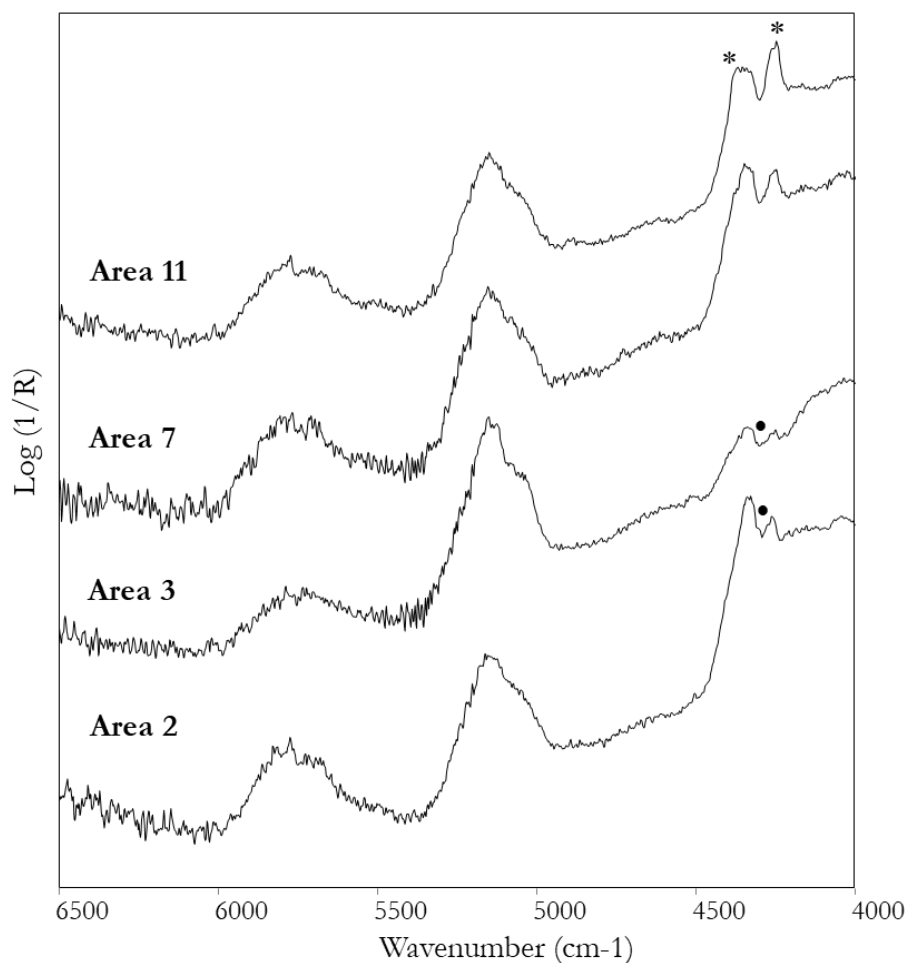


Figure 30. Some exemplificative FT-NIR spectra obtained from *The Virgin and The Child* by A. Boltraffio (1485-1490). The painting is shown at [52]. Legend: * =signals due to azurite and • = signals due to lead white.

The 1st derivatives of the NIR spectra were also tentatively examined to distinguish the type of siccative oil. The obtained results seem to suggest, considering the intensity ratios of the signals between 4450 and 4200 cm⁻¹, the use of linseed oil in area 15, while for the other areas the trend appears more comparable with that of walnut oil (Fig. 31) [48]. However, it is not possible to exclude, especially due to the position of the signals, the coexistence (even in different layers) of several types of oils. Interestingly, this information is in agreement with a previous analysis campaign carried out by the National Gallery of London laboratories, where GC/MS analyses identified the use of walnut oil in primer and of linseed oil in painting layers, while a cross section of the painting demonstrated the presence of a gypsum coating, covered by a pictorial layer thick 60 μm. [53, 54]. The possibility of detecting the gypsum preparatory ground below the colour layer is therefore consistent with what observed on mock-up samples and previously discussed.

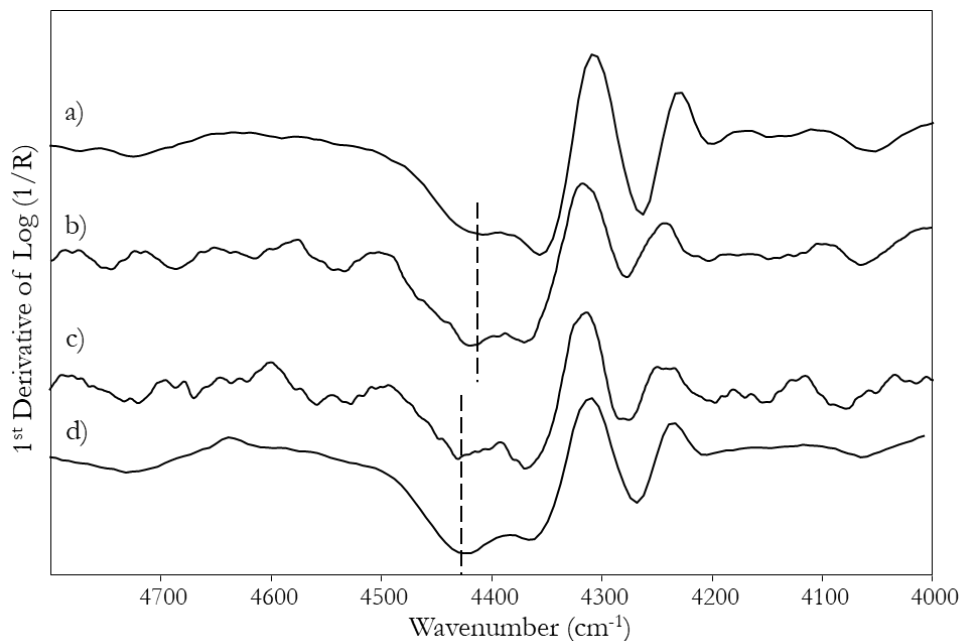


Figure 31. 1st derivatives of NIR spectra of reference a) linseed and d) walnut oils and of b) area 1 and c) area 15.

For the painting *The Virgin and Child* by Francesco Napoletano, the MIR region of the spectra resulted to be still dominated by the signals due to the synthetic varnish used as final coating after the restoration work. In addition, some inorganic pigments were detected, namely azurite, lead white and lead tin yellow, from their characteristic signals [47]. In the NIR region, all the areas under examination showed the characteristic bands of a siccative oil and of gypsum, presumably associated with the ground layer of the painting (some examples are provided in Fig. 32). The presence of the lipidic binder was also supported by the results obtained from the calculation of the ratio between the absorbance values of the bands at 4694 and 5160 cm^{-1} , which results between 1.4 and 1.9 (Fig. 28). The use of gypsum was also confirmed by the analyses made on the back of the painting, where a further coating of the panel was visible (area 11). The presence of lead white (areas 8 and 9) and azurite (area 6) was also confirmed from their peculiar bands in the NIR spectral range.

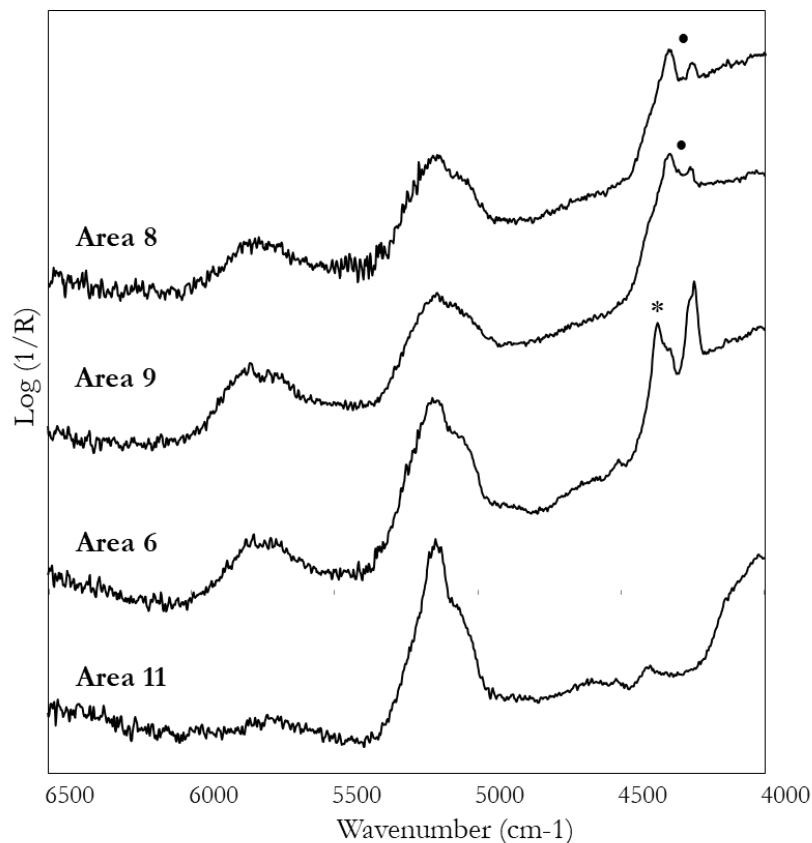


Figure 32. Some exemplificative FT-NIR spectra obtained from *The Virgin and Child* by F. Napoletano (1490 ca). The painting is available at [55]. Legend: * =signals due to azurite and ● = signals due to lead white.

Finally, similar results were obtained also for *The Virgin feeding the Child* by unknown painter of Lombard School. Again, in the MIR region the signals due to the restoration varnish are the predominant ones, sometimes associated with those of lead white [47]. On the other hand, NIR spectra (Fig. 33) confirmed the absence of a gypsum ground layer, and, for pigments, the presence of lead white and azurite in light-coloured (8 and 9) and blue areas (area 9) respectively. The use of a siccativ oil as binder was confirmed also by the calculated ratio between the absorbance values of the bands at 4694 and 5160 cm^{-1} , resulting in the range 1.7-1.9 (Fig. 28).

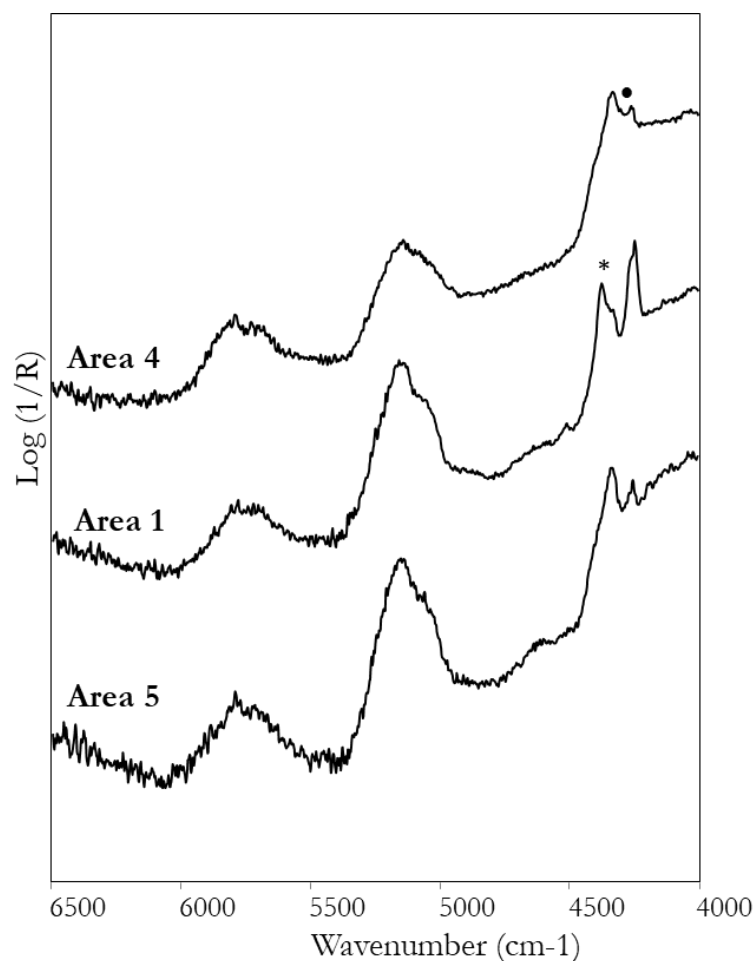


Figure 33. Some exemplificative FT-NIR spectra obtained from *The Virgin feeding the Child* by unknown painter of Lombard School (1500-1510). The painting is available at [56].

5.4.1.2 SS. Augustine and Jerome by Bergognone

Referring to MIR region, it is not particularly diagnostic as the only recognisable signals are those due to the synthetic varnish applied to the surface when the restoration work was complete.

Much more information can be obtained considering the NIR spectral range, demonstrating once again the possibility of exploiting the penetration depth of the near-infrared radiation. First of all, the spectra (Fig. 34) disclosed the presence of a gypsum ground layer (band at 5150 cm^{-1}), clearly recognisable in the spectra acquired from areas 1 (white fur), 2 (blue border) and 3 (blue sky); in areas 4 (red mantle) and 5 (red shoulder), red in colour, it is less pronounced. As far as the binder is concerned, the use of a siccativ oil was indicated by all the spectra obtained from the different areas. However, in the case of the white fur and the blue of the border, a hint of bands at about 4625 and 4850 cm^{-1} also suggested the presence of a protein component, hypothetically used to spread an additional layer of colour over the oil one. The compresence of the proteinaceous binder was also supported by the results obtained from the calculation of

the ratio between the absorbance values of the bands at 4694 and 5160 cm^{-1} , resulting around 0.35 for areas 1 and 2 and around 1.8 for area 3 (Fig. 28).

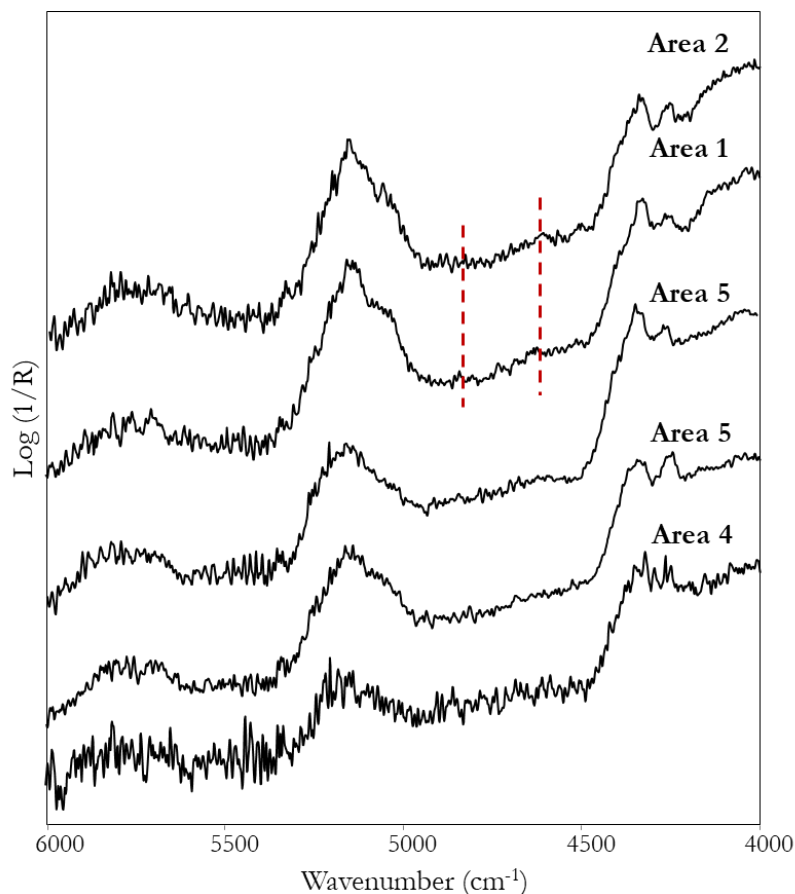


Figure 34. FT-NIR spectra obtained from *St. Augustine and Jerome* by Bergognone (1492-1494). The painting is available at [57].

4.4.1.3 *St. John the Baptist* by Zenale

In the MIR region, the signals due to a superficial varnish applied after the restoration work were invariably observed. On the other hand, the NIR spectra showed in all cases the signals due to the gypsum associated with the preparation layer (Fig. 35). The typical bands of a lipid component were also observed at about 4320 and 4260 cm^{-1} , which refer to the use of a siccative oil as binder. However, in the case of areas 1, 2 and 4, the signals around 4850 and 4620 cm^{-1} associated with a protein component were also distinguishable, which suggested, despite their low intensity, the possible presence of egg tempera. Not being able to obtain information from the spectral response in the MIR (since the analyses were carried out at the end of the restoration), it was not possible to hypothesise whether they are two different layers obtained with the two different binders or if they were used in a mixture. The combined use of a lipidic and a proteinaceous binder was highlighted also by the ratio between the absorbance values of the bands at 4694 and 5160 cm^{-1} , corresponding to 0.4 (Fig. 28).

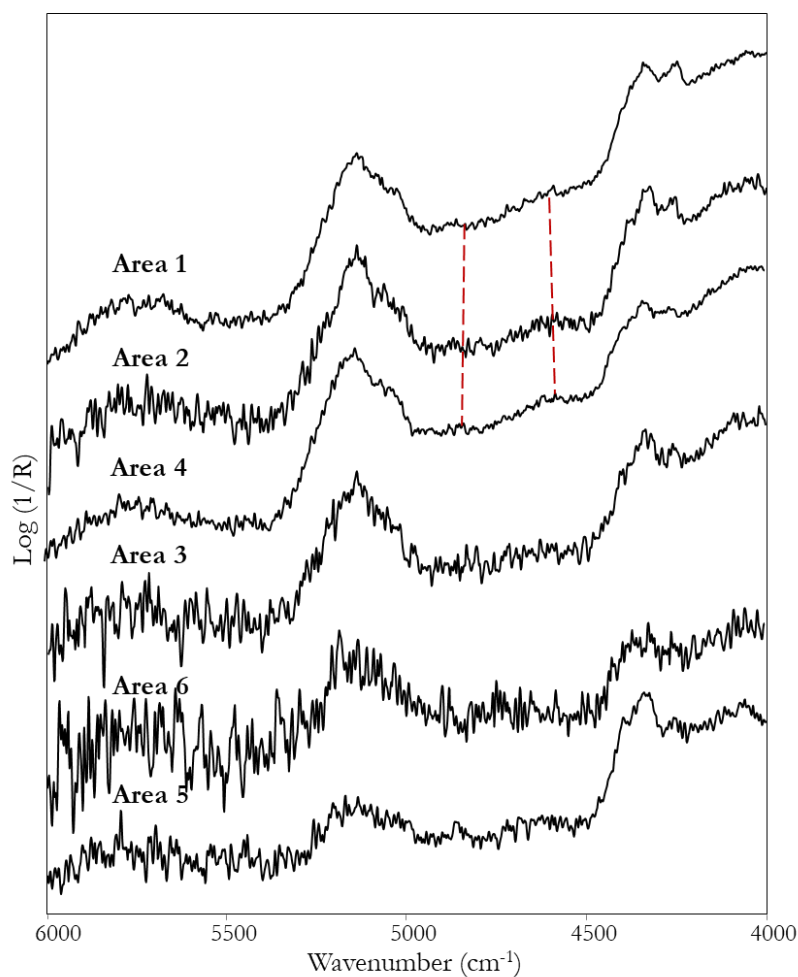


Figure 35. Some exemplificative FT-NIR spectra obtained from *S. Giovanni Battista* by B. Zenale (early 16th century). The painting is available at [58].

5.4.2 *Ecce Homo* by A. Solario

The artwork is painted on paper applied to a wood panel, but the artist's technique is unclear: it is classified as tempera and oil in the catalogue of the Accademia Carrara, to which it belongs [59], while in the catalogue of the Lombard cultural heritage it is considered to be oil [60]. FT-IR measurements were carried out on areas of the painting from which the varnish applied during a previous restoration work had been removed. In the MIR region, the bands at 1640 and 1320 cm^{-1} due to calcium oxalate CaC_2O_4 presumably dihydrate, prevailed. It is evidently a degradation product of the organic substances originally present in the painting and, although it is sometimes particularly associated with the degradation of tempera, it has nevertheless often been observed in oil paintings as well [29]. The presence of a lipidic component of the binder was attested by a weak signal at about 1740 cm^{-1} , but the bands of any proteinaceous component would be hidden by that of calcium oxalate. The spectrum obtained on the complexion was

particular because it still showed intense bands at 1712, 1450 and 1380 cm^{-1} possibly due to a natural resin, probably dammar, used as varnish (Fig. 36).

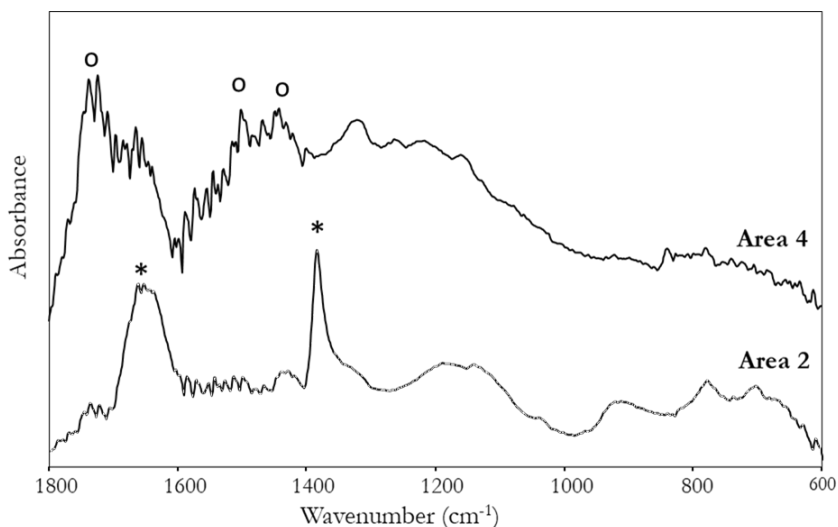


Figure 36. FT-MIR spectra from area 2 and 4, showing respectively the bands due to calcium oxalate (*) and to a residual restoration varnish (o).

In the NIR region, the spectra were dominated by the bands at 5180, 4745, 4390 and 4280 cm^{-1} , typical of cellulose [61] and therefore of the paper that constitutes the support of the painting (Fig. 37). However, for the details of Christ's skin, hair and robe, it was also possible to distinguish the two most intense peaks at about 4330 and 4265 cm^{-1} typical of lipids. The absence of evident signals attributable to gypsum and the possibility of observing the bands of the support led to the supposition that a preparation layer is not present. Moreover, the fact that the characteristic peaks of the lipidic component were not very evident suggested that an oil priming layer was also lacking. However, the predominance of signals due to paper did not allow to recognise even in the NIR region any band associated with a proteinaceous component.

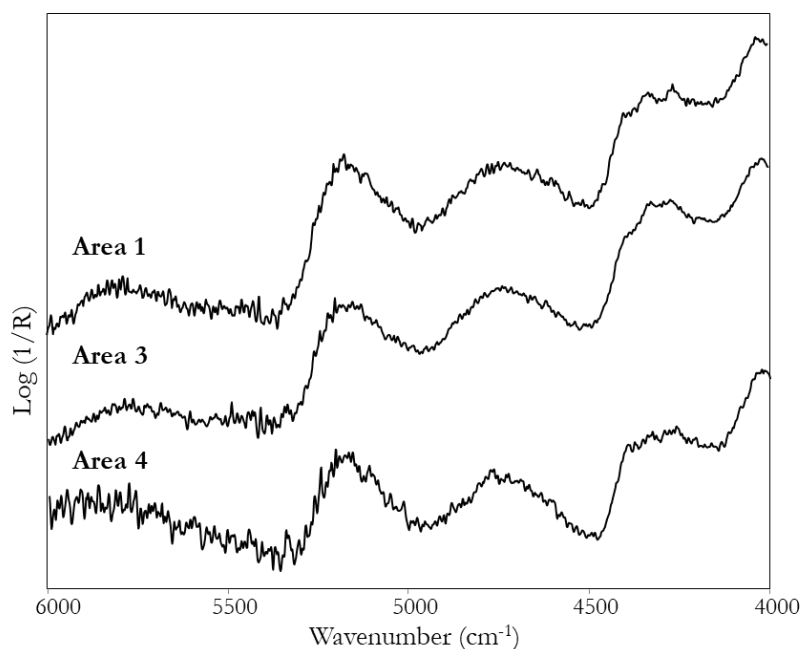


Figure 37. FT- NIR spectra of the corresponding analysed areas of the painting *Ecce Homo* by A. Solario (early 16th century). The painting is available at [59]

In conclusion, thanks to the penetration depth of the NIR radiation, it could be assumed that in this painting both a gypsum preparation and an oil primer are absent. In addition, due to the prevalence of the bands due to the cellulose in the NIR region and those of calcium oxalates in the MIR region, it cannot be excluded that the binder contains a proteinaceous component alongside the lipidic one.

5.4.3 A late baroque Italian painting: *Porter boy sitting on a basket* by Pitocchetto

This painting on canvas dates back to a period (ca. 1735) in which the use of oil binder had been established for two centuries (see section 2.1). On the contrary, the spectro-analytical investigation was of interest from the point of view of the evolution in the characteristics of ground layers (see section 2.2). Also this painting, as well as the one described in the next section, was examined in the studio of restorer Carlotta Beccaria.

FT-IR measurements were carried out on areas of the painting having different colours; moreover, in some of them a surface layer of varnish had already been removed during the ongoing restoration work, while in others it was still present. Referring to MIR spectra, those acquired on varnished areas show signals due to the surface coating; those from cleaned areas, on the other hand, have a completely different pattern, where the main bands are attributable to oil and pigments. In particular, in the light-coloured areas white lead is well recognisable [47] (Fig. 38).

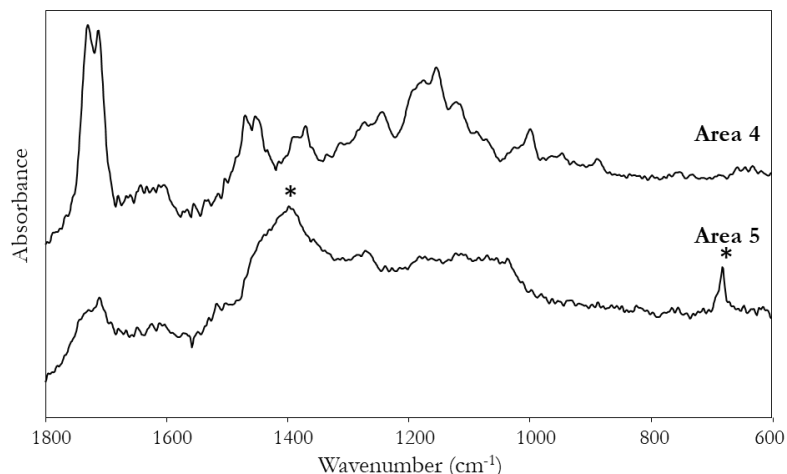


Figure 38. Comparison between FT-MIR spectra from the varnished (area 4) and unvarnished (area 5) areas of the wrist. * =signals due to lead white.

In the NIR region, spectra (Fig. 39) acquired from varnished and unvarnished areas are quite similar to one another, demonstrating once more that in this spectral range it is possible to investigate the inner layers without interference by the surface coating. In all cases, the prevailing signals are those due to an oil binder, but in the spectra of the dark-coloured areas (area 1, 6, 7) and in the lips (area 8), the band at 5200 cm^{-1} is more pronounced than in the remaining areas. This signal can be attributed to the -OH groups presence of an earth pigment, both for its shape and the position. Being reported for this artist the use of dark preparations containing earth pigments, a mock-up sample was prepared by spreading on canvas a mixture of red ochre, lead white and oil, and was then analysed. Actually, a correspondence between the spectral data was found, as shown in Fig. 39, in spite of the fact that the spectrum of the model sample showed evident signals due to canvas. This hypothesis is supported by the fact that this feature is recurrent in the reddish areas, where an earth could have been used as pigment or where the deterioration of the painting film leaves the preparatory layer visible. The possibility that, in the darkest areas of the painting, the ground layer was intentionally left visible by the artist must also be taken into account. Finally, in areas 6 (jacket) and 7 (background), a signal at 4190 cm^{-1} is recognised which could be associated with the presence of lead palmitates (see Fig. 7 and Tab. 7). This information is in agreement with the results obtained from the analyses performed by μ -FT-IR and SEM-EDX on two small fragments collected from the painting during the restoration work (see Appendix B).

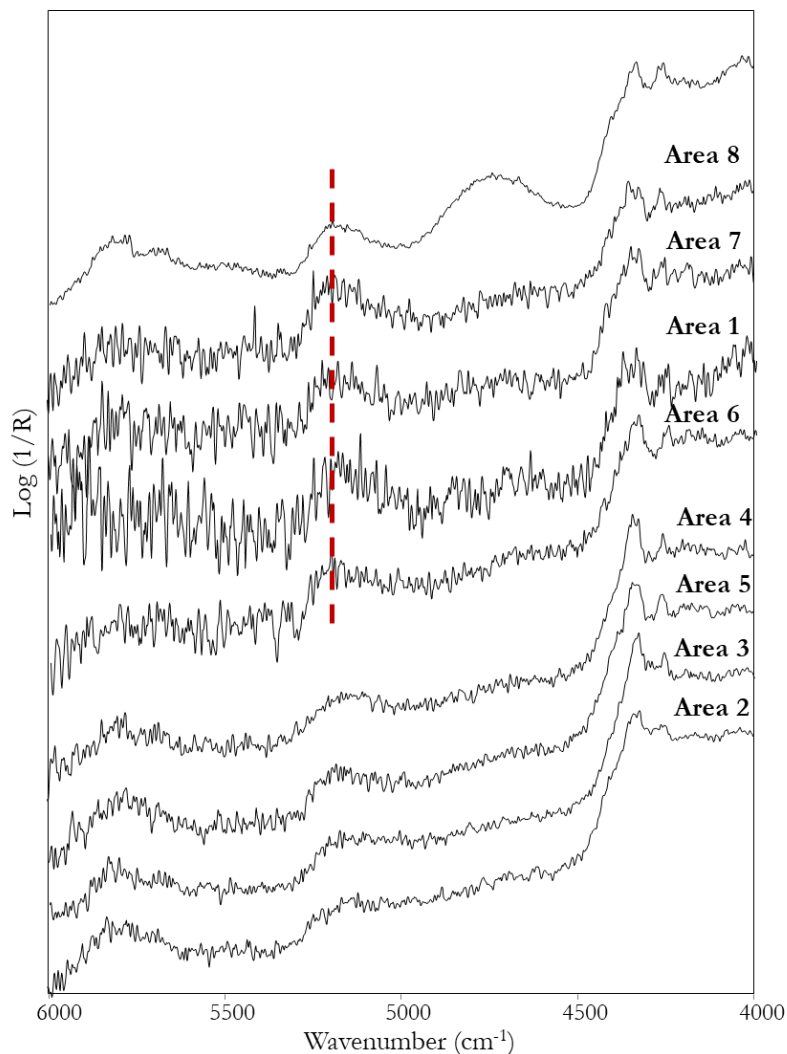


Figure 39. Some exemplificative FT-NIR spectra obtained from *Portarolo sit on a basket* by Pitocchetto (1735). The painting is available at [62].

5.4.4 A neoclassical Italian painting: *Napoleon* by A. Appiani

Also in the case of this painting on canvas, due to the one of the most important representatives of Italian Neoclassicism, the main interest of the FT-IR analyses was related to the identification of the materials of the ground layer, as well as to that of pigments. For the latter, also Raman spectroscopy was employed, as detailed elsewhere [28].

In the MIR range the spectra are often dominated by the signals of the synthetic consolidant spread on the surface after the restoration work; specifically, it is BEVA 371, a mixture of ketone resin and polyvinyl acetate [28]. It is also possible to recognise the oil band at 1740 cm^{-1} and some signals due to pigments: it is the case of lead white in the light-coloured areas, while the use of Prussian blue was identified in the blue and in the green ones. An interesting case is represented by the grey background: the measurements performed in three different areas gave spectra (Fig. 40) that show a variation in the ratio between the oil band at 1740 cm^{-1} and those

attributable to calcium oxalate at 1640 and 1308 cm^{-1} . In particular, as oxalate increases (red arrow) the amounts of oil decreases (green arrow). Therefore, it was possible to map an inhomogeneous degradation process which affects the pictorial surface. In this area the signal due to the synthetic consolidant were not detected.

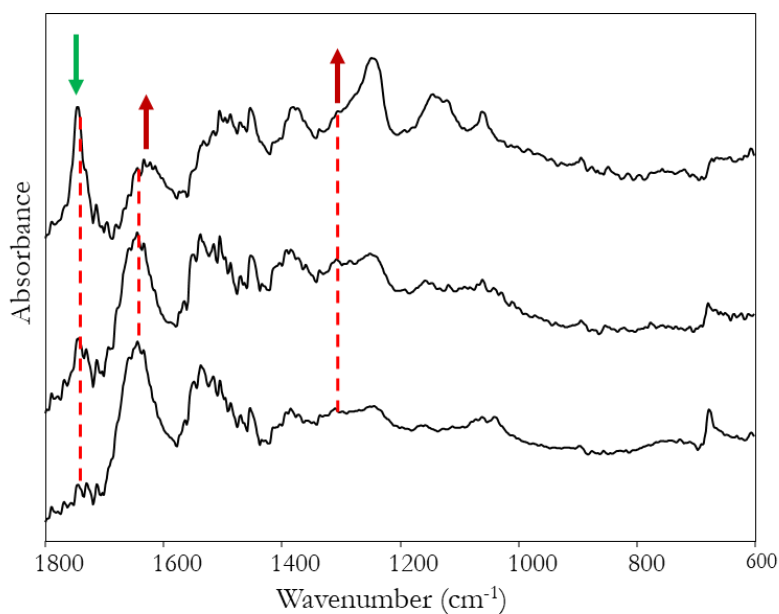


Figure 40. FT-MIR spectra from three areas of the grey background of the painting *Napoleon* by Appiani. A decrease of the signal due to oil is joined by the increase of those corresponding to calcium oxalate.

Referring to the NIR region (Fig. 41), the spectral pattern is that typical of a siccative oil. However, associated with the oil ones, the signal at 4290 cm^{-1} attributable to lead white is well recognisable, disclosing a possible ground layer composed of this pigment dispersed in oil.

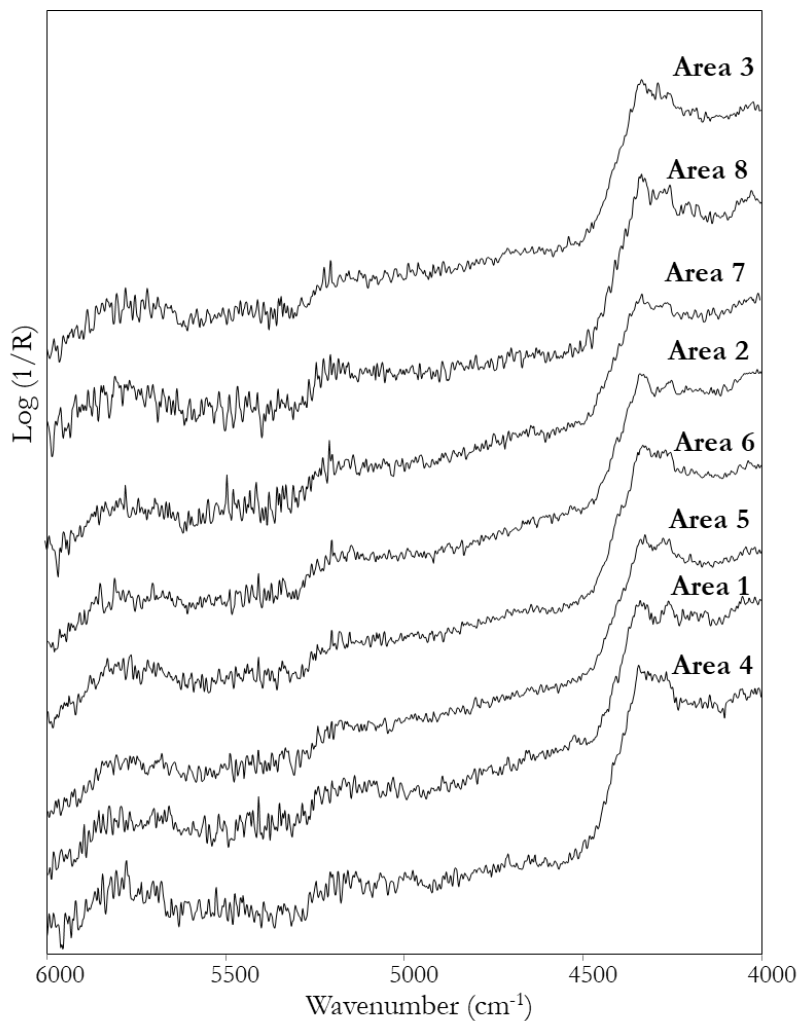


Figure 41. FT- NIR spectra of the corresponding analysed areas of the painting *Napoleone* by A. Appiani (1805).

6. Conclusions

In the present work the potentiality of FT-NIR spectroscopy for the non-invasive characterisation of binders and preparatory layers directly on paintings was investigated. Complex model samples were prepared, with two different compositions of the preparatory layer, gypsum or calcite, and the use of oil and tempera binders, separately, in mixture (*tempera grassa*) or in overlapping layers. Different pigments were also used in the models, including pigments containing hydroxyl groups and therefore prone to absorb NIR radiation. A multivariate approach based on principal component analysis (PCA) was used to emphasize the subtle differences in the spectral patterns, allowing the identification not only of oil and tempera, but also of *tempera grassa* and of superimposed layers containing the two binders. The possibility of individuating the presence of gypsum in the ground layer was correlated with the thickness of the above colour layer. Finally, FT-NIR analyses were carried out on ancient paintings dating from the end of the 15th to the beginning of the 19th century, giving a wide insight on the

applicability of this method for the non-invasive detection of binders, also when different ones were used in the same painting. At the same time, information can be obtained about the presence or absence of a preparatory layer, in particular a gypsum-based one, or of a priming layer, as demonstrated in the particular case of the painting on paper by Solario. Moreover, in the two later paintings the use of a lead white or of earth pigments dispersed in oil as priming layers was recognised, according to the artistic technique of that period.

References

- [1] M. Matteini, A. Moles, *La Chimica nel Restauro. I Materiali dell'arte Pittorica*, Nardini Editore, Florence, 1989.
- [2] G. D'Anna, S. Marconi, C. Merucci, M. L. Papini, L. Traversi, *Preparazione e Finitura delle opere pittoriche. Materiali e metodi. Preparazioni e imprimiture - Leganti - vernici - cornici*, Mursia Editore, 1993.
- [3] S. L. Vallance, *Analyst* 1997, 122, 75R-81R
- [4] R. M. Castro, M.T. D. Carbó, V. P. Martínez, J. V. G. Adelantado, F. B. Reig, *J. Chromatogr. A* 1997, 778, 373-381.
- [5] M. P. Colombini, F. Modugno, E. Menicagli, R. Fuoco, A. Giacomelli, *Microchem. J.* 2000, 67, 291-300.
- [6] M. P. Colombini, F. Modugno, M. Giacomelli, S. Francesconi, *J. Chromatogr. A*, 1999, 846, 113-124.
- [7] M. P. Colombini, A. Andreotti, I. Bonaduce, F. Modugno, E. Ribechini, *Acc. Chem. Res.* 2010, 43, 715-727
- [8] M. Vagnini, C. Miliani, L. Cartechini, P. Rocchi, B. G. Brunetti, A. Sgamellotti, *Anal. Bioanal. Chem.* 2009, 395, 2107-2118
- [9] A. Jurado-López, M. D. Luque de Castro, *Anal. Bioanal. Chem.* 2004, 380, 706-711.
- [10] J. S. Mills, R. White, *The Organic Chemistry of Museum Objects*, Butterworths, London, 1999.
- [11] G. Vasari, *Le vite de' più eccellenti pittori, scultori, e architettori*, Colla Editore, 2012.
- [12] M. Stols, *Grounds, 1400-1900* in *The Conservation of easel paintings*, 2012, 161-185
- [13] G. Socrates, *Infrared and Raman Characteristic Group Frequencies: Third Edition*, John Wiley & Sons Ltd., Chichester, 2001.
- [14] P. R. Griffiths, J. A. De Haseth, *Fourier Transform Infrared Spectrometry: Second Edition*, John Wiley & Sons, New Jersey, 2007.
- [15] C. Invernizzi, T. Rovetta, M. Lichelli, M. Malagodi, *Int. J. Anal. Chem.* 2018, 7823248.
- [16] F. Casadio and L. Toniolo, *J. Cult. Herit.* 2001, 2 (1), 71-78.
- [17] Z. I. Glavcheva, D. Y. Yancheva, Y. K. Kancheva, E. A. Velcheva, B. A. Stamboliyska, *Bulg. Chem. Comm.* 2014, 46, 164 - 169.
- [18] J. J. Bischoff, M. R. Derrick, D. Stulik, and J. M. Landry, *J. Am. Inst. Cons.* 2001, 40, 268, 2001.

- [19] www.irug.org
- [20] M. Spring, C. Ricci, D. Peggie, S. Kazarian, *Anal. Bioanal. Chem* 2008, 392 (1-2), 37-45.
- [21] F. W. Herschel, *Philos. Trans. R. Soc. London* 1800, 90, 255–329.
- [22] K. H. Norris, *J. Near Infrared Spectrosc.* 1996, 4, 31–37.
- [23] W. F. McClure, *J. Near Infrared Spectrosc.*, 2003, 11, 487–518 and papers therein.
- [24] M. Manley, *Chem. Soc. Rev.* 2014, 43, 8200-8214.
- [25] M. Blanco, I. Villarroya, *TRAC-Trend. Analyt. Chem.* 2002, 21, 240-250.
- [26] M. Spring, H. Howard, J. Kirby, J. Padfield, D. Peggie, A. Roy, A. Stephenson-Wright, *Studying Old Master Paintings, Technology and Practice*, The National Gallery Technical Bulletin 30th Anniversary Conference Postprints, Archetype Publications in association with the National Gallery, 2011.
- [27] J. Dunkerton, M. Spring, *The development of painting on coloured surfaces in sixteenth-century Italy*, in “Painting techniques: history, materials and studio practice, contributions to the ICC Dublin Congress”, A. Roy e P. Smith, International Institute for Conservation of Historic and Artistic Works, Londra, 7-11 September 1998.
- [28] A. Marzanni, bachelor thesis, Università degli Studi di Milano, 2021.
- [29] R. Mazzeo, S. Prati, M. Quaranta, E. Joseph, E. Kendix, M. Galeotti, *Anal. Bioanal. Chem.* 2008, 392, 65–76.
- [30] A. A. Christy, S. Kasemsumran, Y. Du, Y. Ozaki, *Anal. Sci.* 2004, 20, 935-940.
- [31] J. Workman Jr., L. Weyer, *Practical Guide to Interpretive Near-Infrared Spectroscopy*, CRC Press, 2007.
- [32] M. R. Derrick, D.C. Stulik, J. M. Landry, *Infrared Spectroscopy in Conservation Science*, The Getty Conservation Institute, Los Angeles, 1999.
- [33] R. L. Frost, B. J. Reddy, D. L. Wain, W. N. Martens, *Spectrochim. Acta A* 2007, 66, 1075-1081.
- [34] M. Bacci in: Ciliberto E, Spoto G (eds) *Modern analytical methods in art and archaeology*, Wiley, New York, 2000, 321-361.
- [35] F. Rosi, A. Daveri, B. Doherty, S. Nazzareni, B. G. Brunetti, A. Sgamellotti, C. Miliani, *Appl. Spectrosc.* 2010, 64, 956-963.
- [36] M. Bacci, R. Chiari, S. Porcinai, B. Radicati, *Chemometr. Intell. Lab. Syst.* 1997, 39, 115-121.
- [37] T. Poli, O. Chiantore, E. Diana, A. Piccirillo, *Coatings* 2021, 11, 171.
- [38] L. Baij, J. J. Hermans, K. Keune, P. Iedema, *Angew. Chem. Int.* 2018, 57,7351-7354.
- [39] G. J. A. M. Eumelen, E. Bosco, A. S. J. Suiker, A. van Loonb, P. D. Iedem, *J. Mech. Phys. Solids* 2019, 132, 103683.
- [40] F. Casadio, K. Keune, P. Noble, A. Van Loon, E. Hendriks, S. A. Centeno, G. Osmond, *Metal Soaps in Art. Conservation and Research*, Cultural Heritage Science, Springer, 2019 and papers therein.
- [41] L. Rampazzi, *J. Cult. Herit.* 2019, 40, 195-214.

- [42] F. Bordignon, P. Postorino, P. Dore M. Laurenzi Tabasso, *Stud. Cons.* 2008, 53 (3), 158-169.
- [43] M. Spring, C. Higgitt, D. Saunders, *Investigation of Pigment-Medium Interaction Processes in Oil Paint Containing Degraded Smalt*. National Gallery Technical Bulletin, 26, 2005, 56–69
- [44] K. Sutherland, B. Price, A. Lins. *The Characterization of Degraded, Oxalate-Rich Surface Layers on Paintings* in The Seventh Biennial Gathering of the Infrared and Raman Users Group (IRUG7), Abstracts and Executive Summaries of Contributions, pp. 41–42. New York: Museum of Modern Art.
- [45] M. Bacci, S. Baronti, A. Casini, P. Castagna, R. Linari, A. Orlando, M. Picollo, B. Radicati, *Mat. Res. Symp. Proc.* 1995, 352, 153-159.
- [46] M. Matteini, A. Moles. *Calcium Oxalate Patinas on Marble Objects*. OPD Restauro: Quaderni dell'Opificio delle Pietre Dure e Laboratori di Restauro di Firenze, 1986, 65-73.
- [47] C. Zaffino, V. Guglielmi, S. Faraone, A. Vinaccia, S. Bruni, *Spectrochim. Acta A Mol. Biomol.* 2015, 136, 1076-1085.
- [48] A. Galli, M. Gargano, L. Bonizzoni, S. Bruni, M. Interlenghi, M. Longoni, A. Passaretti, M. Caccia, C. Salvatore, I. Castiglioni, M. Martini, *Dyes Pigm.* 2021, 187, 109112
- [49] E. Manzano, N. Navas, R. Checa-Moreno, L. Rodriguez-Simón, L. F. Capitán-Vallvey, *Talanta* 2009, 77, 1724-1731.
- [50] R. J. Meilunas, J. G. Bentsen, A. Steinberg, *Stud. Cons.* 1990, 35, 33-51.
- [51] S. Boyatzis, E. Ioakimoglou, P. Argitis, *J. Appl. Polym. Sci.* 2007, 84, 936–949.
- [52]
https://museopoldipezzoli.it/catalogo/#/dettaglio/119305_Madonna%20con%20Bambino
- [53] M. Spring, A. Mazzotta, A. Roy, R. Billinge, D. Peggie, *Painting practice in milan in the1490s: the influence of Leonardo*. Natl. Gallery Tech. Bull. 2011, 32, 78–112
- [54] C. Beccaria, *Some observations on the painting technique of Boltraffio's the Madonna and Child*. Leonardo Vincis Tech. Pract. Paint. Draw. Influ. Paint. Draw. Influ. HERMANN 2014.
- [55] <https://pinacotecabrera.org/collezione-online/opere/madonna-col-bambino-napoletano>
- [56]
https://museopoldipezzoli.it/catalogo/#/dettaglio/121656_Madonna%20che%20allatta%20il%20Bambino
- [57] <https://catalogo.beniculturali.it/detail/HistoricOrArtisticProperty/0300702290-3>
- [58] <https://www.sothebys.com/en/buy/auction/2020/old-masters-including-portrait-miniatures-from-the-pohl-stroeher-collection/bernardo-zenale-saint-john-the-baptist-standing-in>
- [59] <https://www.lacarrara.it/catalogo/81lc00236>
- [60] <https://catalogo.beniculturali.it/detail/HistoricOrArtisticProperty/0302024554>
- [61] X. Li, C. Sun, B. Zhou, Y. He, *Sci. Rep.* 2015, 5, 17210.
- [62] <https://pinacotecabrera.org/collezione-online/opere/portarolo-seduto-su-una-cesta/>

APPENDIX A

1. Reference FT-IR spectra and band assignment

FT-NIR and FT-MIR spectra of tempera painting models with lead white

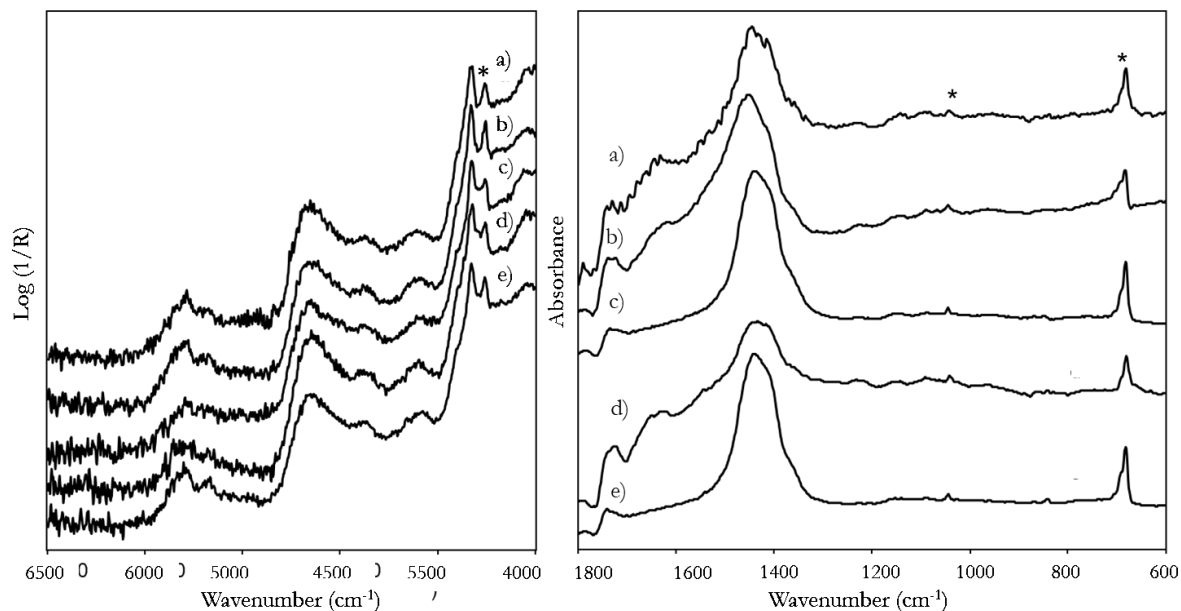


Figure 1. FT-NIR and FT-MIR spectra from painting models of lead white in: a) *tempera grassa* with linseed oil; b) *tempera grassa* with walnut oil, c) egg tempera, (d) linseed oil on egg tempera, (e) walnut oil on egg tempera. Legend: *=signals due to lead white.

Table 1. Wavenumbers (cm^{-1}) of the NIR absorption bands for tempera painting models with lead white.

	Pigment bands	Binder bands - lipidic fraction	Binder bands - proteinaceous fraction
<i>Tempera grassa</i> linseed	4275	4331, 4260	5168, 4869, 4610
<i>Tempera grassa</i> walnut	4273	4333, 4257	5155, 4880, 4605
Tempera	4274	4328, 4262	5160, 4884, 4597
Linseed oil on tempera	4275	4326, 4257	5151, 4876, 4600
Walnut oil on tempera	4275	4333, 4265	5158, 4879, 4578

Table 2. Wavenumbers (cm^{-1}) of the MIR absorption bands for tempera painting models with lead white.

	Pigment bands (cm^{-1})	Binder bands (cm^{-1})- lipidic fraction	Binder bands (cm^{-1})- proteinaceous fraction
<i>Tempera grassa</i> linseed	1440, 1044, 682	1745	1643, 1550
<i>Tempera grassa</i> walnut	1450, 1045, 686	1740	1630
Tempera	1430, 1042, 681	1742	1649, 1653
Linseed oil on tempera	1434, 1045, 681	1735	-
Walnut oil on tempera	1440, 1044, 682	1742	-

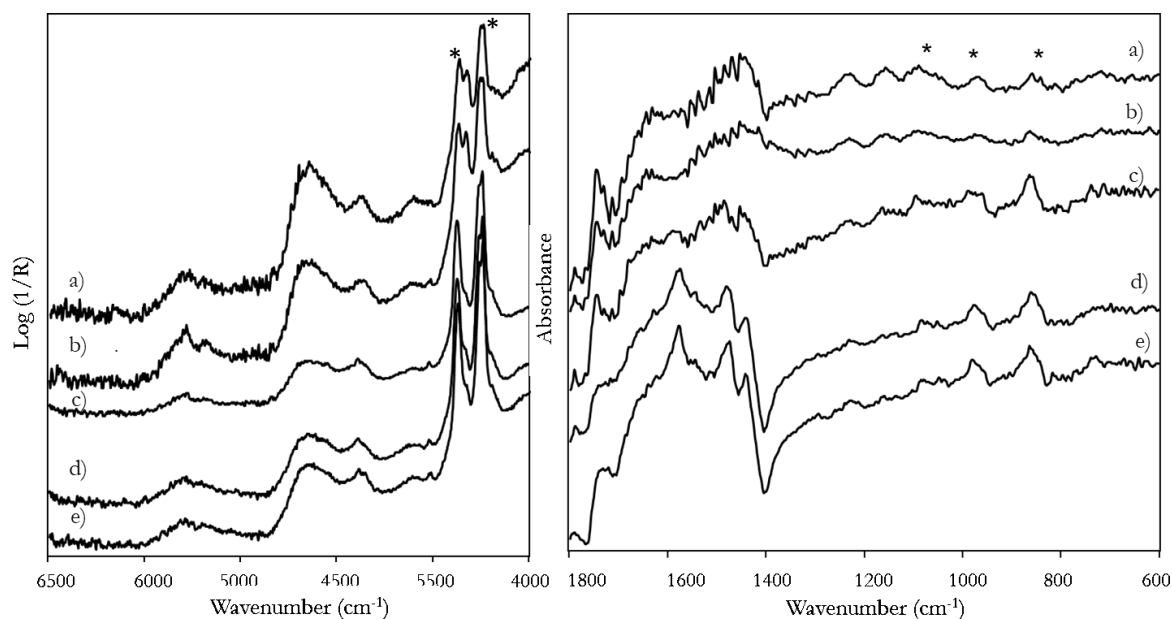


Figure 2. FT-NIR and FT-MIR spectra from painting models of azurite in: a) *tempera grassa* with linseed oil; b) *tempera grassa* with walnut oil, c) egg tempera, (d) linseed oil on egg tempera, (e) walnut oil on egg tempera. Legend: *=signals due to azurite.

Table 3. Wavenumbers (cm⁻¹) of the NIR absorption bands for tempera painting models with azurite.

	Pigment bands	Binder bands - lipidic fraction	Binder bands - proteinaceous fraction
<i>Tempera grassa</i> linseed	4371, 4245	4256, 4330	5160, 4872
<i>Tempera grassa</i> walnut	4368, 4242	4256, 4330	5164, 4864
Tempera	4374, 4243	4259, 4339	5163, 4870
Linseed oil on tempera	4373, 4242	4259, 4332	5156, 4880
Walnut oil on tempera	4373, 4243	4260, 4330	5167, 4875

Table 4. Wavenumbers (cm⁻¹) of the MIR absorption bands for tempera painting models with azurite.

	Pigment bands	Binder bands - lipidic fraction	Binder bands - proteinaceous fraction
<i>Tempera grassa</i> linseed	1091, 963, 860	1745	1649
<i>Tempera grassa</i> walnut	1092, 958, 858	1745	1641
Tempera	1095, 966, 860	1745	1635, 1540
Linseed oil on tempera	1086, 970, 851	1743	1544
Walnut oil on tempera	1087, 960, 862	1743	1646

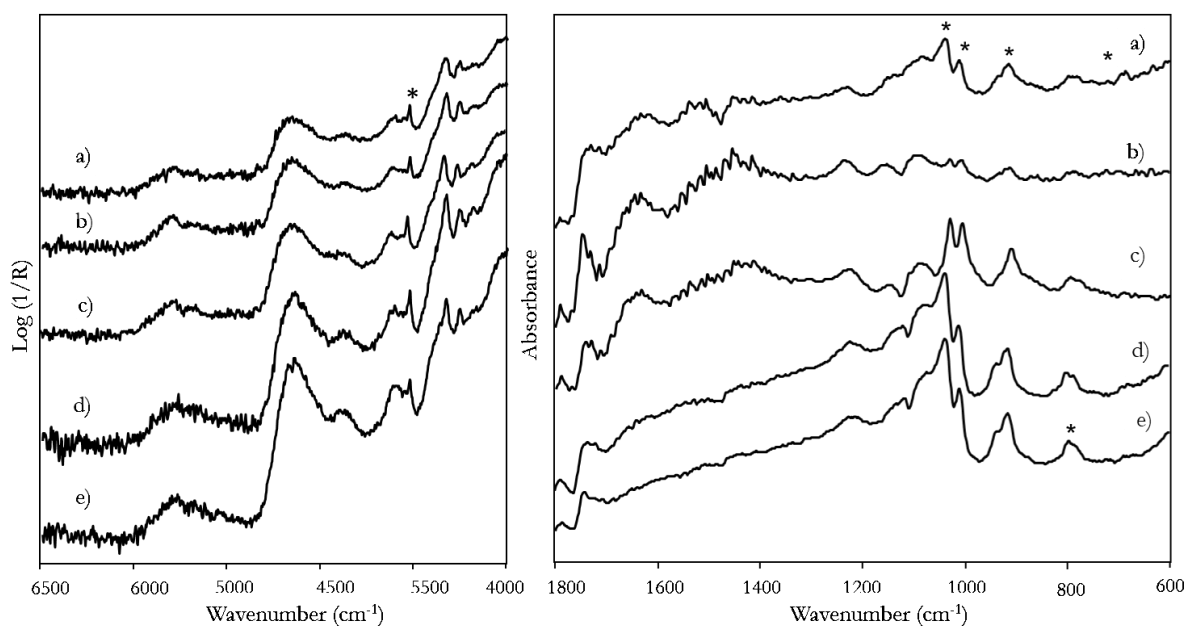


Figure 3. FT-NIR and FT-MIR spectra from painting models of yellow ochre in: a) *tempera grassa* with linseed oil; b) *tempera grassa* with walnut oil, c) egg tempera, (d) linseed oil on egg tempera, (e) walnut oil on egg tempera. Legend: *=signals due to yellow ochre.

Table 5. Wavenumbers (cm⁻¹) of the NIR absorption bands for tempera painting models with yellow ochre.

	Pigment bands	Binder bands - lipidic fraction	Binder bands - proteinaceous fraction
<i>Tempera grassa</i> linseed	4526	4330, 4255	5158, 4866
<i>Tempera grassa</i> walnut	4526	4327, 4255	5158, 4869
Tempera	4526	4330, 4255	5149, 4863
Linseed oil on tempera	4526	4330, 4255	5143, 4872
Walnut oil on tempera	4526	4330, 4258	5152, 4869

Table 6. Wavenumbers (cm⁻¹) of the MIR absorption bands for tempera painting models with yellow ochre.

	Pigment bands	Binder bands - lipidic fraction	Binder bands - proteinaceous fraction
<i>Tempera grassa</i> linseed	1036, 1011, 912	800	1740, 1635, 1532
<i>Tempera grassa</i> walnut	1031, 1006, 912		1745, 1645
Tempera	1030, 1006, 911	796	1743, 1640
Linseed oil on tempera	1037, 1010, 913	800	-
Walnut oil on tempera	1036, 1010, 915	799	1745

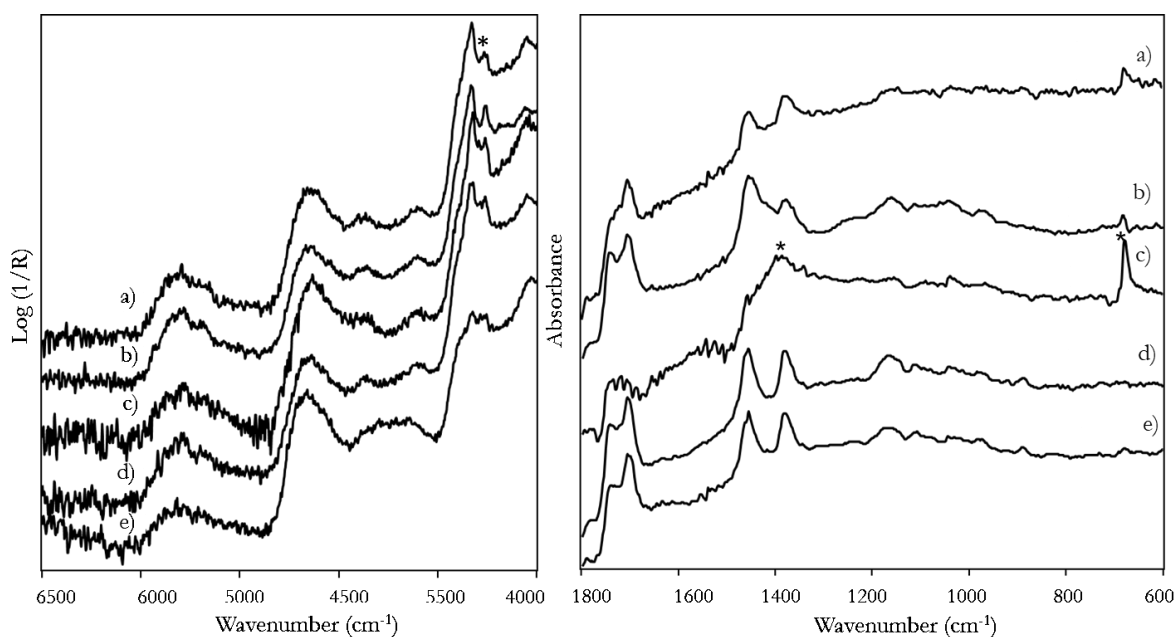


Figure 4. FT-NIR and FT-MIR spectra from painting models of lead white in: a) *tempera grassa* with linseed oil + dammar; b) *tempera grassa* walnut oil + mastic varnish; c) egg tempera + dammar; d) linseed oil on tempera + dammar; e) walnut oil on tempera + dammar. Legend: *=signals due to lead white.

Table 7. Wavenumbers (cm⁻¹) of the NIR absorption bands for tempera painting models with lead white and a superficial layer of varnish.

	Pigment bands -	Binder bands - lipidic fraction	Binder bands - proteinaceous fraction
<i>Tempera grassa</i> linseed	4279	4329, 4255	5160, 4863
<i>Tempera grassa</i> walnut	4275	4332, 4258	5166, 4860
Tempera	4275	4328, 4255	5134, 4864
Linseed oil on tempera	4278	4330, 4258	5161, 4868
Walnut oil on tempera	4275	4328, 4252	5165

Table 8. Wavenumbers (cm⁻¹) of the MIR absorption bands for tempera painting models with lead white and a superficial layer of varnish.

	Pigment bands	Binder bands- lipidic fraction	Binder bands - proteinaceous fraction	Varnish bands
<i>Tempera grassa</i> linseed	681	1742	-	1706, 1456, 1380
<i>Tempera grassa</i> walnut	682	1735	-	1703, 1450, 1381
Tempera	680, 1400	1743	-	1706
Linseed oil on tempera	-	1741	-	1704, 1457, 1379
Walnut oil on tempera	-	-	-	1705, 1457, 1383

FT-NIR and FT-MIR spectra of tempera painting models with azurite and varnish

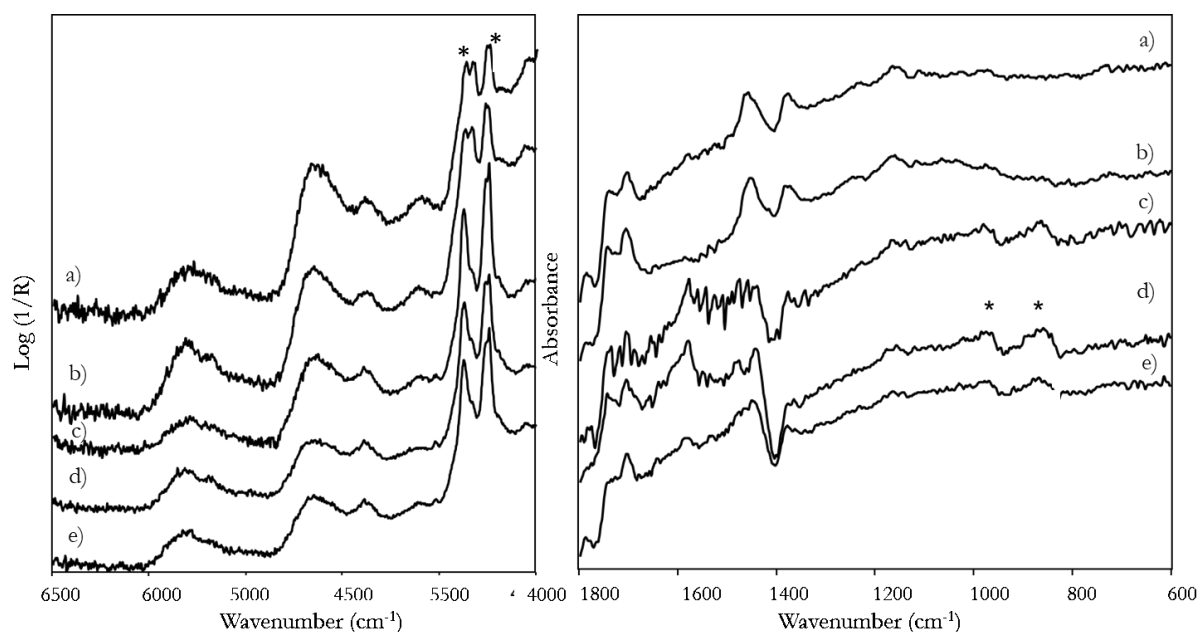


Figure 5. FT-NIR and FT-MIR spectra from painting models of azurite in: a) *tempera grassa* with linseed oil + dammar; b) *tempera grassa* walnut oil + mastic varnish; c) egg tempera + dammar; d) linseed oil on tempera + dammar; e) walnut oil on tempera + dammar. Legend: *=signals due to azurite.

Table 9. Wavenumbers (cm⁻¹) of the NIR absorption bands for tempera painting models with azurite and a superficial layer of varnish.

	Pigment bands	Binder bands - lipidic fraction	Binder bands - proteinaceous fraction
<i>Tempera grassa</i> linseed	4375, 4244, 4331	4259	5156, 4879
<i>Tempera grassa</i> walnut	4369, 4243, 4330	4255	5165, 4874
Tempera	4375, 4243, 4332	4259	5162, 4885
Linseed oil on tempera	4375, 4241, 4333	4260	5162, 4885
Walnut oil on tempera	4372, 4242, 4330	4258	5175, 4866

Table 10. Wavenumbers (cm⁻¹) of the MIR absorption bands for tempera painting models with azurite and a superficial layer of varnish.

	Pigment bands	Binder bands - lipidic fraction	Binder bands - proteinaceous fraction	Varnish bands
<i>Tempera grassa</i> linseed	-	1743	-	1706, 1456, 1380
<i>Tempera grassa</i> walnut	-	1743	-	1703, 1450, 1381
Tempera	-	-	-	1706
Linseed oil on tempera	1579, 971, 844	1741	-	1704, 1457, 1379
Walnut oil on tempera	1577, 969, 860	1740	-	1705, 1457, 1383

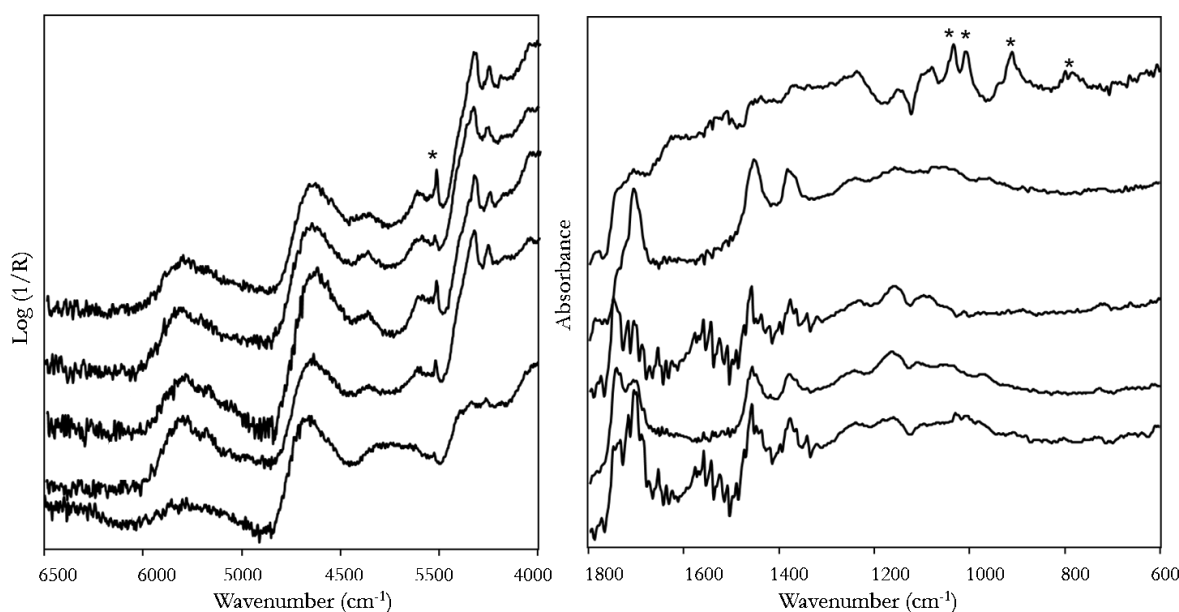


Figure 6. FT-NIR and FT-MIR spectra from painting models of yellow ochre in: a) *tempera grassa* with linseed oil + dammar; b) *tempera grassa* walnut oil + mastic varnish; c) egg tempera + dammar; d) linseed oil on tempera + dammar; e) walnut oil on tempera + dammar. Legend: *=signals due to yellow ochre.

Table 11. Wavenumbers (cm⁻¹) of the NIR absorption bands for tempera painting models with yellow ochre and a superficial layer of varnish.

	Pigment bands	Binder bands - lipidic fraction	Binder bands - proteinaceous fraction
<i>Tempera grassa</i> linseed	4375, 4244, 4331	4259	5156, 4879
<i>Tempera grassa</i> walnut	4369, 4243, 4330	4255	5165, 4874
Tempera	4375, 4243, 4332	4259	5162, 4885
Linseed oil on tempera	4375, 4241, 4333	4260	5162, 4885
Walnut oil on tempera	4372, 4242, 4330	4258	5175, 4866

Table 12. Wavenumbers (cm⁻¹) of the MIR absorption bands for tempera painting models with yellow ochre and a superficial layer of varnish.

	Pigment bands	Binder bands - lipidic fraction	Binder bands - proteinaceous fraction	Varnish bands
<i>Tempera grassa</i> linseed	799, 914, 1009, 1034	1743, 1630	1540	-
<i>Tempera grassa</i> walnut	-	1737	-	1705, 1455, 1383
Tempera	1011	1749	-	1705, 1459, 1377
Linseed oil on tempera	-	1742	-	1706, 1457, 1379
Walnut oil on tempera	1008, 1030	1747	-	1705, 1458, 1377

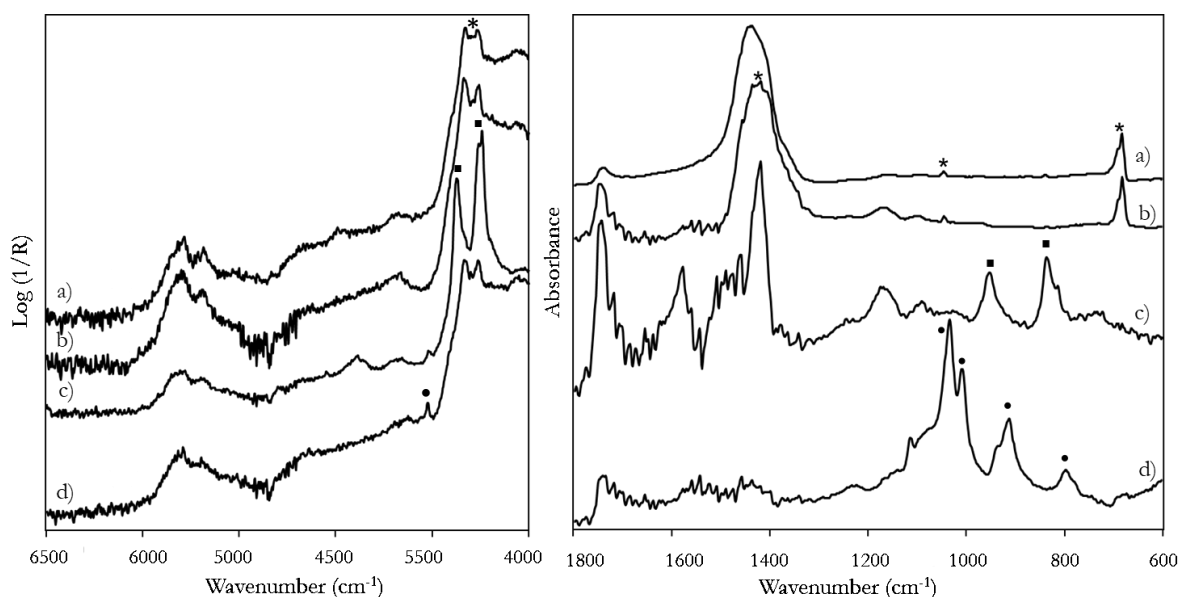


Figure 7. FT-NIR and FT-MIR spectra from painting models of: a) white priming layer with lead white and walnut oil; b) lead white in linseed oil layer on white priming layer; c) azurite in linseed oil layer on white priming layer; d) azurite in linseed oil layer on white priming layer. Legend: *= signals due to lead white, ■ = azurite and • = yellow ochre

Table 13. Wavenumbers (cm⁻¹) of the NIR absorption bands for painting models of linseed oil on a white priming layer.

	Pigment bands	Binder bands lipidic fraction	Other oil bands
Lead white priming layer	4280	4336, 4261	5803, 5685, 4688
Lead white in linseed oil	4280	4336, 4259	5801, 5685, 4680
Azurite in linseed oil	4372, 4244	4339, 4261	5804, 5696, 4881
Ochre in linseed oil	4526	4335, 4261	5796, 5796

Table 14. Wavenumbers (cm⁻¹) of the MIR absorption bands for painting models of linseed oil on a white priming layer.

	Pigment bands	Binder bands- lipidic fraction
Lead white priming layer	1436, 1046, 681	-
Lead white in linseed oil	1420, 1045, 682	1745
Azurite in linseed oil	1579, 1424, 1092, 954, 838	1745
Ochre in linseed oil	1113, 1034, 1010, 914, 798	1742

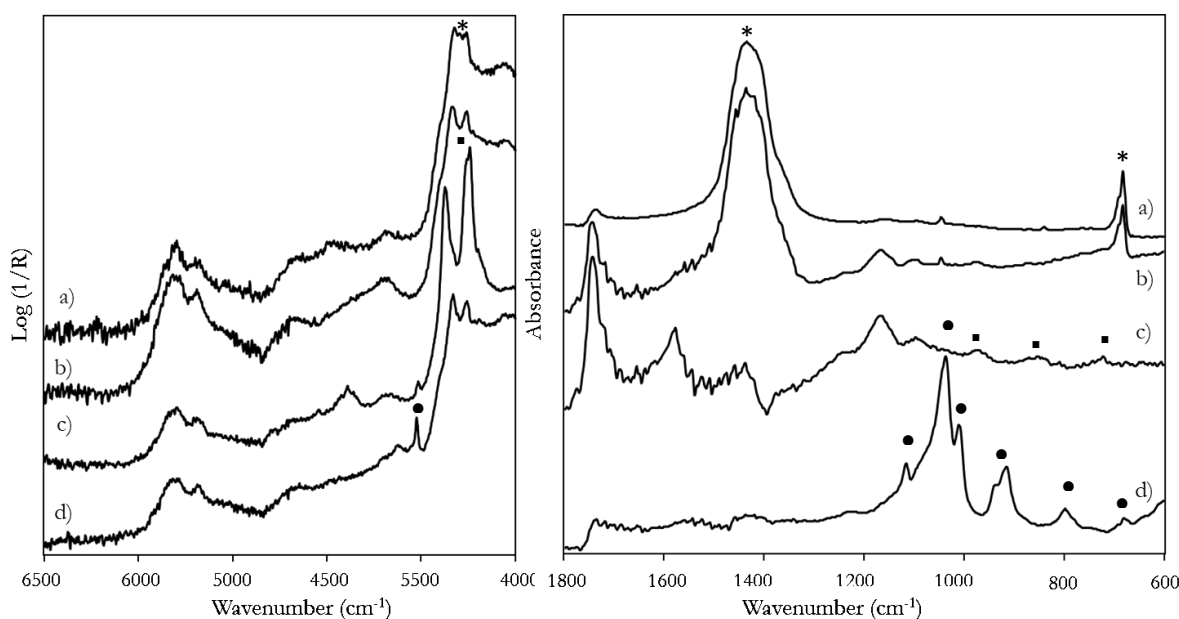


Figure 8. FT-NIR and FT-MIR spectra from painting models of: a) white priming layer with lead white, red lead and lead tin yellow in walnut oil; b) lead white in linseed oil layer on white priming layer; c) azurite in linseed oil layer on white priming layer; d) azurite in linseed oil layer on white priming layer. Legend: *= signals due to lead white. ▪ = azurite and • = yellow ochre

Table 15. Wavenumbers (cm^{-1}) of the NIR absorption bands for painting models of linseed oil on a pink priming layer.

	Pigment bands	Binder bands lipidic fraction	Other oil bands
Lead white priming layer	4282	4339, 4261	5804, 5689, 4685
Lead white in linseed oil	4279	4339, 4261	5808, 5688, 4684
Azurite in linseed oil	4375, 4242	4337, 4261	5803, 5689, 4680
Ochre in linseed oil	4526	4335, 4260	5801, 5686

Table 16. Wavenumbers (cm^{-1}) of the MIR absorption bands for painting models of linseed oil on a pink priming layer.

	Pigment bands	Binder bands- lipidic fraction	Other oil bands
Lead white priming layer	1437, 1045, 682	1740	-
Lead white in linseed oil	1434, 1046, 684	1743	1169, 1101
Azurite in linseed oil	1577, 1460, 1092, 967, 846	1743	1168, 1098
Ochre in linseed oil	116, 1037, 1009, 915, 799	-	-

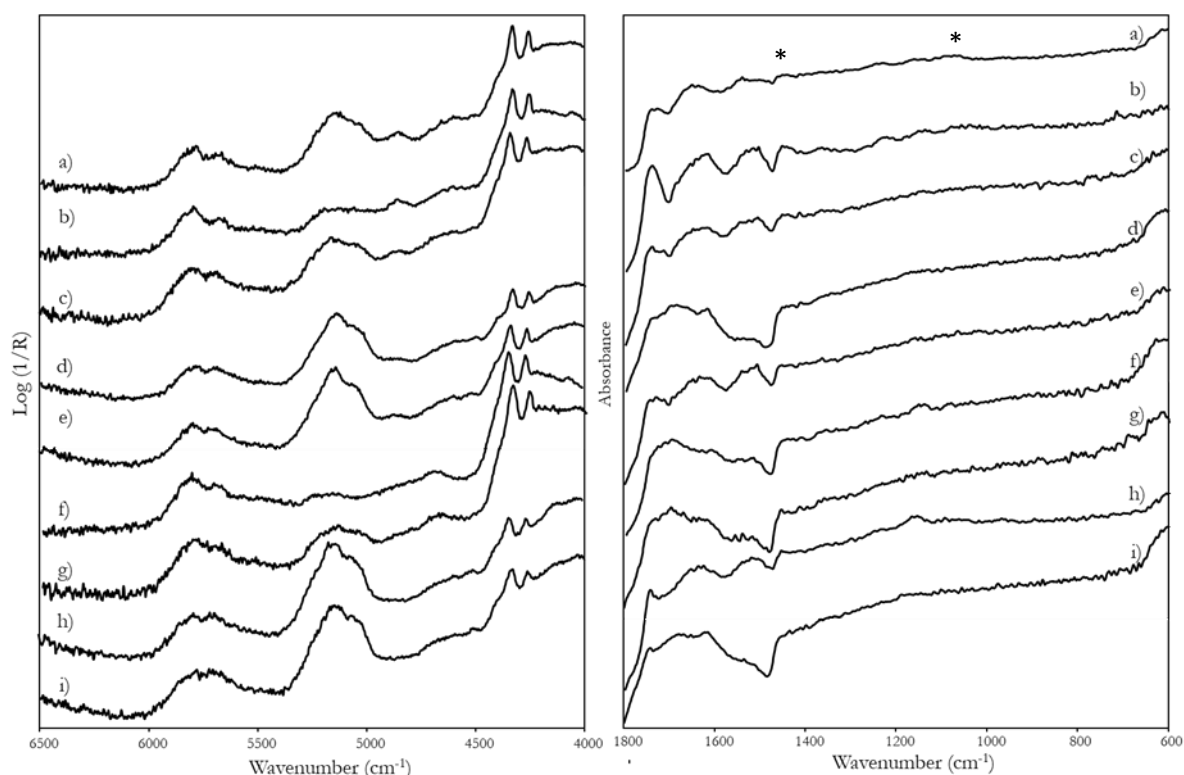


Figure 9. FT-NIR and FT-MIR spectra from painting models of hematite in: a) egg tempera; b) egg tempera on walnut oil; c) egg tempera on linseed oil; d) *tempera grassa* with walnut oil; e) *tempera grassa* with linseed oil; f) walnut oil (2 layers); g) linseed oil (2 layers); h) walnut oil (1 layer); g) linseed oil (1 layer). * = signal due to hematite.

Table 17. Wavenumbers (cm⁻¹) of the NIR absorption bands for painting models of hematite in different binders on a gypsum preparatory layer.

	Pigment bands	Gypsum bands	Binder bands-lipidic component	Binder bands-Proteinaceous fraction	Oil bands
Linseed oil (1 layer)	-	5147, 5058, 4511, 4398sh, 4125, 4029	4337, 4262	-	5788, 5694
Walnut oil (1 layer)	-	5146, 5058, 4506, 4391sh, 4126, 4029	4330, 4257	-	5793, 5697
Linseed oil (2 layers)	-	5047, 4398 sh	4339, 4262	-	5800, 5693, 5220, 4672,
Walnut oil (1 layer)	-	5047, 4399 sh	4338, 4261	-	5800, 5693, 5220, 4651
Tempera grassa linseed	-	5148, 5054, 4512, 4401sh	4334, 4259	4862, 4593	5799, 5714
Tempera grassa walnut	-	5147, 5065, 4511, 4399sh	4334, 4257	4859, 4600	5791, 5701

Tempera on linseed	-	5155, 5049, 4400sh	4334, 4257	4862, 4607	5789, 5701
Tempera on walnut	-	5816, 5674, 5200, 4332, 4257	4332, 4257	4861, 4615	5816, 5674, 5200
Egg tempera	-	5153, 5042, 4512, 4394sh	4331, 4259	4853, 4600	5800, 5681

Table 18. Wavenumbers (cm⁻¹) of the MIR absorption bands for painting models of hematite in different binders on a gypsum preparatory layer.

	Pigment bands	Gypsum bands	Binder bands-lipidic component	Binder bands-Proteinaceous fraction
Linseed oil (1 layer)	600, 480	-	-	-
Walnut oil (1 layer)	614, 483	-	-	-
Linseed oil (2 layers)	610, 477	-	1741	-
Walnut oil (2 layers)	606, 479	-	1740	-
Tempera grassa linseed	472	1168	1745	1640
Tempera grassa walnut	472	1168	1744	1640
Tempera on linseed	600, 470		-	1637
Tempera on walnut	600, 470		1744	1640
Egg tempera	603		-	1646

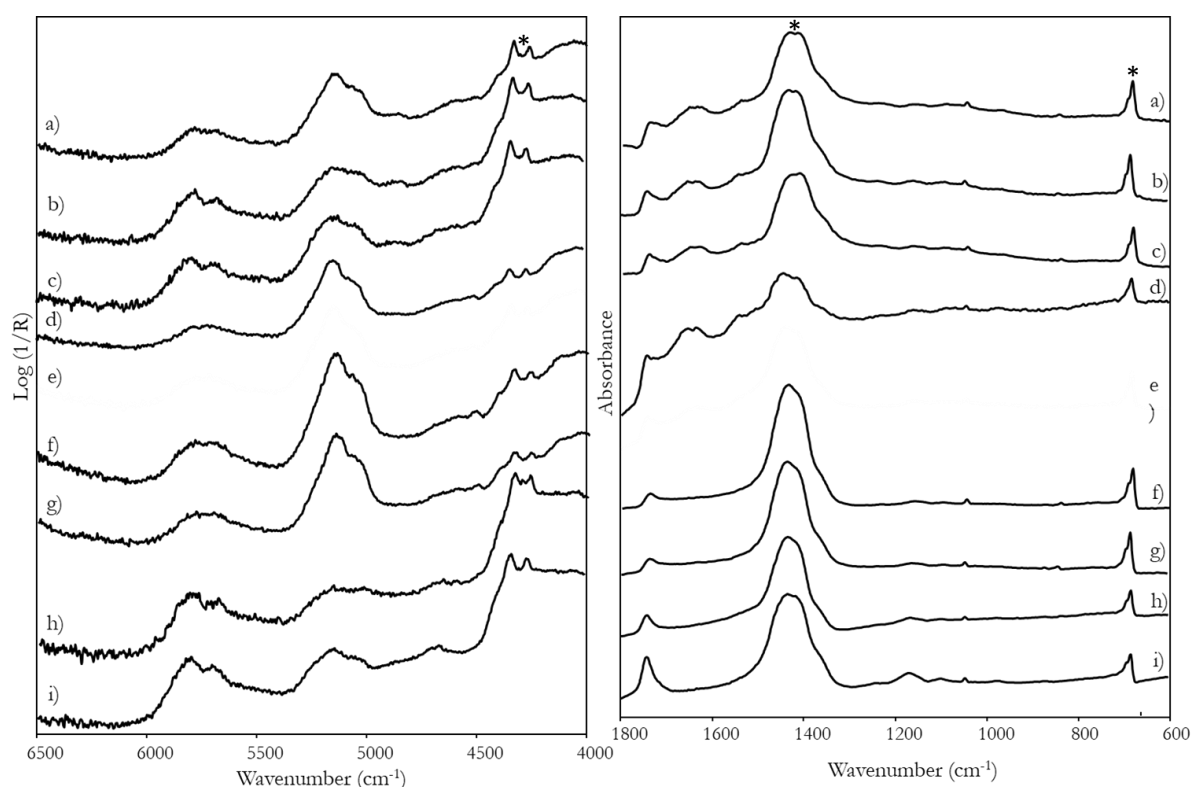


Figure 10. FT-NIR and FT-MIR spectra from painting models of lead white in: a) egg tempera; b) egg tempera on walnut oil; c) egg tempera on linseed oil; d) *tempera grassa* with walnut oil; e) *tempera grassa* with linseed oil; f) walnut oil (2 layers); g) linseed oil (2 layers); h) walnut oil (1 layer); g) linseed oil (1 layer). * = bands due to lead white.

Table 19. Wavenumbers (cm^{-1}) of the NIR absorption bands for painting models of lead white on gypsum preparatory layer.

	Pigment bands	Gypsum bands	Binder bands-lipidic component	Binder bands-Proteinaceous fraction	Oil bands
Linseed oil (1 layer)	4297	5705, 5148, 5047, 4512, 4509	4337, 4261	-	5705, 5148
Walnut oil (1 layer)	4296	5156, 5035	4337, 4261	-	5705, 5148
Linseed oil (2 layers)	4296	5156, 5051	4338, 4262	-	5810, 5700, 4673
Walnut oil (1 layer)	4296	5156, 5051	4331, 4260	-	5810, 5700, 4673
Tempera grassa linseed	4295	5704, 5149, 5072, 4508, 4403	4336, 4259	4840, 4604	-
Tempera grassa walnut	4296	5712, 5148, 5067, 4509, 4400	5787, 4334, 4262	4855, 4600	-

tempera on linseed	4295	5148, 5053, 4508, 4369sh	5791, 5689, 4333, 4259	4855, 4592	-
Tempera on walnut	4298	5154, 4508, 4398 sh	5799, 5689, 4331, 4261	4860, 4594	-
Egg tempera	4303	5147, 5057, 4511, 4402sh	5786, 5701, 4229, 4261	4862, 4593	-

Table 20. Wavenumbers (cm^{-1}) of the MIR absorption bands for painting models of lead white in different binders on a gypsum preparatory layer.

	Pigment bands	Gypsum bands	Binder bands-lipidic component	Binder bands-Proteinaceous fraction
Linseed oil (1 layer)	1435, 1045, 681	1158	1739	1744-
Walnut oil (1 layer)	1433, 1047, 682	1158	1744	-
Linseed oil (2 layers)	682, 1436	-	1742	-
Walnut oil (1 layer)	1451, 1682	-	1740	-
Tempera grassa linseed	1450, 1046, 682	1635, 1166, 683	1744	1657
Tempera grassa walnut	1447, 1044, 682	1631, 1162	1743	1653
Tempera on linseed	683, 1426, 1046, 683	1166	1740	1647
Tempera on walnut	1428, 1045, 684	1166	1742	1649
Egg tempera	1426, 1046, 683	-	1740	1642

2. Score plots from PCA of NIR spectra of model samples

Tempera painting models with azurite

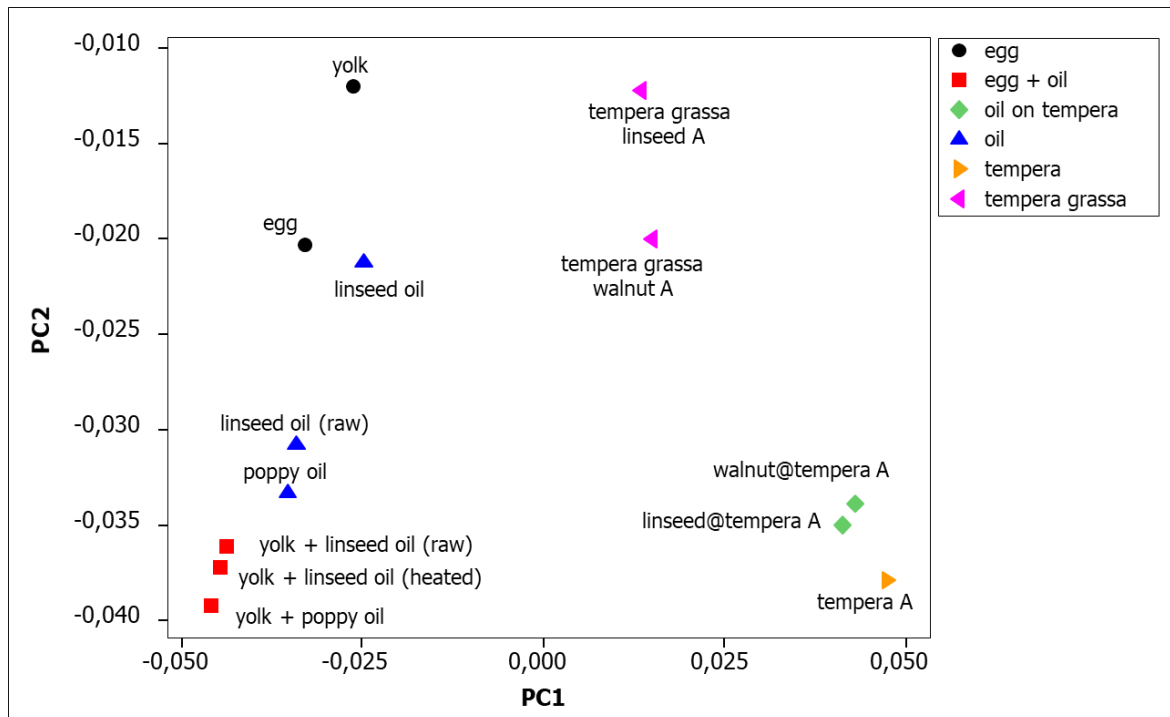


Figure 11. Score plot of NIR spectra (6000-4000 cm^{-1}) of tempera painting models with azurite.

Tempera painting models with yellow ochre

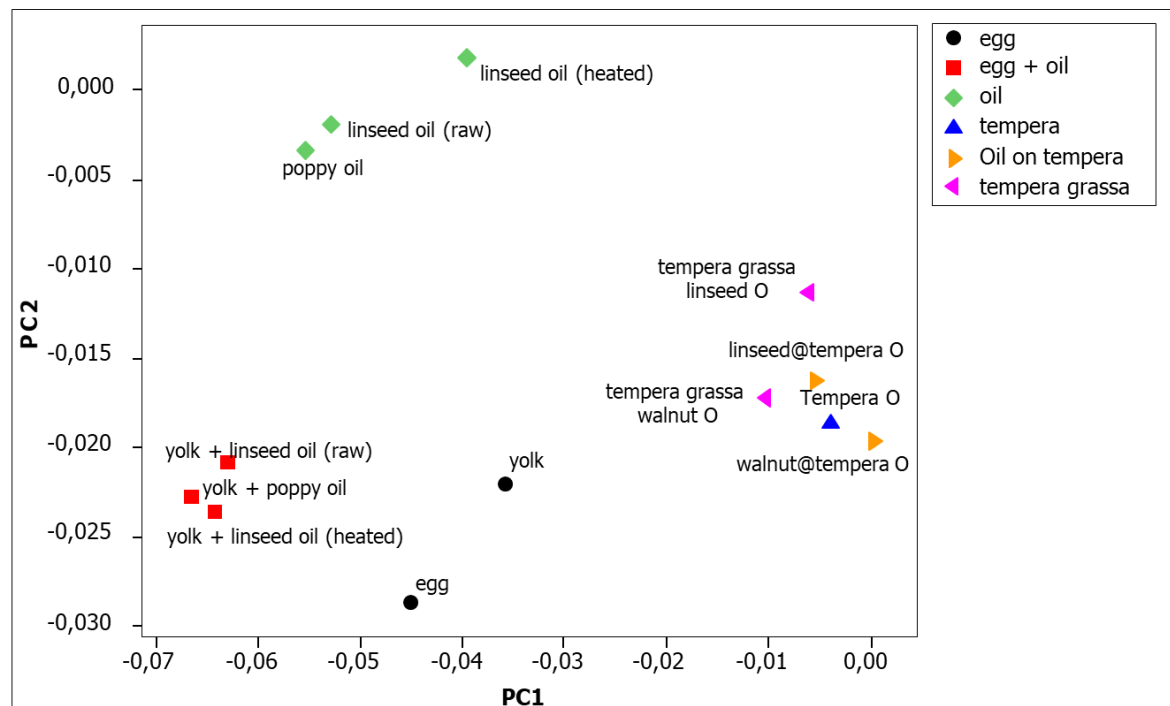


Figure 12. Score plot of NIR spectra (6000-4000 cm^{-1}) of tempera painting models with yellow ochre.

Painting models with azurite in linseed oil on coloured priming layers

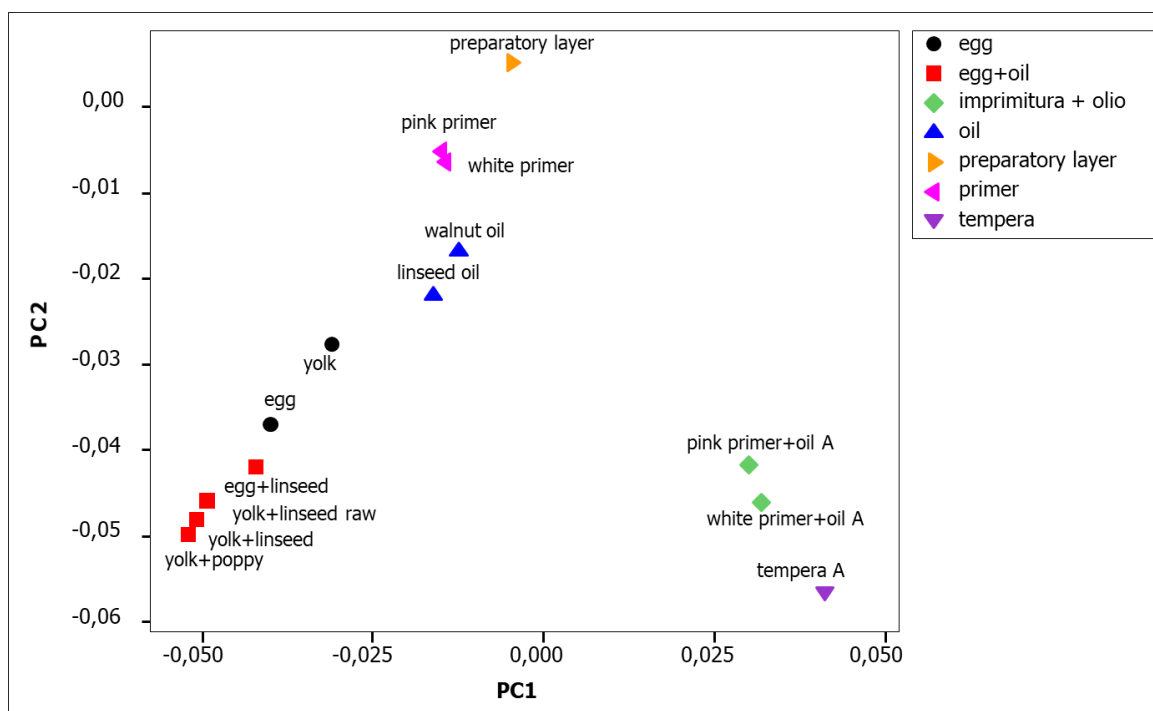


Figure 13. Score plot of NIR spectra (6000-4000 cm^{-1}) of painting models with azurite in linseed oil on white and pink priming layers. A shift of the points corresponding to the spectra of the painting layers containing the blue pigment is due to the overlapping of its bands with those of oil.

Painting layers with yellow ochre in linseed oil on coloured priming layers

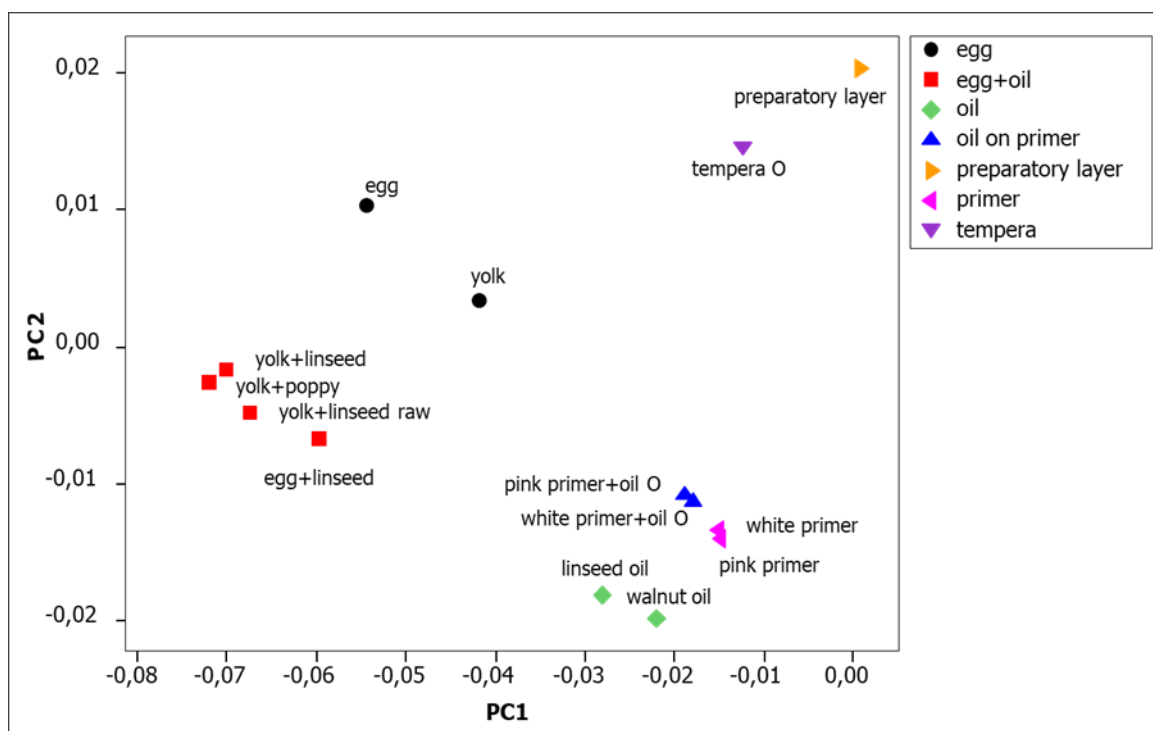


Figure 14. Score plot of NIR spectra (6000-4000 cm^{-1}) of painting models with yellow ochre in linseed oil on white and pink priming layers.

Painting layers with hematite in different binders on a gypsum preparatory layer

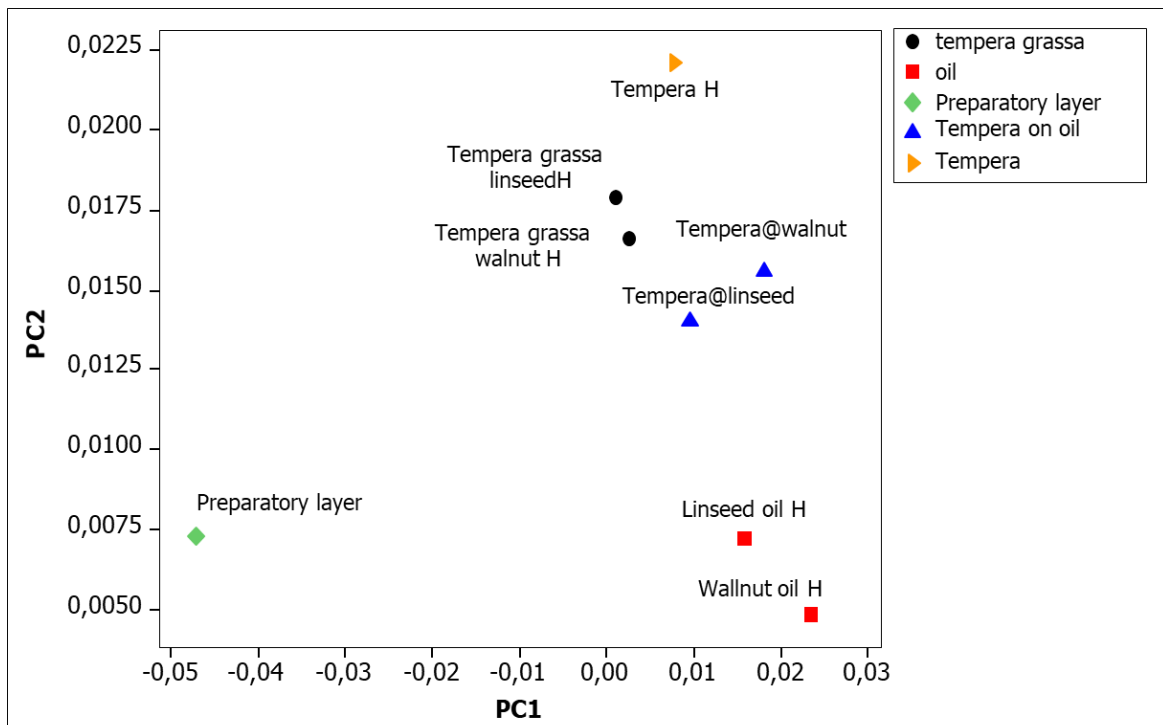


Figure 15. Score plot of NIR spectra (6000-4000 cm⁻¹) of painting models with hematite in different binders on a gypsum preparatory layer.

APPENDIX B

Analyses on micro-samples from the painting *Porter boy sitting on a basket* by Pitocchetto

1. Introduction

During the campaign of in-situ analyses on the painting *Porter boy sitting on a basket* by G. Ceruti, two micro-samples were provided by restorers. They were taken from an area of the edge under the frame, where the colour layer was extremely brittle and detached very easily on its own. The samples consist of a series of microscopic fragments, whose observation under the optical microscope revealed two different natures: some are light in colour (probably small fragments of canvas with possible residues of a first preparatory layer), others are dark (probably coming from the paint layers). Moreover, one of the samples, which seemed to contain all the layers, was embedded in epoxide resin to prepare a cross section. These samples were then studied and characterised by SEM-EDX microscopy and micro-FTIR spectroscopy to have a better insight on the artistic technique of the painter and fully understand the results obtained from the non-invasive analyses presented in chapter 3.

2. Materials and methods

SEM-EDX analyses were performed by means of a Hitachi TM 1000 microscope, having a resolution of 1 nm and equipped with an energy dispersion X-ray (EDX) spectrometer. The accelerating voltage was 15 kV.

Micro-FTIR spectra were recorded both in transmission mode on the fragments and in reflection mode on the cross section in the MIR region ($4000\text{-}600\text{ cm}^{-1}$) by a Jasco IRT 3000 spectrometer, equipped with a 32x objective. The resolution was 4 cm^{-1} and spectra were collected as sum of 256 accumulations.

3. Results and discussion

First, the samples were characterised by SEM in order to investigate their morphology and EDX analyses were performed to understand their elemental composition.

Dark sample - This sample seems to be a fragment from the coloured layer and revealed an almost homogeneous morphology (Fig. 1). The elemental analysis disclosed the presence of Ca, K, Al, Fe and Si, all elements possibly attributable to the use of an earth pigment, as well as

traces of Pb. It is conceivable that this heavy metal is due to the presence of metallic soaps on the surface of the painting itself, as had already been highlighted by FT-NIR spectra acquired in reflection mode during the *in-situ* measurements (see section 5.4.3 of chapter 3).

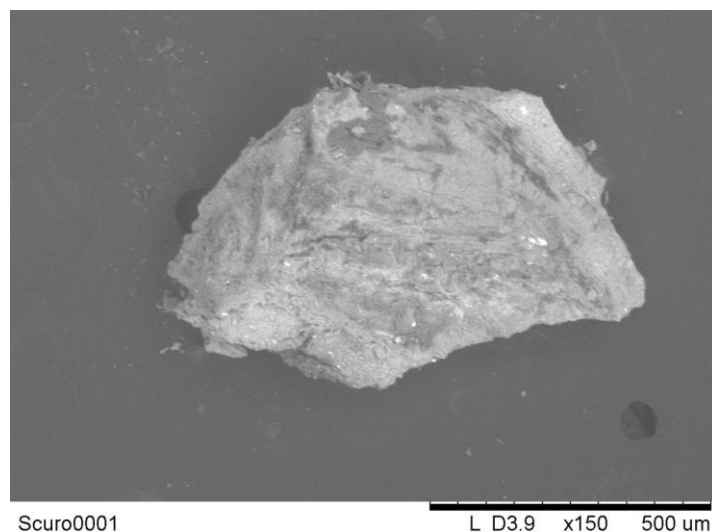


Figure 1. SEM image of the examined dark sample from the painting by Pitocchetto.

Micro-FTIR analyses performed on this sample in transmission mode gave a spectrum (Fig. 4a), characterised by the silicate band at 1030 cm^{-1} . Its position seems to suggest it may be a burnt umber or a Senna earth. The bands at 795 cm^{-1} , in fact, is typical of goethite, a mineral also present in these earth pigments [1]. Finally, the band at 1540 cm^{-1} suggests the presence of metal soaps, probably lead palmitate as EDX analysis recognised this element (Fig. 4a) [2].

Light Sample - In this sample it is possible to recognise two different parts (Fig. 2): the former has a fibrous appearance and probably corresponds to residual fragments of canvas; the latter resembles the paint layer. The elemental analysis on the fibrous part revealed the presence of Ca, leading to the supposition that the artist may have applied a very thin layer of calcite (CaCO_3) preparatory ground to the canvas. On the other hand, in the second layer Al, Si, Ca, Fe possibly attributable to an earth pigment were identified, revealing a correspondence with the dark sample and supporting the hypothesis that it may corresponds to the colour layer.

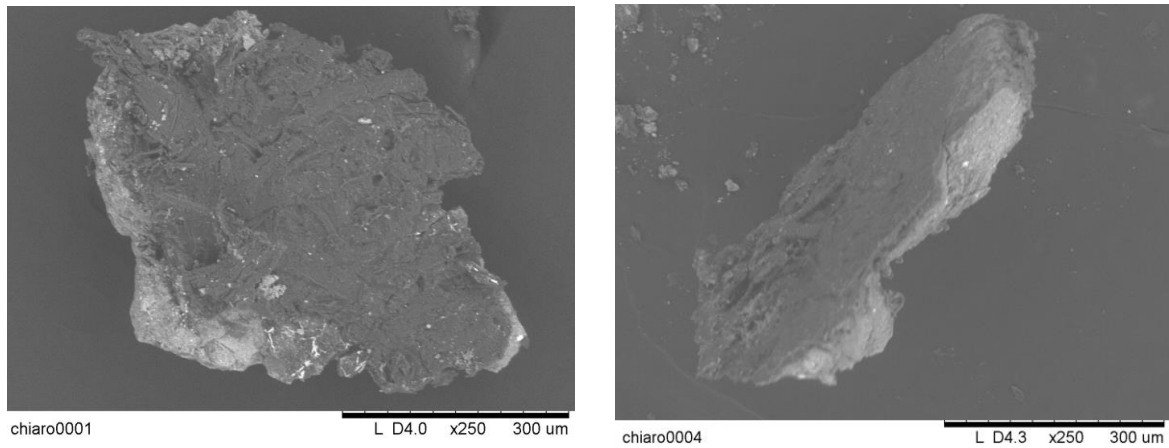


Figure 2. SEM images of the examined dark sample from the painting by Pitocchetto, where two different layers are well recognisable.

The micro-FTR transmission spectrum (Fig. 4b) obtained from the fragment shows a pattern similar to that of cellulose, as suggested by the characteristic band at around 1050 cm^{-1} [3]. The presence of CaCO_3 is then highlighted by the bands at 875 and 1400 cm^{-1} , supporting the supposition made on the basis of SEM-EDX analysis. Finally, the signal at around 1730 cm^{-1} suggests the use of a siccative oil as a binder, confirming once again the results provided by the previous non-destructive analyses.

Cross section - The observation of the cross section, both by an optical microscope (50x magnification) and by SEM, confirmed the presence of two layers (Fig. 3). The darker one showed in the EDX analysis the presence of the aforementioned elements attributable to an earth pigment, while in the light-coloured part the main element was still Ca, attributable to a possible ground layer composed of calcite.

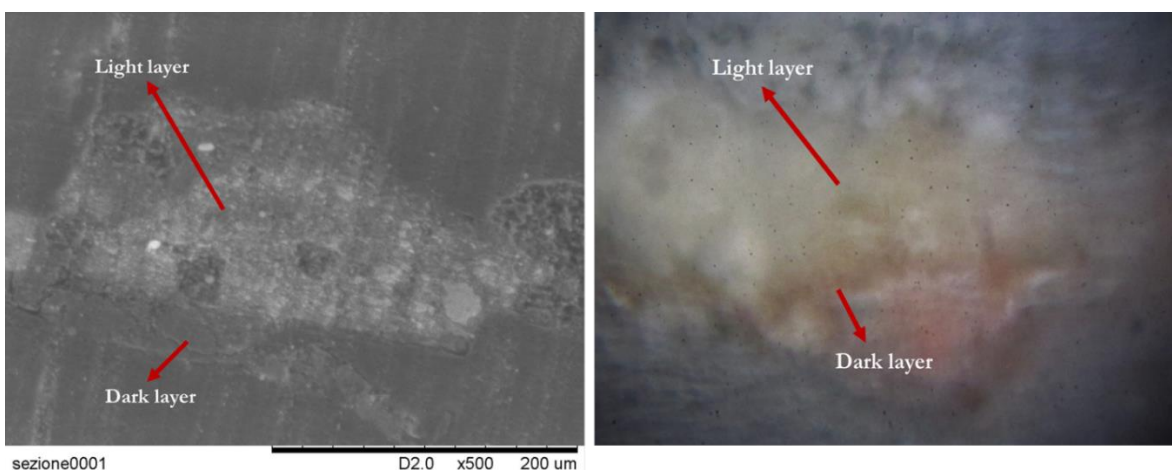


Figure 3. SEM and 50x images of the cross section. The presence of two layer is highlighted.

Micro-FTIR spectra were acquired in reflection mode for each of the two recognisable layers (Fig. 4 c and d). In the dark one, the peculiar band of silicates at 1030 cm^{-1} is still recognisable and always attributable to an earth pigment, while the one at 1538 cm^{-1} seems to suggest the presence of lead palmitate, even if this element has not been identified by EDX. In the light layer, on the other hand, there is the carbonate band, coherently with the detection of calcium in the EDX analysis, leading again to the hypothesis of a calcite ground layer. In the spectrum it is not possible to identify any signal attributable to the binder used by the artist to spread this pigment on the canvas.

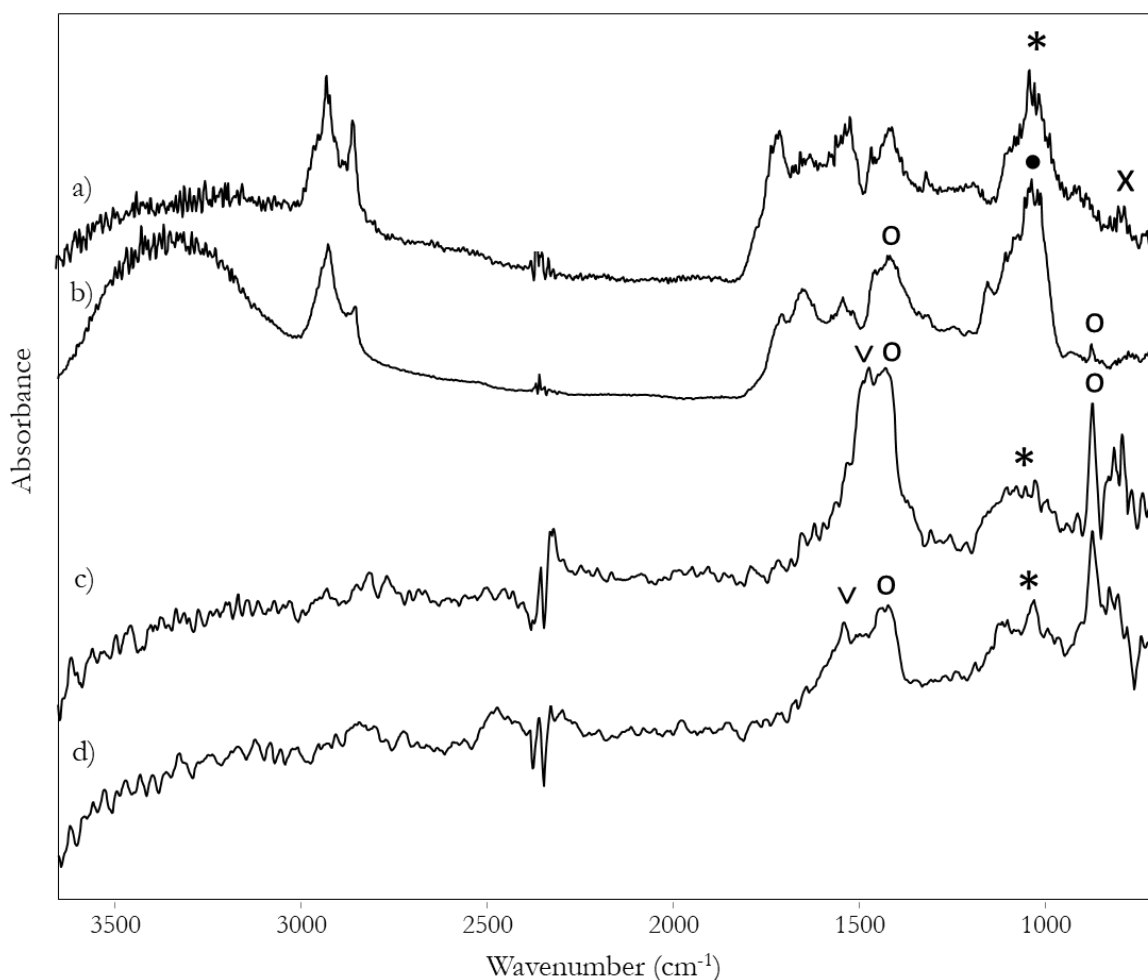


Figure 4. Micro-FTIR spectra obtained in transmission mode from the a) dark and b) light sample from the painting by Pitocchetto and in reflection mode from the c) light and d) dark layer respectively of the corresponding cross section. Legend: * = bands due to a silicate component • = band due to cellulose; o = band due calcite; v = signal due to lead palmitate; x = signal due to goethite.

4. Conclusions

SEM-EDX and micro-FTIR analyses performed on small samples from the painting *Porter boy sitting on a basket* by G. Ceruti provided a further insight on the technique of the artist, confirming on the other hand the results obtained from the in-situ campaign of NIR analyses. In particular,

the use of an earth pigment spread on the pictorial surface to confer a reddish hue was demonstrated, as well as the presence of a thin layer of calcite applied to prepare the canvas. This evidence was not provided by FT-NIR analyses since, as already extensively discussed in chapter 3, this material does not absorb in this spectral range and therefore it cannot be identified. Finally, in some areas lead metal soaps due to a degradation process of the oil binder were also found, in agreement with the results of NIR analyses.

References

- [1] D. Bikiaris, D. Sister, S. Sotiropoulou, O. Katsimbiri, E. Pavlidou, A. P. Moutsatsou, Y. Chryssoulakis, *Spectrochim. Acta A Mol. Biomol. Spectrosc.* 2000, 56A (1), 3-18.
- [2] R. Mazzeo, S. Prati, M. Quaranta, E. Joseph, E. Kendix, M. Galeotti, *Anal. Bioanal. Chem.* 2008, 392, 65-76.
- [3] P. Zaccheoa, G. Cabassia, G. Riccab, L. Crippa, *Org. Geochem.* 2002, 33, 327-345.

Chapter 4

Dry-state SERS for the non-invasive investigation of natural dyes in textiles

Abstract

The present chapter is dedicated to the development of a simple method to identify natural dyes directly on ancient textiles by means of Surface-enhanced Raman spectroscopy (SERS). A dry-state approach, i.e. exploiting only the electromagnetic interaction between a solid nanometallic substrate and the dye molecule absorbed onto a textile fibre, is proposed, pursuing the objective of avoiding sampling. In this respect, a simple method starting from colloids immobilised onto a functionalised microscope glass slide was developed. Silver and gold nanoparticles having different geometries (spheres, stars and rods) were experimented to obtain the most performing sensor and to get the greatest SERS enhancement in dry-state condition, leading to successfully acquire the SERS spectra of four historical dyes from reference dyed wool threads. Moreover, the issues of metal release and of the protection and cleaning of the substrate were considered and investigated.

1. Introduction

Surface-enhanced Raman spectroscopy (SERS) is a powerful analytical technique for the identification at trace level of organic compounds, allowing the overcoming of the drawbacks connected to traditional Raman spectroscopy. As Fleischmann first observed in 1974 [1], a great enhancement of the Raman signal occurs when a molecule is absorbed on, or in the proximity of, a metal nanostructured surface. Indeed, thanks to this close contact, Raman scattering excited by visible light experiences an enhancement up to a factor of 10^8 [2]. In addition, the metallic substrate absorbs most of the fluorescence photons emitted by the molecules, acting as quencher of the fluorescence emission often associated with organic substances.

For its potentiality, SERS has been largely exploited in the field of cultural heritage diagnostics to study natural and synthetic dyes from several artistic and archaeological artefacts [3, 4]. Indeed, these compounds, most of which fluorescent, are not detectable by conventional Raman spectroscopy, whereas SERS, thanks to the strong enhancement of the signal and to the quenching of the fluorescence, is the ideal technique for their univocal identification. Traditionally, SERS experiments are performed with the use of colloidal solutions of metal

nanoparticles (more commonly silver). This method is inherently invasive: in principle, it cannot be used directly on the artistic object as wetting is required, if not the use of extraction methods in order to separate by hydrolysis the colourant from its matrix (i.e. the textile fibre for fabrics or the inorganic substrates for lakes) [3].

In the last years, many attempts have concentrated on the development of non-invasive SERS strategies using different approaches, i.e. hydrogels based on solid phase micro-extraction techniques which extract trace amounts of dyes and are then treated with silver colloid for SERS measurements [5 - 7], or laser ablation followed by the “in-situ” analysis of the ablated substances [8, 9]. A further step towards totally non-destructive SERS analysis is the implementation of dry-state measurements. The possibility to obtain a SERS response starting from a solid nanometric substrate in contact with dyes on textile was already successfully experimented in the artistic field [10, 11]. In this respect, it is worth noticing that the enhancement of the Raman scattering in SERS is due to two different mechanisms, an electromagnetic and a chemical one. The former is a long-range effect, based on the intensification of the electric field of the electromagnetic radiation in proximity of a nanostructured metallic surface, thanks to the excitation of surface plasmons of the metal. The latter needs instead a chemical interaction between the molecules and the SERS substrate to promote charge-transfer transitions. These two phenomena do not contribute at the same extent to the SERS intensification of the Raman scattering: indeed, the electromagnetic one contributes in an order of magnitude of 10^{10} , while the chemical one of 10^2 . Thus, although the interactions are obviously more challenging to establish than those occurring between a solution of the target dye and the same substrate, a dry-state analysis leading to a completely non-invasive approach is, in principle, possible.

In this chapter, the development of a simple protocol to produce dry-state SERS substrates from deposition of silver and gold colloids on an optically transparent support, such as a glass slide, will be presented. The final aim is, in fact, to create simple, accessible and easy-to-produce sensors suitable for *in-situ* analysis by means of portable Raman instrumentation, with no need of complex procedures as those already reported in the literature and cited above [10, 11]. The proposed analytical set-up is shown in Fig. 1: the laser beam passes through the glass support and the metal substrate, and the scattered Raman signal, in principle enhanced by the nanostructured film, is collected back by the microprobe objective. Obviously, also the problem of transparency must be considered.

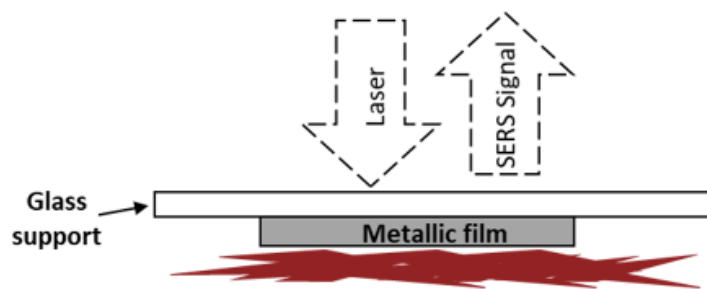


Figure 1. Schematic set-up for dry-state SERS analysis on a dyed wool thread sample.

In this respect, previous studies were carried out in our laboratory to produce SERS substrates starting from Lee-Meisel silver colloid. In particular, thin films of nanoparticles were prepared by immersion of a functionalised glass support in pre-concentrated colloid (depositing from 1 to 5 layers), by air-brush deposition or by silver coating silica micro-spheres [12]. The most promising method, however, proved to be drop deposition, which consists in drop-casting small volumes of suitably pre-treated colloid on a microscope glass slide. In this work, the attention was therefore focused on the optimisation of this procedure in terms of aggregation and deposition condition of the colloid. In addition, in order to try to further enhance the SERS effect of the substrate promoting the acquisition of intense spectra in dry-state condition, silver nanoparticles having different geometries (nanorods and nanostars) were synthesised and deposited. The Raman enhancement generated by spherical nanoparticles and other isotropic nanomaterials can be, in fact, further increased by employing nanostructures characterised by anisotropic features [13-17], reaching a higher enhancement factor [18]. In addition, anisotropic nanoparticles offer the great advantage of not needing activation by aggregating agents, which is an important drawback due to the addition of species which can lead to the appearance of interference bands in SERS spectra. [19, 20] The morphology of the SERS substrates was characterised by scanning electron microscopy (SEM) in order to verify the presence of nanoparticle aggregates, which represent the so-called “hot-spots”, highly localized regions of intense local field enhancement. Dry-state SERS analyses were finally performed by means of a portable spectrometer on mock-up samples of wool yarn dyed with some of the most common ancient natural dyes (alizarin, purpurin, lac dye and indigo).

The issues of metal release on the artefact and the protection of the substrates from environmental degradation were then faced up. During SERS analyses, in fact, residual silver nanoparticles were left on textile fibres. This can potentially be a concern for artefacts, as residual silver can give rise to tarnishing phenomena and a consequent variation in colour. In

this respect, the possibility of embedding nanoparticles in a polymeric matrix was explored, as well as the use of gold instead of silver, again studying the effect of two different nanoparticle geometries, spherical and star-shaped.

Finally, electrochemical-deposited commercial SERS substrates were also tested, considering that not always the analyst of, for example, a museum has the possibility to prepare his own substrates. On the basis of the good results obtained, preliminary studies on the optimisation of electrochemical deposition of silver nanoparticles to prepare our substrates were undertaken thanks to the collaboration of L. Falciola and V. Pifferi of the Università degli Studi di Milano. Lastly, aiming to re-use the substrates, the problem of their cleaning to remove residual molecules of the target analyte and degradation products of the substrate itself was considered by exploiting the self-cleaning properties of titanium dioxide mediated by UV light.

2. Objects of study

2.1 Natural dyes

Since prehistoric times, men have used colouring substances to decorate objects and to create images: dyes and pigments were applied to a wide range of surfaces, becoming integral part of a consistent number of artifacts. Before the advent of modern chemistry and the development of the industry of synthetic dyes in the 19th century, all the colourants were of natural origin. They were obtained from mineral, vegetable - roots, berries, woods and leaves - or animal sources, for example insects or molluscs. Over the centuries, the progressive development of dying art leads to discover which families of plants and which animals were particularly rich in a certain dye and suitable for obtaining a certain colour. Moreover, a wide variety of recipes to improve the fixing of the colour to the fibres was experimented, for example the addition to the dye bath of other substances, both mineral (salts, mud, metal oxides) and organic (urine, fats etc). In this respect, a first classification of natural dyes can be made on the basis of the way in which they were applied to fabrics. [21-24]

Mordant dyes: The most part of natural dyes does not show high chemical affinity for textile fibres, thus a pre-treatment aimed at promoting their lasting and stable adhesion was commonly performed. In particular, fabrics were previously processed with metallic salts, known as mordants, able to fix the dye molecules on fibres. From a chemical point of view, mordant dyestuffs have functional groups, i.e. hydroxyl, amino or carboxyl groups, which are able to form complexes with metal ions. Similarly, textile fibres are rich in functional groups suitable to bond complexed dyes: in particular wool and silk display carboxyl and amino groups. The metal

ions, therefore, seem to mediate the interaction between the dye molecule and the fibre itself. Typical mordants were alum ($\text{KAl}(\text{SO}_4)_2 \cdot 12\text{H}_2\text{O}$) and potassium bitartrate ($\text{KC}_4\text{H}_5\text{O}_6$), sometimes joined by tin, chrome and copper salts to obtain different hues and chromatic shades.

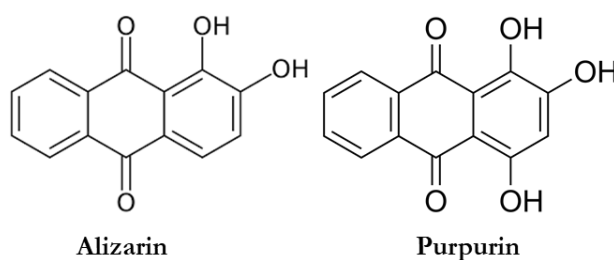
Direct dyes: these dyes do not require special treatments and can be applied directly to the textile fibres. The interaction is based on secondary bonds, such as Van der Waals forces, hydrogen bonds and dipole associations. Such interactions are weaker, determining a lower degree of lightfastness. Chemically, direct dyes are water-soluble molecules characterised by linear and flat shapes, which promote their diffusion into the fibre. [22] A typical example of substances belonging to this category are carotenoids.

Vat dyes: the term *vat* refers to the particular kind of vessel used in the dyeing process. Dyes belonging to this family are water-insoluble in their coloured form, therefore, to be dissolved in the dye-bath, they must be transformed in their reduced, uncoloured, but water-soluble form. Under reducing conditions, in fact, these dyes are converted into their *leuco* form and penetrate into the fibres by immersion of the textiles in the bath. Once the textile is removed from the dyeing bath and exposed to air, they are oxidized again to their coloured form. The most important dyes belonging to this group are the blue indigo and woad and the precious Tyrian purple.

A further classification of dyes can then be made on the basis of their chemical structure. In general, they are large molecules, which exhibit conjugated double bonds, aromatic systems and ketone groups. Their colour depends on the selective absorption of light in the visible range (400-750 nm) of the electromagnetic spectrum. This property is conferred by specific part of the molecule, known as chromophores. They generally consist of functional groups belonging to systems of conjugated double bonds, for example carbonyl ($-\text{C}=\text{O}$), nitroso ($-\text{N}=\text{O}$) and vinylene ($-\text{C}=\text{C}$) groups. In addition, other functional groups can act as auxochromes, such as carboxyl ($-\text{COOH}$), hydroxyl ($-\text{OH}$) and amino ($-\text{NH}_2$) groups. These parts of the molecule are not responsible for colour, but can shift the absorption of an already coloured compound to shorter (hypsochromic effect) or longer (bathochromic effect) wavelengths. [22, 24] Generally, the main chromophores in red dyes are anthraquinones, while the yellow and blue colours are conferred respectively principally by flavonoids and indigoids. In addition, other dyes can belong to the classes of carotenoids, naphthoquinones and tannins. In the following section, a brief overview of the dyes analysed in the present works, which are among the most diffused, will be provided.

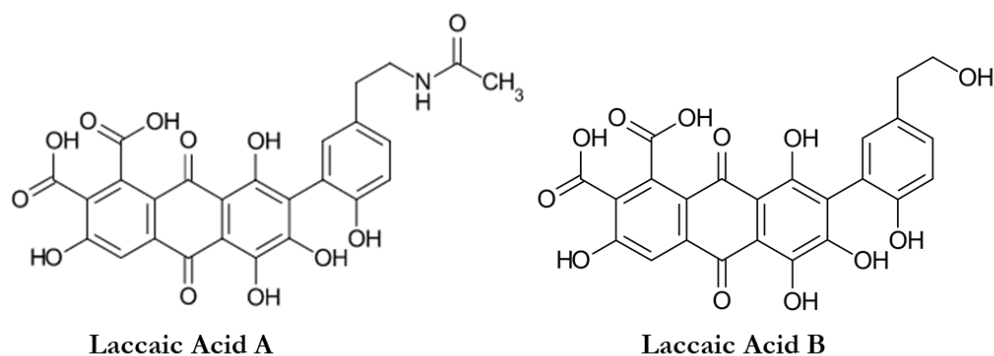
2.1.1 Madder

Madder, belonging to the anthraquinone family, is one of the most historically important and widespread red dyes. Its use, documented since ancient times by Greek and Romans historians [25, 26], lasted for many centuries all over Europe. This red dye was extracted from the roots of plants belonging to the family of *Rubiaceae*, in particular from *Rubia tinctorum*, and owes its success to the fact that these vegetable sources could be cultivated, making this dye much cheaper than the luxury reds obtained from insects. The madder roots contain an impressive number of anthraquinone derivatives, but the main chromophores are alizarin and purpurin. The relative amounts of these two compounds can differ slightly from one botanical source to another. For example, the most common *Rubia tinctorum* is rich in alizarin, while wild madder, derived from *Rubia peregrina* R., owes its colour mainly to purpurin and pseudo-purpurin. [21] In this respect, the chemical characterisation of this dye can provide interesting information about the origin of the raw material and thus about its geographical provenance.



2.1.2 Lac dye

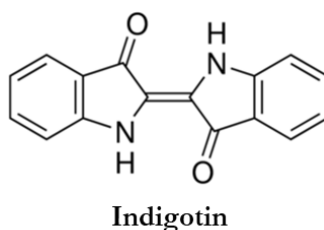
Lac dye is probably the most ancient anthraquinone dye of animal origin. It was extracted from the resinous exudation produced by female insects *Laccifer lacca* Kerr, also known as *Coccus lacca* L., on host trees typical of the geographical area ranging from Northern India to Indochina. Because of its origins, it was mainly employed for dyeing silks in Asian countries, while its early use as textile dye in Europe is only rarely documented. It is known that for a certain period lac dye replaced cochineal in an attempt to stop the Spanish monopoly on this precious substance, but it was a failure because of the lower tinting strength of this dye and the presence of impurities which could damage the fibres. Anyway, since the 13th century it was extensively used as pigment by artists. [27] Laccic Acid A and B are the main chromophores of this dye.



2.1.3 Indigoids

The most diffused blue dyes, indigo and woad, belong to the chemical class of indigoids. They are vat-dyes: in the dyeing process their molecules were reduce to their water-soluble form and, once penetrated inside the textile fibres, re-oxidated to their coloured form by atmospheric oxygen (section 2.1).

Indigo is one of the most ancient dyes (its use dates back to ancient Egypt in 2000 B.C.). The main source of this very stable organic dye were fermented leaves of *Indigofera tinctoria* L., an herbaceous plant typical of India, or of *Isatis tinctoria*, more widespread in Europe, from which woad was extracted [24]. Indigo and woad were often employed in mixture with yellow, red and brown dyes to obtain green, purple and black hues. Because of their high stability, these colourants were still extensively exploited in oil paintings by the greatest masters of the 17th and 18th centuries. [28]



3. SERS spectroscopy

Surface-enhanced Raman spectroscopy (SERS) is an analytical technique which takes advantage from the enhancement of the Raman signal of an analyte, when it is absorbed, or in proximity of, a rough metallic surface. SERS effect was firstly observed by Fleishmann and co-workers in 1974, while studying by Raman scattering the electrochemical reactions of pyridine at the surface of a silver electrode [1]. Thanks to this close contact, Raman scattering excited by visible light can experience an enhancement up to a factor of 10^8 , as observed by Van Duyne [2] and Albrecht and Creighton [29].

A large variety of substrates have been exploited to amplify Raman scattering, ranging from modified electrodes to colloidal nanoparticles and, more recently, metal nanostructures fabricated directly on solid supports by nano-lithography, electrodeposition or template-based synthesis. [30] The preferred metals are silver and gold, even if also the use of copper is documented. Wet chemical synthesis of SERS-active nanoparticles is, anyway, the most common method, being cheap and versatile. Briefly, metal nanoparticles are obtained by reducing silver or gold ions in a solution, typically aqueous, by means of reducing agents such as citrate, sodium borohydride, hydrazine or hydroxylamine hydrochloride [31]. Moreover, chemical reduction methods often employed capping agents, having the double aim of binding to the surface of the nanoparticle, preventing aggregation by either repulsive or steric forces [32] and directing the shape to nanoparticles with peculiar morphologies. [33] Typical capping agents are sodium citrate, polyvinylpyrrolidone (PVP), cetyltrimethylammonium bromide (CTAB) and hydroxylamine hydrochloride.

The exact mechanism underlying the SERS effect is still not completely clear. The most accredited theory states that two different effects are responsible for it: the chemical and the electromagnetic one. They involve different processes and contribute to SERS in different extents; in addition, different kinds of interaction between the analyte and the substrates occur. In the following sections, the complex mechanisms underlying SERS will be briefly explained.

3.1 Optical properties of metals

The enhancement of Raman signal in SERS is due to the optical properties of metals, typically silver and gold, which are able to intensify the signals emitted by the molecules in their proximity. Materials are characterised by two parameters, the dielectric function $\epsilon(\omega)$ and the refraction index $n(\omega)$, depending on the frequency of light ω and linked by the following equation: [34]

$$n(\omega) = \sqrt{\epsilon(\omega)}$$

In the simpler case of transparent material, both the dielectric function and the refraction index are positive real numbers. Dealing with metals, and in general with non-transparent materials, however, $\epsilon(\omega)$ becomes a complex number, expressed by an imaginary (small and positive) and a real (large and negative) function. Considering for simplicity only the real part, the dielectric function of metals can be described by the *lossless Drude model* as function of the frequency ω , or of the wavelength λ :

$$\varepsilon = \varepsilon_{\infty} \left(1 - \frac{\omega_R^2}{\omega^2} \right) = \varepsilon_{\infty} \left(1 - \frac{\lambda^2}{\lambda_R^2} \right)$$

where ω_R is the plasma frequency of the metal. This value is proportional to the square root of the density of free electrons and corresponds to the frequency at which the conduction electrons naturally oscillate. Silver and gold have actually very similar electronic densities, since the real parts of their dielectric functions are not so different from each other. Anyway, in real metals the imaginary part of the dielectric function is not neglectable and determines the absorption of light. For Ag, the imaginary part of $\varepsilon(\omega)$ is approximatively zero [$\text{Im}[\varepsilon(\lambda)] = 0$], meaning that almost all the incoming photons are reflected. Differently, in the case of Au, the imaginary function assumes higher values for wavelengths lower than 600 nm, causing the absorption of photons in that spectral region and thus the typical colour of this metal. However, it is worth noticing that, for $\lambda \geq 600$ nm, the imaginary parts of $\varepsilon(\omega)$ for both Ag and Au is comparable, meaning that both materials are similar from the viewpoint of their electromagnetic response in the near and far infrared range, while are slightly different in the visible one. In addition, their surface chemical behaviours are of course different and one material might be preferred over the other for specific chemical reasons. [34]

Once the complex dielectric function $\varepsilon(\lambda)$ is known, all the electromagnetic properties of the material can be calculated for different geometries: geometry-induced resonances, in fact, have a great importance in SERS [34]. However, the most typical SERS substrate is composed by nanoparticles, whose shape is approximately a sphere with a diameter ranging from 20 to 100 nm. Size is, in fact, an another fundamental issue since increasing this parameter causes a red-shift of the surface plasmon resonance.

When an external electric field E interacts with a metal nanosphere an induced dipole μ is produced. It depends on the dielectric function of the embedding medium, generally the air ($\varepsilon_M = 1$), and on the one, wavelength-dependent, of the metal, $\varepsilon(\lambda)$:

$$\mu \propto \frac{\varepsilon(\lambda) - \varepsilon_M}{\varepsilon(\lambda) + 2\varepsilon_M}$$

When $\varepsilon(\lambda) = -2\varepsilon_M$, the denominator equals zero and the induced dipole tends to infinite. In detail, the real part of the dielectric function satisfies the condition [$\text{Re}[\varepsilon(\lambda)] = -2\varepsilon_M$], limited only by the imaginary function whose influence, especially for Ag, can be neglected. As a consequence, the system will show a large response, known as dipolar localised surface plasmon resonance (LSPR) of the sphere. [34]

Therefore, when the wavelength of the incident field satisfies the boundary conditions for the resonance ($\lambda \sim \lambda_R$), the surface of the sphere will undergo a strong local field enhancement, expressed by the local field enhancement factor (LFIEF). LFIEF is a dimensionless parameter expressing the change in local intensity caused by the presence of objects which perturb the electric field of light. In the case of a sphere, it is maximum at the two extremities of the axis passing through its centre, where the external field and the induced dipole add up (Fig. 2). If a molecule is placed at those positions, it experiences the consistent enhancement of the local field, allowing the SERS effect to take place [34]. LFIEF can be calculated as the ratio between the normalised value of the local field intensity at position r and depending on the incident wavelength λ and the intensity of the incoming field $E_0(r,\lambda)$ at that point:

$$\text{LFIEF}(r,\lambda) = \frac{|E(r,\lambda)|^2}{|E_0(r,\lambda)|^2}$$

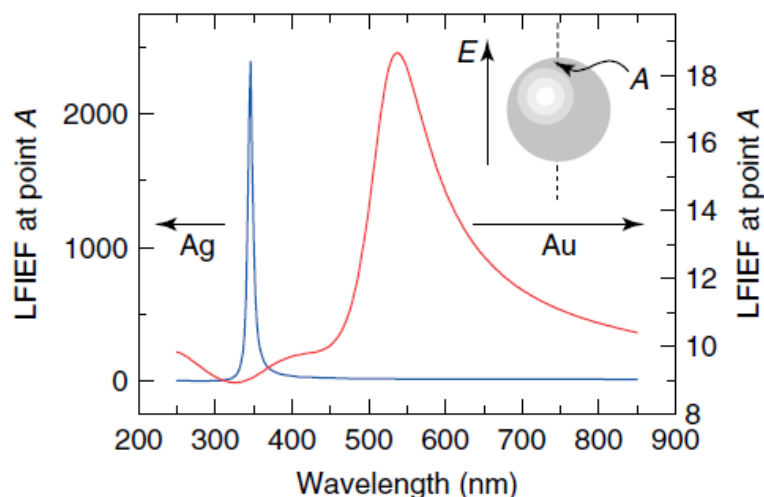


Figure 2. Schematic representation of LFIEF of a metal sphere (Ag or Au) in the point A. when resonance conditions are satisfied, the intensification is maximum. The LFIEF of Ag is stronger due to its low level of absorption compared to that of Au. Adapted from [34]

Silver is the most suitable metal and, in fact, it is widely used for SERS application. Gold and copper can also be employed, but only at longer exciting wavelengths (typically ≥ 600 nm). As explained above, at such wavelengths, the optical absorption of gold in fact becomes comparable to that of silver. Au is therefore more recommended for application in the red and near IR. [35]

3.2 The SERS effect

The exact mechanism underlying SERS effect is still not completely clear. As already mentioned, the most accredited theory states that two different effects are responsible for it: the chemical (CE) and the electromagnetic (EM) one. The former involves charge-transfer processes between

molecular orbitals of the analyte and the conduction band of the metallic substrate [36]; the formation of a chemical bond is therefore mandatory. The latter is based on the intensification of Raman scattering caused by the enhancement in the electric field generated thanks to the optical properties of the nanostructured metal surface; in this case, a physisorption of the analyte on the surface is enough. [37.] In fact, while the chemical effect is short-range, the electromagnetic one is long-range. Moreover, it is worth recall again that the two phenomena contribute a different extent to the SERS enhancement of Raman scattering: an order of magnitude of 10^{10} for EM, of 10^2 for CE. [38]

In order to understand how electromagnetic and chemical effect works, the origin of Raman effect must be considered. When the electric field of an incident photon interacts with a molecule of polarizability α , a magnetic dipolar moment, μ , is induced. The intensity of the Raman scattering depends both on the square of the applied electric field and of the polarizability: $I_{\text{Raman}} \propto E^2 \alpha^2$.

In the electromagnetic effect, the intensification of the Raman scattering is due to an enhancement of the electric field in proximity of the metal surface; in the chemical one, the polarizability of the adsorbed molecule is modified itself. [34]

3.2.1 Electromagnetic mechanism

When a molecule is absorbed onto a nanoparticle, it experiences an electric field which is the sum of two components: the electric field of the laser, E_0 , and the electric field scattered by the metal itself, E_s . The photons of these two components have the same frequency ω_0 and, when it corresponds to the surface plasmon resonance of the metal, the field scattered by the metal is strongly intensified of a g factor. In this case the total electric field affecting the molecule can be approximated to the one scattered by the metal substrate. The total Raman scattering radiation which is recorded by the detector is the sum of that emitted by the molecule (E_R) and the one enhanced by the nanoparticle (E_{RS}). A schematic representation of this process is represented in Fig. 3. The resulting energy of the scattered electric field or, in other terms, of the enhanced Raman effect, corresponds to E_{RS} : [39]

$$E_{\text{SERS}} \cong E_{\text{RS}} \propto g' E_R \propto g' \alpha_R E_S \propto g g' \alpha_R E_0$$

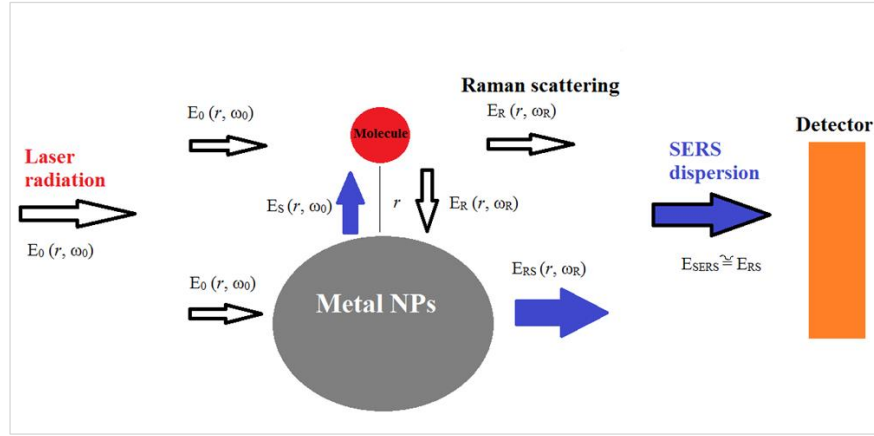


Figure 3. Schematic representation of electromagnetic mechanism in SERS. Adapted from [39]

On the other hand, the intensity of the scattered photons due to SERS effect is proportional to the intensity of the incident electric field multiplied by the square of the enhancing factors and the polarizability of the molecule:

$$I_{SERS} \cong (g g')^2 \alpha_R^2 E_0$$

Generally, the difference between the frequency of the incident photons and the Raman ones can be neglected, therefore it is possible to approximate the enhancing factor of the impinging radiation and that of the scattered one. In this way, the amplification of the incident radiation results multiplied by the fourth power of the enhancing factor, g^4 . It is important to define the G intensification factor in order to understand the relation between the SERS and Raman intensity of the scattered photons:

$$G = \frac{I_{SERS}}{I_{Raman}} = \frac{\alpha_R}{\alpha_{R0}} (g g')^2$$

where I_{Raman} is the intensity of the scattered electric field without the metal and α_{R0} the polarizability of the molecule in absence of the SERS substrate. [38, 39]

3.2.2 Chemical mechanism

In opposition to the electromagnetic mechanism, the chemical one is based on charge-transfer processes, so a chemical interaction between the analyte molecule and the substrate is required [37]. If a chemisorption takes place, the molecule forms a complex with the metal and new electronics transitions can occur, leading to different energy levels of the adsorbates. These transitions, induced by an external incident radiation, consist in charge-transfer processes in which the electrons belonging to the HOMO (highest occupied molecular) orbital of the adsorbate pass to its LUMO (lowest unoccupied molecular orbital) or to the Fermi level of the metal. This last transition is the predominant, as the stronger interaction molecule-nanoparticle

implies a higher degree of connection of their molecular orbitals. Charge transfer more likely occurs the most when the molecule presents π electrons, prone to be yielded and, as a consequence, involved in this process. [38, 39]

3.2.3 Hot spots and SERS enhancement

So far, only the case of an isolated spherical particle was considered; however, it is possible to obtain a further enhancement of the SERS signal in the presence of aggregates of nanoparticles. Experimental evidence and theoretical calculations show that when two spherical nanoparticles are at a distance of less than 5 nm, at the intermediate point between them, an amplification of the local electric field of several orders of magnitude higher than in the case of isolated nanoparticles takes place [40]. This enhancement of the electric field derives from the constructive interference of the surface plasmon resonance of the two particles and the interparticle region where this field amplification is experienced is called *hot spot*. The SERS signals, therefore, increase dramatically when the molecules to be detected are found in a hot spot (Fig. 4a) rather than on the surface of an isolated nanoparticle. [41] Although the determining factor remains the interparticle distance (if it is too large, the SERS effect is strongly penalised), also the size and the morphology of the nanoparticles have a certain influence on the enhancement factor. In particular, the amplification is greater when the two nanoparticles have very similar dimension [42] or when they have anisotropic geometry associated with sharp tips and narrow gaps (Fig. 4b). [43]

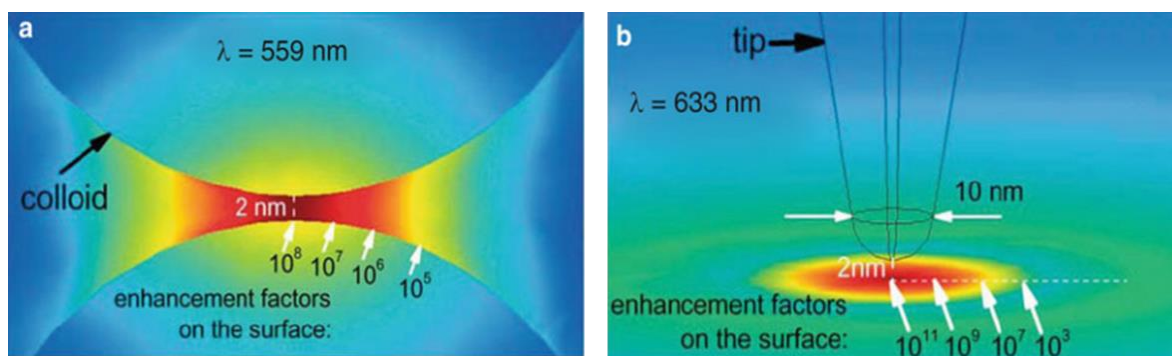


Figure 4. Examples of different types of hot spot: (a) hot spot formed between two closely placed nanoparticles, (b) hot spot formed at a sharp geometrical feature. Reproduced from [44].

3.1.5 Quenching of the fluorescence emission

Beside the enhancement of the Raman scattering, the second aspect that makes SERS a powerful technique for the analysis of organic molecules is the quenching of the fluorescence emission, generally associated with such compounds. To understand this event, it is worth

underlining that these two effects arise from radically different mechanisms and processes [34, 35, 38].

A Stokes Raman vibrational scattering event is an instantaneous optical process: an incoming photon from the laser at ω_L excites a molecular vibration with frequency ω_v while emitting a scattered photon at $\omega_S = (\omega_L - \omega_v)$. The absorption of the incoming photon is therefore not implied. Fluorescence, on the other hand, involves that the incoming photon is absorbed by the molecule, which passes from the ground state S_0 to an excited electronic state S_1 . Subsequently, the photon is re-emitted after undergoing a series of steps which lower its energy: before relaxing to the ground state, in fact, a part of it is dissipated in a non-radiative way (i.e. heat). As a consequence, the fluorescence phenomenon takes more time to happen than the Raman scattering, which is almost instantaneous. Both fluorescence and Raman scattering are positively affected by the absorption of the incoming photons, but, while in the instantaneous emission process Raman scattering experiences a beneficial enhancement of its intensity, proportional to the fourth power of the incident electric field ($|E^4|$), in fluorescence the only possible effect of the environment on emission is to modify the radiative efficiency η , that is the relative contribution of radiative and non-radiative decay. The radiative decay, also known as quantum yield, is generally inhibited by the presence of a metal as it is able to absorb the emitted photons in other way. Therefore, the combination of the enhanced absorption and the lowering of the radiative efficiency ($0 \geq \eta \leq 1$) results in a strong quenching of the fluorescence for a molecule in the proximity of a metal substrate. [34]

3.4 SERS in cultural heritage diagnostics

SERS spectroscopy has been largely exploited in the field of cultural heritage diagnostics for the detection of natural dyes in textiles and lakes. Actually, SERS was firstly applied for the detection of colourants extracted from ancient artistic and archaeological objects in 1987 by Guineau and Guichard [45], but, because of the low reproducibility and the unavailability of suitable instrumentation, it is only in the last two decades that this method has become of common use in this field of research [3, 46-49]. The potentiality of this technique for the identification of natural dyes lies in the fact that, as described in the previous sections, the close contact with a nanostructured metal substrate leads to an enhancement of the Raman signal and a simultaneous quenching of the fluorescence emission typical of organic compounds. Moreover, natural dyes have chemical structures rich in π -electron systems or atoms having lone pair of electrons, conditions which promote their absorption on metal substrate. Finally, since organic dyes, because of their high tinting strength, were used in very low concentrations, a very sensitive

technique is mandatory for their identification and SERS spectroscopy fulfils this requirement. [3, 49]

The most typical SERS substrates are colloidal suspensions of metal nanoparticles, as they can be quickly prepared and easily used. This traditional approach involves the analysis in solution of the target analyte. Anyway, since dyes are present in works of art as complexes with aluminium or other metal ions and in this form their absorption on metal nanoparticle surface is prevented, the first step towards SERS analysis of lake pigments and mordanted dyes is the extraction of the colourants from their matrix. Extraction procedures are generally carried out in strong acids or alkali, such as HCl or NaOH [3, 4], and allow the hydrolysis of the chemical bond between the dye molecules and the substrate, aiming to isolate the dye. Despite the very small amount of sample required, this method is invariably invasive towards the host material. In this respect, progressively, gentler methods have been developed, such as non-extractive *in situ* hydrolysis and non-hydrolysis approaches. The former alternative methods involve selective removal of the target dye by milder extracting reagents [46, 47, 48] or the use of room temperature acid vapours (typically HF) instead of heated solutions [47, 52]. Referring to the latter, the possibility of detecting some anthraquinone dyes directly on microscopic fragment of the artistic object put in contact with a colloidal paste was demonstrated [53-55], as well as the effectiveness of the use of photo-reduced silver nanoparticles to generate SERS signal directly from dyed fibres [56-58]. These results confirmed that the SERS effect can be recorded even if the molecules are still in form of metal complexes, even if it has been demonstrated that the introduction of the hydrolysis step is the best method to ensure high reproducibility and the certain identification of the dyes. [47, 59-60]

In most recent years, researchers dealt with the issue of transforming SERS into a less invasive method. All the strategies described above, in fact, shall be considered as micro-destructive. Recently the use of peelable gels associated with a SERS-active substrate was proposed by different research groups [5-7]. This procedure involves the use of hydrogels loaded with suitable organic solvents and chelating agents to extract micro-amounts of dyes directly from the artistic object, followed by SERS analysis directly onto the gel surface. Anyway, even if these strategies are non-invasive and applicable *in situ*, a close contact with a wet substrate is mandatory and this could represent a limitation when dealing with artworks and ancient objects. For example, close observation of detached composites showed that analytical surface fragments (40 μm) underwent removal and trapping into the composite matrix, making the method slightly invasive in nature.

Another recently developed technique which reduce invasiveness of SERS spectroscopy by improving the degree of spatial resolution is laser ablation (LA)-SERS [8, 9]. This method involves the ablation of the target dye molecules by an intense visible laser pulse and its collection onto a SERS-active substrate, typically silver nano-islands made by vapor-deposition. This procedure certainly required a more complex equipment and, although it seems non-invasive, the high intensity of the laser beam causes a damage, although on a microscopic scale, to the artefact.

In this scenario, an increasing interest towards dry-state methodology is arising. The use of silver island fabricated by vapor deposition to detect dyes in textiles was proposed in [10] and also the production of complex substrates obtained by deposition of self-assembled silver nanoparticles on glass and polydimethylsiloxane (PDMS) substrates [11]. Anyway, these methodologies involve the use of specific equipment and/or a complex procedure, not always accessible for diagnostics laboratory. The aim of the present work was to develop a simpler and effective protocol to produce dry-state SERS substrates starting from metal nanoparticles prepared on the basis of simple wet chemistry.

4. Materials and methods

4.1 Materials

Trisodium citrate dihydrate, silver nitrate, hydroxylamine 50 % w/w in water, sodium chloride, sodium perchlorate, magnesium sulphate, sodium hydroxide, methanol, 3-(aminopropyl)trimethoxysilane, hydrochloric acid (37 %), sulfuric acid (95-97 %), $\text{HAuCl}_4 \cdot \text{H}_2\text{O}$, hydroxylamine hydrochloride, hexadecyltrimethylammonium bromide, iron sulphate eptahydrate, indigo and alizarin were purchased from Sigma-Aldrich, purpurin from Fluka and lac dye from Zecchi. Tylose H300 YP2 hydroxyethylcellulose was from ShinEtsu, the acrylic polymer Exodisp C 4502 from Novachem and polyvinyl alcohol (PW 61000) was from Sigma Aldrich. All solutions were prepared in Milli-Q water unless otherwise specified

4.2 Syntheses of silver colloids

4.2.1 Lee-Meisel nanospheres

The colloid was synthesised according to the procedure reported by Lee and Meisel [61]. Briefly, 150 mL of a 10^{-3} M AgNO_3 solution were prepared, using water previously degassed under a gentle N_2 flow. This solution was heated to boiling under constant magnetic stirring and then 3 mL of a 1% trisodium citrate aqueous solution were slowly dropped into the flask. After 60 minutes at the boiling point, the colloid became of a light green-grey opalescent colour. After

cooling, it was stored in the refrigerator overnight before use. The obtained nanoparticles have a diameter ranging from 60 to 150 nm [62] and the concentration of silver is 10^{-3} M. The UV-visible spectrum of the Lee-Meisel colloid shows an absorption maximum at 420 nm (Fig. 5).

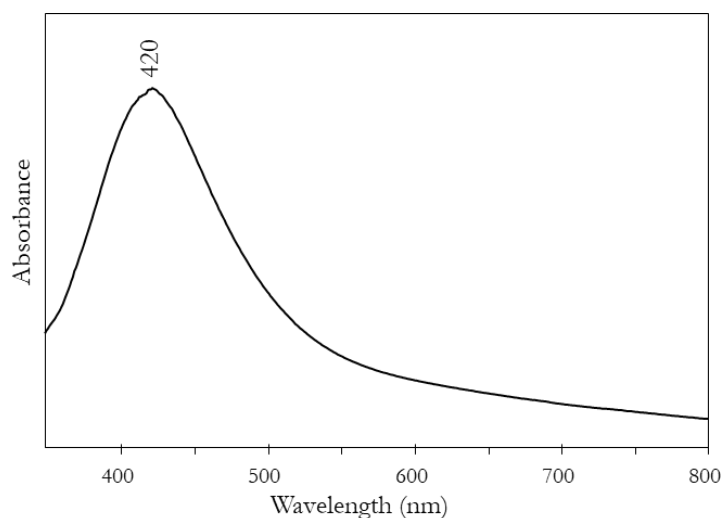


Figure 5. UV-visible absorption spectrum of Lee-Meisel colloid, showing a band at 420 nm.

4.2.2 Leopold-Lendl nanospheres

For the synthesis of Leopold-Lendl colloid [63], 90 mL of a 10^{-3} M aqueous solution of AgNO_3 were prepared at room temperature and quickly added under fast magnetic stirring to a second solution obtained by mixing 4.5 mL of sodium hydroxide 0.1 M with 5 mL of hydroxylamine hydrochloride 0.06 M. The resulting colloid had a final pH around 7 and showed a milky grey colour. The average diameter of the nanoparticles is 67 nm and the final concentration of silver is 10^{-3} M. The UV-vis absorption spectrum is characterised by a band centered at 426 nm.

A modified synthesis of Leopold-Lendl colloid, allowing the formation of larger nanoparticles, was also tested following the procedure proposed in [64]. 90 mL of a AgNO_3 10^{-3} M aqueous solution was heated in a water bath at $45\text{-}50^\circ\text{C}$, with constant magnetic stirring. Then, a second solution obtained by mixing 1 mL of 0.1 M sodium hydroxide with 5 mL of 0.02 M hydroxylamine hydrochloride was quickly added under continuous stirring. The mixture was cooled until it reached room temperature. The colloid showed a milky white-grey colour with a final pH around 5. The average diameter of these nanoparticles is 100 nm and their UV-vis spectrum exhibits an absorption maximum at 408 nm (Fig. 6).

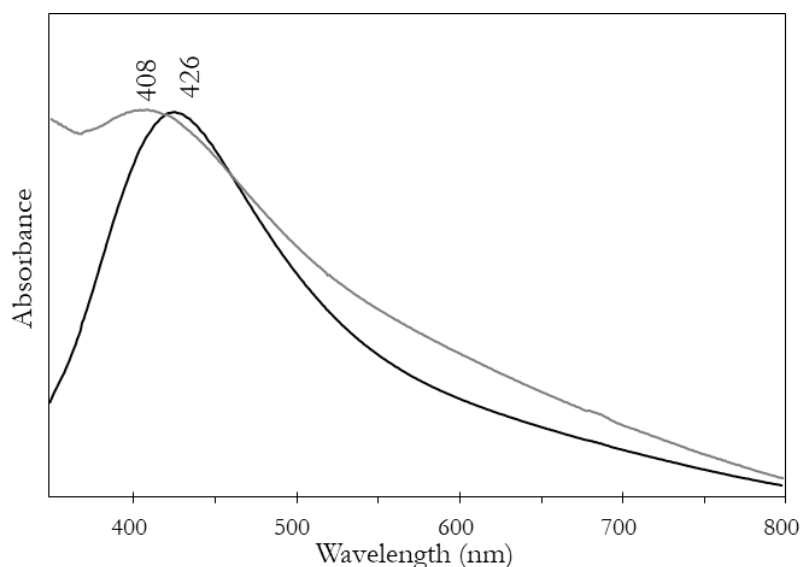


Figure 6. UV-visible absorption spectrum of Leopold-Lendl colloid obtained from the standard (black line) and modified (grey line) synthesis. They show respectively emission maxima at 426 and 408 nm.

4.2.3 Garcia-Leis nanostars

The star-shaped nanoparticles were produced following the procedure reported by Garcia-Leis [17]. Briefly, 500 μL of a 0.05 M NaOH solution were mixed for 1 minute with 500 μL hydroxylamine 50 % w/w one, then 9 mL of AgNO_3 10^{-3} M were added and the mixture was stirred at 670 rpm for 5 minutes. Finally, 100 μL of a 1% trisodium citrate solution were dropped and the stirring was continued for 15 minutes. The reduction of Ag^+ ions is operated by hydroxylamine but this process is very slow at low temperature. In order to make the long arms of these spiky nanoparticles grow faster citrate was added. The resulting colloid, having a dark green-black color, was stored overnight in the dark before use, in order to allow nanostars to develop their final branched shape. The pH should be in the range 8-10: an acid pH prevents the formation of the nanoparticles, while a too basic one leads to the formation of a polydisperse system of nanospheres and nanostars. The average diameter of these nanoparticles is 100-200 nm and the final concentration of silver in the colloid is 10^{-3} M. The UV-visible spectrum is characterised by a sharp band at 380 nm associated to an ascent from 600 nm (Fig. 6). Comparison with the literature supports the formation of star-shaped nanoparticles since the absorption at 380 nm can be due to the core while the broad increase in absorbance at longer wavelengths can be attributed to the tips [15]. Indeed, this double absorption is responsible for the greater SERS enhancement in comparison with spherical nanoparticles [65].

Moreover, the traditional procedure to obtain nanostars was slightly modified during the optimisation of the substrates. In particular, the attempt of eliminating citrate from the synthesis replacing it by hydroxylamine was made. In this respect, the standard procedure was followed

but, instead of adding a 1% trisodium citrate solution, a corresponding volume of hydroxylamine 50% w/w solution was added again. The obtained colloid was characterised by UV-visible spectroscopy and its spectrum, as can be seen in Fig. 7., shows the typical features of nanostars; anyway, the problem of this colloid proved to be its instability as the day after its preparation it precipitated.

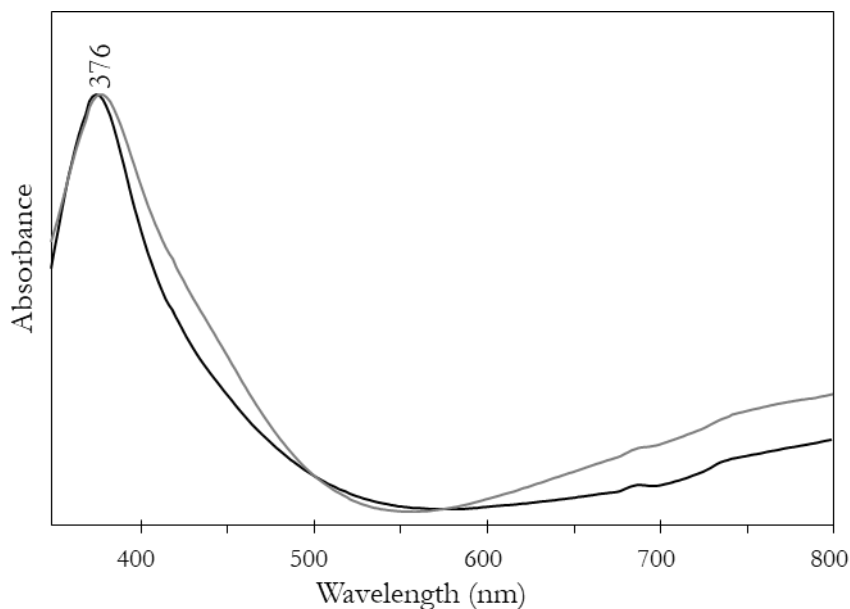


Figure 7. UV-visible absorption spectrum of silver nanostar colloid obtained from the standard (black line) and modified (grey line) synthesis. They show emission maxima at 376 nm.

4.2.4 Nanorods

Silver nanorods were synthesised according to the method recently proposed in [66] and adapted from [67].

It is a seed-mediated procedure, so it involves two different steps: the synthesis of small spherical nanoparticles acting as nuclei and their addition to a growth solution to form nanorods.

For seeds, 100 mL of a AgNO_3 0.01 M were mixed with 400 μL of CTAB 0.1 M and 10 mL of NaBH_4 0.01 M aqueous solutions. The mixture was stirred for two minutes and left to rest for 1 hour. The obtained seed colloid shows a greenish colour and its UV-vis spectrum shows an absorption maximum at 420 nm (Fig. 8).

For the growth solution, 50 mL of a 0.01 M aqueous solution of CTAB were prepared under magnetic stirring and gentle heating to promote the dissolution of the surfactant: in this way, the mixture turns to opalescent white and becomes transparent. Then, 1.25 mL of a 0.02 M solution of AgNO_3 in water and 2.5 mL of 0.1 M ascorbic acid (the reducing agent) were added, leading to the development of a yellow colour.

Finally, to produce nanorods an aliquot of seeds (ranging from 625 to 375 μL) was added to the growth solution together with 500 μL of NaOH 1 M to adjust the pH, thereby enhancing the growth and the formation of nanorods [68]. After ten minutes, the final nanorods colloid, having a dark colour, was obtained. Different attempts demonstrated that better results were obtained if the seed solution was added while heating the growth solution. It is worth noticing that the rod diameter corresponds to the diameter of the seeds, while the amounts of seeds added to the growth solution determines their final length: more seeds lead to shorter rods. In particular nanorods were synthesised by adding 625, 400 and 375 μL of seeds. Their spectra are showed in Fig. 7. As can be seen, they are characterised by two plasmon bands, corresponding to the transverse (TSPR) and longitudinal surface plasmon (LSPR) resonance respectively [66]. The former is centred around 405 - 415 nm, while the latter changes its position from 500 to 600 nm according to the amounts of seeds added to the growth solution. The plasmon surface properties of these nanorods are, in fact, highly sensitive to the seed concentration: its decrease determines a shift of the LSPR band towards lower wavelengths.

The final concentration of the nanorods colloid was calculated as approximatively 10^{-4} M.

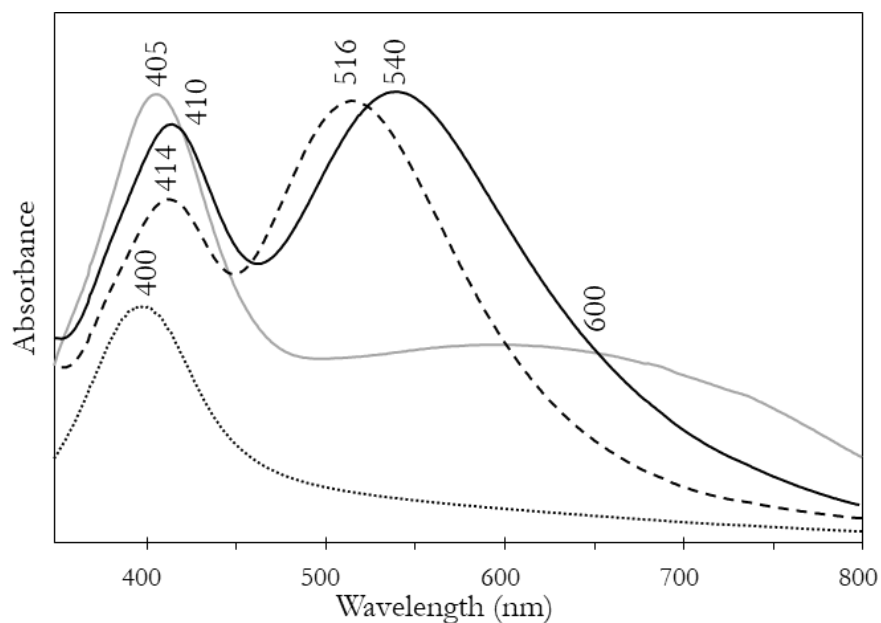


Figure 8. UV-visible absorption spectrum of silver seeds (pointed line) and of nanorods obtained from different amounts of seeds: 625 μL (grey line), 400 μL (black line) and 375 μL (dotted line). The two plasmon bands are due to TSPR and LSPR respectively.

4.3 Syntheses of gold colloids

4.3.1 Frens nanospheres

10 mg of $\text{HAuCl}_4 \cdot \text{H}_2\text{O}$ were dissolved in 100 mL of water in a three-neck flask and the solution was heated up to boil in an oil bath under reflux, with constant stirring. 420 μL of a 1% trisodium citrate solution was then added: after 1-2 minutes the colour became intense blue, but it turned progressively to red after 40 minutes. The final colloid has an intense Tyndall effect: its colour changes from red to blue-violet depending on the light. The final pH is 3-4. The concentration of gold is $2.94 \cdot 10^{-5}$ M and the average diameter of the nanoparticles is comprised between 45 and 60 nm, as suggested by the band at 542 nm in the UV-visible spectrum of the colloid Fig. 9). [69]

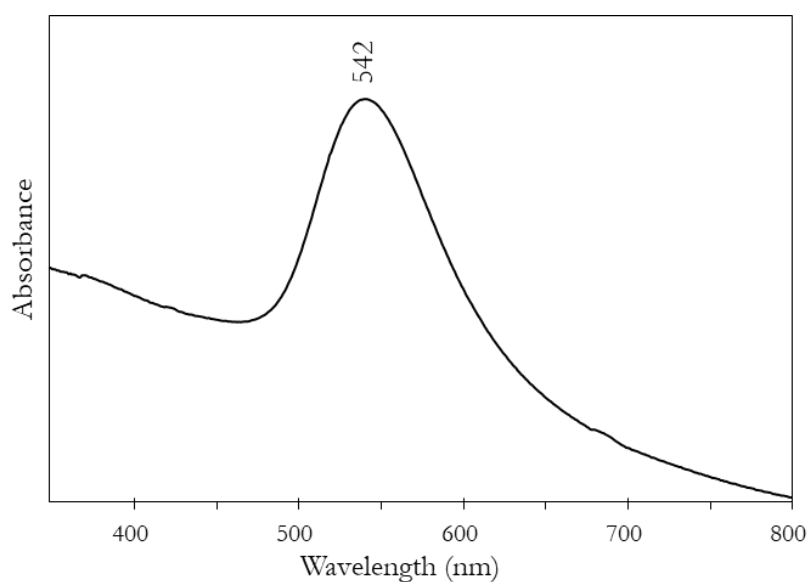


Figure 9. UV-visible absorption spectrum of Frens colloid, showing a band at 542 nm.

4.3.2 Gold nanostars

Gold nanostars were synthesised following two different procedures reported in the literature, both seed-mediated.

The method proposed in [70] involves the preparation of four starting aqueous solutions: 22.5 mL of CTAB 0.1 M, 1.5 mL of $\text{HAuCl}_4 \cdot 3\text{H}_2\text{O}$ 0.01 M, 300 μL of AgNO_3 0.01 M and 320 μL of ascorbic acid 0.1 M. The seeds were prepared following the method reported in section 3.3.1. For the growth solution, 1 mL of $\text{HAuCl}_4 \cdot 3\text{H}_2\text{O}$ 0.01 M was added to the surfactant solution under magnetic stirring, followed by 150 μL of AgNO_3 0.01 M: the colour turned to brown-yellow. Then, 160 μL of ascorbic acid solution were added, making the colour of the solution turn to transparent again. Finally, 50 μL of seeds were added and the colloid was left for 2 hours

in a water bath at room temperature, developing its final blue-violet colour. The final nanoparticles have an average diameter of 140 nm and the concentration of gold in the colloid is calculated to be $2.6 \cdot 10^{-4}$ M. The absorption spectra of seeds and nanostars are shown in Fig. 10.

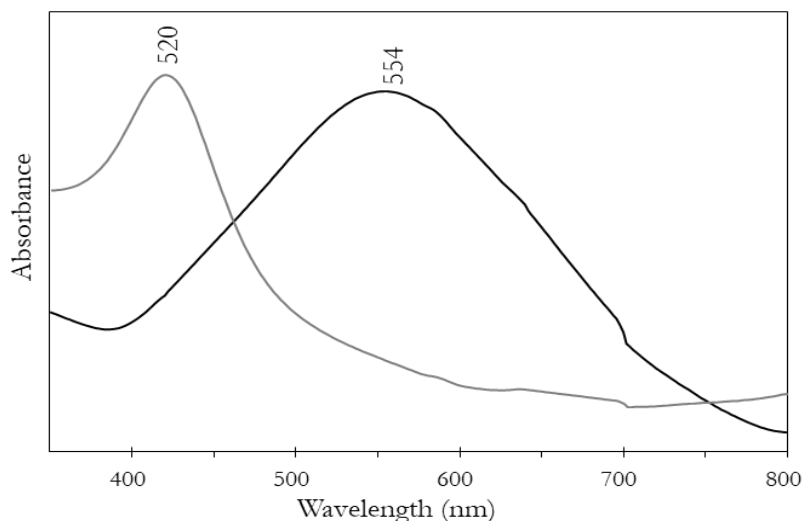


Figure 10. UV-visible absorption spectra of gold nanostars (black line) and their seeds (grey line), showing bands at 554 and 520 nm respectively.

This second synthesis was chosen as it specifically does not require the use of surfactants, which can cause problem in the drop deposition step. It was proposed in [71]. For the seed synthesis, 20 mL of $\text{HAuCl}_4 \cdot \text{H}_2\text{O}$ 1 mM aqueous solution were heated to boiling and 3 mL of a 1% trisodium citrate solution were added. During the whole procedure, the flask was maintained under reflux to avoid solvent evaporation and with constant magnetic stirring. The colloid soon developed a transparent dark-red colour. The UV-vis spectrum, showing an absorption maximum at 524 nm, suggests the formation of small seeds, having an average diameter of around 50 nm. [70]

For nanostars, 100 μL of HCl 1 M were added to 100 mL of a 0.25 mM $\text{HAuCl}_4 \cdot \text{H}_2\text{O}$ aqueous solution. 1 mL of seed was then quickly dropped into it and subsequently 1 mL of a 1 mM AgNO_3 and 500 μL of ascorbic acid 100 mM were quickly added simultaneously. After few seconds, the colloidal suspension became blue. The final concentration of gold is $2.6 \cdot 10^{-4}$ M.

A second synthesis was repeated adding a double concentrated AgNO_3 solution in order to promote the formation of more branched nanoparticles. The concentration of this reagent is, in fact, a determinant parameter for the anisotropic growth and leads to obtaining longer arms. The absorption maximum of this colloid is at 694 nm, red-shifted in comparison with the previous one because of a larger diameter of the stars (Fig. 11).

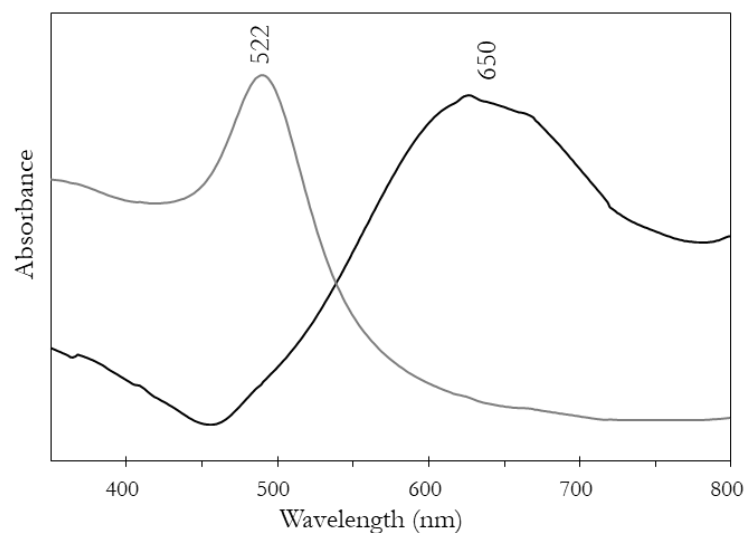


Figure 11. UV-visible absorption spectra of gold nanostars (black line) and their seeds (grey line), showing bands at 650 and 522 nm respectively.

4.4 Preparation of the substrates

4.4.1 Functionalisation of the glass supports

In order to promote the adherence of the nanoparticles to the glass support and to prevent the so-called “coffee ring” effect, a functionalisation procedure of the glass slides with (3-aminopropyl)trimethoxysilane was developed, combining different methods reported in the literature [72-75]. The “coffee ring effect” is an evaporation-driven self-assembly and self-organization. [76, 77] When a droplet of solutions containing non-volatile solutes (i.e. nanoparticles) dries on a substrate, it leaves a dense, ring-like deposit of the solutes along the perimeter. In more detail, the evaporation flux at the edge of the droplet is much higher than that at the centre, leading to more solvent loss. The solvent must flow from the droplet centre toward the edge to compensate for the solvent loss. Consequently, a flow is generated in the evaporating droplet and more particles are carried to the edge. Translating this phenomenon in the physics of colloidal solutions, it obviously hinders the possibility to obtain homogenous films from colloids.

The developed functionalisation process consists of two phases: washing and immobilisation. The former allows to make the hydroxyl groups of the glass slide free for the latter, that involves the reaction between the glass substrate and the immobilising agent (Fig. 12). In particular, 3-(aminopropyl)trimethoxysilane (APTMS) was chosen as it binds the Ag nanoparticles to the surface of the salinized substrate through the amine groups.

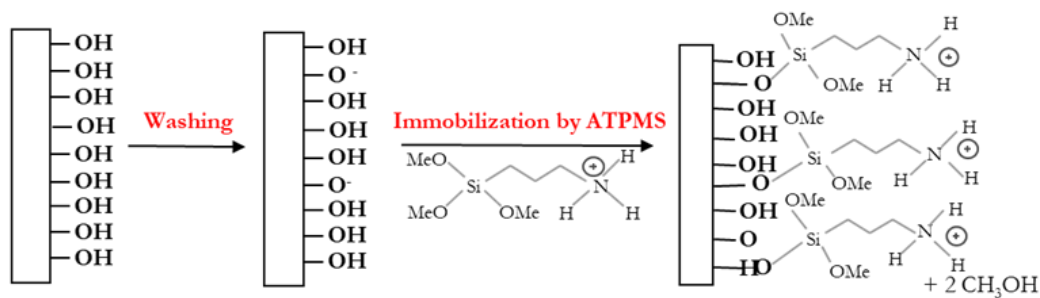


Figure 12. Schematic representation of the functionalisation process.

For washing, the glass slide was dipped in a 1:1 methanol and hydrochloric acid solution for 30 minutes, washed copiously with distilled water until a neutral pH is reached and then dried under a N_2 flux. Then, it is immersed into concentrated sulfuric acid for 30 minutes and washing and drying were repeated as described above. For the immobilisation, the glass slide was dipped in a solution containing 45 mL of methanol, 2.5 mL of deionized water and 2.5 mL of APTMS. After 15 minutes it was carefully washed by immersion in methanol and subsequently in water in order to eliminate all the residual traces of APTMS and finally put in the oven at $90^\circ C$ for 30 minutes. The functionalised glass slide must be used in the day.

4.4.2 Drop deposition

Before drop casting, the colloid was centrifuged (time and rpm depend on the type of colloid and varies from 30 minutes at 3000 rpm to 10 minutes at 6000 rpm) and re-dispersed in water to obtain the right concentration factor (between 1:50 and 1:100). In this respect, after removing the supernatant, a suitable volume of water was added to the nanoparticles paste deposited at the bottom of the centrifuge tube and the suspension was homogenized by quick magnetic stirring. Moreover, when requested, nanospheres were aggregated by adding a suitable electrolyte agent; for spherical particles, in fact, the aggregation step is crucial in order to induce the formation of the hot-spots, i.e. highly localised regions of intense local field enhancement, and to increase the magnitude of the SERS effect [78, 79]. Different salts ($NaClO_4$, $NaCl$, $MgSO_4$) were tested aiming to choose the most effective one (see section 5.1.1). On the other hand, nanostars and nanorods were deposited without the addition of aggregating agents: the anisotropic shape of these nanoparticles, in fact, allows a large intensification of the electromagnetic field, taking place directly on the tips or in the spaces between the arms [13-17, 80]. Finally, a micro-drop ($10 \mu L$) of the treated colloid was deposited by a micropipette on the functionalised glass slide and put in the oven at $50^\circ C$ for about 2 hours, inducing a slow evaporation of the solvent to obtain a homogeneous film. Fig. 13 shows an example of the

obtained substrate, with (a) or without (b) the functionalisation step: in the latter case a more pronounced coffee-ring effect is well evident.

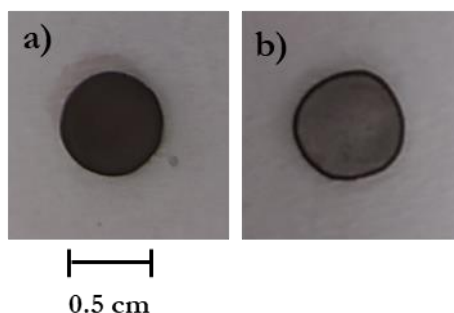


Figure 13. SERS substrate obtained from drop deposition of pre-treated silver nanostars on a) functionalised and b) not-functionalised glass slide.

4.4.3 Multi-layered deposition

The multi-layered deposition involves the application of two layers of nanoparticles, Lee-Meisel nanospheres and Garcia-Leis nanostars respectively, as described below.

1st layer of Lee-Meisel nanospheres: the deposition of Lee-Meisel colloid was deposited by immersion. In this respect, the functionalised glass slide was dipped for 24 hours in 8 mL of pre-concentrated colloid. The concentration factor was set to 1:10, aiming to obtain a quite transparent layer of nanoparticles in view of the deposition of the second layer. The glass slide was finally extracted, gently rinsed with milliQ water and dried under a nitrogen flux.

2nd layer of nanostars: to start, the first layer of nanoparticles was functionalised using a sol-gel method [81]. A solution containing 80 mL of water, 970 μ L of APTMS and 805 μ L of HCl 0.1 M was prepared and stirred for 1 hour. The glass slide covered with the first layer of Lee-Meisel colloid was therefore dipped into it for 20 minutes, afterwards it was copiously rinsed with water and immersed for 2 hours in pre-concentrated nanostar colloid. Two concentration factors were experimented, aiming to obtain a film rich in nanoparticles but at the same time transparent enough to perform SERS measurements through it. They were 1:10 and 1:20. Finally, the second layer was dried into a tubular graphite oven at 110° C for 15 minutes. As the deposition of the second layers by immersion did not lead to satisfying results, a further attempt was made of depositing nanostars by drop deposition on the first layer of functionalised nanoparticles. The stars were concentrated up to a factor of 1:25 and 10 μ L were deposited as described for drop-deposition in section 4.4.2.

4.4.4 Films based on modified coffee-ring effect

This procedure for the deposition of gold nanoparticles was adapted from [82]. A non-functionalised glass slide was cut into small stripes (3 x 0.5 cm ca), then cleaned by sonication in an ultrasonic bath for 10 minutes using deionized water. These glass supports were then laid in a Petri dish maintaining an angle of inclination of approximately 10°.

The solution of concentrated nanoparticles was poured into the Petri dish and the evaporation was carried out inside an oven set at 50°C until complete drying.

4.5 Metal nanoparticles embedded into polymeric matrixes

4.5.1 Exodisp C 4502 matrix

Exodisp C 4502 polymer is an aqueous emulsion of an acrylic copolymer, which crosslinks because of the solvent evaporation. Thanks to its form, it could be added directly to the colloid. Silver nanoparticles were not pre-aggregated by addition of an electrolyte assuming that the evaporation of the solvent gives rise to the formation of the so-called “dynamic hot spots”, i.e. aggregates of nanoparticles originated as the network volume decreases and the nanoparticles get close to each other [83]. In this respect, 5 mL of Lee-Meisel colloid were concentrated up to 1:100 factor and then re-dispersed under magnetic stirring in 25 µL of milliQ water and 25 µL of polymer. When 50 µL of polymer were added directly, in fact, a very strong aggregation of the nanoparticles was induced, as demonstrated by the colour of the colloid which turned immediately from opalescent yellowish-green to black. By diluting the polymer in water (1:1) the aggregation process induced by the polymer itself was less effective, leading to a dark green colour. Finally, 5 µL of this suspension were deposited by a micro-pipette on a non-functionalised glass slide, trying hardly to avoid the formation of air bubbles. The deposited drops were left to dry overnight at room temperature to promote a slow evaporation process and prevent cracking phenomena. Once dried, in fact, this polymer becomes very stiff.

4.5.2 Hydroxyethylcellulose 250 matrix

As described elsewhere [84], Ag nanoparticles polymeric films have been prepared by drying an aqueous mixture of hydroxyethylcellulose (HEC) and pre-aggregated nanoparticles. The procedure was adapted to our experimental conditions in the following way. After centrifuging 10 mL of the colloid and removing the supernatant, the nanoparticles were re-dispersed in 90 µL of ultrapure milliQ water and it was aggregated by 10 µL of MgSO₄ 10 mM, thus achieving a concentration factor of 1:100. The gelation of the concentrated colloid was then progressively induced by adding 100 µL of an aqueous solution containing 160 g/L of HEC, which were gradually dropped by a micro-pipette in ten minutes (around 1 µL per minute). 5 µL of the

obtained suspension were then collected after different times of stirring (0, 10, 30, 40 minutes) and deposited onto a glass slide. The drops were left to dry in a dark place overnight. The final concentration factor of silver in these substrates is 1:50, as 1:100, when experimented, led to a very concentrated film having a mirror-effect surface and low transparency.

4.5.3 Silver nanoparticle-doped polyvinyl alcohol films

The procedure was adapted from [85]. A 5% w/w polyvinyl alcohol solution was prepared by dissolving 0.1 g of polymer in 2 mL of water, under gentle heating and stirring. In our experiment, a PVA having a molecular weight of 61000 was used (in reference it was 88000). After a homogeneous solution was obtained, 0.24 g of AgNO_3 were added and the mixture was stirred at room temperature for 24 hours. Glass microscope slides were cut into rectangular strips and cleaned in ethanol several times. For spin coating deposition, 150 μL of PVA- AgNO_3 solution was delivered to the surface of the glass plate making sure that the whole surface of the glass was covered, afterwards the glass plate was spun at 2000 rpm for 20 s (using a spinning device) in order to spread the composite on the glass surface uniformly. The coated supports were then dried overnight at 60° C and then further dried at 100° C for two hours. Finally, to reduce Ag^+ ions to silver metal nanoparticles, the dried substrates were dipped into 4% w/w $\text{FeSO}_4 \cdot 7\text{H}_2\text{O}$ for 30 s and then placed into the oven at 100° C for 15 minutes. The PVA- AgNO_3 solution-coated glasses, which were transparent after spin coating, changed their colour into yellow with time and became red after the drying step.

4.6 Commercial SERS substrates

Commercial SERS substrates commercialised by the company SERSitive™ were used. They are obtained from electrochemical deposition of silver or silver and gold nanoparticles on an ITO (indium tin oxide) conductive glass. Moreover, they are available in two forms according to the nature of their surface, if hydrophobic or hydrophilic. In our work, both silver and combined silver-gold substrates were tested, as well as both types of surfaces.

4.7 Electrochemical deposition of silver nanoparticles

Electrochemical deposition of silver nanoparticles is a well-assessed method to produce SERS substrates and a consistent number of procedures was reported [86-88]. We followed the method reported in [89], which allows the production of silver dendrite fractal nanostructures by a facile electrochemical deposition method.

The substrate was a FTO (fluorine tin oxide) glass, previously cut in strips of about 2x1 cm, and cleaned in an ultrasonic bath for 15 minutes in acetone, distilled water and ethanol respectively,

in order to remove any impurities from the surface. The electrolytic deposition solution was then freshly prepared, containing citric acid (40 g/L) and silver nitrate (2 g/L) in ultrapure milliQ water. The deposition was carried out by chronoamperometry in an electrochemical cell composed of three electrodes: an Ag/AgCl reference electrode (maintained in the saline bridge to avoid the formation of KNO_3 in the deposition solution), a platinum counter electrode and the working electrode made up of the FTO plate. The electrodes were placed triangularly at close range, making sure that the conductive side of the plate was facing the other electrodes. The deposition solution was then added and, under constant magnetic stirring at 200 rpm, the chronoamperometric deposition was started. The potential applied to induce the reduction of silver nitrate to metallic silver was + 0.8 V, confirmed by cyclic voltammetry performed on the solution itself.

The first test was carried out following the conditions reported in [89], which involves a time of 90 s, while the second was continued for a total of 600 seconds.

At the end of the deposition, the slides were immediately rinsed with abundant milliQ water, dried under nitrogen flow and stored in a dark place to avoid the degradation of silver.

4.8 The cleaning of substrates by TiO_2

Two of the obtained films which gave good results in the dry-state detection of alizarin were selected for the test. They were put in close contact with an alizarin-dyed wool yarn overnight so that, possibly, some residual dyed fibres were released on the metal film. Indeed, SERS spectra showing signals typical of alizarin could be acquired afterwards on different spots of the substrate surface. Then, the substrates were put in contact with a FTO glass covered with a thin layer of titania synthesised according to the procedure reported in [90] and exposed to UV light for 4 hours. SERS analyses were repeated after different cycles of irradiation to check the decrease in the signal intensity. The total irradiation time was 14 hours. In a further experiment, the substrate was gently washed after irradiation to promote the elimination of degradation products.

4.9 Preparation of reference mock-up samples

To prepare reference samples, firstly wool threads were washed and mordanted with alum, ($\text{KAl}(\text{SO}_4)_2 \cdot 12\text{H}_2\text{O}$) for a lasting and stable adhesion of the colorants to the fibre. Then wool threads were dyed following ancient recipes, as described elsewhere [91]. Before analysis, a small piece of the dyed thread was washed in 1 mL of pure methanol in order to remove the not-mordanted dye possibly remaining on the fibre. In the present work wool was dyed with the red anthraquinone dyes alizarin, purpurin, lac dye and the blue dye indigo (Fig. 14).

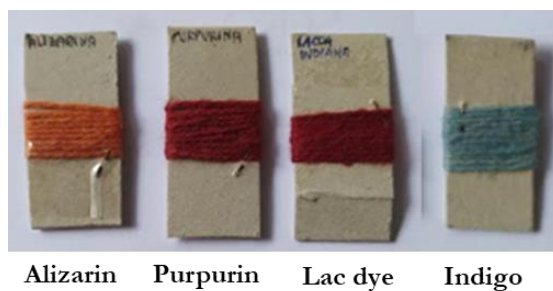


Figure 14. Image of the wool dyed mock-up samples used for dry-state SERS analyses.

4.10 Instrumentation

4.10.1 Raman spectroscopy

SERS spectra were collected with a portable micro-Raman microprobe, equipped with a notch filter and an Olympus 50× microscope objective. The microprobe is connected by fibre optics with a Lotoriel MS 125 spectrometer with a 1800 lines/mm grating and an Andor Peltier-cooled CCD detector. The source, again connected to the microprobe by fibre optics, is a Nd : YAG laser providing the exciting radiation at 532 nm, with an output laser power of about 100 mW. Alternatively, the Raman probe can be coupled with a near-infrared diode laser, emitting at 785 nm. All SERS spectra were recorded between 2000 and 200 cm^{-1} by collecting 30 scans with an exposure time of 2 s.

As the contact between the SERS-active substrate and the sample is fundamental to obtain a good SERS response (the surface-enhanced electromagnetic field is a short range one [21]), the wool thread is fixed in close contact with the SERS substrate. The measurements were then performed by focusing the laser beam on an area of the film where both an aggregate of nanoparticles and the dyed wool thread below were visible through the SERS substrate thanks to the use of a visualization system integrated in the Raman probe.

4.10.2 UV-visible spectroscopy

UV-visible spectra were acquired in the spectral range 400 – 800 nm using a JASCO UV/VIS/NIR V-570 spectrometer, allowing measurements both in transmission and, when equipped with an integrating sphere, in reflection mode.

4.10.3 Scanning Electron Microscopy (SEM-EDX)

SEM images were obtained using a Hitachi TM 1000 microscope, having a resolution of 1 nm and equipped with an energy dispersion X-ray (EDX) spectrometer. The accelerating voltage was 15 kV.

4.10.4 Profilometry

The average thickness of the SERS substrates was evaluated by means of a Bruker DektakXT contact profilometer, having a repeatability of 4 Å and capable of measuring <10 nm step heights.

4.10.5 Potentiometry

Electrochemical depositions were carried out with an Autolab PGStat30 (Ecochemie, The Netherlands) potentiostat/galvanostat equipped with FRA module and controlled by NOVA and FRA softwares. No N₂ degassing of the solution was necessary, since dissolved O₂ did not affect the procedure.

5. Results and discussion

5.1 Silver substrates

5.1.1 Lee-Meisel nanosphere substrates

Lee-Meisel silver nanospheres are the most common colloid employed for SERS detection of natural dyes in the artistic field [3, 52, 54, 92-95]. These nanoparticles, in fact, are easy to synthesise and lead to a great enhancement of the Raman signal. For this reason, it was the first colloid to be chosen to produce our substrates. As already mentioned, previous experiments carried out in our laboratory demonstrated that the best method to obtain SERS substrates from this colloid is drop deposition. A consistent part of the work was therefore dedicated to the optimisation of this procedure, aiming to obtain homogeneous and reproducible SERS substrates, able to induce a high enhancement of SERS signal in dry-state conditions.

In order to induce the formation of hot-spots, the Lee-Meisel colloid must be aggregated by a suitable electrolyte. This aggregating process is generally explained by electrostatic interaction between the ions derived from the dissociated salts and the surface of the nanoparticles, which causes a decrease in repulsion between them. Typical aggregating salts are NaClO₄, NaCl and MgSO₄. The effect of these different electrolytes was studied in order to choose the most effective one and the results are summarised in Tab. 2. Electrolyte solutions, having a 10 mM concentration, were therefore prepared and added to the pre-concentrated (1:100) nanoparticles in a ratio water to electrolyte of 9:1. The aggregating properties of the different salts was then studied by UV-visible spectroscopy and SEM microscopy. As shown in Fig. 15 a and b, the UV-vis spectra of the colloid aggregated by NaCl and NaClO₄ do not differ significantly from those of the non-aggregated colloid. This suggests that the aggregation process is only partial and this feature is reflected in SEM images of the films, where only small aggregates can be distinguished.

On the other hand, when MgSO_4 is added, the absorption band shifts towards longer wavelength indicating the formation of aggregates (Fig. 15c). This is due to the fact that Mg^{2+} ions, thanks to their higher charge, induce stronger aggregation than singly charged cations [96]. The better aggregation properties of Mg salts, in comparison with alkaline metal ones, are demonstrated by the SEM images, where larger ensembles of nanoparticles can be seen.

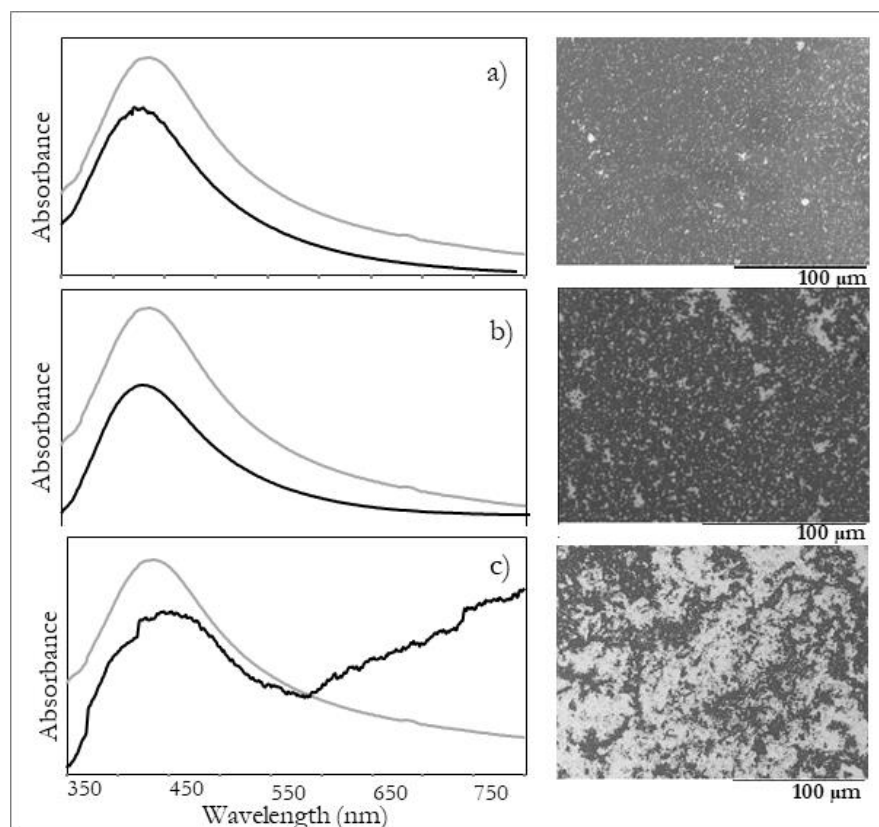


Figure 15. UV-visible absorption spectra of the reference Lee-Meisel colloid (grey line) compared with the same colloid aggregated with a) NaCl , b) NaClO_4 , c) MgSO_4 . On the right, SEM images of the substrates obtained from the corresponding aggregated colloid.

The latter electrolyte was therefore selected and further studies were carried out to find the best water to electrolyte ratio for aggregating and re-dispersing the concentrated colloid. 6:1, 9:1 and 9:2 ratios were experimented and 9:1 proved to be the best one, as it results in obtaining a substrate rich in nanoparticle aggregates, but also having the required transparency. In fact, to reach the detector the scattered Raman signal has to pass through the nanoparticle film and the glass support, undergoing invariably a loss of intensity.

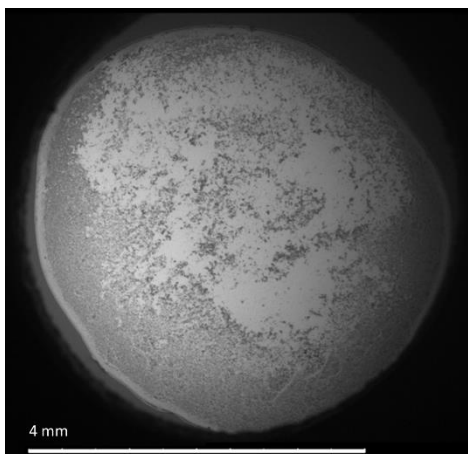


Figure 16. SEM image of a substrate aggregated by MgSO_4 showing the overall inhomogeneity of the surface.

The main problem of substrates aggregated by MgSO_4 is their inhomogeneity. The large aggregates of nanoparticles, in fact, are concentrated in the centre of the drop (Fig. 16), so the metal coating of the substrates is extremely random from deposition to deposition. To solve this problem, different experiments were carried out, for example re-dispersing the aggregated nanoparticles by sonication rather than by magnetic stirring or aggregating the colloid *in situ*, i.e. depositing a drop of pre-concentrated colloid on the functionalised glass slide and then applying a micro drop of extremely

diluted 2 mM electrolyte solution directly on it. Among all experiments, the method selected as the most performing, despite its low reproducibility and the inhomogeneity of the metal coating, was: redispersion of the concentrated nanoparticles in milliQ water to obtain a concentration factor of 1:100 and aggregation by MgSO_4 10 mM (the ratio water to electrolyte was therefore 9:1). These SERS substrates obtained by deposition of the concentrated and aggregated colloid were then further characterised by UV-vis spectroscopy and profilometry. The average thickness of the film is 200 μm and the UV-vis spectrum shows a broad absorption band centred around 625 nm (Fig. 17). The position of the plasmonic band is in accordance with the fact that better results are obtained by using the 532 nm excitation wavelength rather than the 785 nm one.

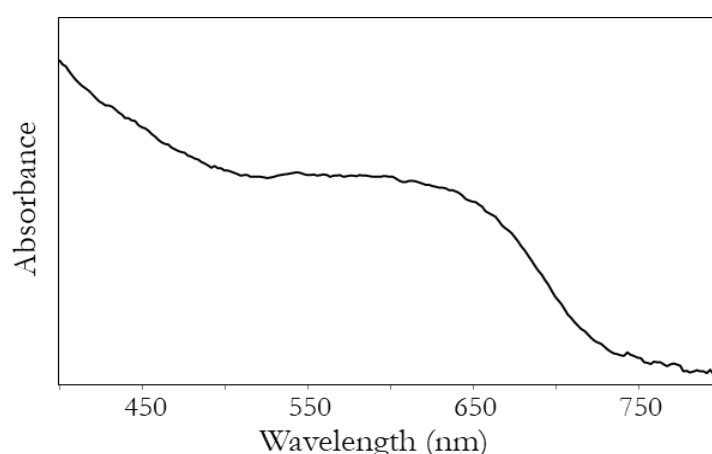


Figure 17. UV-visible reflectance spectra of the SERS substrate synthesised with Lee-Meisel colloid aggregated by MgSO_4 10 mM.

These substrates were then successfully used for the detection of two anthraquinone dyes, alizarin and purpurin, absorbed onto a mordanted wool thread. The acquired SERS spectra (Fig. 18) show intense signals (Tab. 1) due to the two analytes and a low fluorescence background, allowing their certain identification. This is demonstrated by comparison with the spectra of the same compounds analysed in solution on the same substrate, corresponding to those reported in the literature for the dyes [27].

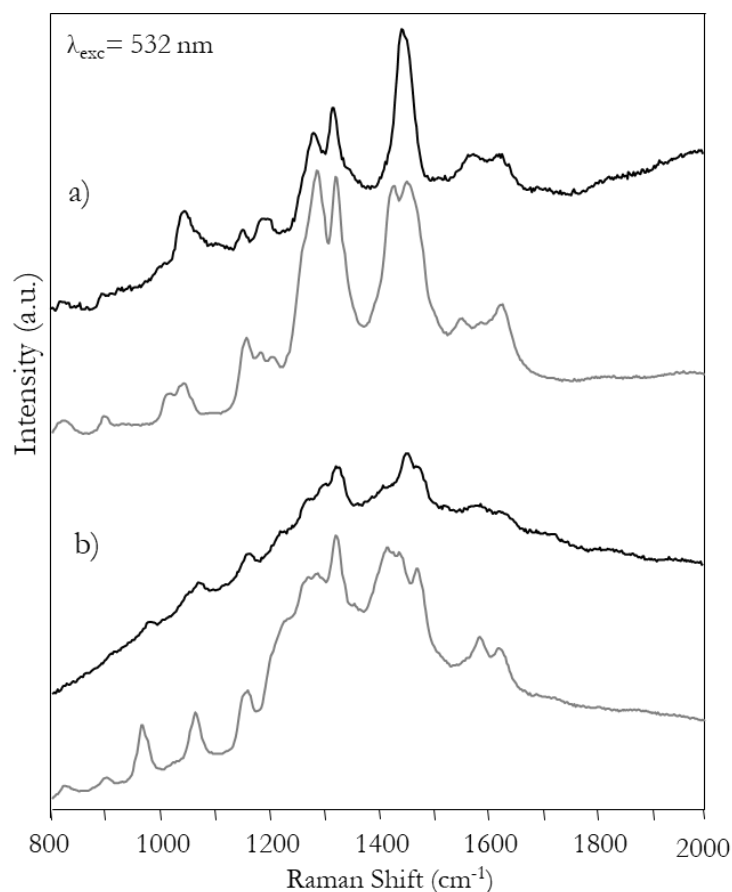


Figure 18. Dry-state SERS spectra acquired on Lee-Meisel substrates from wool samples (black line) dyed with a) alizarin and b) purpurin in comparison with those recorded on the same substrate from a 10^{-3} methanolic solution of the same dye (dotted line).

Table 1. Wavenumber (cm^{-1}) of SERS spectra of alizarin and purpurin obtained from Lee-Meisel nanosphere substrates.

		SERS signals (cm^{-1})
Alizarin	solution	1043, 1157, 1183, 1206, 1289, 1325, 1427, 1454, 1152, 1586, 1625.
	fibre	1047, 1161, 1191, 1285, 1319, 1448, 1578, 1623.
Purpurin	solution	967, 1064, 1158, 1228, 1287, 1323, 1418, 1438, 1472, 1586, 1625.
	fibre	974, 1056, 1157, 1218, 12277, 1329, 1450, 1467, 1585.

Anyway, a strong dependence on the analysed micro-area of the surface was found: intense SERS spectra with low fluorescence background were obtained when the laser beam was

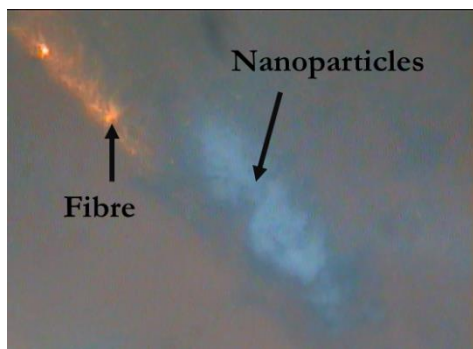


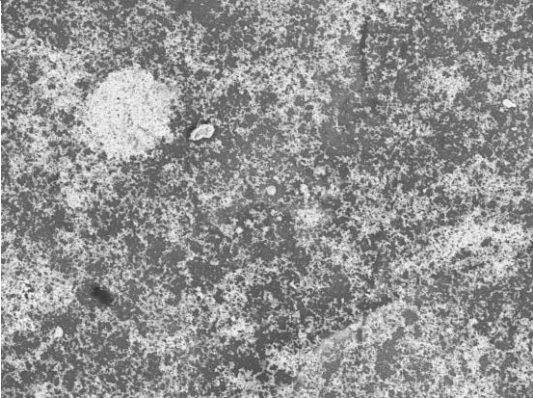
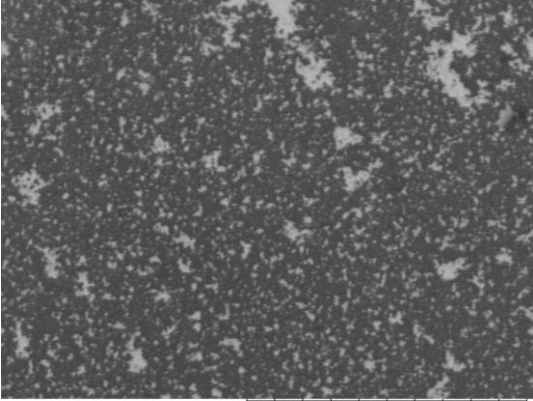
Figure 19: 50x image showing a large aggregate of nanoparticles (a hot spot) aggregates together with the dyed fibre.

focalized onto an area of the substrates where a large aggregate of nanoparticles and, as a consequence, a hot-spot were located (Fig. 19). In this respect, in fact, it must be underlined that almost all these experiments (including those on the substrates aggregated by NaCl and NaClO₄) led to obtain SERS spectra of the reference dye alizarin from a dyed wool thread when this condition is satisfied. However, when the available aggregates are few and small, the selection of an area

suitable for SERS analysis becomes challenging, as well as obtaining intense signals.

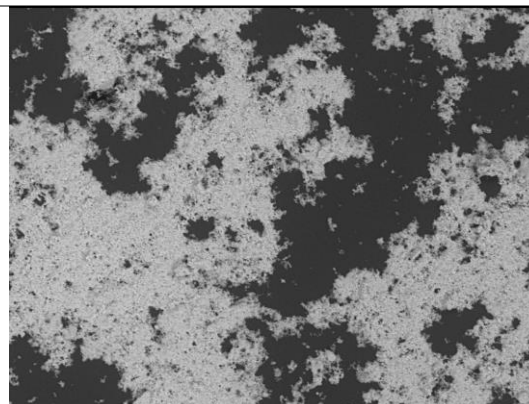
Pursuing the objective of reducing the dependence on the analysed area, also the possibility of coupling the portable Raman probe with a 10x objective in order to lower the magnification power and investigating a larger area was experimented. However, even if from this point of view this could represent an advantage, it causes a loss of intensity of the scattered Raman signal and, as a consequence, dry-state spectra were more difficult to obtain and of worst quality.

Table 2. Summary of the results of the experiments performed to optimise Lee-Meisel nanosphere substrates.

Electrolyte	Water to electrolyte (v/v) ratio	SEM images	Observations	SERS spectra
NaCl 10 mM	9:1	 <p data-bbox="748 788 1279 807">D1-10006 L D4.4 x800 100 um</p>	Uniform morphology, but only small aggregates.	From reference solutions and in dry state condition from alizarin and purpurin dyed wool (weak).
NaClO₄ 10 mM	9:1	 <p data-bbox="748 1251 1279 1267">NaClO410mM0003 L D4.7 x1.0k 100 um</p>	Very small aggregates and very low metal concentration on the surface.	From reference solutions and in dry state condition from alizarin dyed wool (very weak).

MgSO₄ 10 mM

9:1



D9_B0012

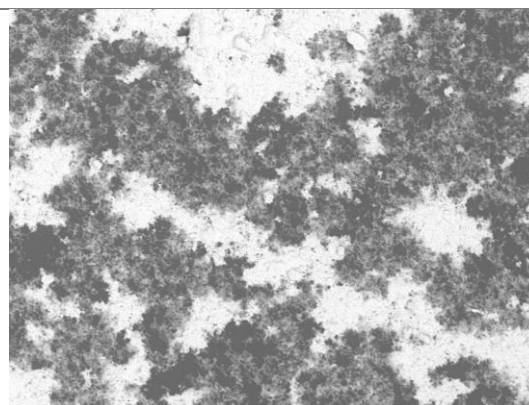
L D3.8 x800 100 um

Large aggregates, although concentrated only in the centre of the deposited drop, which is overall quite inhomogeneous.

From reference solutions and in dry state condition from alizarin and purpurin dyed wool (very intense).

MgSO₄ 10 mM

8:2



D8_A0005

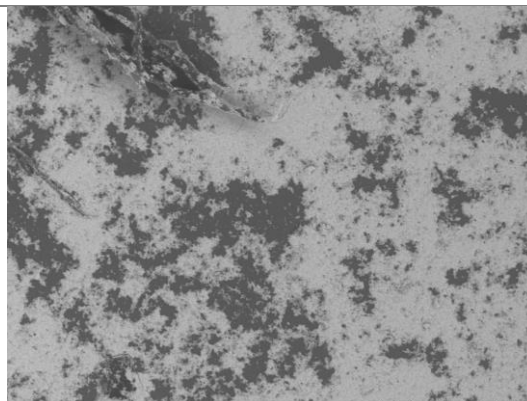
L D4.9 x600 100 um

Large aggregates together with smaller ones. They are still not homogeneously distributed along the surface.

From reference solutions and in dry state condition from alizarin and purpurin dyed wool (very intense).

MgSO₄ 10 mM

19.1



D9_C0005

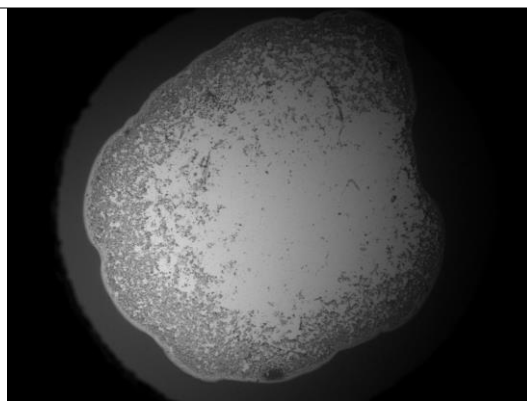
L D3.5 x600 100 um

Large aggregates, although concentrated only in the centre of the drop: overall inhomogeneity.

From reference solutions and in dry state condition from alizarin dyed wool.

MgSO₄ 2 mM

1 μ L of electrolyte 2mM deposited directly on a drop (5 μ L) of concentrated nanoparticles.



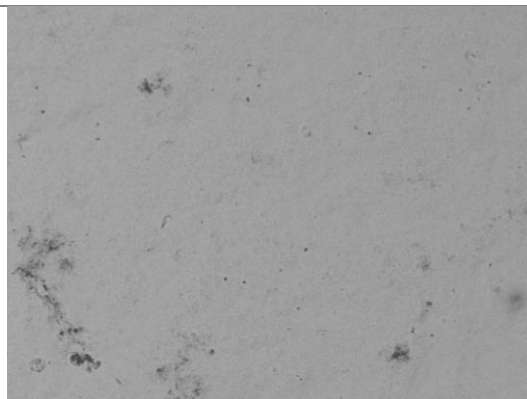
D13C0001

L D4.0 x30 2 mm

Thick and uniform metal layer where the μ -drop of electrolyte is deposited. Very small aggregates along the perimeter.

No SERS signals.

The electrolyte solution was added for small subsequent rates of 1 μ L.



D13B0002

L D4.1 x1.0k 100 μ m

Uniform metal coating of the surface. No SERS signals.

5.1.2 Leopold-Lendl colloids

Even if it does not prevent the identification of dyes in dry-state conditions, the substrates obtained from Lee-Meisel colloids are characterised by blank spectra (i.e. spectra acquired on the surface of the substrate in the same experimental conditions, but without the analyte) dominated by intense signals (Fig. 18a). Together with the peak at 230 cm^{-1} attributed to the interaction between colloidal Ag and ions adsorbed from the preparation solution [97], between 1000 and 1200 cm^{-1} there is a group of signals mainly attributable to degradation products of citrate [98]. After the reduction process, in fact, the oxidised products from the reducing agent can remain on the surfaces of the nanoparticles and act as interferents. For example, molecules such as 1,3-acetonedicarboxylic acid ($\text{C}_5\text{H}_6\text{O}_5$) and acetoacetic acid ($\text{C}_4\text{H}_6\text{O}_3$) are likely to be found. [39]. This issue can be overcome when the analysis is performed focusing the laser beam on a large aggregate, that means an active hot-spot, but when the signal of the analyte is very weak, their presence can interfere and prevent a successful identification. Therefore, some attempts were made to obtain substrates whose blank spectra had less intense signals. Firstly, a washing of the substrate was experimented. In this respect, milliQ water and subsequently methanol were gently dropped on the substrate by a Pasteur pipette, aiming at the removal of possible degradation products of citrate left on the silver surface during the evaporation of the solvent. SERS measurements were then repeated and the comparison of the blank spectra revealed that this method did not provide a significant improvement. The hypothesis was therefore that the degradation by-products are strictly bonded to the surface of the nanoparticles, and thus trapped in the substrate itself. For this reason, a further attempt was to wash the nanoparticles themselves: after the centrifugation step and the removal of the supernatant, nanoparticles were dispersed again in an equal volume of water and centrifuged again before proceeding with drop deposition. Anyway, some problems were encountered because the washed nanoparticles aggregated by themselves, tending to precipitate.

Finally, pursuing the aim of eliminating citrate by-products, a further experiment consisted in removing this reagent from the synthesis of the metal nanoparticles. Lee-Meisel colloid was therefore replaced by the one proposed by Leopold and Lendl [63]. It contains spherical nanoparticles too, but the reduction of Ag^+ ions is induced by hydroxylamine hydrochloride instead of citrate. This represents a main advantage since its oxidation products are gaseous H_2O and N_2 which are dispersed without leaving residues in the colloid [39]. The procedure for obtain suitable substrates is therefore optimised again for these nanoparticles by experimenting two different syntheses and by testing different aggregation conditions.

The first colloid tested to obtain a SERS substrate was the conventional Leopold-Lendl colloid (see section 4.2.2). In all the experiments the concentration factor of silver was set to 1:100. First, silver films were produced without aggregating the nanoparticles, only exploiting the effect of the solvent evaporation to induce their aggregation. The resulted films appeared quite transparent, even if SEM observation revealed the presence of small aggregates of nanoparticles, forming a homogeneous net along the surface. Despite the functionalisation step, a little coffee-ring effect was observed in most cases. Aiming to obtain larger aggregates of nanoparticles, a micro-volume of a 10 mM NaCl solution was added to the pre-concentrated nanoparticles in a volume ratio water to electrolyte volume equal to 9:1. After the addition of NaCl to the nanoparticles, their colour did not change significantly, suggesting that only a weak aggregation effect took place as already discussed for the Lee-Meisel colloid (section 5.1.1). This hypothesis was reflected in SEM images, where the aggregates were still small, although more massive, as if they were formed by a higher number of nanoparticles. Overall, the morphology of the film was quite inhomogeneous, showing a little coffee ring effect and a major distribution of metal along the perimeter of the deposited drop. MgSO₄ was thus tested to induce a stronger aggregation effect. The procedure was analogous to that followed for NaCl, but immediately after the addition of the salt a greater aggregation effect was obtained, as suggested by the colour variation of the nanoparticles. SEM observation of the substrate showed however that the dimension of the aggregates was still very small, similar to that of the unaggregated nanoparticles (Tab. 4).

A modified synthesis of Leopold-Lendl colloid (see section 4.2.3), leading to larger nanoparticles, whose average diameter is similar to that of Lee-Meisel nanospheres, was therefore experimented. The films were again prepared starting from unaggregated or aggregated by NaCl or MgSO₄ colloids. The concentration factor for the silver colloid was 1:100 for all the experiments. The substrate obtained from the unaggregated colloid showed a homogeneous morphology and a characteristic milky-grey colour. SEM images demonstrated the homogeneity of the surface, where a net of small aggregates can be seen (Tab. 4). When NaCl or MgSO₄ were added, the situation was similar to that presented for the unaggregated colloid films with a homogeneous distribution of the aggregates along the surface. Anyway, the addition of both salts did not seem to provide any advantage. On the contrary, the ensembles of nanoparticles appeared smaller, even if more massive, i.e. made of a large number of nanoparticles closely spaced. Tab. 4 resumes the results obtained from these experiments.

Referring to SERS measurements, firstly the blank spectrum was acquired on the surface of the substrates. For both colloids, a good result is obtained: it presents few signals of low intensity

(Fig. 20 b and c), confirming that the absence of citrate is a main advantage. This is clearly demonstrated by the comparison with the blank spectrum of the substrate obtained from Lee-Meisel nanospheres (Fig. 20a).

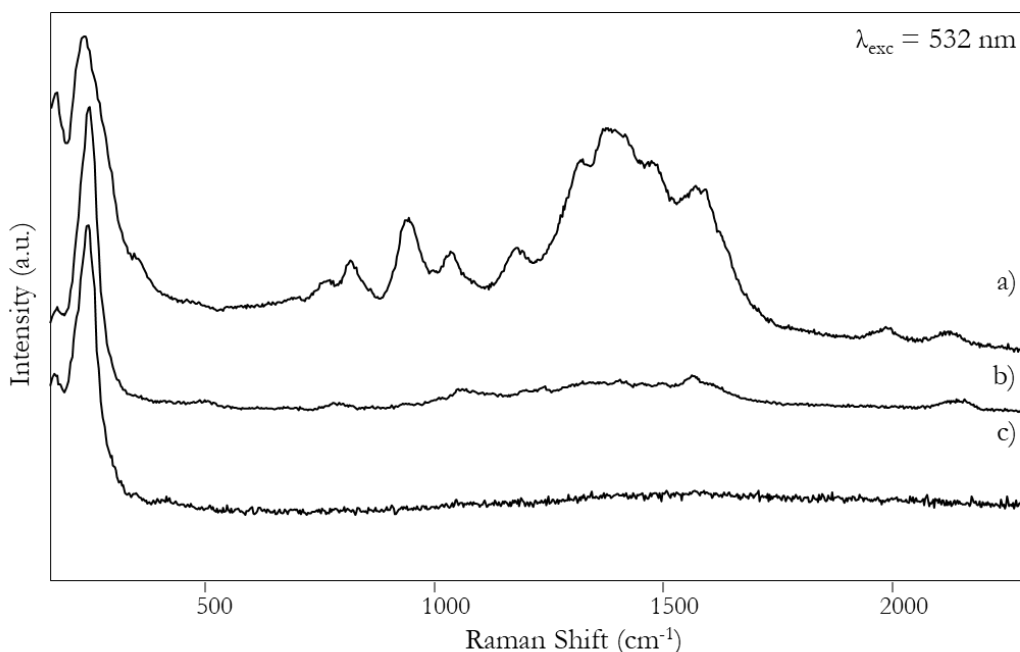


Figure 20. Raman spectra of the blank substrates obtained from: a) Lee-Meisel colloid aggregated by MgSO_4 ; b) unaggregated traditional Leopold-Lendl and c) unaggregated modified Leopold-Lendl.

Regarding SERS analyses on the probe dye alizarin, the best results were provided unexpectedly by those substrates obtained from the unaggregated conventional colloid. An intense spectrum was collected from alizarin in methanolic solution (Fig. 21a) and, in dry-state conditions, from a grain of the powdered dye (Fig. 21b), while extremely weak signals were detected from the dyed textile fibre (Fig. 21c). The SERS bands are listed in Tab. 3. By using the substrates obtained from aggregated colloids, no spectra in dry-state condition could be detected. It seems that the obtained aggregates, despite being rich in nanoparticles, are too small and the resulting metal coating is really inhomogeneous. As a consequence, during SERS measurements especially in dry-state condition, focusing the laser on a single aggregate in order to obtain the maximum SERS enhancement is really difficult.

The modified synthesis did not yield a significant advantage, although the dimension of these nanoparticles is closer to those of the Lee-Meisel colloid: SERS spectra were obtained only from the target dye in solution, i.e. when the chemisorption of alizarin molecules is possible and therefore the chemical effect of the SERS enhancement can be exploited.

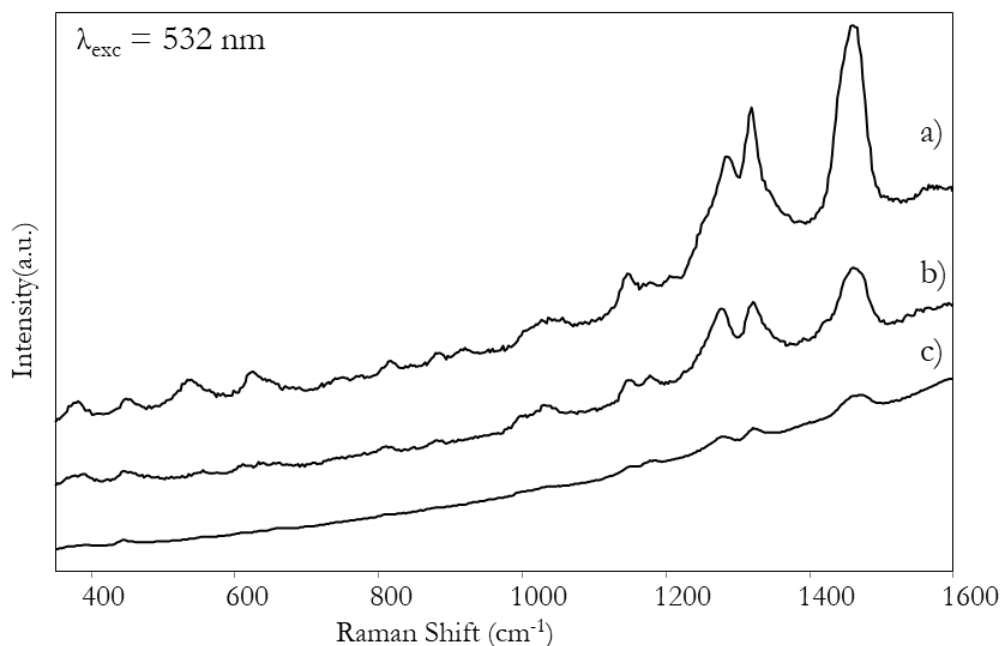


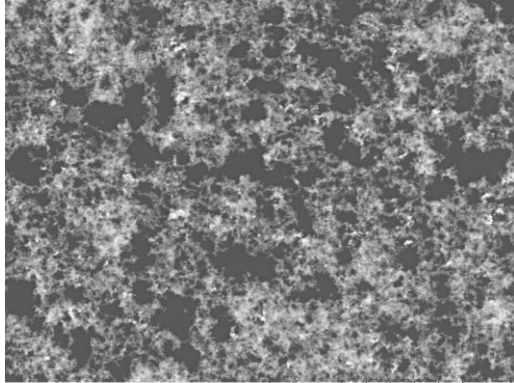
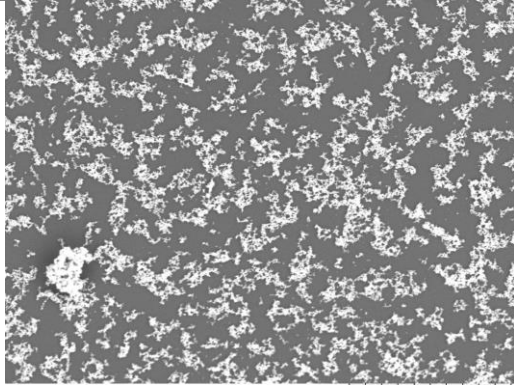
Figure 21. Dry-state SERS spectra of alizarin on a substrate obtained from the unaggregated Leopold-Lendl colloid: a) methanolic solution; b) powdered alizarin; c) dyed fibre. These results are obtained from unaggregated modified Leopold-Lendl substrates, the most effective one.

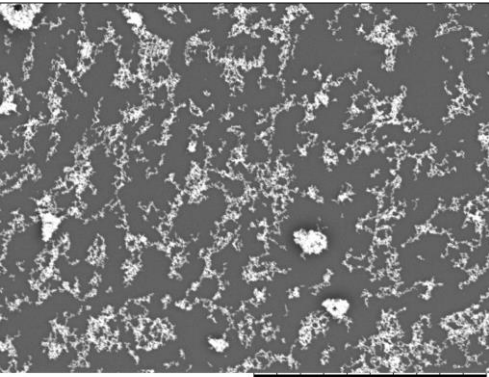
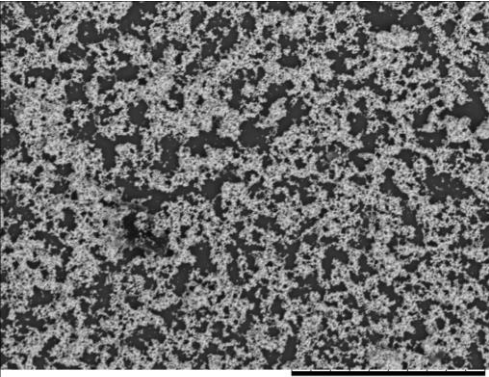
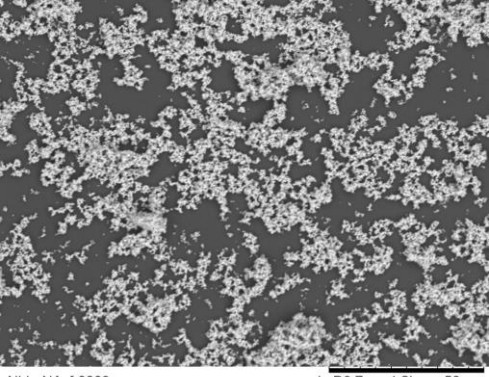
Table 3. Wavenumbers (cm^{-1}) of SERS bands of alizarin obtained from Leopold-Lendl nanosphere substrates.

		SERS signals (cm^{-1})
Alizarin	solution	656, 830, 903, 1015, 1052, 1157, 1183, 1292, 1325, 1466, 1152, 1586, 1625.
	powder	344, 406, 474, 826, 1012, 1045, 1156, 1187, 1286, 1328, 1460, 1625.
	fibre	1159, 1184, 1284, 1326, 1465.

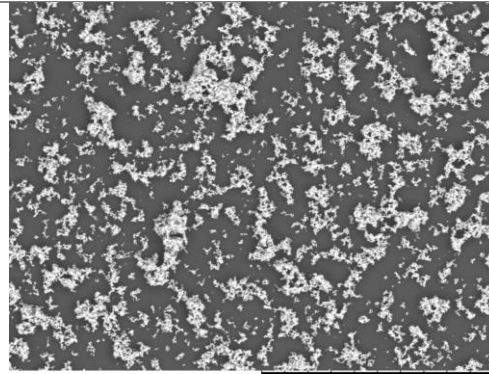
In conclusion, the use of a colloid obtained from the reduction of Ag^+ ions by hydroxylamine hydrochloride provided the main advantage of a blank spectrum characterised by few and low-intensity signals due to the absence of trisodium citrate and its oxidation by-products. However, SERS spectra did not improve: although very good results were obtained from alizarin methanolic solution (demonstrating that the substrates are SERS-active) in all cases, dry-state analyses led to some results only for the substrates obtained from unaggregated Leopold-Lendl colloid.

Table 4. Summary of the results of the experiments performed to optimise Leopold-Lendl nanosphere substrates.

Colloid	Aggregation	SEM Images	Observations	SERS signal
Standard	Unaggregated		Homogeneous distribution of aggregates, quite small and not very massive.	From alizarin in solution and in dry-state condition (powdered dye and dyed fibre)
	NaCl 10 mM		Homogeneous distribution of aggregates, but very small.	From alizarin in solution, no results in dry-state condition.

MgSO ₄ 10 mM	 <p>LLmgso40001 L D4.6 x1.8k 50 um</p>	Homogeneous distribution of aggregates, but very small.	From alizarin in solution, no results in dry-state condition.
Modified Unaggregated	 <p>NewLL_30001 L D3.5 x1.5k 50 um</p>	Homogeneous distribution of aggregates, quite small and not very massive.	From alizarin in solution, no results in dry-state condition.
NaCl	 <p>NLL_NAcr0003 L D3.7 x1.2k 50 um</p>	Homogeneous distribution of aggregates, but very small although massive.	From alizarin in solution, no results in dry-state condition.

MgSO₄ 10 mM



NLL_MsSo4b0002

L D3.2 x1.8k 50 um

Homogeneous distribution of aggregates, but very small.

From alizarin in solution, no results in dry-state condition.

5.1.3 Silver nanostar substrates

As discussed above, the main problem of SERS substrates obtained from nano spherical colloids is the difficulty in setting a standard procedure for a uniform and reproducible result. In fact, the aggregation step, which is crucial to form hot-spots and to enhance Raman scattering, results in an unequal distribution of the metal in the surface of the film. Moreover, also the colloid itself is affected by low reproducibility and its aggregation response can slightly vary from synthesis to synthesis. This irreproducibility derives from both from even slight changes in parameters such as temperature and concentration and from a typically broad distribution of nanoparticle size and shape in the colloidal solution [99]. To overcome these limitations, colloids based on nanoparticles having different geometries can be exploited. Nanoparticles with sharp corners and edge, in fact, are particularly attractive as their anisotropic morphologies give rise to highly concentrated local electromagnetic fields, leading to a further amplification of the Raman scattering in SERS [13-17, 80]. Moreover, these nanoparticles, because of the presence of long tips and their particular geometry, are able to interact directly to form hot-spots without requiring activation by aggregation [17]. Nanostars were therefore tested to produce the SERS substrates avoiding the aggregation step and the consequent inhomogeneity of the surface.

Different concentration factors of the colloid (1:5, 1:20, 1:30, 1:40, 1:50, 1:75 and 1:100) were tested to have a substrate dense in nanoparticles and hot spots, but in the meanwhile transparent enough to allow the passage of the laser radiation and of the scattered Raman signal. The best results were obtained for the concentration factor equal to 1:50. SEM images revealed a considerable presence of aggregates and a homogeneous distribution of the nanoparticles (Fig. 22). On the other hand, when the concentration is lower there are too few nanoparticles and the distance between them during the evaporation of the solvent is maintained, preventing the interaction between their branches and thus the formation of a consistent number of hot spots (it should be remembered that a distance lower than 5 nm between the nanoparticles is mandatory). However, when it is higher, the substrate is too covering, preventing the passage of the laser radiation and of the scattered Raman signal. The results of the experiments are summarised in Tab. 7.

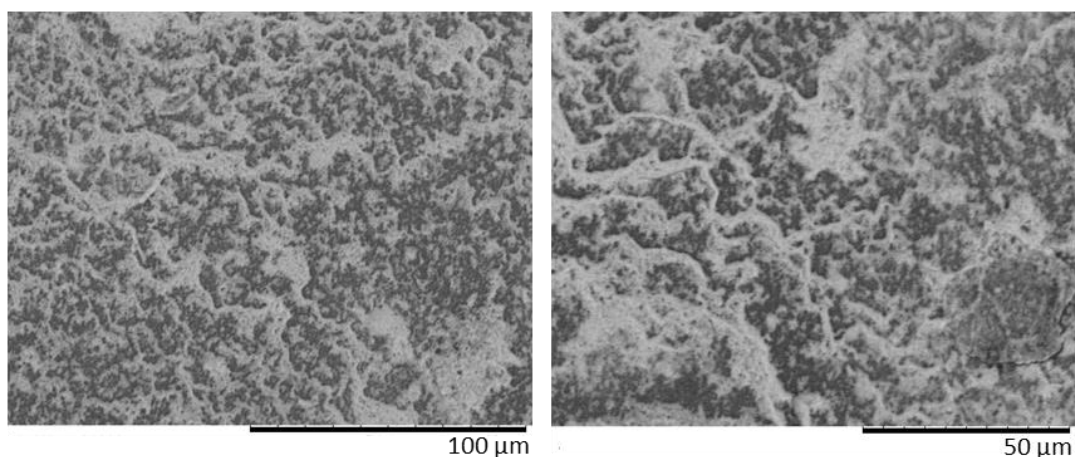


Figure 22. SEM images of the substrates obtained from silver nanostars (concentration factor 1:50).

The best nanostar substrate (concentration factor 1:50) was further characterized by profilometry and UV-visible spectroscopy. Profilometric analyses estimated an average thickness of 200 μm and the UV-vis spectrum was characterized by a broad absorption band centered at 608 nm (Fig. 23). Again, this result is consistent with the greater enhancement obtained by the 532 nm laser excitation wavelength, in comparison with the 785 nm one.

A strong dependence on the examined micro area was observed again, but in comparison to Lee-Meisel nanosphere substrates, the higher number of aggregates make easier to select a suitable spot to perform SERS measurement on the dyed yarn. In fact, the nanostar substrates were finally successfully tested for dry-state SERS analysis of wool dyed with the anthraquinone dyes alizarin, purpurin and lac dye and also with the blue dye indigo. In Fig. 24, the acquired spectra are shown in comparison with the reference ones obtained from a solution of the same analyte on the same substrate. Again, the SERS signals (listed in Tab. 5) correspond to those reported in literature [24, 25]

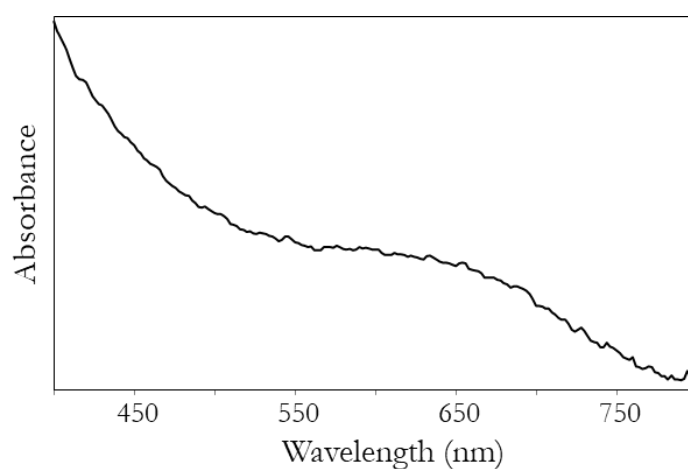


Figure 23. UV-visible reflectance spectra of the SERS substrate synthesised with Lee-Meisel colloid aggregated by MgSO_4 10 mM.

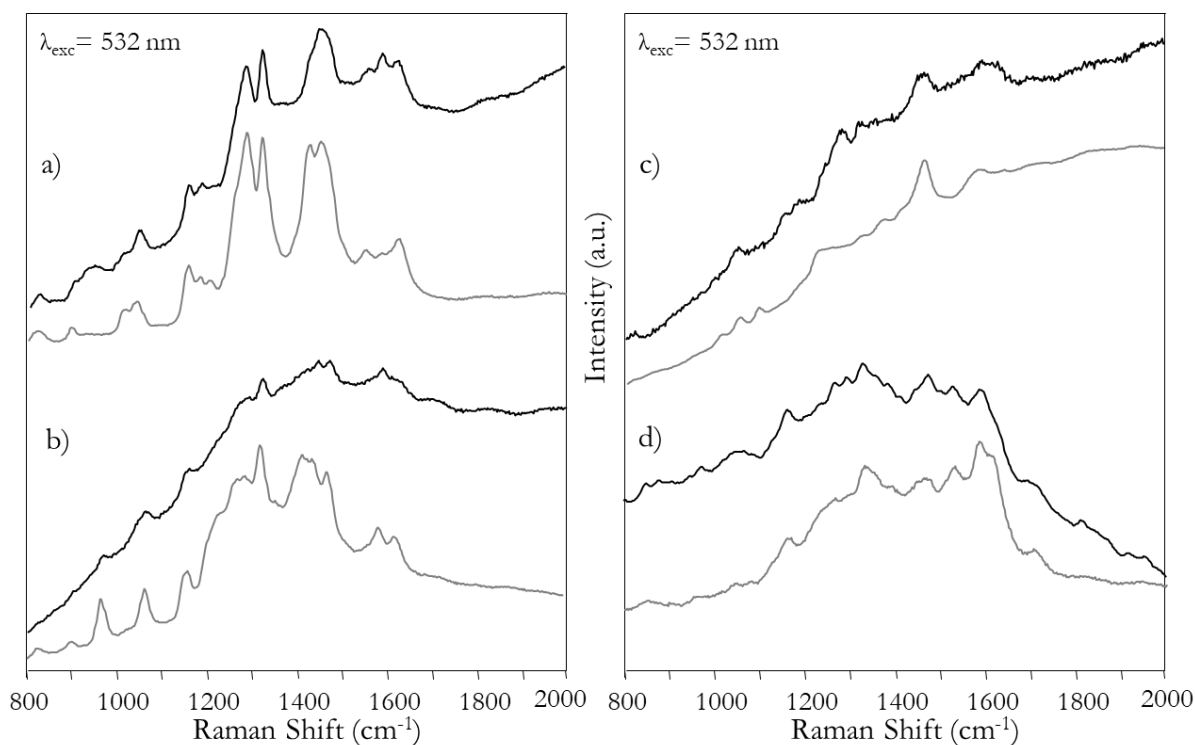


Figure 24. Dry-state SERS spectra acquired on Garcia-Leis substrates from wool samples (black line) dyed with a) alizarin, b) purpurin, c) lac dye and d) indigo in comparison with those recorded on the same substrate from a 10^{-3} methanolic solution of the same dye (dotted line).

Table 5. Wavenumbers (cm^{-1}) of SERS bands of alizarin obtained from Garcia-Leis nanostar substrates.

			SERS signals (cm^{-1})
Alizarin	solution		824, 898, 1015, 1043, 1157, 1183, 1206, 1289, 1325, 1427, 1454, 1152, 1586, 1625.
	fibre		821, 1043, 1156, 1212, 1281, 1326, 1619.
Purpurin	solution		826, 901, 967, 1064, 1158, 1228, 1287, 1323, 1418, 1438, 1472, 1586, 1625.
	fibre		1065, 1155, 1286, 1321, 1443, 1475, 1590, 1629.
Lac dye	solution		1009, 1050, 1098, 1194sh, 1230sh, 1368, 1461, 1578, 1625.
	fibre		1051, 1094, 1187, 1293, 1325, 1465, , 1588, 1629.
Indigo	solution		958, 1045, 1081, 1160, 1266, 1332, 1391, 1461, 1527, 1584, 1616, 1703.
	fibre		930, 1044, 1361, 1458, 1585

In addition, also the issue of the identification of dyes in mixture was faced. In this respect, a wool thread was dyed with a mixture of alizarin and purpurin (1:1). Such combination of colouring molecules, in fact, is typical of one of the most widespread red dyes, madder. The SERS spectrum obtained from the dyed wool thread showed quite intense signal (Fig. 25b and Tab. 6). By comparing it with reference spectra of pure alizarin (Fig. 25a) and purpurin (Fig.

25c), it seems, apparently, more similar to purpurin, although minor signals due to alizarin are recognisable too. It must be said that these two anthraquinone compounds are very similar in their chemical structure, and, as a consequence, their SERS spectra are comparable too, especially referring to the position of the signals at 1290 and 1320 cm^{-1} (corresponding to $\delta\text{OH} + \delta\text{CH}$ [100]). The higher similarity to the spectral pattern of purpurin can be explained by the fact that, as already demonstrated, when a green excitation wavelength is used, lower detection limits can be achieved for purpurin by exploiting resonance condition. The strong electronic absorption band for this dye at 481 nm originates a strong resonance Raman enhancement for an excitation wavelength of 514.5 nm (not too different from the one used in this work). [101, 102]

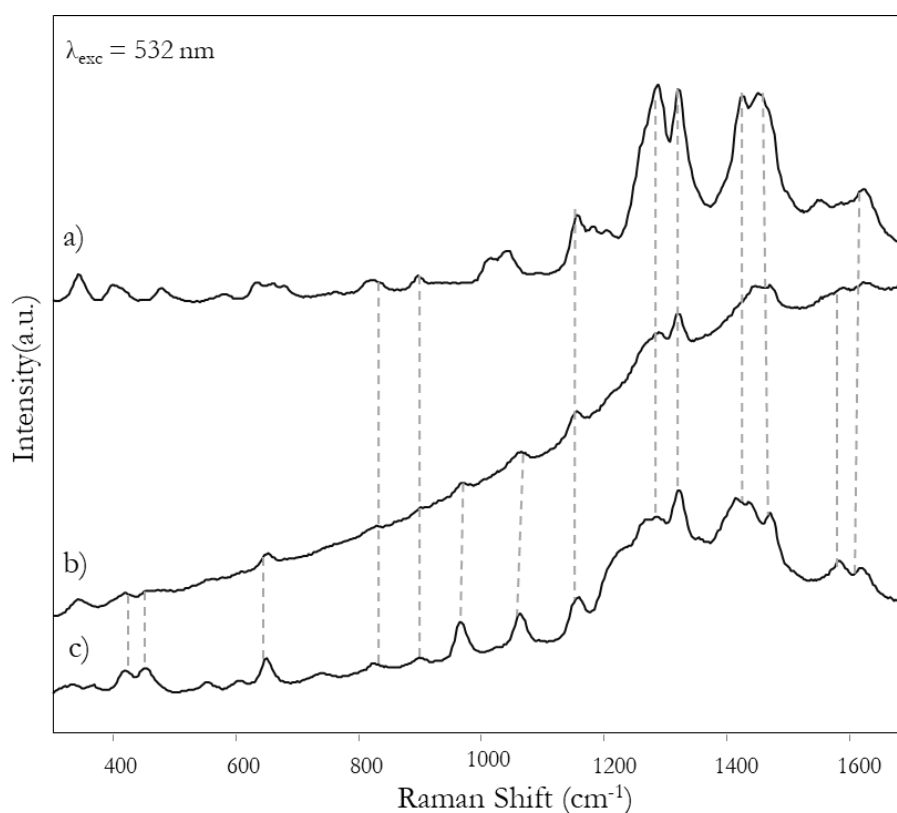


Figure 25. Comparison between SERS spectra of alizarin and purpurin and the one obtained in dry-state from a wool thread dyed with a mixture of the two anthraquinone dyes. The substrate was a film obtained from Garcia-Leis nanostar colloid.

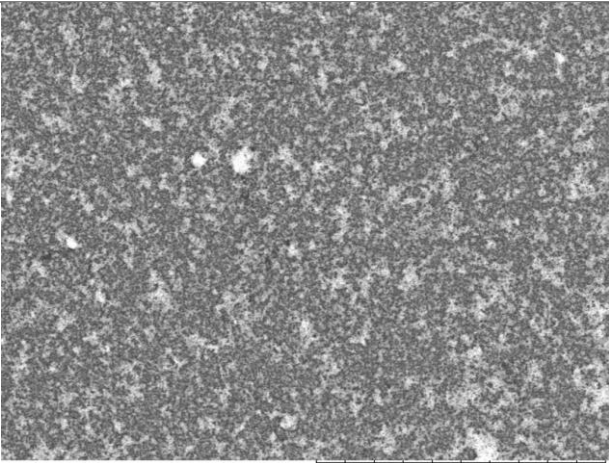
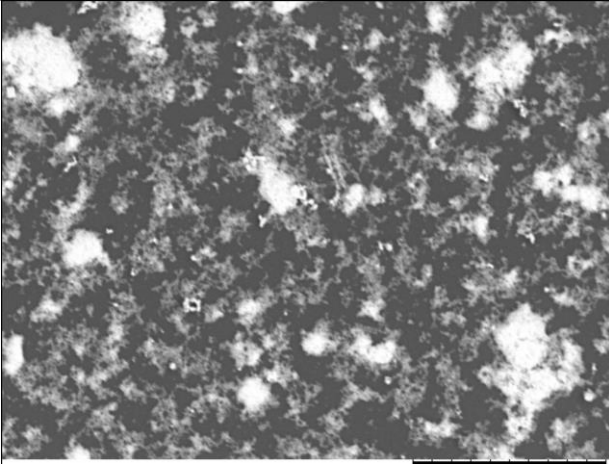
Table 6. Wavenumbers (cm^{-1}) of SERS bands of a mixture of alizarin and purpurin (1:1) obtained from Garcia-Leis nanostar substrates.

	SERS signals (cm^{-1})
Alizarin +	343, 418, 451, 649, 827, 900, 967, 1064, 1157, 1290, 1321, 1447,
Purpurin (1:1)	1471, 1548, 1625.

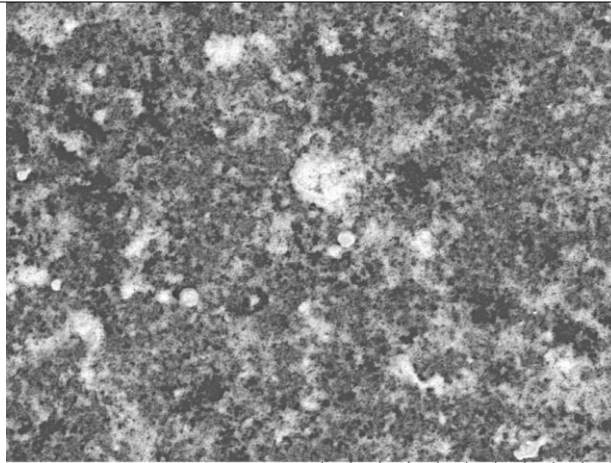
Finally, it must be underlined that, also in this case, some problems with blank spectra were encountered in case of weak dry-state SERS signals. The second reduction step involved in

producing star-shaped nanoparticles is, in fact, induced by trisodium citrate. As for Lee-Meisel colloid, some experiments were performed to solve this problem: washing of the film with water and then methanol, washing of the colloid by centrifugation (both leading once again to unsatisfying results) and finally, the synthesis was slightly modified. In particular, also the second reduction step was performed by means of hydroxylamine. Anyway, the obtained nanoparticles proved to be really unstable and impossible to be deposited by drop deposition. Nevertheless, silver nanostars demonstrated to be a very effective colloid to obtain performing dry-state SERS substrates. The absence of activation by aggregation leads to very homogeneous and reproducible surfaces, where, when the right concentration factor of the nanoparticle is adopted, numerous aggregates are uniformly distributed. This is obviously a great advantage for the selection of the measurement area during the dry-state analysis directly on the textile fibre.

Table 7. Summary of the results of the experiments performed to optimise Garcia-Leis nanostar substrates.

Colloid concentration	SEM images	Observations	SERS spectra
1:5		<p>Very small aggregates: the low concentration prevent the interactions of nanoparticles. transparent film.</p>	<p>Only from alizarin in solution, not in dry-state condition.</p>
1:20		<p>Very small aggregates joined by larger ones: the concentration is still too low. Transparent film.</p>	<p>Only from alizarin in solution, not in dry-state condition.</p>

1:30



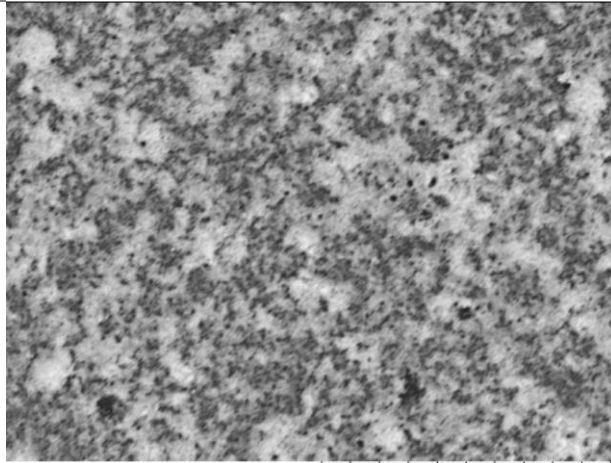
1_30a0002

L D3.8 x1.8k 50 um

Very small aggregates joined by larger ones: the concentration is still too low. Transparent film.

Only from alizarin in solution, not in dry-state condition.

1:40



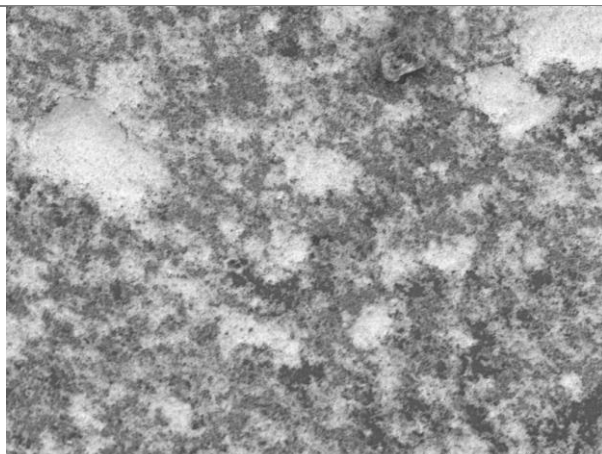
1_40b0001

L D3.9 x1.8k 50 um

The aggregation effect becomes more evident, leading to a homogeneous coating.

From alizarin in solution and, even if weak, in dry-state condition from alizarin dyed wool.

1:50



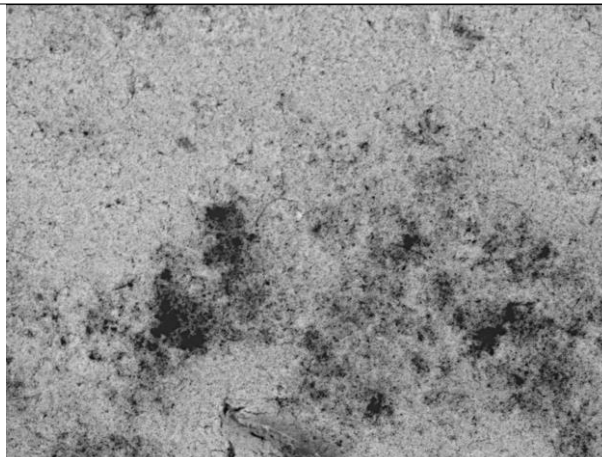
1-50a0002

L D3.5 x1.2k 50 um

Homogeneous coating of the surface and large aggregates of nanoparticles. Although rich in nanostars, the substrates are still transparent.

From four dyes, alizarin, purpurin, lac dye and indigo, in solution and from dyed wool.

1:75



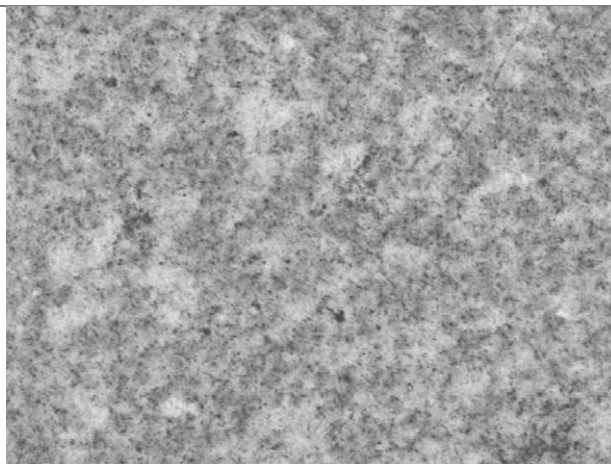
1-75 20002

L D3.0 x1.2k 50 um

Nanostars cover almost uniformly the surface in many areas of the drop. Overall low transparency of the substrate preventing the analyses on the fibre.

Only from alizarin in solution, not in dry-state condition: the substrate resulted too covering.

1:100



1_100a0001

L D3.4 x2.5k 30 um

Nanostars cover almost uniformly the surface in many areas of the drop. Low transparency of the substrate preventing the analyses on the fibre.

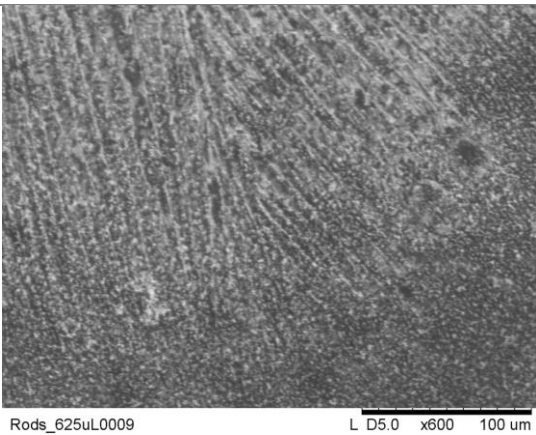
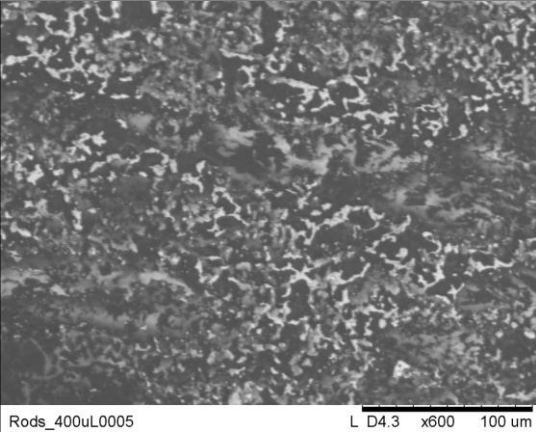
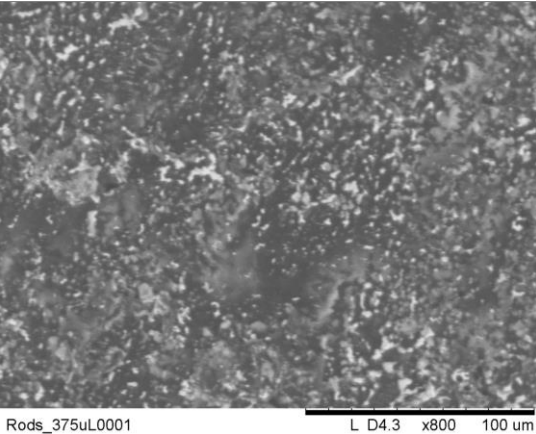
Only from alizarin in solution, not in dry-state condition: the substrate results too covering.

5.1.4 Nanorods

In the framework of experimenting nanoparticles having different geometries to obtain larger SERS enhancement and avoid activation by aggregation, silver nanorods were also tested. Due to their optical properties, these nanostructures have attracted extensive research interest: their absorption, in fact, can be fine-tuned by varying their aspect ratio [103-105]. According to the amounts of seeds added to the growth solution, the length of the obtained rods differs, and the resonance plasmon band of the nanomaterials is shifted towards longer wavelengths, as described in section 4.2.4.

To obtain the SERS substrates, the depositions were carried out on functionalised glass slides and, as the final concentration of the colloid is one order of magnitude lower than the previous ones ($\approx 10^{-4}$ M), the concentration factor of silver was set to 1:1000. Very low final volumes of the concentrated nanorods were thus obtained, resulting in a complication of the deposition step. Moreover, the surfactant CTAB, which acts as stabilizer for the nanoparticles, also represented an issue as it flocculated and formed a foam which trapped the nanoparticles themselves. SEM observation confirmed this fact, as the substrate surface appeared extremely transparent and rich in residual CTAB, as demonstrated by the presence of air bubbles and a mat and glossy appearance. The consistent amount of Br detected by EDX confirmed the hypothesis. In addition, substrates exhibited an evident coffee ring effect and the low amount of metal was concentrated in few determined areas of the drops. The obtained results did not improve significantly by varying the length of nanorods (Tab. 8). No dry-state SERS signals were obtained neither from powdered alizarin nor from the dyed fibre in all the conditions. It seems that the low metal concentration of these colloid and the presence of the surfactant represent strong limitations to obtain substrates having the required features for a SERS enhancement high enough to be exploited in dry-state condition. For these reasons, this geometry was discarded for our purposes.

Table 8. Summary of the results of the experiments performed to optimise nanorod substrates.

Seed amounts	SEM Images	Observations	SERS signal
625 μL		Inhomogeneous surface, matt appearance because of CTAB. Small amounts of silver nanoparticles deposited.	No SERS signals.
400 μL		Inhomogeneous surface, matt appearance because of CTAB. Small amounts of silver nanoparticles deposited.	No SERS signals.
375 μL		Inhomogeneous surface, matt appearance because of CTAB. Small amounts of silver nanoparticles deposited.	No SERS signals.

5.1.5 Multi-layered substrates: nanostars on nanospheres

In principle, a hierarchically-organised structure of nanomaterials having different morphologies can promote the plasmonic effect leading to a remarkable improvement of the SERS response [106-110]. On this basis, we wanted to verify the possibility of obtaining a further enhancement

of the SERS signal by the combined deposition of two colloids. In particular, the effect of Garcia-Leis nanostars deposited on Lee-Meisel silver nanospheres was investigated. The first problem to face was how to obtain a film transparent enough to allow the passage of the laser radiation and of the scattered Raman signal of the analyte. For these reasons, different approaches were tested, aiming to optimise the conditions for a multi-layer deposition. In particular, the first layer was deposited by immersion and the concentration factor of the colloid was set to 1:10, 10 times lower than that commonly adopted for drop-deposition. As verified by SEM, this method led to a quite inhomogeneous results, with a marked coffee ring effect and an inhomogeneous distribution of the deposited nanoparticles. When a second layer of nanostars (concentration factor 1:10) was applied also by immersion on the first layer of nanospheres previously functionalised (section 4.4.3), the result was not satisfying as it seemed that only a few nanostars were deposited. The concentrations factor was increased up to 1:20, but in both cases SEM analyses confirmed that the star-shaped nanoparticles were identifiable only in some extremely localised area of the glass slide (Fig. 26a).

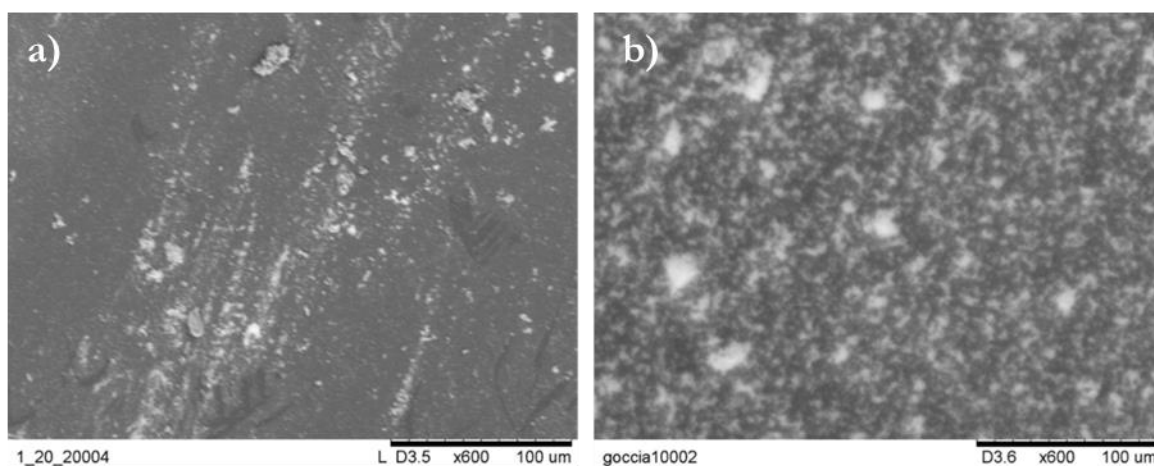


Figure 26. SEM images of multi-layered substrates obtained by depositing silver nanostars (1:20) a) by immersion or b) by drop deposition on a layer of Lee-Meisel nanospheres (1:10).

From such substrates obtained by immersion, a dry-state SERS of wool dyed with alizarin was obtained for both the concentration factor of nanostars (Fig. 27 a and b), but the enhancement is similar to that achieved starting from a mono-layer film. Comparable results were provided by the two experiments. In fact, the spectra were acquired from areas visually selected for the analyses as rich in nanoparticles, therefore the result was not determined by the whole concentration of nanoparticles on the glass slide, but by their amounts in a certain area. A strong dependence on the examined spot is thus confirmed once again.

The multi-layer deposition was therefore repeated by applying a first layer of Lee-Meisel nanospheres by immersion and the second of nanostars by drop deposition (Fig. 26b). In this

respect the concentration of nanostars was lowered in comparison with that optimised for the mono-layer deposition (1:25 vs 1:50). The film, in fact, would have been too covering. This procedure led to a better result for the deposition of the second layer of colloid, as confirmed by the comparison of SEM images (Fig. 26). The second layer of nanostars, in fact, was more homogeneous and the amounts of deposited nanoparticles was considerably higher. The signals due to alizarin in dry-state SERS spectrum (Fig. 27c) were, in fact, more intense and defined, but there was no considerable improvement in comparison with the results obtained by the mono-layered drop-deposited substrates.

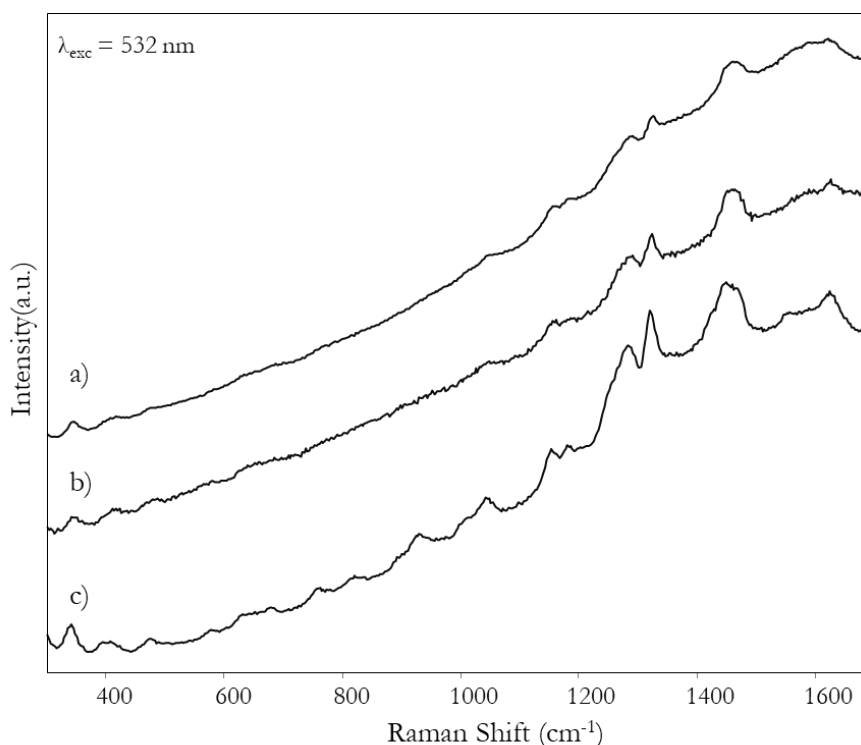


Figure 27. Dry-state SERS spectra from an alizarin dyed wool thread obtained from the multi-layered substrates: a) nanostars (1:10) on nanospheres (1:10) by immersion; b) nanostars (1:20) on nanospheres (1:10) by immersion and c) nanostars (1:25) by drop deposition on nanospheres (1:10) by immersion.

In conclusion, it seems that the SERS enhancement is mainly due to the effect of nanostars, as demonstrated by the fact that upon increasing the concentration factor of these nanoparticles (from 1:10 to 1:20 by immersion and 1:25 for drop deposition) a more intense signal is found. As a consequence, the SERS enhancement is comparable with that obtained starting from the standard drop-deposited nanostar film.

5.2 Silver nanoparticles embedded into polymeric matrixes

The release of silver from the SERS substrates to the analysed textile fibres and the lack of stability under environmental conditions of the deposited nanoparticles represent two limitations to take into account. In fact, SEM-EDX analyses performed on the fibre put in

contact with the substrate revealed that a small quantity of silver remained on the sample (Fig. 28). Obviously, this is a problem that must be considered and avoided, as the silver left behind can react with the surrounding environment and tarnish, causing alteration effects on the artistic objects. Moreover, silver nanoparticles have a limited temporal stability and their deterioration can influence the spectral response, leading to a considerable decrease of the SERS enhancement.

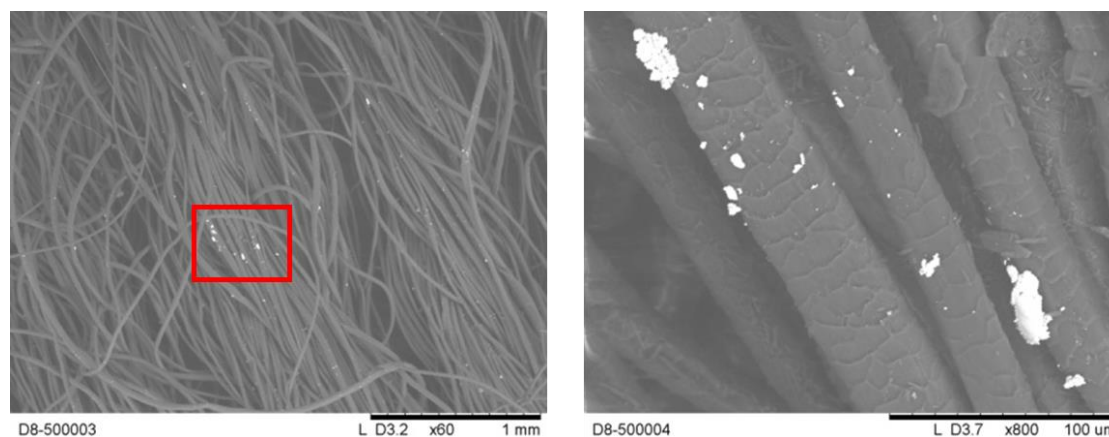


Figure 28. SEM images showing residual silver nanoparticles left on the textile fibre after dry-state SERS analysis.

Therefore, the possibility of embedding silver nanoparticles in a thin, optically transparent polymeric matrix was investigated. To allow the simultaneous protection of nanoparticles and the decrease of the metal amount released on the sample. In the literature, a large number of such experiments are reported referring to SERS analyses in solution [111-115]. Thus we investigated the applicability of this method also for dry-state SERS analyses. To this aim, two different polymers (the acrylic copolymer Exodisp C 4502 and the HEC 250 polymer) were tested as embedding matrix for Lee-Meisel and Garcia-Leis silver colloids. In addition, a different procedure involving the reduction of silver nanoparticles directly into a PVA solution was experimented.

Exodisp C 4502 is an acrylic, aqueous-based copolymer, which crosslinks because of the solvent evaporation. In this preliminary test silver nanoparticles were not pre-aggregated assuming that the evaporation of the solvent gives rise to the formation of “dynamic hot spots” [83]. However, the films resulted strongly cracked from the centre to the sides because of a lack of flexibility and no nanoparticle aggregates were highlighted by SEM examination (Fig. 29). Furthermore, EDX analysis, performed on an area where silver nanoparticles could be, revealed a major contribution due to light elements, while silver is almost not-detectable in comparison with the polymeric matrix. No SERS spectra could be recorded from the probe molecule alizarin neither in solution nor adsorbed onto the wool fibre.

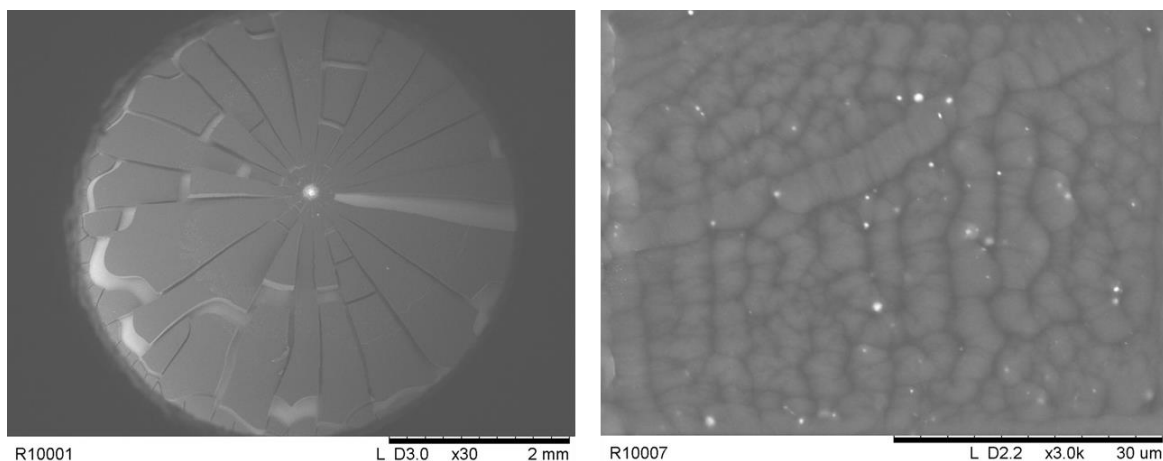
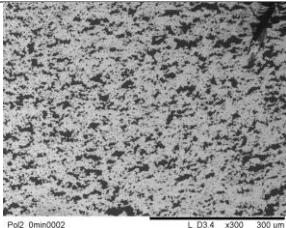
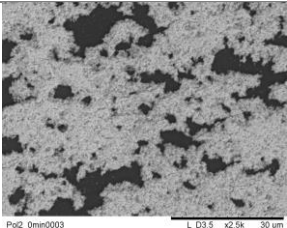
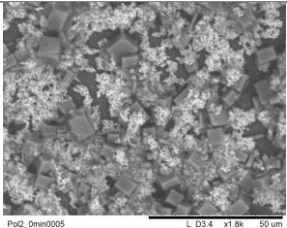
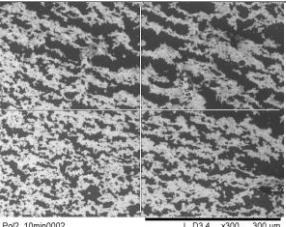
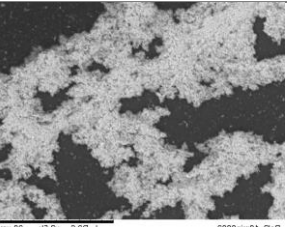
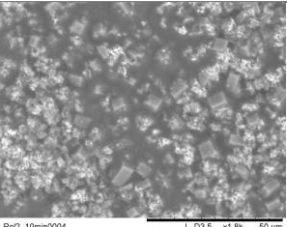


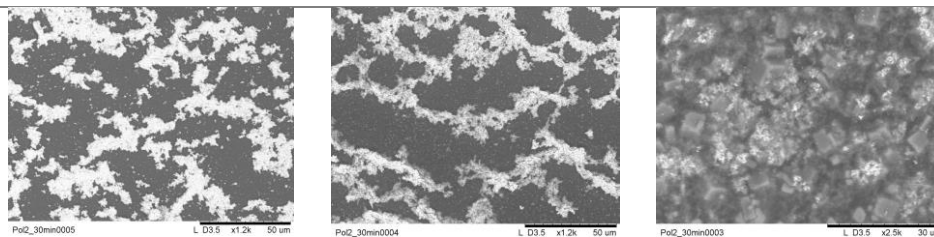
Figure 29. SEM images of the substrates obtained by embedding Lee-Meisel nanospheres into Exodisp C 4502 polymer.

Consequently, a more flexible polymer was chosen: hydroxyethyl cellulose HEC 250 YP2. Silver nanoparticle polymeric films were prepared by drying an aqueous mixture of the polymer and pre-aggregated nanoparticles (section 4.5.2). HEC proved to be more suitable than the acrylic copolymer as its higher flexibility prevents cracking phenomena during the crosslinking process. This method gave indeed a more promising result: the films were quite transparent, with an extensive, but recognisable net of aggregates. As a drawback, a higher concentration of metal was located in the centre of the deposited drop. The effect of different polymerisation times, i.e. the time the colloid was stirred in the polymeric solution before being deposited, were studied by they did not result in different situations. Tab. 9 shows the SEM images of the obtained substrates.

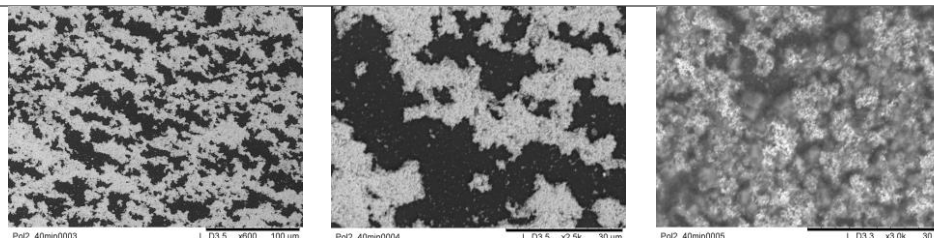
Table 9. SEM images of the substrates obtained after different polymerization times.

Time	Sides	Centre	
0 minutes			
10 minutes			

30 minutes



40 minutes



It is worth noting that the central area of every deposition is affected by the presence of anomalous cubic structures in addition to silver aggregates. EDX analyses performed on them revealed the presence of Cl and Na (deriving from NaCl used as aggregating agents), besides Mg, Si and S which are the same elements dominating the spectrum of the pure polymer.

The possibility of using these polymeric films for dry-state SERS analysis was finally investigated. Considering the SEM-EDX observations, the measurements were made on the lateral areas of the depositions, where the aggregates were prevalent and no anomalous structures were observed. First, the Raman spectrum of pure HEC polymer was acquired to confirm the absence of Raman bands that could interfere with the spectrum of the analyte (Fig. 28). Then the blank spectra of the silver films were recorded, showing a satisfying pattern, where only less intense signals attributable to silver nanoparticles were recognisable (datum not shown). Finally, SERS analyses were performed to investigate the possibility of detecting the probe dye alizarin. At first, the SERS activity of the substrate was tested: a drop of a 10^{-3} M methanolic solution was applied on the substrate and the SERS analysis was performed, showing the typical spectral pattern of this anthraquinonic compound. However, the spectrum was dominated by an intense fluorescence background due to the polymeric matrix and only the main signals of the analyte were clearly recognisable (Fig. 30).

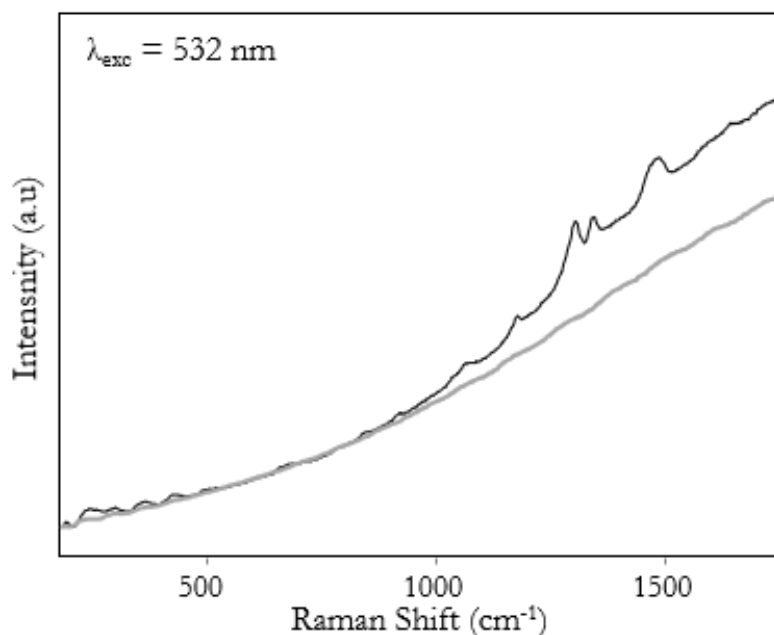


Figure 30. SERS spectrum obtained from a 10^{-3} M alizarin solution (black line) and of HEC polymer (grey line).

In dry-state condition, it was not possible to collect any spectrum. Probably, the presence of the polymeric matrix embedding the colloid could prevent a close contact between the analyte and the substrate required also to achieve an efficient electromagnetic enhancement. This problem does not exist when the analysis is performed on a solution, as the analyte molecules permeate the substrate spreading through it. To overcome this limitation, a chemical etching of the HEC matrix was tested, aiming to uncover the surface of the nanoparticles.

The etching procedure was made by immersing the substrate for 1 minute into a mixed solvent composed of water and ethanol in different ratios (1:1, 7:3, 4:1). HEC is, in fact, water-soluble, and these attempts pursue the aim of eliminating only the most superficial layer of it, avoiding the complete detachment of the substrate from the glass. After this treatment, the 7:3 water to ethanol solution was selected as the most efficient (1:1 was ineffective, while 4:1 led to the partial detachment of the film from the glass) as the substrates did not show loss of silver and the Raman spectrum collected as a blank exhibited strong signals due to the sub-products of the colloid synthesis, confirming the removal of part of the polymeric matrix. Anyway, no Raman spectra of alizarin could be obtained in dry-state condition and only fluorescence was detected: it seems that the partial etching of the polymer is not enough to allow the electrochemical interaction between the analyte molecules and the embedded nanoparticles.

The same embedding and etching procedures were tested for silver nanostars, but in this case the polymer had a negative effect on the interaction between the nanoparticles (Fig. 31). In fact,

in comparison with the substrates obtained re-dispersing nanostars in an aqueous medium, very small aggregates were formed. Analogous results were obtained for different concentration factors of the colloid (1:25, 1:35 and 1:50) and also in this case the etching procedure did not seem to provide great advantages. As a consequence, no SERS signal were obtained.

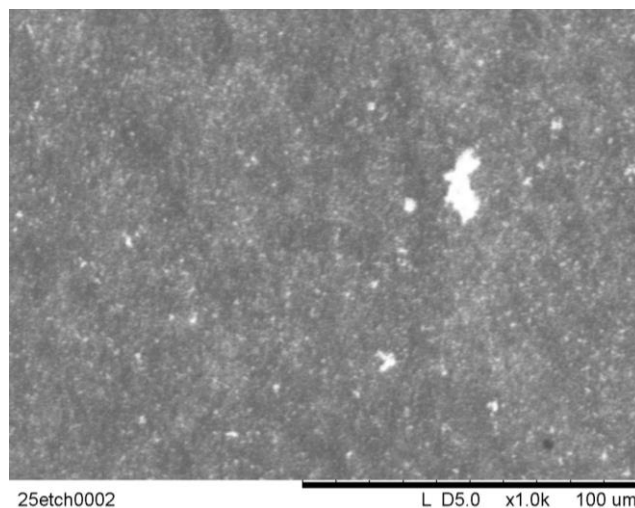


Figure 31. SEM image of the substrate obtained embedding nanostars into a HEC matrix. The polymer seems to prevent the interaction between the nanoparticles and the hot spot formation.

Considering the poor results given by the embedding of the nanoparticles into polymers, a different approach was tested. It involves the reduction of the nanoparticles directly into a PVA thin film containing the metallic precursor AgNO_3 and applied by spin-coating method. Also this experiment did not lead to remarkable outcomes: SEM images disclosed the presence of a stiff layer of polymer, where silver is mainly unidentifiable (Fig. 32). Once again, significant SERS results were not obtained and also this method was discarded.

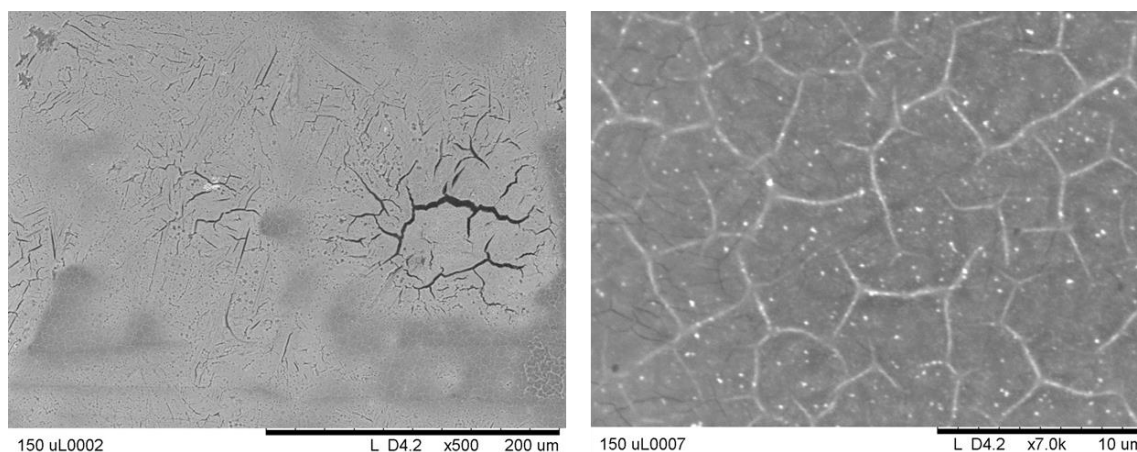


Figure 32. SEM images of the substrate obtained by reducing silver nanoparticles into a PVA solution.

5.3 Gold substrates

In this part of the work the possibility of exploiting gold rather than silver nanoparticle substrates was explored. The choice was dictated by trying to overcome the already mentioned problem of the release of silver on ancient artefacts. Gold, in fact, in comparison with silver, does not suffer from tarnishing problems, representing a minor potential damage for artworks if some residuals are left. In literature many procedures to obtain gold substrates for biological applications are reported [116, 117], but they are suitable for target analytes in solution. In this work, two colloids were tested. The former is characterised by spherical nanoparticles, the latter by a star-shaped morphology. The conditions of synthesis, aggregation (if required) and deposition were optimised and the SERS response was evaluated first by analysing a 10^{-3} M methanolic solution of alizarin and then a wool thread dyed with the same dye.

5.3.1 Frens nanosphere substrates

The gold colloid obtained according to the method reported by Frens (section 4.3.1) has a final metal concentration of gold equal to $3 \cdot 10^{-4}$ M, corresponding to almost a third of that in silver colloids (10^{-3} M). The drop deposition procedure was therefore optimised through different attempts to obtain a film that is transparent enough, but in the meanwhile has an appreciable amounts of metal aggregates. In this respect, the possibility of avoiding the aggregation step by exploiting the self-assembling effect produced on nanoparticles by slow solvent evaporation was firstly exploited; subsequently the colloid was aggregated by different electrolytes, namely NaClO_4 and MgSO_4 , always redispersing the colloid in a ratio water to electrolyte equal to 9:1. Finally, a method which exploits a modified coffee-ring effect was tested (section 4.4.4). Table 11 summarises the different experiments made and the corresponding results are discussed in the following.

The substrates obtained from the unaggregated colloid showed, in general, some coffee ring effect and a slight inhomogeneity of the nanoparticle distribution on the surface. Anyway, even if the metal coating is diffuse, only very small aggregates were formed. The situation was similar for the two concentration factors of gold (1:100 and 1:200), although the aggregates obtained from the double concentrated colloid appeared slightly larger. The colloid was therefore aggregated to intensify the hot spot formation. The first salt to be tested was NaClO_4 , as its use for the aggregation of gold nanoparticles in SERS has been reported [118]. The concentration was kept at 1.8 M, even if this value is much higher than those experimented for drop-deposition of aggregated silver colloids. When the micro-volume of perchlorate solution was added to the concentrated colloid, the colour suddenly turned from intense red to dark blue, suggesting a consistent aggregation. Anyway, the high concentration of NaClO_4 gave rise to the presence in

SEM images of parallelepiped crystals precipitated during the evaporation of the solvent (Fig. 33a). EDX analysis, detecting as main elements Na and Cl in association with Au, Ca and Si (due to glass), confirmed this hypothesis. To overcome this limitation, films were gently washed by dropping milliQ water from a Pasteur pipette to remove this highly-soluble (2090 g/L at 15° C) by-product. This washing resulted in the dissolution of the salt crystals, without an apparent loss of gold nanoparticles, but with voids remaining in their place. (Fig. 33b) Aggregated films are characterised by larger aggregates than the unaggregated ones, however the ensembles of nanoparticles are mainly localised in the centre of the drop, determining an overall inhomogeneity of the drop surface. Few differences were observed between the film concentrated 100 rather than 200 times. In addition, a further attempt was to concentrate the colloid 300 times in order to obtain the same metal concentration of the films prepared from silver colloids, whose concentration is 10 mM versus 0.3 mM. Anyway, the experiment did not lead to a significantly better results and the metal coating was still inhomogeneous. Surely a loss of metal nanoparticles occurred during the concentration and re-dispersion steps because of the very low volumes involved when higher concentration factor are used.

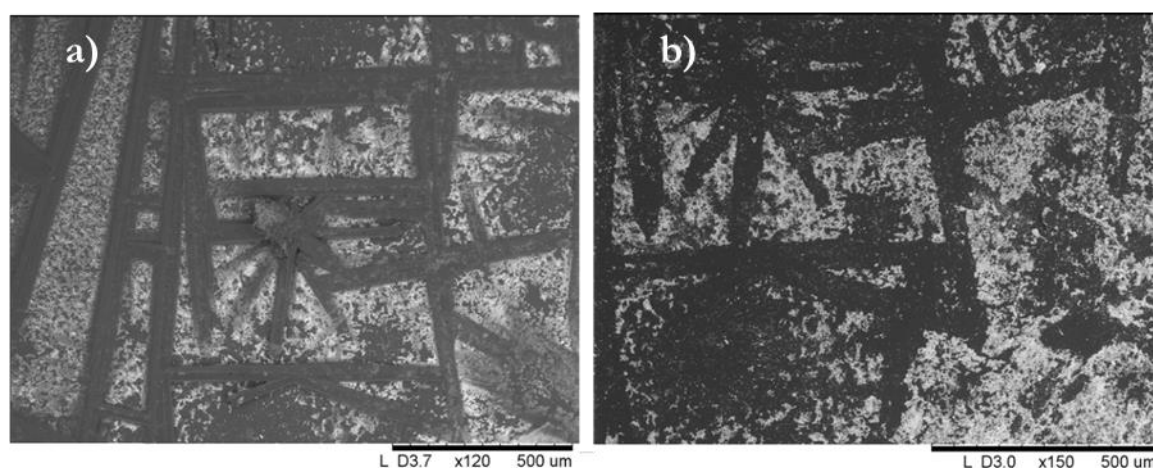


Figure 33. SEM images of an Au-nanoparticle substrate before and after washing. The crystals of NaClO_4 are dissolved but their print remains on the surface.

To overcome the problem of precipitation of the NaClO_4 , MgSO_4 solutions with lower electrolyte concentration were tested on its behalf. The use of this salts is documented in the literature for SERS with gold nanoparticles as it bonds only weakly to their surfaces and does not compete with target analytes [119]. The solution of magnesium salt was added (always in a ratio 9:1 to water) at two different concentration, 0.1 M and 10 mM. When the less concentrated MgSO_4 solution was dropped into the concentrated colloid (1:200), the colour of the suspension turned from red to purple-red, indicating a lower aggregation effect in comparison with perchlorate. This is expected according to the lower concentration of the salt in the aggregating

solution. The obtained gold substrates appeared quite homogeneous and characterised by a net of small aggregates (see corresponding figure in the resuming Tab. 11). In addition, EDX analysis showed that Au was the major element, while magnesium was present only in a low percentage, suggesting that the salt did not precipitate on the surface. On the other hand, using an electrolyte solution ten times more concentrated led to a strong aggregation with the precipitation of the aggregates at the bottom of the centrifuge tube. As an obvious consequence, drop-deposition gave an unsatisfying result, with a transparent film having only sporadic ensembles of nanoparticles.

In addition, a different experiment was carried out aiming to obtain films with a suitable metal concentration and a uniform substrate. This method, already tested for SERS analyses of drugs in solution [82], exploits the evaporation of the solvent by controlling the coffee-ring effect simply tilting the substrate. Anyway, despite a uniform coating of gold nanoparticles deposited on the functionalised glass support, the metal concentration progressively decreased from the top to the bottom of the support itself (Fig. 34). This can be explained by the fact that, while nanoparticles progressively deposited on the support during the evaporation of the solvent, the colloidal solution is depleted. Moreover, SEM observation suggested that no remarkable aggregation took place.

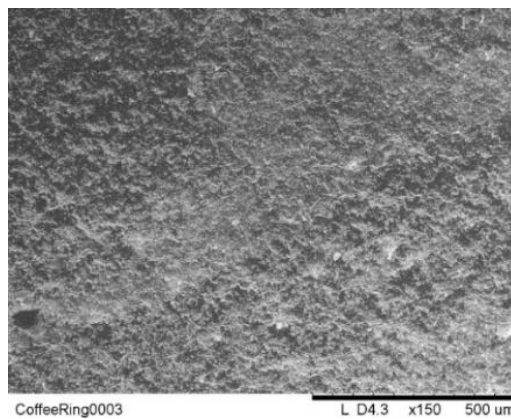


Figure 34. Substrate based on modified coffee-ring effect. Gold concentration decreases from the upper (right in the image) to the lower part (left).

The described gold substrates were then tested for SERS analyses. Two different excitation wavelengths were experimented: 532 and 785 nm. The former has the disadvantage of not being in resonance with the metal, but it is absorbed by red dyes; the latter is, in principle, more suitable for SERS analyses on gold substrates, but in this case resonance conditions with the target dyes are not satisfied. Therefore, in order to select the best excitation wavelength, a preliminary study was made by analysing a methanolic solution of alizarin (10^{-3} M) to establish the most advantageous conditions to perform SERS measurements in dry-state mode on both unaggregated and aggregated films. The obtained results revealed that in any case the near-infrared excitation wavelength leads to a more intense SERS spectrum. However, also the excitation at 532 nm allowed the identification of alizarin, but only the three main signals are recognisable, whereas by exciting at 785 nm also the peaks at lower wavenumbers can be detected and the signal-to-noise ratio is lower.

The spectra presented in Fig. 33 for the two different excitation wavelengths (a and b respectively) were obtained from the substrate aggregated with NaClO₄, previously washed to eliminate the residual salt. As expected, the results achieved for alizarin in solution by using the aggregated film are better than those acquired on the unaggregated one (Fig. 35 c vs d) and, upon equal aggregation, when gold is more concentrated. An exception is represented by those films obtained from gold nanoparticles concentrated 300 times, but this is attributable to the problems encountered in the deposition step, as already described in the previous section. Finally, NaClO₄-aggregated substrates proved to be more performant than those aggregated by MgSO₄, despite their inhomogeneity, but this is probably due to the higher electrolyte concentration.

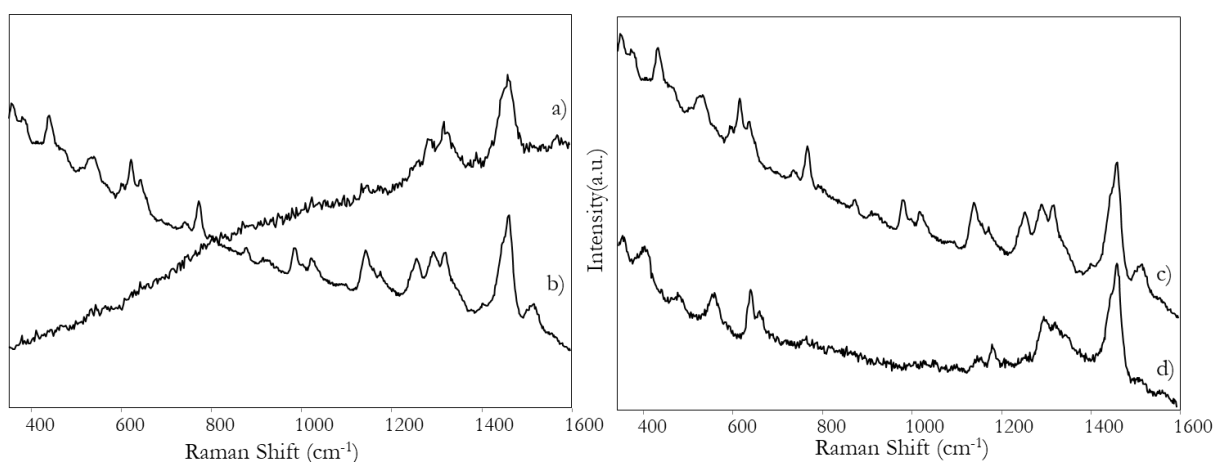


Figure 35. SERS spectra of alizarin (10^{-3} methanolic solution) obtained from gold substrates concentrated 1:200, aggregated by NaClO₄ and washed a) excited at 532 nm and at b) 785 nm; comparison between the spectra obtained from an c) aggregated by NaClO₄ and d) unaggregated film at $\lambda_{exc} = 785$ nm.

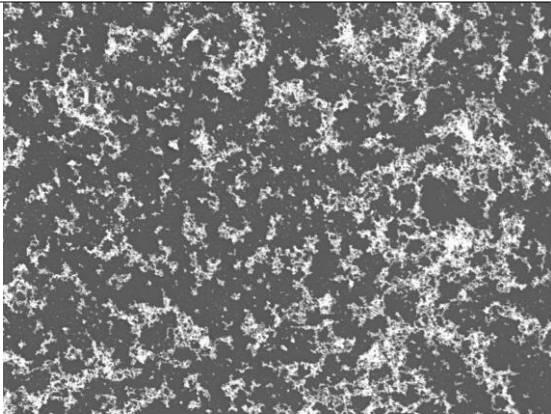
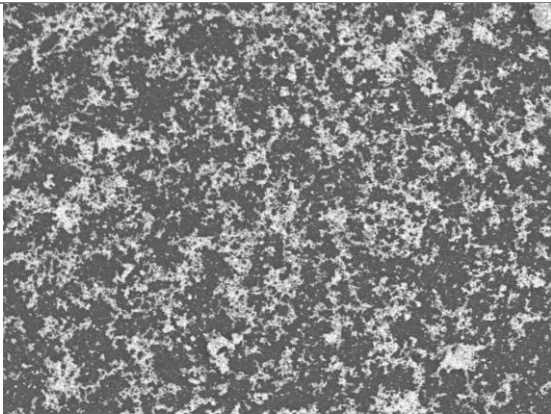
Table 10. Wavenumbers (cm^{-1}) of SERS bands of alizarin obtained in solution from Frens nanosphere substrates.

SERS signals (cm^{-1})	
$\lambda_{exc} = 532 \text{ nm}$	1158, 1191, 1296, 1326, 1572, 1639.
$\lambda_{exc} = 785 \text{ nm}$	360, 413, 483, 563, 652, 765, 833, 934, 1152, 1185, 1302, 1326, 1461.

All substrates were finally tested for the detection of alizarin in dry-state condition, using the NIR-emitting laser on the basis of the just showed results. A first attempt was made on pure powdered dye, but both on it and on the textile fibre no signal due to alizarin could be detected. This unsuccessful result can be possibly attributed to a too low concentration of metal in the starting colloid (a third in comparison with that of silver colloids) and to the impossibility of

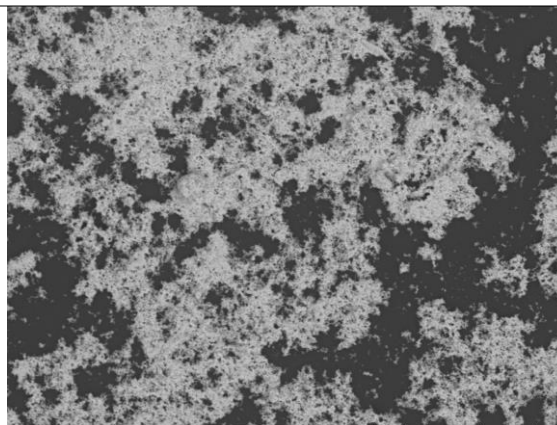
creating a homogeneous system of aggregates and hot spots. In conclusion, the NIR excitation wavelength, although fulfilling resonance conditions with the gold substrate, is not in resonance with the red dye molecules, penalising in this way the enhancement of the Raman signal.

Table 11. Summary of the results of the experiments performed to optimise Frens gold nanosphere substrates.

	Concentration factor	SEM image	Observations	SERS spectra
Unaggregated	1:100	 <p>AuFr_1a30004 L D2.8 x1.2k 50 um</p>	Small aggregates, overall homogeneous distribution.	From alizarin solution, both exciting at 532 and 785 nm. No results in dry-state conditions
	1:200	 <p>AuFr_2b20003 L D3.1 x1.8k 50 um</p>	Larger aggregates, overall homogeneous distribution on surface.	From alizarin solution, both exciting at 532 and 785 nm. No results in dry-state conditions

NaClO₄ 1.8 M

1:100



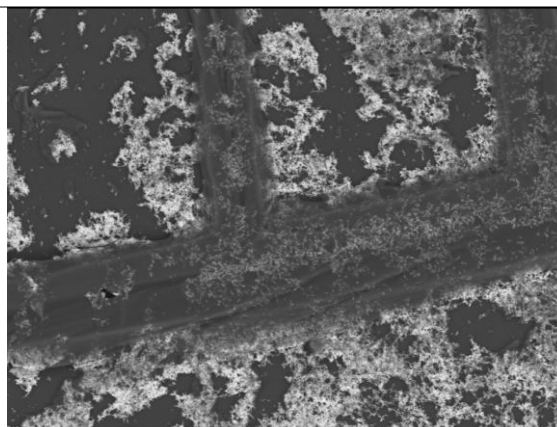
FrAgg_4b20003

L D4.0 x1.8k 50 um

Large aggregates mainly concentrated in the centre of the drop. Precipitation of NaClO₄, removable by washing.

From alizarin solution, both exciting at 532 and 785 nm. No results in dry-state conditions

1:200



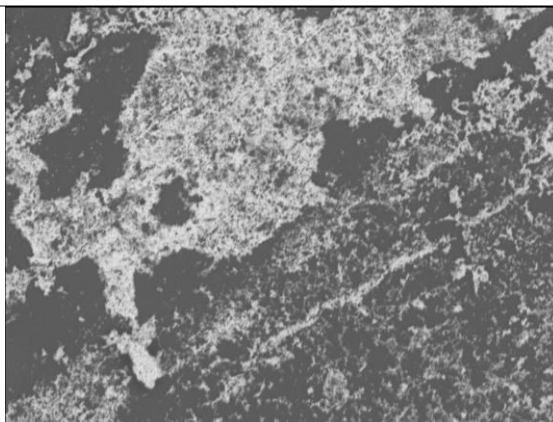
AuFr_3b30005

L D3.4 x1.5k 50 um

Large aggregates mainly concentrated in the centre of the drop. Precipitated NaClO₄.

From alizarin solution, both exciting at 532 and 785 nm. No results in dry-state conditions

1:300



FrAgg_5a3a0006

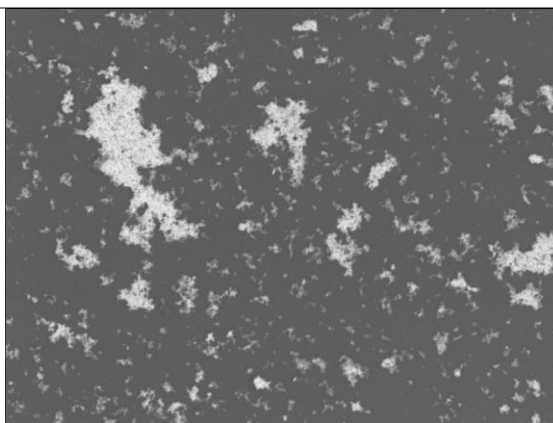
L D4.5 x1.2k 50 um

Large aggregates mainly concentrated in the centre of the drop. Precipitated NaClO_4 .

From alizarin solution (very weak and noisy), both exciting at 532 and 785 nm. No results in dry-state conditions

MgSO_4 0.1 M

1:200



Fr_0.1M_10002

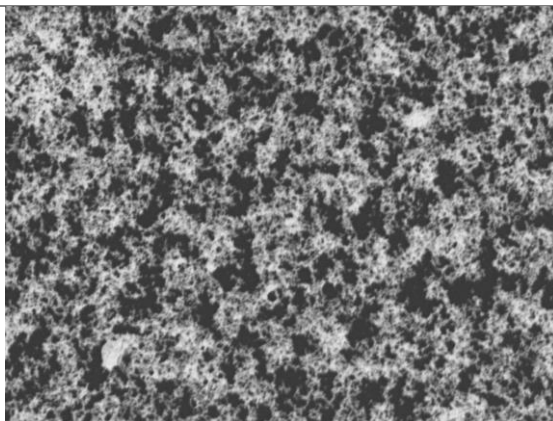
L D3.8 x1.2k 50 um

Very small aggregates together with larger ones, already formed before depositing the colloid.

No SERS signals.

MgSO₄ 0.01 M

1:200



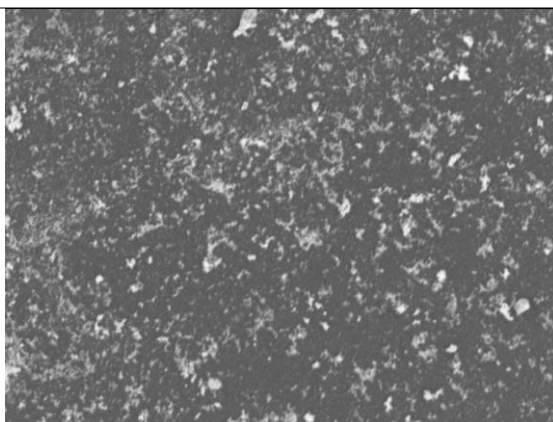
Fr_10mM_30002

L D3.9 x1.5k 50 um

Homogeneous distribution of small aggregates, apparently forming a net of hot-spots.

No SERS signals.

Modified coffee-ring effect



CoffeeRing0006

L D4.3 x1.5k 50 um

Inhomogeneity in the concentration of nanoparticles from the bottom to the top of the glass support. Very small nanoparticles, mainly unaggregated.

No SERS signal in dry-state conditions.

5.3.2 Nanostar substrates

Substrates obtained from nanostars synthesised following the traditional seed-method involving CTAB as stabilizer [71], did not yield remarkable results. The deposition of the colloid, in fact, as already described for Ag-nanorods in section 5.1.4, was strongly affected by the presence of the surfactant. During the centrifugation step, it formed a foam hindering the redispersion of the nanoparticles in water and also their deposition, because of the presence of air bubbles, which left voids printed on the film surface after the drying process (Fig 36, blue box), and residual CTAB (Fig 36, orange box). Moreover, SEM-EDX analyses demonstrated the prevalence of the surfactant itself, being Br the major element observed in the EDX spectrum gold was deposited, as the main substance was the surfactant itself.

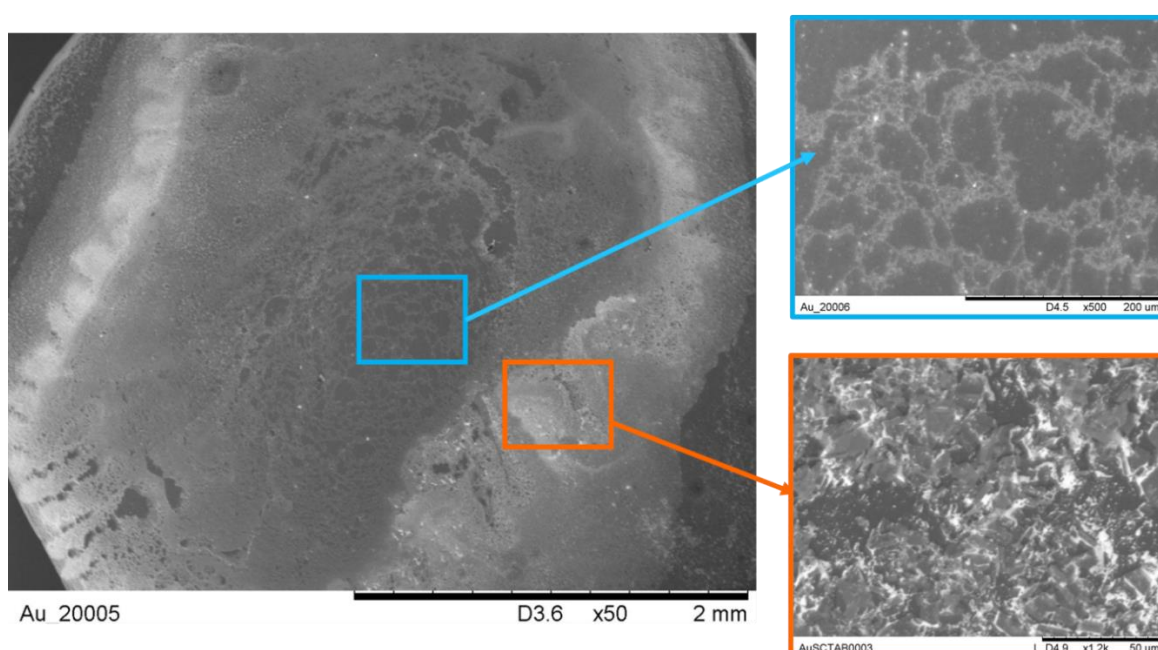


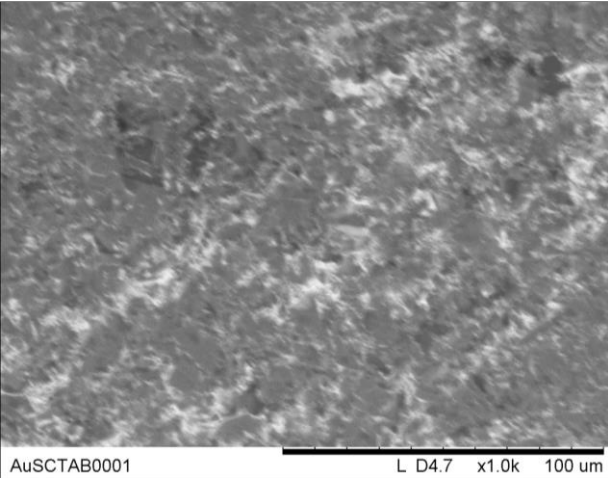
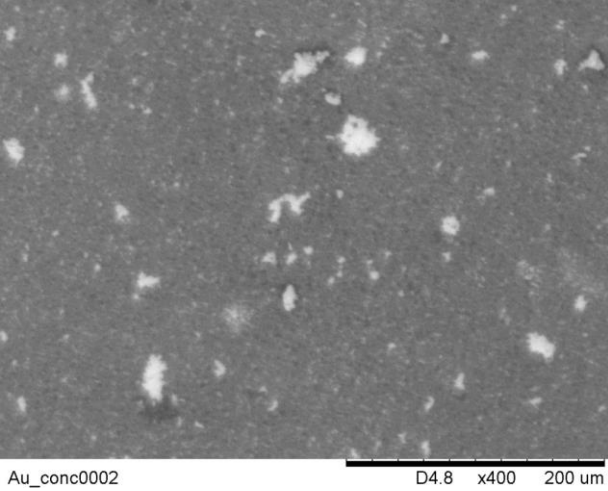
Figure 36. SEM images of gold-nanostars substrate. The boxes show two details of air bubbles printed on the surface (blue line) and of residual CTAB (orange line).

The synthesis was therefore repeated following a method which does not involve the use of any surfactant (section 4.3.2). The final concentration of gold in the colloid was $2.6 \cdot 10^{-4}$ M: to obtain a suitable concentration of the metal comparable to that of silver substrates, concentrated nanostars must be dispersed in very small micro-volumes of water, very difficult to handle. No aggregating salts were added as the peculiar morphology of stars, rich in tips, should induce by itself the formation of hot-spots and the activation of the colloid. As mentioned in the reference paper [71], the degree of branching of the stars can be settled by changing the concentration of AgNO_3 added to the growth solution. This reagent is, in fact, responsible for the anisotropic growth of the nanoparticles leading to the develop of longer tips. When a 1 mM silver solution

was added, no consistent results were obtained: the morphology of the substrates was inhomogeneous and only small aggregates were formed. The deposition was therefore repeated starting from more branched nanoparticles, synthesised doubling the concentration of AgNO_3 , and the resulting substrates showed more promising features as a net of aggregates was recognised. Anyway, also these metal films did not allow the acquisition of a SERS spectrum neither from the alizarin-dyed textile fibre nor from the dye solution, suggesting that they are not SERS-active. The experiments are summarised in Tab. 12.

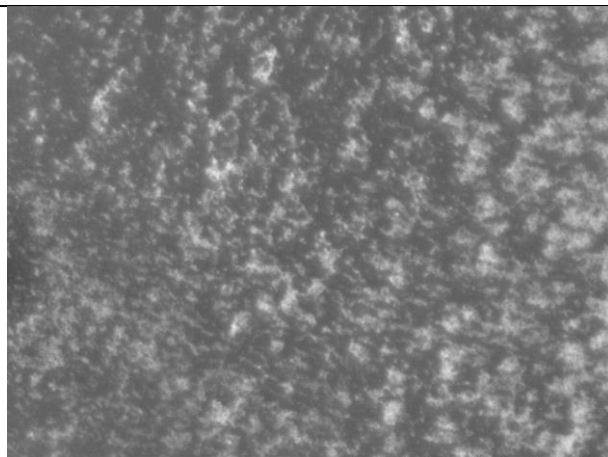
In conclusion, all experiments revealed that silver is the best metal for the analysis of natural dyes, both in solution and in dry-state condition. The reasons lies in the SERS enhancement properties of the metal itself (silver nanoparticles have the largest SERS enhancement capabilities due to their relatively high sensitivity and sharpness of scattered signals [120, 121]) and in the difficulties to produce suitable substrates starting from very-diluted colloidal suspensions, such as those of gold nanoparticles.

Table 12. Summary of the results of the experiments performed to optimise gold nanostar substrates.

Colloid	SEM Images	Observations	SERS
CTAB-nanostars		Small aggregates of nanostars trapped in a layer of residual surfactant.	No SERS signals.
Surfactant-free nanostars [AgNO ₃] = 1 mM		Few and very small aggregates, very low amounts of deposited gold.	No SERS signals.

Surfactant-free nanostars

[AgNO₃] = 2 mM



Appreciable number of aggregates,
although small and inhomogeneous.

No SERS signals.

5.4 Commercial SERS substrates

Despite the final aim of this work was to develop a simple and accessible method to prepare SERS substrates, it should be considered that a chemistry laboratory is not always available for conservation scientists. Hence, the possibility of exploiting commercial SERS substrates for the detection of natural dyes in textile fibres was investigated for the first time, to the best of our knowledge.

First, the commercial substrates SERSitive, already described in section 4.6, were characterised by SEM to check their morphology: the observations revealed a uniform and homogenous distribution of metal nanoparticle aggregates. They appear smaller than those obtained from our procedure and exhibit a three-dimensional structure, with a highly branched structure (Fig. 37).

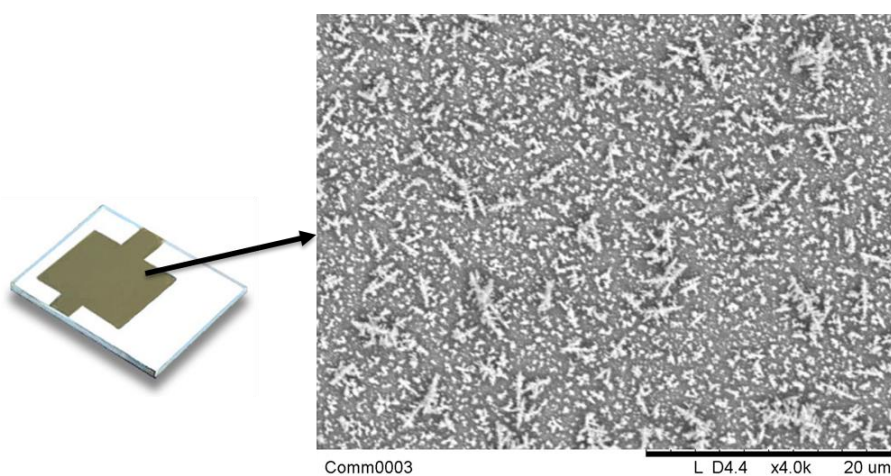


Figure 37. SEM image of a SERSitive substrate and its schematic representation.

SERS analyses performed on dyed wool threads lead to obtain SERS spectra of the three anthraquinone dyes alizarin, purpurin and lac dye (Fig. 38 and Tab. 13). In particular, alizarin and purpurin gave spectra of excellent quality, while that of lac dye, whose detection is notoriously more difficult [122], had a more intense fluorescence background and weaker signals.

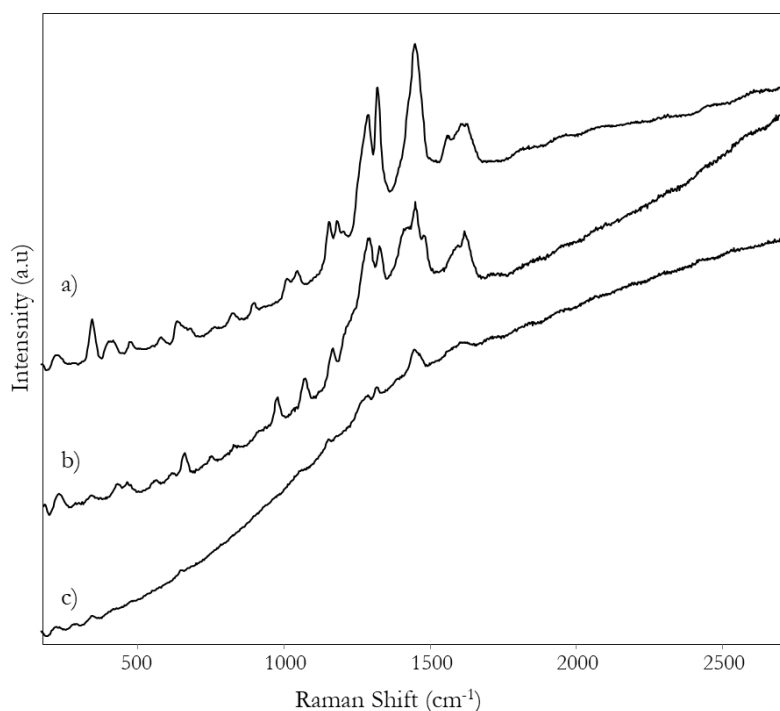


Figure 38. Dry-state SERS spectra of the anthraquinonic dyes a) alizarin; b) purpurin; c) lac dye obtained from SERSitive Ag-substrates.

Table 13. Wavenumber (cm^{-1}) of SERS bands of alizarin obtained from nanostars substrates.

SERS bands wavenumber (cm^{-1})	
Alizarin	344, 400, 416, 478, 579, 633, 681, 828, 897, 1011, 1047, 1155, 1183, 1204, 1290, 1323, 1423 sh, 1451, 1558, 1563, 1611, 1629.
Purpurin	424, 456, 556, 608, 650, 741, 822, 965, 1061, 1158, 1205 sh, 1228 sh, 1282, 1318, 1408 br, 1442, 1474, 1581, 1610.
Lac dye	650, 1061, 1155, 1288, 1322, 1453, 1605 br.

The best results were obtained from Ag-substrates: the Ag-Au combined ones allowed as well the identification of alizarin and purpurin, but the signals are less intense and resolved. For these substrates both excitation wavelengths (532 and 785 nm) were tested and the green radiation gave the best results. Besides satisfying the resonance conditions for red dyes, it was also more suitable for the nature of the substrate itself, as EDX semi-quantitative analysis (Fig. 39) showed that silver is the prevalent metal (87 vs 4%).

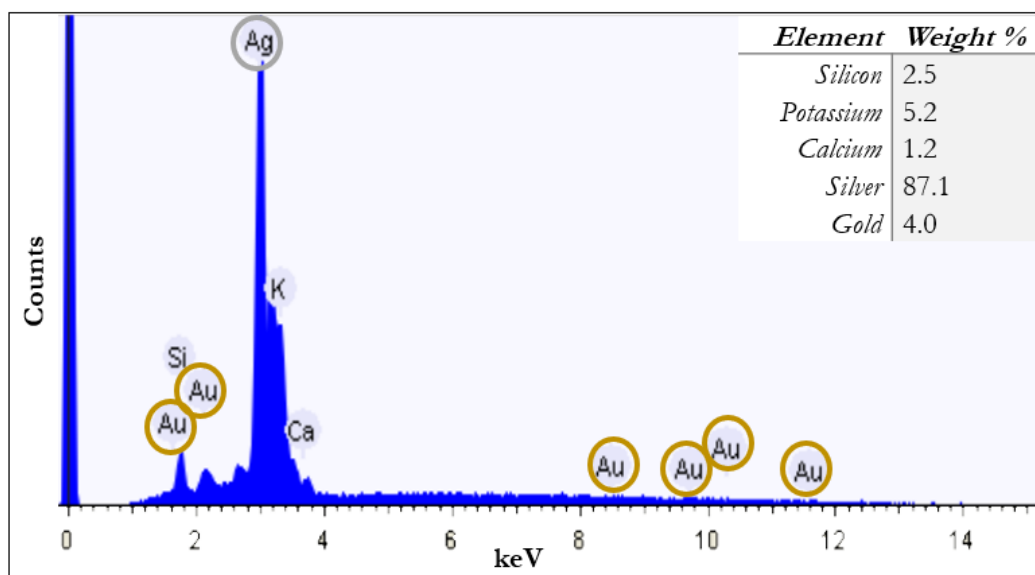


Figure 39. EDX spectrum acquired on the surface of a commercial SERSitive Ag-Au substrate. The table reports the semi-quantitative analysis of the detected elements (normalised).

Despite the positive results obtained from commercial SERSitive substrates, some drawbacks must be underlined: first, the substrates (whose dimensions are 9 x 7 x 0.7 mm) are very difficult to handle and to keep in contact with the textile without damaging their extremely fragile SERS-active surface. Moreover, when analyses are performed in dry-state conditions, the blank spectra gave very intense signals which, as already observed for substrates prepared from colloid in our silver colloid, can prevent in some cases the identification of the analyte. Two different commercial substrates were also tested, the former having a hydrophobic surface, the latter hydrophilic. Obviously, this difference can be of interest when performing SERS analysis on analytes dissolved in certain solvents, but the results in dry-state conditions were very similar and the problem of the blank bands was not solved.

A further step was therefore to develop a strategy that allows us to produce electrochemically-deposited Ag-film having a similar morphology, as will be discussed in the following section.

5.5 Electrochemically-deposited substrates

A preliminary study of the possibility to deposit electrochemically nano-structured substrates suitable for SERS detection was carried out thanks to the collaboration of Prof. Valentina Pifferi and Prof. Luigi Falciola of the Università degli Studi di Milano.

The best condition to reduce Ag^+ ions was selected by cyclic voltammetry in order to find the suitable reducing potential. The deposition was carried out by chronoamperometry starting from a solution containing the metallic precursor AgNO_3 (2 g/L) and citric acid (40 g/L) as reducing agent (section 4.7).

Two explorative experiments of electrochemical deposition of silver nanoparticles on a conductive FTO glasses were made. In both cases, at the end of the deposition, the FTO slides took on an opalescent yellow colour, indicating the successful deposition of silver. The first deposition lasted 90 s and led to obtain nanostructures characterised by a pseudo-round shape (approximative diameter around 3 μm), even if the presence of little branches could be supposed (Fig. 40a). On the basis of the followed procedure [89], in fact, nano-dendritic structures should be produced. The second lasted 600 s and originated larger structures, characterised by a pseudo-round shape (approximative diameter around 5 μm). Their “mushroom” morphology led to assume that they are the result of the association of the single nanoparticles because of an excessive growth (Fig. 40b). In general, an overall uniform and homogenous distribution of metal nanoparticles could be observed.

The elemental analysis performed by EDX in correspondence of this area revealed the presence of silver, together with silicon and tin due to the FTO glass in a minimum percentage. Compared to the previous case, a larger amount of silver was detected after the second deposition, as suggested by the uniform coverage of the FTO glass surface and by the larger dimension of the nanostructures themselves.

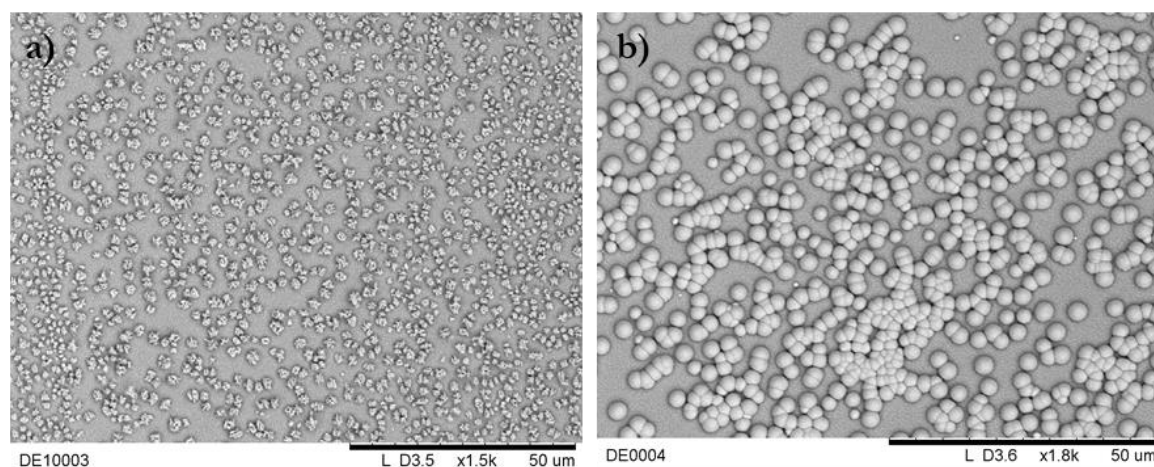


Figure 40. SEM image of nanoparticles electrochemically deposited for 90 (left) and 600 s (right).

In conclusion, these two explorative experiments demonstrated the possibility of producing substrates for dry-state SERS analyses by electrochemical route. Anyway, further studies will be mandatory to optimise the experimental conditions in terms of deposition time, concentration of silver, choice of the best reducing agent and morphology of the nanoparticles. The described substrates, in fact, did not allow the detection of alizarin in dry-state conditions because of the formation of too small or too large nanoparticles.

5.6 Exploiting the self-cleaning properties of titanium dioxide

Finally, the problem of the cleaning of the dry-state SERS substrates was considered. Measurements performed on the side of the metal substrate previously put in contact with the alizarin-dyed wool thread revealed that sometimes residual traces of the dyed fibres are released on the nanostructured surface. This cause, as a consequence, to obtain a memory effect of the SERS spectrum of the anthraquinone dye. In addition, the removal of the upper layer of the Ag films, prone to oxidation and tarnishing, would be of interest, disclosing the possibility of reusing the same substrate for more than a single analysis. In this context, the self-cleaning properties of titanium dioxide (TiO_2) mediated by UV and visible light were explored. TiO_2 is inexpensive, non-toxic, photostable and highly effective as a photocatalyst material. When it undergoes band gap excitation, electron-hole pairs are generated, which can initiate reduction and oxidation of organic compounds, leading to their decomposition. So, TiO_2 self-cleaning properties can be used to prevent passivation caused either by silver oxidation or by the presence of residual organic molecules, as already studied for electrode surfaces in [90]. In principle, this method could represent a valuable approach to remove the degradation products of silver and the organic compounds left on the silver surface after the SERS analysis. The possibility of exploiting the self-cleaning properties of titanium dioxide mediated by UV light to remove residual molecules of alizarin, just putting a thin film of it in contact with SERS substrates, was studied. SERS analyses performed on an artificially alizarin-contaminated substrate after different irradiation times (4, 9 and 14 hours), revealed that the SERS signal due to alizarin progressively lost its intensity. Fig 41 shows how the intensity of the SERS signals sensibly decreases with the extension of the irradiation time. In addition, a second artificially contaminated substrate was monitored to check if only irradiating by UV-light, in absence of contact with the titania thin layer, could produce a partial removal of alizarin from the film surface. Actually, a slight reduction was observed but the result is not comparable to that obtained in the presence of the titanium dioxide layer.

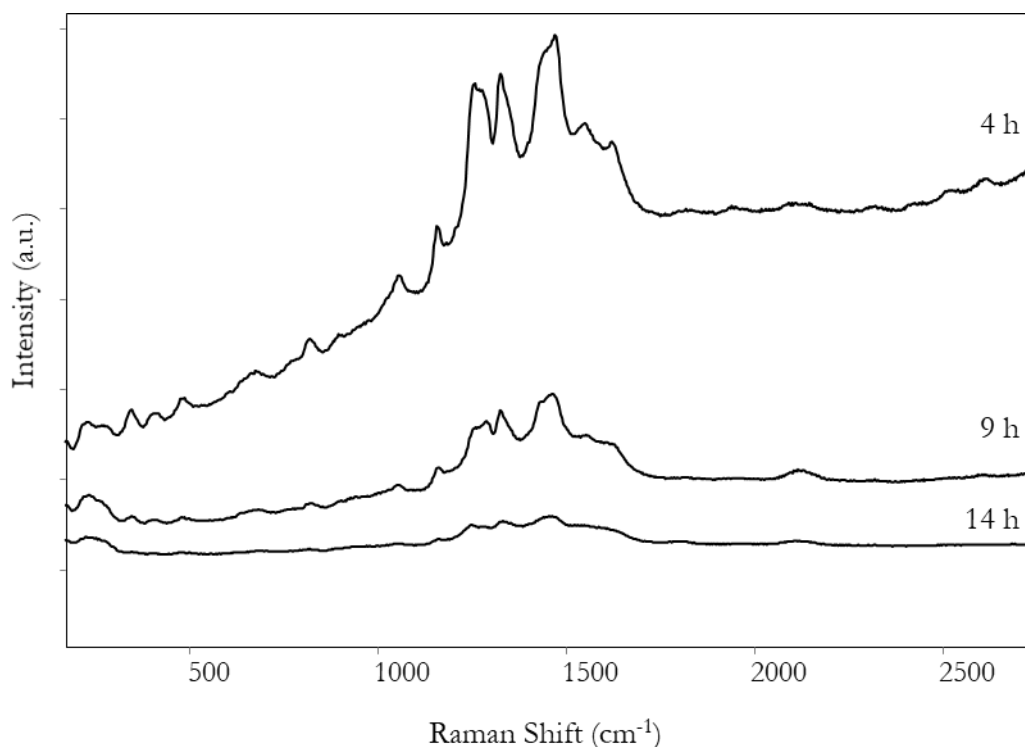


Figure 41. SERS spectra of alizarin after 4, 9 and 14 hours under UV-irradiation in contact with a titania thin layer.

In conclusion, the self-cleaning properties of TiO_2 mediated by UV light can be successfully exploited to eliminate the memory effect of the SERS spectrum of alizarin on the silver substrate. From silver substrate surface residual molecules of alizarin. After different irradiation cycles, a decrease of the SERS signal due to the natural dye was observed, suggesting a progressive removal of the residual organic molecules. In addition, a further step will surely involve trying to deposit titanium dioxide on the silver film itself in order to enhance the cleaning properties and also to prevent the release of metal. Anyway, it is necessary to verify if the presence of an upper titania layer can interfere with the acquisition of the SERS spectrum in dry-state condition.

6. Conclusion and future perspectives

In the present work, the development of SERS substrates for the non-invasive identification of natural dyes in textiles was implemented. The objective was to create accessible and easy-to-produce sensors able to provide a high SERS enhancement in dry state conditions, i.e. exploiting the electromagnetic effect between a solid nanometallic substrate and the dye molecules absorbed onto a textile fibre. A consistent number of experiments was carried out pursuing this objective: different silver colloids were deposited on functionalised glass slides and the experimental conditions were optimised to obtain reproducible and effective substrates, rich in

hot spots. These highly localised regions of intense local field enhancements, in fact, are of critically importance for SERS and, if in sufficient density, can dominate the properties of any SERS active substrate within which they reside [34, 99]. For spherical nanoparticles, the hot spot formation is induced by a suitable electrolyte, but this aggregation step proved to be the main cause of the irreproducibility of the substrates, as it depends from experimental factor during the synthesis and from the colloid itself. To overcome this issue, nanoparticles having anisotropic geometries (stars and rods) were used, as their peculiar morphology with sharp corners and edges gives rise to highly concentrated local electromagnetic fields and in the meanwhile makes them able to interact directly to form hot-spots without requiring activation by aggregation [17]. Among all experiments, silver nanostar substrates proved to be the most reproducible and effective ones and were successfully used for the detection of four dyes of artistic interest (alizarin, purpurin, lac dye and indigo). Moreover, the issue of metal release on the artefact was faced by trying to embed the nanoparticles into an optically transparent polymeric matrixes or depositing gold, a tarnish resistant metal, instead of silver nanoparticles, but the original silver substrates still proved to be the most performing ones. The possibility of exploiting SERS commercial substrates was finally demonstrated and some promising preliminary studies about the possibility of obtaining the substrates by electrochemical deposition of nanoparticles on conductive glass were made.

In perspective, the production of electrochemically deposited substrates will be carried on, as well as the study of the possible protection of the nanoparticles by a thin titania layer, in order to better exploit the self-cleaning properties of this smart material and protecting in the meanwhile the substrate surface. In addition, silver nanostar substrates will be applied to detect a larger number of natural and synthetic dyes, not only on mock-up samples but also on artistic objects. The final aim should be to reduce the diameter of the support where the metallic substrate is deposited, possibly creating a system based on fibre optics, to make this non-invasive approach even more suitable and easy-to-apply for in situ analyses in museums and exhibitions.

References

- [1] M. Fleischmann, P.J. Hendra, A.J. McQuillan, *Chem. Phys. Lett.* 1974, 26, 163-166.
- [2] D. L. Jeanmaire, R.P. Van Duyne, *J. Electroanal. Chem. Interfacial Electrochem.* 1977, 84, 1-20.
- [3] M. Leona, J. Stenger, E. Ferloni, *J. Raman Spectrosc.* 2006, 37, 981- 992.
- [4] K. Chen, M. Leona, T. Vo-Dinh, *Sens. Rev.* 2006, 27, 109-120.

- [5] M. Leona, P. Decuzzi, T. A. Kubic, G. Gates, J. R. Lombardi, *Anal. Chem.* 2011, 83, 3990-3993.
- [6] B. Doherty, B. G. Brunetti, A. Sgamellotti, C. Miliani, *J. Raman Spectrosc.* 2011, 42, 1932-1938.
- [7] E. Platania, J. R. Lombardi, M. Leona, N. Shibayama, C. Lofrumento, M. Ricci, M. Becucci, E. Castellucci, *J. Raman Spectrosc.* 2014, 45, 1133.
- [8] P. S. Londero, J. R. Lombardi, M. Leona, *Anal. Chem.* 2013, 85, 5463.
- [9] A. Cesaratto, M. Leona, J. R. Lombardi, D. Comelli, A. Nevin, P. Londero, *Angew. Chem.* 2014, 53, 14373-14377.
- [10] C. Zaffino, H. T. Ngo, J. Register, S. Bruni, T. Vo-Dinh, *Appl. Phys. A.* 2016, 122, 707.
- [11] A. Alyami, A. Mirabile, D. Iacopino, *Herit Sci.* 2019, 7, 87.
- [12] V. Merletti, Master degree thesis, Università degli Studi di Milano, 2019.
- [13] Javier Reguera, Judith Langer, Dorleta Jimenez de Aberasturi, Luis M. Liz-Marzán, *Anisotropic Metal Nanoparticles for Surface-Enhanced Raman Scattering in Colloidal Synthesis of Plasmonic Nanometals*, Jenny Stanford Publishing, 2020.
- [14] A. Shiohara, Y. Wang, L. M. Liz-Marzán, *J. Photochem. Photobiol. C: Photochem. Rev.* 2014, 21, 2-25.
- [15] A. Guerrero-Martínez, S. Barbosa, I. Pastoriza-Santos, L. M. Liz-Marzán, *Curr. Opin. Colloid Interface Sci.* 2011, 16, 118-127.
- [16] Y. Wang, P. H. C. Camargo, S. E. Skrabalak, H. Gu, Y. Xia, *Langmuir* 2008, 24, 12042.
- [17] A. García-Leis, J. V. García-Ramos, S. Sánchez-Cortés, *J. Phys. Chem. C* 2013, 117, 7791.
- [18] L. Litti, J. Reguera, F. J. García de Abajo, M. Meneghetti, L. M. Liz-Marzán, *Nanoscale Horiz.* 2020, 8, 102-108.
- [19] S. Sánchez-Cortés, J. V. García-Ramos, G. Morcillo, *J. Colloid Interface Sci.* 1994, 167, 428-436.
- [20] S. Sánchez-Cortés, J. V. García-Ramos, G. Morcillo, A. Tinti, *J. Colloid Interface Sci.* 1995, 175, 358-368.
- [21] D. Cardon, *Natural Dyes: Sources, Tradition, Technology and Science*, Archetype Publications, London, 2007.
- [22] J. H. Hofenk de Graaff, *The colourful past. origins, chemistry and identification of natural dyestuffs*, Archetype Publications, London, 2004.
- [23] E. S. B. Ferreira, A. N. Hulme, H. McNab, A. Quye, *Chemical Society Reviews* 2004, 33, 329-336.
- [24] J. S. Mills, R. White, *The Organic Chemistry of Museum Objects*, Butterworths, London, 1994.
- [25] H. Schweppe, J. Winter, *Artists' pigments, Vol. 3*, Oxford University Press, New York, 1997.
- [26] Z. C. Koren, in *Archaeological Chemistry: Organic, Inorganic and Biochemical Analysis*, American Chemical Society, 1996, 269-310.
- [27] A. V. Whitney, R. P. Van Duyne, F. Casadio, *J. Raman Spectr.* 2006, 37, 993-1002.
- [28] J. S. de Melo, A. P. Moura, M. J. Melo, *J. Phys. Chem. A* 2004, 108, 6975-6981.
- [29] M. G. Albrecht, J. A. Creighton, *J. Am. Chem. Soc.* 1977, 99, 5215-5217.

- [30] P. A. Mosier-Boss, *Nanomaterials* 2017, 6, 142-172.
- [31] R. Stiuflu, C. Iacovita, C. M. Lucaci, G. Stiuflu, A. G. Dutu, C. Braescu, N. Leopold, *Nanoscale Res. Lett.* 2013, 8, 47.
- [32] N. D. Israelsen, C. Hanson, E. Vargis, *Sci. World J.* 2015, 2015, 124582
- [33] Y. Xie, D. Kocafe, C. Chen, Y. Kocafe, *J. Nanomat.* 2016, 2016, 2302595.
- [34] S. Schlucker ed., *Surface Enhanced Raman Spectroscopy: Analytical Biophysical and Life Science Applications*, Wiley-VCH, Weinheim, Germany, 2011.
- [35] E. Le Ru, P.G. Etchegoin, *Principles of surface enhanced Raman spectroscopy and related plasmonics effects*, Elsevier, Oxford, 2009.
- [36] J. A. Frank, *J. Chem. Phys.* 1982, 77, 5302.
- [37] G. J. Kovacs, R. O. Loutfy, P. S. Vincett, C. Jennings, R. Aroca, *Langmuir* 1986, 2, 689-694.
- [38] R.F. Aroca, M.C. Vallete, J.V. García-Ramos, S. Sánchez-Cortés, J.A. Sánchez-Gil, P. Sevilla, *Amplificación plasmónica de espectros Raman y de fluorescencia SERS y SEF sobre nanoestructuras metálicas*, ed. CSIC, Madrid, 2014.
- [39] M. V. Cañamares, Ph.D. thesis, Universidad Complutense de Madrid, 2005.
- [40] E. C. Le Ru, P. G. Etchegoin, *Principles of Surface-enhanced Raman Spectroscopy and Related Plasmonic Effects*, Elsevier, Amsterdam, 2009.
- [41] M. Moskovits, *J. Raman Spectrosc.* 2005, 36, 485-496.
- [42] V. Amendola, M. Meneghetti, *Adv. Funct. Mater.* 2012, 22, 353-360.
- [43] M. I. Stockman, *Phys. today* 2011, 64, 39-44.
- [44] P. G. Etchegoin, E. C. Le Ru, *Phys. Chem. Chem. Phys.* 2008, 10, 6079-6089.
- [45] B. Guineau, V. Guichard, in *ICOM Committee for Conservation: 8th Triennial Meeting, Vol. 2*, The Getty Conservation Institute, Marina del Rey, 1987, 659-666.
- [46] C. L. Brosseau, F. Casadio, R. P. Van Duyne, *J. Raman Spectr.* 2011, 42, 1305-1310.
- [47] F. Pozzi, J. R. Lombardi, S. Bruni, M. Leona, *Anal. Chem.* 2012, 84, 3751-3757.
- [48] F. Casadio, M. Leona, J. R. Lombardi, R. Van Duyne, *Acc. Chem. Res.* 2010, 43, 782-791.
- [49] M. Leona, F. Pozzi, *Journal of Raman Spectroscopy* **2016**, 47, 66-67.
- [50] S. Bruni, V. Guglielmi, F. Pozzi, A. M. Mercuri, *J. Raman Spectros.* 2011, 42, 465-473.
- [51] F. Pozzi, G. Poldi, S. Bruni, E. De Luca, V. Guglielmi, *Anthropol. Sci.* 2012, 4, 185-197.
- [52] M. Leona, J. R. Lombardi, *J. Raman Spectros.* 2007, 38, 853-858.
- [53] E. Van Elslande, S. Lecomte, A.-S. Le Hô, *J. Raman Spectros.* 2008, 39, 1001-1006.
- [54] A. El Bakkali, T. Lamhasni, M. Haddad, S. Ait Lyazidi, S. Sanchez-Cortes, E. del Puerto Nevado, *J. Raman Spectros.* 2013, 44, 114-120.
- [55] A. Idone, M. Aceto, E. Diana, L. Appolonia, M. Gulmini, *J. Raman Spectros.* 2014, 45, 1127-1132.
- [56] M. V. Cañamares, J. V. Garcia-Ramos, J. D. Gómez-Varga, C. Domingo, S. Sanchez-Cortes, *Langmuir* 2007, 23, 5210-5215.

- [57] Z. Jurasekova, C. Domingo, J. V. Garcia-Ramos, S. Sanchez-Cortes, *J. Raman Spectros.* 2008, 39, 1309-1312.
- [58] Z. Jurasekova, E. del Puerto, G. Bruno, J. V. García-Ramos, S. Sanchez-Cortes, C. Domingo, *J. Raman Spectros* 2010, 41, 1455-1461.
- [59] C. Zaffino, S. Bruni, V. Guglielmi, E. De Luca, *J. Raman Spectros.* 2014, 45, 211-218.
- [60] F. Pozzi, K. J. Van den Berg, I. Fiedler, F. Casadio, *J. Raman Spectros.* 2014, 45, 1119-1126.
- [61] P. C. Lee, D. Meisel, *J. Phys. Chem.* 1982, 86, 3391-3395.
- [62] Y. Wan, Z. Guo Z., X. Jiang, K. Fanga, X. Lub, Y. Zhanga, N. Gu, *J. Colloid Interface Sci.* 2013, 394, 263-268.
- [63] N. Leopold, B. Lendl, *J. Phys. Chem. B* 2003, 107, 5723–5727.
- [64] C. Garrido, B.E. Weiss-López, M.M. Campos Vallette, *Spectrosc. Lett.* 2016, 49, 11–18.
- [65] M. V. Canãmares, J. V. Garcia-Ramos, J. D. Go´mez-Varga, C. Domingo, S. Sanchez-Cortes, *Langmuir* 2005, 21, 8546-8553.
- [66] C. R. Rekha, V. U. Nayar, K. G. Gopchandran, *J. Sci.-Adv. Mat. Dev.* 2018, 3, 196-205.
- [67] M. Bottacchiari, bachelor thesis, 2019, Politecnico di Milano.
- [68] R. Jana, L. Gearheart, C.J. Murphy, *Chem. Commun.* 2001, 617-618.
- [69] G. Frens, *Nat. Phys. Sci.* 1973, 241, 20-22.
- [70] E. N. Esenturk, A. R. H. Walker, *J. Raman Spectrosc.* 2009, 40, 86-91.
- [71] H. Yuan, C. G. Khoury, H. Hwang, C. M. Wilson, G. A. Grant, T. Vo-Dinh, *Nanotechnology* 2012, 23, 075102.
- [72] J. A. Howarter, J. P. Youngblood, *Langmuir* 2006, 22, 11142-11147.
- [73] N. Shahidzadeh, M. F. Schut, J. Desarnaud, M. Prat, D. Bonn, *Sci. Rep.* 2015, 27, 10335.
- [74] A. Lucotti, G. Zerbi, *Sens. Actuators B Chem.* 2007, 121, 356-364.
- [75] R. G. Freeman, K. C. Grabar, K. J. Allison, R. M. Bright, J. A. Davis, A. P. Guthrie, M. B. Hommer, M. A. Jackson, P. C. Smith, D. G. Walter, M. J. Natan, *Science* 1995, 267, 1629-1632
- [76] R. D. Deegan, O. Bakajin, T. F. Dupont, G. Huber, S. R. Nagel, T. A. Witten, *Nature* 1997, 389, 827-829.
- [77] F. Parisse, C. Allain, *J. Phys. II (Paris)* 1996, 6, 1111-1119.
- [78] F. Tian, F. Bonnier, A. Casey, A. E. Shanahan, H. J. Byrne, *Anal. Methods* 2014, 6, 9116-9123.
- [79] M. Cyrankiewicz, T. Wybranowski, S. Kruszewski, *J. Phys. Conf. Ser.* 2007, 79, 012013.
- [80] V. Giannini, R. Rodriguez-Oliveros, J. A. Sanchez-Gil, *Plasmonics* 2009, 5, 99-104.
- [81] G. F. S. Andrade, M. Fan, A. G. Brolo, *Biosens. Bioelectron.* 2010, 25, 2270-2275.
- [82] W. Zhou, A. Hu, S. Bai, Y. Ma, Q. Su, *Nanoscale Res. Lett.* 2014, 9, 87
- [83] P. Aldeanueva-Potel, E. Faucher, R. A. Alvarez-Puebla, L. Marzán, B. Mathias, *Anal. Chem.* 2009, 81, 9233-9238.
- [84] W. W. Y. Lee, V. A. D. Silversen, C. P. McCoy, R. F. Donnelly, S. E. J. Bell, *Anal. Chem.* 2014, 86, 8106-8113.
- [85] S. Karabiçak, M. Kaya, T. Vo-Dinh, M. Volkan, *J. Nanosci. Nanotechnol* 2008, 8, 955-960.

- [86] Renáta Oriňáková, Lenka Škantárová, Andrej Oriňák, Jakub Demko, Miriam Kupková, Jan T. Andersson, *Int. J. Electrochem. Sci.* 2013, 8, 80-99.
- [87] K. H. Yang, Y. C. Liu, C. C. Yu, *Langmuir* 2010, 26, 11512-11517 and paper therein
- [88] M. Fu-Der, Y. Kuang-Hsuan, L. Yu-Chuan, H. Ting-Chu, J. Ming-Yu, *RSC Adv.* 2011, 7, 2, 1324-1332 and paper therein.
- [89] Z. Cheng, Y. Qiu, Z. Li, D. Yang, S. Ding, G. Cheng, Z. Hao, Q. Wang, *Opt. Mater. Express* 2019, 9, 860-869.
- [90] G. Sliveri, V. Pifferi, G. Panzarasa, S. Ardizzone, G. Cappelletti, D. Meroni, K. Sparnacci, L. Falciola, *Analyst* 2015, 140, 1486-1494.
- [91] S. M. Edelstein, H.C. Borghetty, *The Plietho of Gioanventura Rosetti: Instructions in the Art of the Dyers which Teaches the Dyeing of Woolen Cloths, Linens, Cottons, and Silk by the Great Art as well as by the Common*, translation of the First Edition of 1548, M.I.T. Press, Cambridge, 1969.
- [92] J. Chang, M. V. Cañamares, M. Aydin, W. Vetter, M. Schreiner, W.Q. Xu, J.R. Lombardi, *J. Raman Spectrosc.* 2009, 40, 1557-1563.
- [93] M. V. Cañamares, M. Leona, M. Bouchard, C.M. Grzywacz, J. Wouters, K.Trentelman, *J. Raman Spectrosc.* 2010, 40(4), 391-397.
- [94] C. L. Brosseau, A. Gambardella, F. Casadio, C. M. Grzywacz, J. Wouters, R. P. V. Duyne, *Anal. Chem.* 2009, 81, 7443-7447.
- [95] C. L. Brosseau, F. Casadio, R. P. Van Duyne, *J. Raman Spectrosc.* 2011, 42, 1305-1310.
- [96] S. E. J. Bell, N. M. S. Sirimuthu, *J. Am. Chem. Soc.* 2006, 128, 15580-15581.
- [97] Y. Zhao, X. Li, Y. Liu, L. Zhang, F. Wang, Y. Lu, *Sens. Actuators B* 2017, 247, 850-857.
- [98] S. Sánchez-Cortés, J. V. García-Ramos, *J. Raman Spectrosc* 1998, 29, 5, 365-371.
- [99] C. S. S. R. Kuma Ed., *Raman Spectroscopy for Nanomaterials Characterization*, Springer, Berlin, 2012.
- [100] C. Gellini, M. Macchiagodena, M. Pagliai, *Nanomaterials* 2021, 11, 860.
- [101] S. Bruni, V. Guglielmi, F. Pozzi, *J. Raman Spectrosc.* 2011, 42, 1267-1281.
- [102] I. T. Shadi, B. Z. Chowdry, M.-J. Snowden, R. Whitnall, *J. Raman Spectrosc.* 2004, 35, 800-807.
- [103] E. B. Guidez, C. M. Aikens, *J. Phys. Chem. C* 2013, 117 (2013) 12325-12336.
- [104] M. A. Mahmoud, M. A. El-Sayed, *J. Phys. Chem. Lett.* 2013, 4, 1541-1545.
- [105] K. M. Ratheesh, P. Prabhathan, L. K. Seah, V. M. Murukeshan, *Biomed. Phys. Eng. Express* 2016, 2, 55005.
- [106] M. S. Zalaffi, L. Litti, P. Canton, M. Meneghetti, L. M. Moretto, P. Ugo, *Nano Ex.* 2020, 1, 020006
- [107] X. Guo, Z. Guo, Y. Jin, Z. Liu, W. Zhang, D. Huang, *Microchim. Acta* 2012, 178, 229-236.
- [108] M. Longoni, M. S. Zalaffi, L. de Ferri, A. M. Stortini, G. Pojana, P. Ugo, *Nanomaterials* 2021, 11, 518.
- [109] K. Kwan, H.S. Lee, *J. Phys. Chem. B* 2005, 109 (40), 18929-18934.
- [110] C. Y. Fu, K. W. Kho, U. S. Dinish, Z. Y. Koh, O. Malini, *J. Raman Spectrosc.* 2012, 43, 8, 977-985.

- [111] G. Schmidl, J. Dellith, H. Schneidewind, D. Zopf, O. Stranik, A. Gawlik, S. Anders, V. Tympel, C. Katzer, F. Schmidl, W. Fritzsche, *Mater. Sci. Eng. B* 2015, 193, 207-216.
- [112] T. Hasell, L. Lagonigro, A. C. Peacock, S. Yoda, P. D. Brown, P. J. A. Sazio, S. M. Howdle, *Adv. Funct. Mat.* 2008, 18, 1265-1271.
- [113] X. Ma, Y. Xia, L. Ni, L. Song, Z. Wang, *Spectrochim. Acta A: Mol. Biomol. Spectrosc.* 2014, 121, 657-661.
- [114] Z. Gong, C. Wang, C. Wang, C. Tang, F. Cheng, H. Du, M. Fan, A. G. Brolo, *Analyst* 2014, 139, 5283-5289.
- [115] R. V. Kesava Rao, T. P. Radhakrishnan, *ACS Appl. Mater. Interfaces* 2015, 7, 2767-12773.
- [116] A. Kaminska, O. Inya-Agha, R. J. Forster, T. E. Keyes, *Phys. Chem. Chem. Phys.* 2008, 10, 4172-4180.
- [117] *SERS Microscopy: Nanoparticle Probes and Biomedical Applications* in [34].
- [118] M. Suzuki, Y. Niidome, Y. Kuwahara, N. Terasaki, K. Inoue, S. Yamada, *J. Phys. Chem. B* 2004, 108, 11660-11665.
- [119] S. E. Bell, M. R. Mc Court, *Phys. Chem. Chem. Phys.* 2009, 11, 7455-7462.
- [120] Q. Fu, Z. Zhan, J. Dou, X. Zheng, R. Xu, M. Wu, Y. Lei, *ACS Appl. Mater. Interfaces* 2015, 7, 13322-13328.
- [121] T. Tan, C. Tian, Z. Ren, J. Yang, Y. Chen, L. Sun, Z. Li, A. Wu, J. Yin, H. Fu, *Phys. Chem. Chem. Phys.* 2013, 15, 21034-21042.
- [122] M. V. Cañamares, M. Leona, *J. Raman Spectrosc.* 2007, 38, 1259-1266.

Final conclusions

The present doctoral thesis work aimed at developing innovative and effective strategies based on molecular spectroscopies for the non-invasive identification of organic materials of artistic interest. Three different methods, namely spectrofluorimetry, infrared and Raman spectroscopy, were successfully study for the detection of as many categories of organic substances: synthetic organic pigments, painting binders and natural dyes.

First, the approach based on the combination of visible-excited spectrofluorimetry and visible reflectance spectroscopy with a multivariate processing of data demonstrated to be an effective method for the non-invasive identification of synthetic organic pigments. Such approach allowed us to overcome the issues related to these electronic spectroscopies, which yield spectra with broad bands and thus affected by a lack of specificity and strongly dependant on different factors, such as the concentration of the pigments and the interference due to binders. Moreover, the fluorescence emission exhibited by several synthetic pigments upon visible excitation was confirmed under UV radiation and the possibility of individuating such materials in paintings by ultraviolet fluorescence images was disclosed for the first time, to the best of our knowledge. The importance of a multiwavelength approach in imaging to reduce the dependence on the binder to pigment ratio was also evidenced and explained thanks to the comparison with the results provided by spectrofluorimetric analyses.

As a second aspect, interesting results were obtained from FT-NIR spectroscopy as a non-invasive method to recognise binding media directly in a very complex system such as a painting, implementing and further developing the application of measurements in this spectral range, reported in the literature for the characterisation of pure reference materials. The possibility of exploiting FT-NIR spectroscopy for the investigation of paintings was at first studied in complex multi-layered reference samples, aiming both at the identification of binders and the understanding of the stratigraphy taking advantage of the higher penetration power of the NIR radiation in comparison with the MIR one. The study was therefore carried out on reference mock-up samples simulating different situations: pigments were dispersed in different binders - pure, in mixture or in superimposed layers- and the support was coated with two different preparatory layers (calcite and gypsum). In both cases, the characteristic absorption bands in the range $6500\text{-}4000\text{ cm}^{-1}$ proved to be useful to distinguish among the different binders and once again, the elaboration of the spectral data by means of a multivariate approach demonstrated to be an effective method to highlight minimal differences in the spectral patterns. Moreover, the

greater penetration depth of the NIR radiation was exploited to gain information about the inner layers of the painting disclosing the possible presence of a gypsum preparatory layer, as this material show strong absorption bands in this spectral range. The comparison between the spectral results and the thickness of the colour layers evaluated on cross-sections of the corresponding samples, highlighted a penetration depth of around 100 μm . Finally, as a proof of concept, FT-NIR analysis were carried out *in situ* on eight masterpieces dating from 15th to 18th century, giving a wide insight on the applicability of this method for the non-invasive detection of binders and the comprehension of the stratigraphy in real paintings.

Finally, the proof of concept of performing SERS analyses in dry-state conditions by means of easy-to-prepare and inexpensive substrates for the identification of natural dyes directly on wool yarns was given. This was possible by exploiting only the electromagnetic component of the SERS effect, which takes place when the analyte is in proximity of the substrate and not necessarily chemisorbed to it. This goal was reached by producing SERS sensors through the immobilization of colloidal silver nanoparticles on commercial microscopes glass slides. The best conditions to obtain reproducible and homogeneous substrates leading to a strong enhancement of the Raman signal in dry-state conditions were evaluated by experimenting different aggregation processes and nanoparticles having spherical or anisotropic geometries. The most reproducible and effective sensor proved to be the one obtained from a silver nanostar colloid, which allowed us to detect alizarin, purpurin, lac dye and indigo from dyed wool thread by means of a portable Raman instrument, suitable for non-invasive, *in-situ* analysis directly on artefacts. Some related issues were also faced, in particular the possibility of exploiting the self-cleaning properties of titanium dioxide under UV light to clean the substrates after SERS analyses.

In conclusion, the present work proposed solutions to the problem of the non-invasive identification of organic materials of artistic interest in complex systems, such as contemporary and ancient paintings and ancient textiles, and disclosed new applications and potentialities for spectroscopic methods commonly available in the conservation science field.

List of publications and conference presentations

Publications

M. Longoni, M. Gargano, A. Buttarelli, S. Bruni. *A multiwavelength approach for the study of contemporary painting materials by means of fluorescence imaging techniques: a comparison with spectroscopic methods* Applied Science (2022), 12, 94-

M. Longoni, N. Cicala, V. Guglielmi, G.Poldi. *The art of everyday objects: a non-invasive in situ investigation of materials and techniques of Italian Pop Art paintings on aluminium*. Heritage (2022), 5, 42-60

M. Longoni, S. Bruni. *Development of dry-state SERS substrates for the non-invasive detection of artistic dyes in textiles*. Optical Engineering (2021), 60 (12), 127105.

S. Bruni, M. Longoni, S. De Meo, F. Scalzo, A. Dibenedetto, V. Guglielmi. *Visible-induced spectrofluorimetry as a non-invasive tool for the “in situ” identification of natural dyes in historical textiles* accepted for publication by Dyes in History and Archaeology (October 2021).

A. Galli, M. Gargano, L. Bonizzoni, S. Bruni, M. Interlenghi, M. Longoni, A. Passaretti, M. Caccia, C. Salvatore, I. Castiglioni, M. Martini. *Imaging and spectroscopic data combined to disclose the painting techniques and materials in the fifteenth century Leonardo atelier in Milan*. Dyes and Pigments (2021) 187, 109112.

M. Longoni, M.S. Zalaffi, L. De Ferri, A. M. Stortini, G. Pojana, P. Ugo. *Surface Enhanced Raman Spectroscopy with electrodeposited copper ultramicro-wires with/without silver nanostars decoration*. Nanomaterials (2021) 11, 518 - 533.

M. Longoni, S. Bruni. *Identification of Synthetic Organic Pigments in Contemporary Artists' Paints by FT-IR and FT-Raman: An Advanced Analytical Experiment*. Journal of Chemical Education (2021) 98, 966 - 972.

M. Longoni, A. Freschi, N. Cicala, S. Bruni. *Non-invasive identification of synthetic organic pigments in contemporary art paints by visible-excited spectrofluorimetry and visible reflectance spectroscopy*. Spectrochimica Acta Part A: Molecular and Biomolecular Spectroscopy (2020) 229, 117907.

Conference presentations

Colors in historical textiles: “in-situ” identification of natural dyes by dry-state SERS, accepted poster, **InArt 2022**, to be held in Paris (France).

Dry-state SERS for the “in-situ” identification of natural textile dyes, oral presentation, **SPIE Digital Forum**, 20-25 June 2019, Munchen (Germany).

Dry-state SERS for the “in-situ” identification of historical textile dyes, poster, **Fitzpatrick Institute for Photonics (FIP) Virtual Symposium**, 16-18 May 2021, Duke University (NC USA).

Dry-state SERS for the “in-situ” identification of natural textile dyes, oral presentation, **VISPEC ONLINE**, 19 February 2021, Politecnico di Milano (Italy).

Visible-excited spectrofluorimetry as a non-invasive tool for the “in situ” identification of natural dyes in historical textiles, oral presentation **Dyes in history and archeology (DHA38)**, 6-9 November 2019, Amsterdam (The Netherlands).